

UCSF

UC San Francisco Electronic Theses and Dissertations

Title

Computer assisted discovery and design of non-peptide inhibitors of the HIV I protease ; Thianthrene 5-oxide as a probe of the electronic properties of hemoprotein oxidizing species

Permalink

<https://escholarship.org/uc/item/3cb1z9rk>

Author

Alvarez, Juan Carlos

Publication Date

1992

Peer reviewed|Thesis/dissertation

- I Computer Assisted Discovery and Design of Non-Peptide Inhibitors of the HIV I Protease**
- II Thianthrene 5-Oxide as a Probe of the Electronic Properties of Hemoprotein Oxidizing Species**

by

Juan Carlos Alvarez

DISSERTATION

Submitted in partial satisfaction of the requirements for the degree of

DOCTOR OF PHILOSOPHY

in

Pharmaceutical Chemistry

in the

GRADUATE DIVISION

of the

UNIVERSITY OF CALIFORNIA

San Francisco



ACKNOWLEDGEMENTS

I would like to thank the many individuals who have contributed to my education along my academic career. I would especially like to thank my graduate advisor Dr. Paul Ortiz de Montellano for his guidance and support, and for allowing me the freedom to pursue my individual interests. I would also like to thank Dr. "Tack" Kuntz for turning me on to computational chemistry and giving me the opportunity to interact with his group. In addition, I would like to thank many of my peers, and in particular Dr. Brian Shoichet and Robert Harris with whom I have engaged in many fruitful discussions, and Elaine Meng for help with DOCK. I am also grateful to the staff of the Computer Graphics Laboratory and the Mass Spectrometry Laboratory for technical support and the University of California for financial support. Many thanks also go to Dr. Gregory Petsko who provided valuable guidance in my selection of a graduate program.

Finally, I would like to thank my family. My mother and father for placing an emphasis on education and giving me the opportunity to pursue it to the fullest extent, my wife, Debbie, for her patience and understanding, and all of them for their endless support and encouragement.

I. COMPUTER ASSISTED DISCOVERY AND DESIGN OF NON-PEPTIDE INHIBITORS OF THE HUMAN IMMUNODEFICIENCY VIRUS 1 PROTEASE

JUAN CARLOS ALVAREZ

ABSTRACT

Using the shape-fitting algorithm DOCK, haloperidol, a known antipsychotic, was identified as a competitive inhibitor of the HIV-1 protease with a K_i of 100 μM . Systematic modification of the haloperidol skeleton by traditional medicinal chemistry methods has yielded improvements in inhibitory potency as high as 18-fold. The observed improvements in the activity of many of the derivatives are in agreement with the binding orientation observed in the structure of the complex of UCSF8, the derivative in which the ketone moiety of haloperidol is replaced by a thioketal group, with the HIV-1 protease. The observed binding orientation as well as structure-activity relationships of the haloperidol derivatives led to the proposal of a pharmacophore pattern for the binding site of the enzyme. A high (85%) success ratio for the discovery of novel HIV-1 protease inhibitors resulted from a database search based on this pattern. Inhibitors identified by this method have resulted in potent second generation lead compounds. $N\alpha$ -FMOC amino acids appear to be promising drug leads. In particular, $N\alpha$ -FMOC $N\omega$ -tosylarginine, with an IC_{50} of 2.0 μM of the HIV-1 protease and an IC_{50} of 700 nM for the HIV-2 protease, is a potent non-peptide inhibitor for the HIV proteases. In addition, preliminary cell viability assays suggest that

derivatives of this compound, with LD₅₀'s of greater than 250 μM, are much less toxic than haloperidol derivatives. Using a distance geometry and rigid-body docking approach, a binding orientation in agreement with experimental evidence has been generated. The methodology for the structure-based discovery and design of novel HIV-1 protease inhibitors described can be applied to any target for which the three dimensional structure is known, and therefore comprises a powerful tool for the development of drugs.

II. THIANTHRENE 5-OXIDE AS A PROBE OF THE ELECTRONIC PROPERTIES OF HEMOPROTEIN OXIDIZING SPECIES

JUAN CARLOS ALVAREZ

ABSTRACT

Thianthrene 5-oxide (T-5-O), a compound previously used to probe the electronic character of chemical oxidants, was incubated with several hemoprotein oxidative systems. Nucleophilic and electrophilic oxidants convert T-5-O to its 5,5-dioxide and its 5,10-dioxide, respectively. Cytochrome P450 and chloroperoxidase convert T-5-O exclusively to the 5,10-dioxide, in agreement with direct oxygenation by an electrophilic ferryl species. Horseradish peroxidase in the presence of dihydroxyfumaric acid (DHFA) catalyzes the aerobic oxidation of T-5-O, generating the T-5,5-dioxide. The fact that the oxygen atom incorporated into the product is derived from molecular oxygen, as well as the failure of γ -radiolytically-generated hydroxyl radicals to oxidize the substrate under analogous conditions, has led to the proposal of a co-oxidative mechanism for the transformation. T-5-O is converted to both the 5,5- and 5,10- dioxides by hemoglobin and H_2O_2 . Thus, it appears as though multiple oxidative mechanisms are involved. Incubations using ^{18}O -labeled hydrogen peroxide have identified it as the primary source of the transferred oxygen atom in both products. The electrophilic oxidant product (T-5,10-dioxide) is consistent with oxidation by a cytochrome P450-like ferryl species, whereas a

mechanism invoking an activated ferrous dioxygen complex ($\text{Fe}^{\text{II}}\text{-O-O}^-$) is proposed for the formation of the 5,5-dioxide. Stereochemical analysis of the 5,10-dioxide produced by cytochrome P450, chloroperoxidase, and hemoglobin reveals *cis:trans* ratios of 1.3:1, 2.5:1, and 1:10, respectively. Since all three products are thought to be generated by analogous mechanisms, the differences in the isomer ratios are thought to reflect the geometrical constraints imposed on the substrate by the protein. These results demonstrate the utility of T-5-O as a probe of the electronic properties of biological oxidants.

TABLE OF CONTENTS

I. Computer assisted discovery and design of non-peptide inhibitors of the HIV 1 protease

Chapter 1	Introduction	
1.1	Introduction	1
1.2	How are drugs discovered?	1
1.3	The quest for lead compounds	
1.3.1	Random screening	2
1.3.2	Substrate and transition-state analogue inhibitors	2
1.3.3	Structure-based design	3
1.4	Human immunodeficiency virus and the AIDS problem	7
1.4.1	The life cycle of HIV	8
1.4.2	HIV-1 protease as a therapeutic target	11
1.4.3	The biochemistry of HIV-1 protease	12
1.4.4	Peptides as drugs	20
Chapter 2	Haloperidol and its analogues as inhibitors of the HIV-1 protease	
2.1	The discovery of haloperidol as an inhibitor of the HIV-1 protease	21
2.2	"Random" modifications of haloperidol	30
2.2.1	Additions to the haloperidol ketone	30
2.2.2	Biphenyl analogues of haloperidol	32
2.2.3	Double modifications to the haloperidol structure	35

2.3	X-ray structure of the complex of HIV-1 protease and the thioetal derivative of haloperidol (UCSF8)	36
2.4	Rationalization of the inhibitory potency of haloperidol derivatives based on the structure of the thioetal derivative (UCSF8)- HIV-1 protease complex	48
2.4.1	Products of the additions to the haloperidol ketone	49
2.4.2	Biphenyl analogues of haloperidol	52
2.4.3	Products with two modifications of the haloperidol structure	59
Chapter 3	The search for additional inhibitor leads using a pharmacophore-based approach	
3.1	Introduction	64
3.2	Defining the pharmacophore	65
3.3	Search results	66
3.4	Evaluation of compounds	68
3.5	Results of inhibition assays	69
3.5.1	Compounds similar to haloperidol	69
3.5.2	N-FMOC protected amino acids	75
3.5.3	Additional compounds	78
3.6	Conclusions	79
Chapter 4	Derivatives of haloperidol and cinnarizine attempting to fill the hydrophobic pockets defined by the UCSF8-protease complex x-ray structure	
4.1	Introduction	81
4.2	Synthesis of derivatives	82
4.3	Results of HIV-1 protease inhibition assays	85

Chapter 5	Nα-FMOC amino acids as inhibitors of the HIV-1 protease	
5.1	Introduction	91
5.2	Evaluation of potency of various N α -FMOC amino acids	92
5.3	N α -FMOC arginine derivatives as HIV-1 protease inhibitors	94
5.4	Attempts at elucidating the binding orientation of N α -FMOC N ω -tosylarginine	100
Chapter 6	Conclusions and future directions	110
6.1	Perspective	115
Chapter 7	Experimental	
7.1	Equipment	126
7.2	Chemicals	126
7.3	Synthetic methods	127
7.3.1	Purification of haloperidol (UCSF1)	127
7.3.2	Additions to ketones by organometallic reagents	128
7.3.3	LAH reductions of biphenyl acids	133
7.3.4	Pyridinium chlorochromate (PCC) oxidations	134
7.3.5	Alpha keto cyclopropyl ring openings	136
7.3.6	Thioketalization	139
7.3.7	N-oxidation	140
7.3.8	Acylation of heterocyclic amines	140
7.3.9	LAH reduction of amides	145
7.3.10	Reductive alkylation of heterocyclic amines with 3-phenyl cinnamaldehyde	147
7.3.11	Catalytic hydrogenation	149

7.4	Calculations	
7.4.1	DOCK	151
7.4.2	MACCS-3D	152
7.4.3	DGEOM	152
References		154
II. Thianthrene 5-oxide as a probe of the electronic properties of hemoprotein oxidizing species		
Chapter 1	Introduction	
1.1	Hemoproteins	160
1.2	Thianthrene 5-oxide as a probe of the electronic character of chemical oxidants	161
1.2.3	T-5-O as a probe of the electronic character of oxygenations in biological systems	162
Chapter 2	Direct oxidation of thianthrene 5-oxide by the ferryl species of cytochrome P450	
2.1	Introduction	164
2.2	Oxidation of T-5-O by cytochrome P450	165
2.3	Stereochemical course for the oxidation of T-5-O by cytochrome P450 2B1	167
2.4	Discussion fo the results of the cytochrome P450-catalyzed oxidation of T-5-O	168
Chapter 3	Chloroperoxidase: Another ferryl oxygen transfer reaction	
3.1	Introduction	169
3.2	The chloroperoxidase-catalyzed oxidation of T-5-O	170
3.3	Stereochemical course for the oxidation of T-5-O by chloroperoxidase	171

3.4	Discussion of the results of the chloroperoxidase-catalyzed oxidation of T-5-O	173
Chapter 4	The horseradish peroxidase/dihydroxyfumarate/O ₂ oxidizing system	
4.1	Introduction	175
4.2	The aerobic oxidation of T-5-O by horseradish peroxidase and dihydroxyfumarate	178
4.3	Oxidation of the thianthrene dioxides by the HRP/DHFA/O ₂ system	182
4.4	Involvement of the hydroxyl radical in the aerobic oxidation of T-5-O by HRP and DHFA	183
4.5	Implications of T-5-O oxidation data on the mechanism of HRP/DHFA-mediated reactions	185
Chapter 5	The hemoglobin-mediated oxidation of T-5-O	
5.1	Introduction	188
5.2	Oxidation of T-5-O by the hemoglobin/H ₂ O ₂ system	190
5.3	Stereoselectivity of the conversion of T-5-O to T-5,10-dioxide by hemoglobin/H ₂ O ₂	192
5.4	Implications of the results of T-5-O oxidation by hemoglobin/H ₂ O ₂ on the mechanism	193
Chapter 6	Summary and Conclusions	195
Chapter 7	Experimental	
7.1	Equipment	198
7.2	Materials	198
7.3	Synthetic procedures	199
7.4	Incubation procedures	201
7.5	Product identification	206

LIST OF TABLES

I. Computer assisted discovery and design of non-peptide inhibitors of the HIV 1 protease	
Table 2.1: Relative enzyme activity in the presence of 0.5 mM haloperidol and IC ₅₀ 's for various aspartic proteases. (DeCamp and Craik, unpublished results; Desjarlais <i>et al.</i> , 1990).	29
Table 2.2: Structures and IC ₅₀ 's of haloperidol-based inhibitors.	31
Table 3.1: Inhibitory potency against the HIV-1 protease of the compounds originating from the pharmacophore-based search of the FCD using MACCS-3D.	71
Table 4.1: Inhibitory potencies against the HIV-1 protease of various derivatives of cinnarizine and haloperidol (Craik <i>et al.</i> , unpublished results).	88
Table 5.1: Structures and inhibitory potencies (Craik <i>et al.</i> , unpublished results) of N α -FMOC amino acids.	93
Table 5.2: Structures and inhibitory potencies (Craik <i>et al.</i> , unpublished results) of arginine derivatives modified at the amino and guanidino groups.	95
Table 5.3: Structures and inhibitory potencies (Craik <i>et al.</i> , unpublished results) of N α -FMOC N ω -tosylarginine derivatives modified at the carboxyl group (adapted from DeVoss, 1992).	98
Table 5.4: Structures and inhibitory potencies of N α -FMOC amino acid derivatives assayed to explore the tolerance of substitution in the alkyl guanidino sidechain of SF75.	99

Table 6.1: DOCK candidates with the potential of being attached to a thioketal methylene group of UCSF8. 125

II. Thianthrene 5-oxide as a probe of the electronic properties of hemoprotein oxidizing species

Table 6.1: Isomeric composition of the T-5,10-dioxide product obtained from the electrophilic oxidation of T-5-O. 197

LIST OF FIGURES

I. Computer assisted discovery and design of non-peptide inhibitors of the HIV 1 protease	
Figure 1.1: Polyprotein translation products of the HIV-1 genome. Adapted from Darke <i>et al.</i> , 1990.	10
Figure 1.2: X-ray crystallographic structure of the uncomplexed HIV-1 protease reported by Wlodawer <i>et al.</i> , 1989.	14
Figure 1.3: Ribbon diagram depicting secondary structure elements of the uncomplexed HIV-1 protease (Wlodawer <i>et al.</i> , 1989).	15
Figure 1.4: Comparison of the alpha carbon backbone of the x-ray crystallographic structures of the uncomplexed HIV-1 protease (Wlodawer <i>et al.</i> , 1989), and the protease-MVT-101 complex (Miller <i>et al.</i> , 1989).	17
Figure 1.5: Proposed catalytic mechanism for aspartyl proteases (Meek <i>et al.</i> , 1990).	18
Figure 1.6: Summary of the biochemical properties of the HIV-1 protease (Meek <i>et al.</i> , 1990).	19
Figure 2.1: Template candidates obtained from the DOCK 1.1 search of a subset of the Cambridge Crystallographic Database.	23
Figure 2.2: Structures of bromperidol, R = Br; and haloperidol, R = Cl; and UCSF8.	24
Figure 2.3: Top view of the highest scoring orientation obtained from DOCK 1.1 of bromperidol within the HIV-1 protease active site.	25

Figure 2.4: Side view of the highest scoring orientation obtained from DOCK 1.1 of bromperidol within the HIV-1 protease active site.	26
Figure 2.5: Side view of the highest scoring orientation obtained from DOCK 1.1 of bromperidol within the HIV-1 protease active site.	27
Figure 2.6: X-ray structure of the HIV-1 protease (blue) complexed with UCSF8 (yellow). The crystallographic chloride ion is shown in green, and the catalytic aspartate residues are shown in red. (Rutenber <i>et al.</i> , 1992)	38
Figure 2.7: Side view comparison of the structures of the uncomplexed, peptide inhibitor bound, and UCSF8 bound forms of the HIV-1 protease.	39
Figure 2.8: Top view comparison of the structures of the uncomplexed, the peptide inhibitor bound, and the UCSF8 bound forms of the HIV-1 protease.	40
Figure 2.9: Close-up view of UCSF8 bound within the HIV-1 protease active site.	41
Figure 2.10: Both two-fold related binding modes observed crystallographically for UCSF8 within the HIV-1 protease active site.	42
Figure 2.11: Side view comparison of the binding modes of UCSF8 and MVT-101 (Miller <i>et al.</i> , 1989) within the active site of the HIV-1 protease.	44
Figure 2.12: Top view comparison of the binding modes of UCSF8 and MVT-101 (Miller <i>et al.</i> , 1989) within the active site of the HIV-1 protease.	45
Figure 2.13: Side view comparison of the binding modes of UCSF8 proposed by DOCK and observed in the x-ray structure within the active site of the UCSF8 bound HIV-1 protease.	46

Figure 2.14: Top view comparison of the binding modes of UCSF8 proposed by DOCK and observed in the x-ray structure within the active site of the HIV-1 protease.	47
Figure 2.15: Result of the superposition of the R isomer of 2 on the x-ray structure of UCSF8 within the protease active site.	50
Figure 2.16: Result of the superposition of the S isomer of 2 on the x-ray structure of UCSF8 within the protease active site.	51
Figure 2.17: Alternative binding mode for the S isomer of 3 obtained from its superposition on the x-ray structure of UCSF8, followed by rotation of a single bond placing the benzyl group of 3 in the site occupied by the fluorenyl group of UCSF8.	53
Figure 2.18: HIV-1 protease cleft created by residues 32, 47, 54, 56, and 79-81.	54
Figure 2.19: Comparison of the structures of UCSF8 and the proposed binding orientation for the meta biphenyl analogue of haloperidol (19).	55
Figure 2.20: Proposed binding orientation for the meta biphenyl haloperidol derivative, 19 , to the HIV-1 protease.	56
Figure 2.21: Space-filling representation of the proposed binding orientation for the meta biphenyl haloperidol derivative, 19 , to the HIV-1 protease.	57
Figure 2.22: Proposed binding orientation for the para biphenyl haloperidol derivative, 20 , to the HIV-1 protease.	58
Figure 2.23: Proposed binding orientation for the ortho biphenyl haloperidol derivative, 18 , to the HIV-1 protease.	60

Figure 2.24: Proposed binding orientation for 21 , to the HIV-1 protease.	61
Figure 2.25: Proposed binding orientation for 22 , to the HIV-1 protease.	62
Figure 2.26: Proposed binding orientation for 23 , to the HIV-1 protease.	63
Figure 3.1: (A) Relative distances between the centroids of the chlorophenyl, fluorophenyl, and thioketal groups of UCSF8 in the HIV-1 protease bound conformation. Top: intramolecular distances; Bottom: intermolecular distances of the symmetry related inhibitor molecules observed crystallographically. (B) Query used for the pharmacophore search of the FCD using MACCS-3D.	67
Figure 3.2: Structures of compounds originating from the pharmacophore-based search of the FCD using MACCS-3D which were tested for inhibition of the HIV-1 protease.	70
Figure 3.3: Orientation of cinnarizine, SF17, within the HIV-1 protease active site proposed by DOCK 3.0.	72
Figure 3.4: Alternative possible binding orientation of cinnarizine, SF17, within the HIV-1 protease active site.	74
Figure 3.5: Possible orientations of the FMOC group proposed by DOCK 3.0 for N α -FMOC amino acid-based inhibitors of the HIV-1 protease.	76
Figure 3.6: Comparison of binding orientations of SF33 proposed by DOCK, and UCSF8 within the HIV-1 protease.	77
Figure 3.7: Orientation of SF37 within the HIV-1 protease active site proposed by DOCK 3.0.	80

Figure 5.1: Superposition of a manually generated conformation of N α -FMOC N ω -tosylarginine on the x-ray structure of UCSF8 in its bound conformation to the HIV-1 protease.	102
Figure 5.2: Superposition of the highest scoring DOCK orientation of a computationally generated conformation of N α -FMOC N ω -tosylarginine on the x-ray structure of UCSF8 in its bound conformation to the HIV-1 protease.	104
Figure 5.3: Side view comparison of the orientations of N α -FMOC N ω -tosylarginine obtained manually and by computational methods within the HIV-1 protease.	105
Figure 5.4: Top view comparison of the orientations of N α -FMOC N ω -tosylarginine obtained manually and by computational methods within the HIV-1 protease.	106
Figure 5.5: Close-up view of the acid functionality the highest scoring orientation of N α -FMOC N ω -tosylarginine.	107
Figure 5.6: Primary structure of the HIV-2 protease.	109
Figure 6.1: Cross-section of the spheres generated by DOCK within the remaining volume in the UCSF8-bound active site of the HIV-1 protease.	117
Figure 6.2: Result of the DOCK search of the FCD for ligands complementary to the remaining volume in the UCSF8-bound active site of the HIV-1 protease using the force-field scoring option.	118
Figure 6.3: Result of the DOCK search of the FCD for ligands complementary to the remaining volume in the UCSF8-bound active site of the HIV-1 protease using the contact only scoring option.	119
Figure 6.4: Result of the DOCK search of the FCD for ligands complementary to the remaining volume in the UCSF8-bound active site of the HIV-1 protease using the normalized force-field scoring option.	120

Figure 6.5: Result of the DOCK search of the FCD for ligands complementary to the remaining volume in the UCSF8-bound active site of the HIV-1 protease using the normalized contact scoring option.	121
Figure 6.6: DOCK orientation of the top scoring molecule (methyl-4-azidobenzoimidate) obtained from the search for ligands complementary to the remaining volume in the UCSF8-bound active site of the HIV-1 protease.	123
II. Thianthrene 5-oxide as a probe of the electronic properties of hemoprotein oxidizing species	
Figure 1.1: Oxidation of thianthrene-5-oxide by electrophilic or nucleophilic oxygen-transfer agents.	162
Figure 1.2: <i>Cis</i> and <i>trans</i> isomers of thianthrene 5,10-dioxide.	163
Figure 2.1: The catalytic cycle of cytochrome P450.	164
Figure 2.2: Time course for the oxidation of T-5-O by microsomal cytochrome P450.	166
Figure 2.3: Time courses for T-5,5,10-trioxide formation from the microsomal cytochrome P450-catalyzed oxidation the thianthrene dioxides.	167
Figure 3.1: Time course for the oxidation of T-5-O to T-5,10-dioxide by chloroperoxidase.	171
Figure 3.2: Time course for the chloroperoxidase-catalyzed conversion of T-5,5-dioxide to T-5,5,10-trioxide.	172
Figure 4.1: Time course of the conversion of T-5-O to the 5,5-dioxide by horseradish peroxidase in the presence of DHFA and O ₂ .	179
Figure 4.2: Dose-dependent inhibition of HRP/DHFA/O ₂ -mediated oxidation of T-5-O.	180

Figure 4.3: Effect of catalase and exogenous H ₂ O ₂ on the HRP/DHFA/O ₂ -mediated oxidation of T-5-O.	181
Figure 4.4: Time course of the conversion of <i>cis</i> -T-5-O to the 5,5,10-trioxide by horseradish peroxidase in the presence of DHFA and O ₂ .	183
Figure 4.5: Mechanism for the formation of a hypothetical DHFA-peroxyl species ultimately responsible for the conversion of T-5-O to T-5,5-dioxide in the HRP/DHFA system.	187
Figure 5.1: Mechanism proposed for the incorporation of molecular oxygen into styrene oxide in the H ₂ O ₂ -dependent oxidation of styrene by hemoglobin.	189
Figure 5.2: Time course for the oxidation of T-5-O by human hemoglobin and H ₂ O ₂ .	191
Figure 7.1: High pressure liquid chromatogram of the thianthrene oxides standards and phenyl sulfone (internal standard).	208

LIST OF SCHEMES

I. Computer assisted discovery and design of non-peptide inhibitors of the HIV 1 protease

- Scheme 1.1: Iterative cycle for designing and evaluating ligands of a target enzyme. 6
- Scheme 2.1: Synthetic pathway for the de novo synthesis of the biphenyl analogues of haloperidol. 34
- Scheme 4.1: Formation of cinnarizine and haloperidol amide derivatives by the acylation of various heterocycles. 83
- Scheme 4.2: Reduction of cinnarizine and haloperidol amide derivatives to generate the corresponding amines. 84
- Scheme 4.3: Formation of cinnarizine and haloperidol olefin derivatives by alkylation of various heterocyclic starting materials. 86
- Scheme 4.4: Reduction of cinnarizine and haloperidol olefin derivatives to generate the corresponding saturated compounds. 87

II. Thianthrene 5-oxide as a probe of the electronic properties of hemoprotein oxidizing species

- Scheme 4.1: Proposed mechanism for the DHFA/O₂-dependent aromatic hydroxylation catalyzed by HRP. 177

CHAPTER 1

INTRODUCTION

1.1 INTRODUCTION

Whether a disease is caused by a biochemical pathway gone awry or by a microbial organism, enzymes are often the targets of choice for its therapeutic control. Elimination of an invading organism can be accomplished by the inhibition of an enzyme essential for its survival but not present in the host. Three years ago, we undertook the task of "rationally" designing non-peptide inhibitors of the human immunodeficiency virus 1 (HIV-1) protease, defining methodology which can be applied to countless other diseases where the three-dimensional structure of the target enzyme is known.

1.2 HOW ARE DRUGS DISCOVERED?

Many drugs, including quinine and penicillin have been found through serendipity (Roberts, 1989). More often, however, drugs are developed through iterative cycles of modifying and evaluating analogues of a lead compound. The goal of a medicinal chemist is to improve on the inhibitory activity of the compound and/or reduce its side effects. Although the pharmaceutical industry has become efficient in carrying out these steps, the process, being largely based

on trial and error, is quite slow and expensive. It has been estimated that for every 10,000 or more compounds synthesized less than one makes it to the market as a drug (Sheridan & Venkataraghavan, 1987). In addition, the method is limited by the fact that a lead compound is necessary, and that if the original lead fails, one is left to find a new lead compound. There are several avenues one can take for finding lead compounds.

1.3 THE QUEST FOR LEAD COMPOUNDS

1.3.1 RANDOM SCREENING

Traditionally, lead compounds have been discovered through the screening of thousands of synthetic chemical compounds or natural products for desirable effects. Although the screening process has the drawbacks of being a crude, repetitious, and time-consuming method it has the advantage of requiring relatively little knowledge of the disease, the target, or even the lead itself (Propst and Perun, 1989), and it has the potential of uncovering structural classes of compounds not previously known or never before used in a particular therapeutic area (Sheridan & Venkataraghavan, 1987).

1.3.2 SUBSTRATE AND TRANSITION-STATE ANALOGUE INHIBITORS

When some information is available on the enzyme target, such as its substrate specificity or the mechanism by which it carries out its

function, it becomes possible to begin rationally designing inhibitors. Structural analogues of the substrate, or products, incapable of being turned over by the enzyme, are often good starting points for the development of new drugs since one can frequently retain the binding affinity to the desired target (Propst and Perun, 1989).

Enzymes catalyze reactions by stabilizing the highest energy species, or transition state (Eyring, 1935), along the reaction pathway, thereby lowering the activation energy barrier. The structure of the transition state generally resembles the midpoint between the reactants and the products (Haldane, 1930) of the rate-determining step. Analogues of this putative entity often bind much more tightly than the endogenous substrates themselves thereby making them excellent lead compounds.

1.3.3 STRUCTURE-BASED DESIGN

Due to inherent limitations of peptides as drugs (discussed in section 1.3.4) substrate or transition state analogues are not practical as protease inhibitors, making it necessary to follow an alternate strategy. The approach we decided to take for discovering a lead compound was that of structure-based design. Certainly the most creative, if not the most elegant, of lead generation methods, it provides an opportunity for the discovery of entirely novel leads. Structure-based design, however, also requires the largest amount of knowledge; a three-dimensional structure for the target is necessary. Although such a structure may be obtained from NMR, or

inferred from modelling by homology or secondary structure predictions, we opted to use the x-ray structure of the HIV-1 protease (Wlodower *et al.*, 1989) as our starting point.

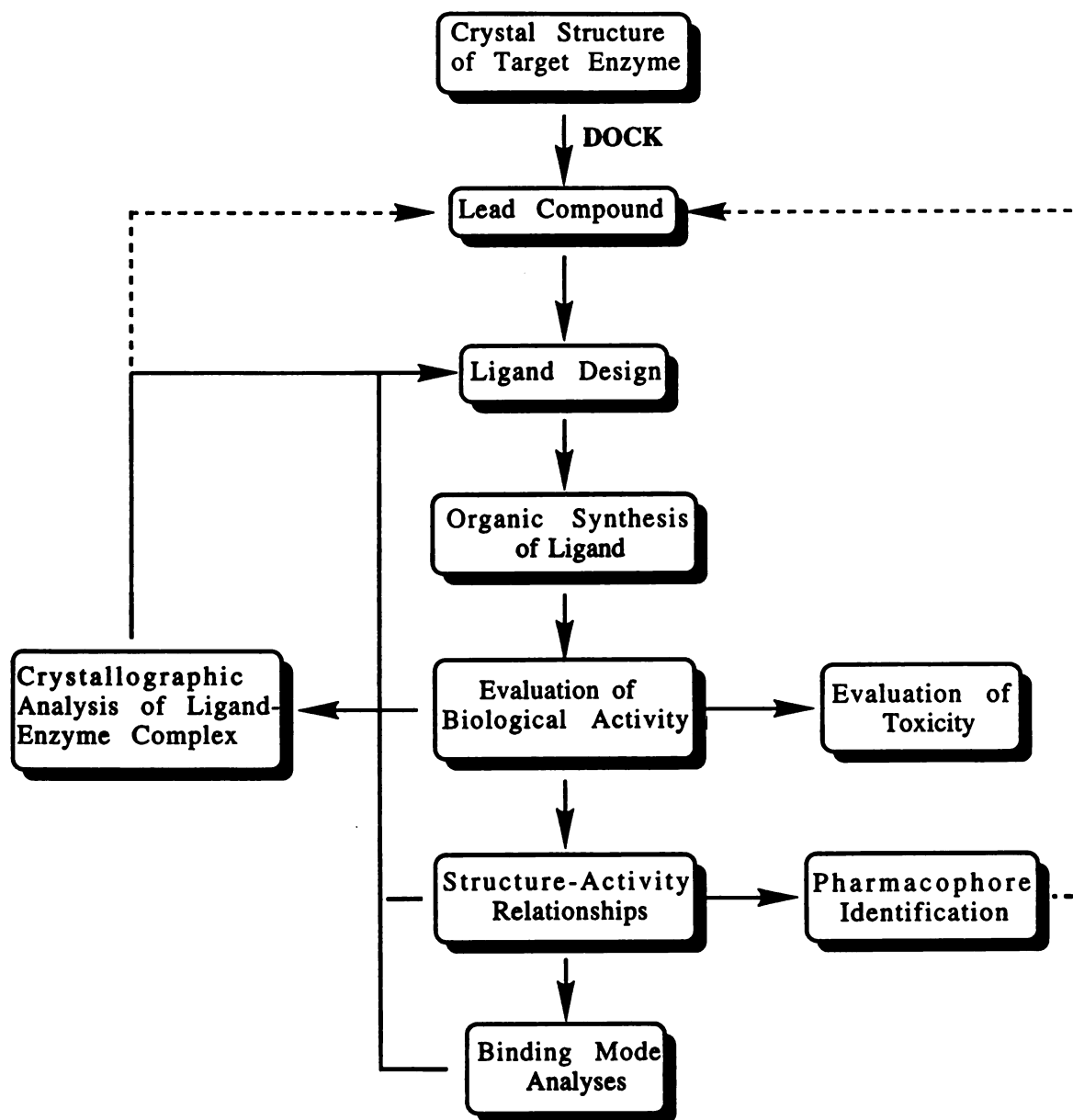
In 1878, Langley suggested the theory that certain antagonists, in that case atropin and pilocarpin, carry out their effect by interacting with substances (receptors) on cells. Fischer, in 1894, and Ehrlich, in 1909, expanded on this idea by suggesting lock-and-key type of interactions between the receptor and the ligand; a concept essential to structure-based design. In addition to the implicit steric complementarity between the two entities, there is a requirement for electronic, or chemical, complementarity, such as ion pairs, hydrogen bond formation, and hydrophobic interactions. In structure-based design, one attempts to engineer this complementarity not only in finding a lead compound, but also in designing the appropriate analogues. Initially, we attempted to incorporate the necessary steric complementarity into our inhibitor using a set of computer algorithms called DOCK (Kuntz *et al.*, 1982). The following section outlines the approach we envisioned for designing our inhibitors.

DOCK is in essence a rigid body matching program. The program generates sets of spheres that fill the invaginations on the surface of the target molecule. These spheres are subdivided into clusters. Databases of small molecules are searched for templates whose shapes are complementary to the cluster of interest, generally the active site (Desjarlais *et al.*, 1988). Correspondence between the

ligand atom centers and the site sphere centers is sought using their respective distance matrices. Although subsequent generations of the program also allow for grid-based energy scoring (Meng et al., 1992), the DOCK version (1.1) we used for our initial search scored and ranked the potential ligands exclusively on steric interactions. Thus, it was expected that these templates would require modifications to introduce the chemical and electronic complementarity.

After visually evaluating the compounds obtained from DOCK, the top candidates themselves can be tested for the desired activity or atomic changes can be introduced prior to testing. Once a lead compound is identified, that is, one which exhibits reasonable inhibition, modifications of the structure can begin. Although the binding orientations proposed by DOCK cannot be considered predictions, they can be used as hypotheses to suggest initial modifications in lieu of an enzyme-inhibitor complex crystal structure.

An iterating cycle of design, synthesis, activity evaluation, and binding model analysis is introduced (Scheme 1.1). Initial modifications of the structure, which are mostly done at random, can include variation/addition of substituents, changes in chain length, introduction of rigidity, and pruning of the molecule. Provided that the derivatives can bind in an analogous conformation, structure-activity relationships can be established, and once groups important for binding are identified, a pharmacophore pattern for the target enzyme can be postulated. The more potent inhibitors of the target



Scheme 1.1: Iterative cycle for designing and evaluating ligands of a target enzyme.

enzyme can also be tested for their toxicity in cell culture assays, and inhibitor-enzyme complex crystallizations can be attempted to unambiguously determine the inhibitor binding orientation. Once the actual binding orientation is established, rational modifications targeted to interact with particular sites in the enzyme can begin. The knowledge obtained can be applied to the improvement of the existing lead as well as the search for new lead compounds.

Due to the large number of expertises necessary, such projects are possible only through the collaboration of many groups. The discovery of lead compounds, and the design and synthesis of various derivatives are the subjects which will be primarily discussed.

1.4 HUMAN IMMUNODEFICIENCY VIRUS AND THE AIDS PROBLEM

Human immunodeficiency virus (HIV) is the causative agent for the acquired immune deficiency syndrome (AIDS). Since the first AIDS cases diagnosed in 1981 (Gallo and Montagnier, 1988), the virus has spread rapidly and has reached epidemic proportions. No cure or vaccine is yet available for combatting the disease, which generally proceeds to a fatal endpoint. Although dideoxynucleotides, such as 3'-azido-2',3'-dideoxythymidine (AZT), have been used to prolong the survival of infected individuals, these carry multiple serious side effects including bone marrow suppression, insomnia, nausea, vomiting, myalgias, myopathy, seizures, severe headaches, and liver

function abnormalities (Fischi *et al.* , 1987, Richman *et al.*, 1987). Moreover, the long-term administration of AZT has resulted in the emergence of AZT-resistant HIV variants (Larder *et al.*, 1989). Thus, new drugs which alone or in combination with other agents reduce viral infectivity must be developed.

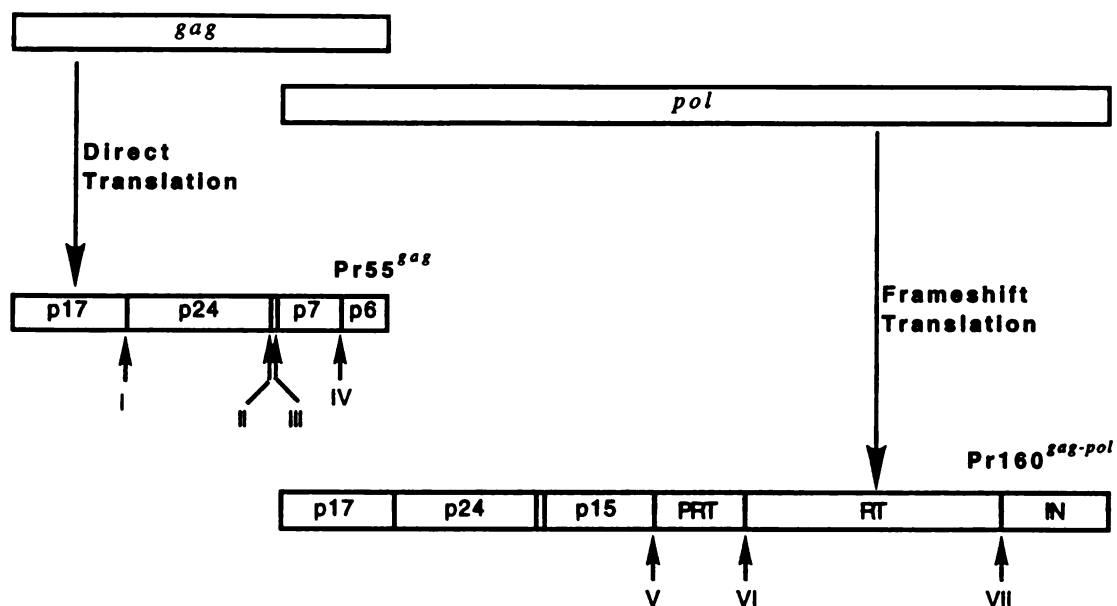
1.4.1 THE LIFE CYCLE OF HIV

HIV is a member of the family of retroviruses, *Retroviridae* (Gallo & Montagnier, 1988). Retroviruses, which like other viruses largely depend on the host's cellular machinery for their propagation, are characterized by a genome composed of RNA instead of DNA. The life cycle of the virus begins when a virion attaches to the surface of a T4-lymphocyte by the binding of gp120, a glycoprotein on the viral envelope, to the CD4 receptor of the lymphocyte (Dalgleish *et al.*, 1984; McDougal *et al.*, 1986; Smith *et al.*, 1987). The viral membrane then fuses to the cellular membrane injecting the viral core, structural proteins, enzymes, and two identical strands of RNA (Haseltine and Wong-Staal, 1988).

The next phase is the permanent installation of the HIV genome into the host cell. A viral polymerase, reverse transcriptase, uses the viral RNA as a template for the synthesis of a single-stranded cDNA copy of the viral genome. An associated enzyme, ribonuclease H, destroys the original RNA, allowing the polymerase to make a second DNA copy using the first as a template. The resulting double-stranded DNA translocates to the nucleus where a third viral enzyme,

integrase, inserts the HIV genome into the host cell's DNA. Once integrated, the viral genomic DNA, known as the provirus, is permanently established in the lymphocyte, and a variable latency period ensues (Meek *et al.*, 1990).

The final stage of the HIV life cycle involves the expression of the proviral genome resulting in the formation of new virus particles. Upon activation, the proviral DNA is transcribed to viral genomic RNA by host RNA polymerases. This RNA transcript serves a dual purpose; it is the source of mRNA from which viral proteins are made, and the genomic RNA in the core of new virions. Translation of the mRNA results in the synthesis of polyprotein precursors to viral structural proteins as well as viral enzymes (Figure 1.1). Post-translational modifications, including glycosylation and myristoylation, catalyzed by cellular enzymes take place as the proteins migrate to the periphery of the cell. Immature virions composed of a glycoprotein envelope, viral genomic RNA, and viral polyproteins begin to bud from the cell. The final maturation step for the virion is carried out by the fourth virally-encoded enzyme, the HIV protease. The protease frees itself, intermolecularly, from one of the polyproteins, and then cleaves the viral polyproteins into the individual enzymes and structural proteins of the virion core (Figure 1.1). The resulting mature virions are now capable of infecting adjacent T-lymphocytes, thus completing the cycle (Meek *et al.*, 1990).



<u>HIV-1 Sites</u>	<u>Peptides Hydrolyzed</u>
I GAG 129-136	SQNY*PIVQ
II GAG 360-367	ARVL*AEAM
III GAG 374-381	ATIM*MQRG
IV GAG 445-452	PGNF*LQSR
V POL 65-72	SFNF*PQIT
VI POL 164-171	TLNF*PISP
VII POL 724-731	RKIL*FLDG

Figure 1.1: Polyprotein translation products of the HIV 1 genome. Viral protease cleavage sites are designated by arrows, and their amino acid sequence is shown below. Adapted from Darke *et al.*, 1990.

1.4.2 HIV-1 PROTEASE AS A THERAPEUTIC TARGET

There are multiple steps, reviewed recently by Mitsuya *et al.* (1990), in the HIV life cycle described above amenable for therapeutic intervention. The viral enzymes are attractive drug targets since they are vital to viral replication and serve no role in normal cell function. The proposed approach for rational inhibitor design necessitates a three-dimensional structure of the target molecule. The availability of the coordinates for both the unliganded (Navia *et al.*, 1989; Wlodawer *et al.*, 1989) and an inhibitor-complexed form (Miller *et al.*, 1989) of the HIV-1 protease made it the most attractive therapeutic target.

The essential role of the HIV-1 protease has been established by studies in which mutations within the viral genome, or inhibition by peptide-based inhibitors, have been shown to interfere with viral propagation. Inactivation of the HIV-1 protease through a single base substitution in the 9-kilobase viral genome, mutating the catalytic residue Asp-25, leads to the formation of non-infectious, immature virions with reduced reverse transcriptase activity (Kohl *et al.*, 1988). In addition, removal of either the p17-p24 or p24(p1)-p9 proteolytic cleavage site of the Pr55^{gag} polyprotein also produces non-infectious virions (Gottlinger *et al.*, 1988). Finally, analogous results are observed in cultured T4 cells when the HIV-1 protease is inhibited using peptide-based compounds (Meek *et al.* 1990).

1.4.3 THE BIOCHEMISTRY OF HIV-1 PROTEASE

The HIV-1 protease is a member of the aspartyl protease family, as first suggested for retroviral proteases by Toh *et al.* (1985) based on the presence of the Asp-Thr-Gly sequence characteristically conserved in members of this class. Non-retroviral aspartyl proteases are two-domain proteins of more than 300 residues with each domain contributing one copy of the conserved triad to the active site. The similarity in the sequence and structure of the two domains led to the proposal that they evolved from a single domain by gene duplication (Tang *et al.*, 1978). Using pattern-recognition, structure prediction, and molecular modelling techniques, Pearl and Taylor (1987) concluded that the HIV-1 protease, with only 99 amino-acid residues, as well as other retroviral proteases, correspond to a single domain of the non-retroviral aspartic proteases. In their proposal they invoked the formation of homodimers, in which each monomer contributes an Asp-Thr-Gly to the active site formed at the subunit interface.

Additional support for this theory was obtained through inhibition and mutagenesis experiments. The HIV-1 protease is weakly inhibited by pepstatin A (isovaleryl-Val-Val-Sta-Ala-Sta), where Sta is the amino acid statine, (4S,3S)-4-amino-3-hydroxy-6-methylheptanoic acid), with a $K_i \leq 2 \mu\text{M}$. This natural product, a transition-state analogue, is a characteristic inhibitor of aspartyl proteases (Richards *et al.*, 1989). Furthermore, the protease is inactivated by 1,2-epoxy-(4-nitrophenoxy) propane (EPNP) in a

time-dependent manner (Meek *et al.*, 1989). This inactivator has been shown to esterify one or both of the active-site aspartate residues of this family of proteases. Meek *et al.* (1989) showed that inactivation of the HIV-1 protease by EPNP depends on the presence of the unprotonated form of a residue of $pK_a = 3.8$, in agreement with a mechanism of inactivation in which participation of an unprotonated aspartyl residue is necessary. Site-specific mutagenesis of Asp-25 to an alanyl (Kohl *et al.*, 1988), threonyl (Seelmeier, 1988), or arginyl (Gottlinger *et al.*, 1989) residue eliminates the proteolytic activity of the enzyme. However, a glutamate residue at position 25 can, although poorly, substitute for the natural residue (Pichuantes *et al.*, 1989).

The proposal by Pearl and Taylor (1987) that the HIV-1 protease is an aspartic protease in which dimerization is necessary to create the active site and juxtapose the catalytic aspartate residues was confirmed by solution of the three-dimensional structure of both a recombinant (Navia *et al.*, 1989) and a synthetic form (Wlodawer *et al.*, 1989) of the enzyme (Figure 1.2). The general topology of the HIV-1 protease molecule, as was expected, is similar to that of a single domain in pepsin-like aspartic proteases. The tertiary structure of the monomer primarily consists of β -sheet elements with only a single helix at residues 86-94 (Figure 1.3). The completely symmetrical dimer is held together by a four-stranded antiparallel β sheet, two strand from each monomer, comprised of amino-terminus residues 1-5 and the carboxy-terminus residues 95-99 (Wlodawer *et al.*, 1989).

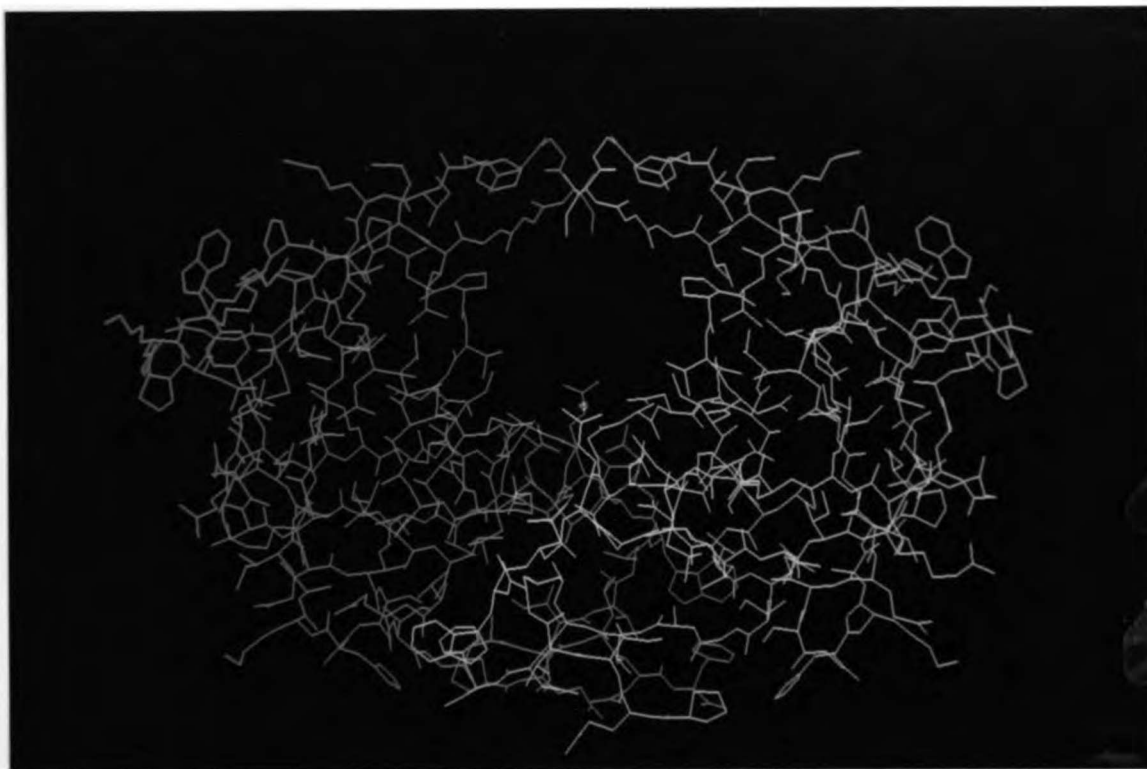


Figure 1.2: X-ray crystallographic structure of the uncomplexed HIV-1 protease reported by Wlodawer *et al.*, 1989. The two monomers are distinguished by different shades of blue. The catalytic aspartate residues and the crystallographic water molecule bound between them are shown in red.

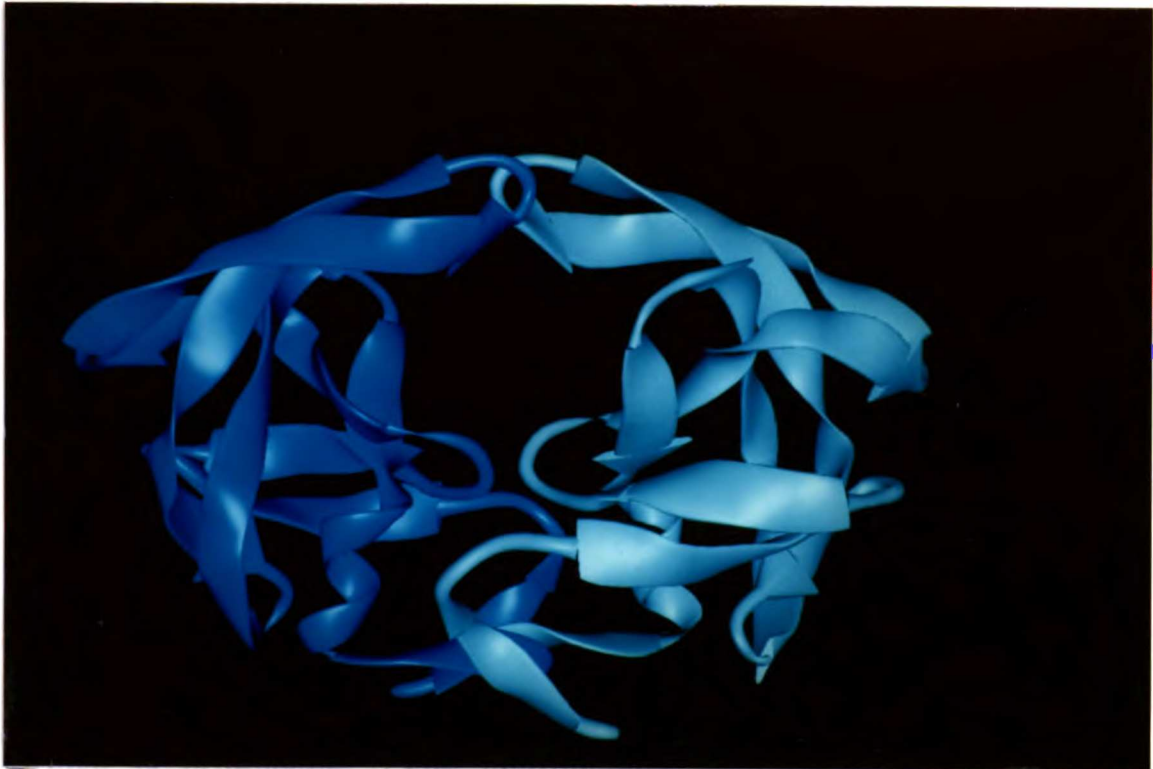


Figure 1.3: Richardson(1985) ribbon diagram depicting secondary structure elements of the uncomplexed HIV-1 protease (Wlodawer *et al.*, 1989).

Upon binding of an inhibitor, or presumably also a substrate, significant changes in the structure of the enzyme take place as observed in the crystal structure of a complex of the HIV-1 protease with the substrate-based inhibitor MVT-101, N-acetyl-Thr-Ile-Nle-Ψ[CH₂-NH]-Nle-Gln-Arg.amide (Miller *et al.* , 1989) (Figure 1.4). Reduction of the scissile peptide bond to the -CH₂-NH- function prevents hydrolysis by the enzyme. The inhibitor lies in a single orientation as an extended β-strand, thereby perturbing the original C₂ symmetry of the unliganded enzyme. The largest motions observed, as large as 7 Å, occur in the "flaps", residues 35-57 of each chain, that apparently serve to sequester the peptide substrate.

The proposed catalytic mechanism based on kinetic data is shown in Figure 1.5 (Meek *et al.*, 1990). A water molecule is hydrogen-bonded to the catalytic aspartates (residue 25 in each monomer), only one of which is protonated. The unprotonated Asp-25 elicits general-base deprotonation of the lytic water, activating it to attack the peptide carbonyl while the protonated Asp-25 acts as a general-acid to protonate the carbonyl oxygen. This forms the initial tetrahedral intermediate. Collapse of the intermediate to the products is also facilitated by the aspartate residues by general-acid/base catalysis.

Additional properties of the HIV-1 protease are summarized in Figure 1.6. The 99 residues of the primary structure correspond to a molecular weight of 11,000. However, a molecular weight of 22,000 is obtained by analytical gel filtration, glycerol density gradient

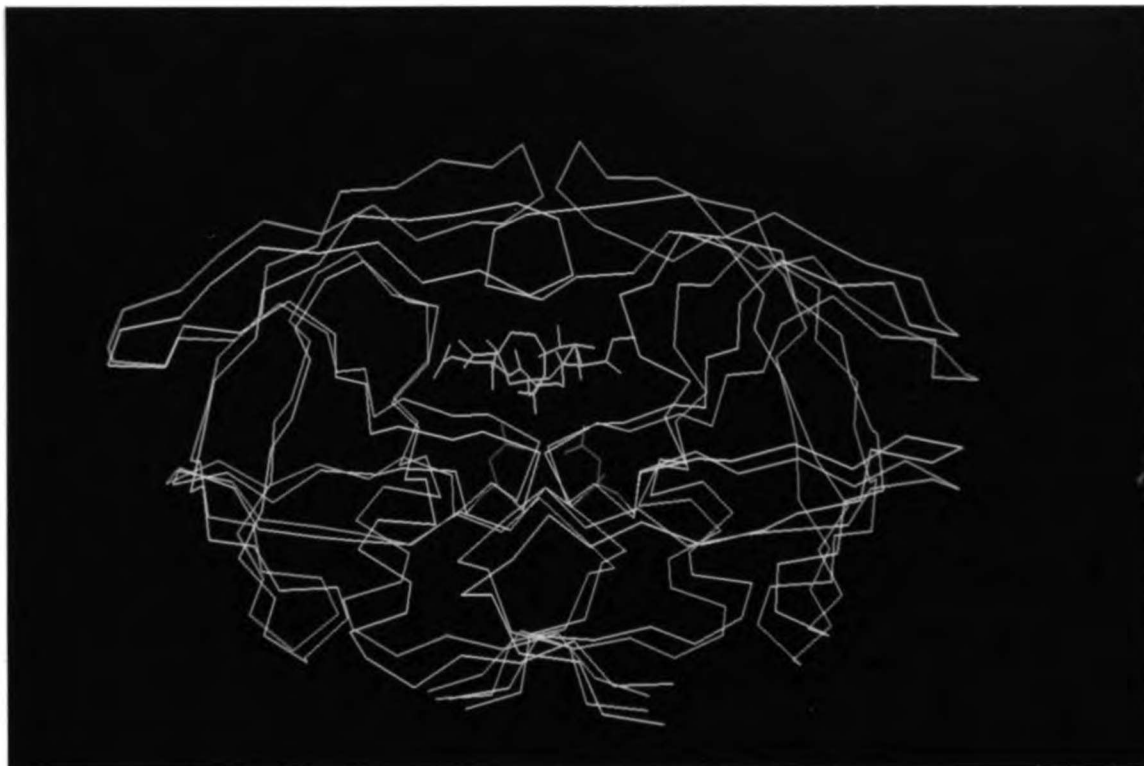


Figure 1.4: Comparison of the alpha carbon backbone of the x-ray crystallographic structures of the uncomplexed HIV-1 protease (Wlodawer *et al.*, 1989) in cyan, and the protease-MVT-101 complex (Miller *et al.*, 1989) in magenta. The peptide-based inhibitor is shown in yellow. The catalytic aspartate residues of the complexed structure are shown in red.

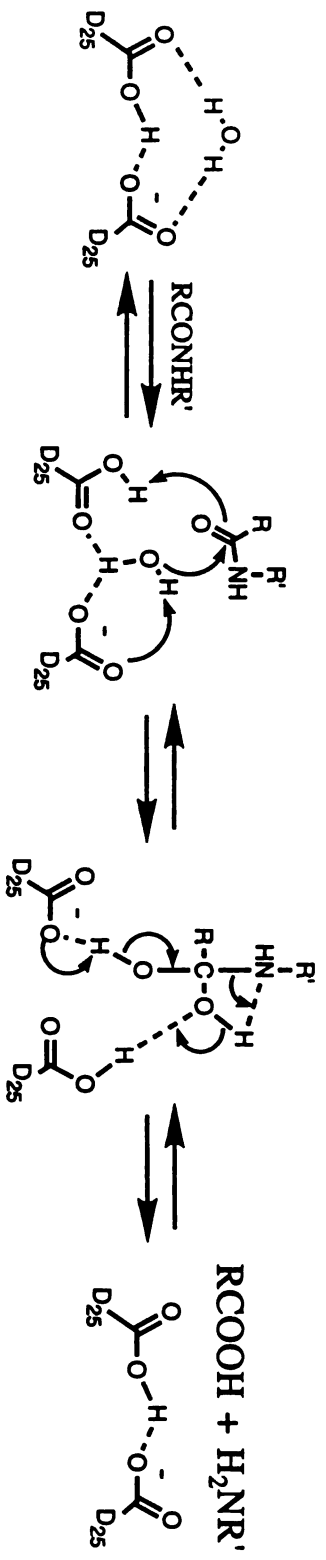


Figure 1.5: Proposed catalytic mechanism for aspartyl proteases (Meek *et al.*, 1990).

Protease Class: Aspartic Protease

Molecular Weight: 22,000 (non-denaturing)

11,000 (denaturing)

Primary Structure:

1 10 20
SFNF*PQITLWQRPLVTIKIGGQLKEALL DTGA
30 40 50 60
DDTVLEEMSLPGRWKPKMIGGIGGPIKVRQYD
70 80 90
QILIEICGHKAIGTVLVGPTPVNIIGRNLLTQI
99
GCTLNF*PI

Quarternary Structure: Homodimer, Asp25 residues from each subunit comprise the catalytic unit.

Substrate Specificity: P4 = Ser, Thr, Ala, Pro, Arg
P3 = Gln, Glu, Phe, Arg, Leu, Lys, Gly, Thr
P2 = Val, Ile, Asn, Thr
P1 = Tyr, Phe, Leu, Met
P1' = Pro, Leu, Ala, Met, Tyr
P2' = Ile, Val, Leu, Gln, Glu
P3' = Val, Ser, Asp, Arg, Ile

Figure 1.6: Summary of the biochemical properties of the HIV-1 protease (Meek *et al.*, 1990). The triad conserved in aspartic proteases is boxed, and auto-proteolytic sites are denoted by asterisks.

centrifugation, or chemical crosslinking with dimethylsuberimidate followed by NaDodSO₄-polyacrylamide gel electrophoresis as expected for the dimer (Meek *et al.*, 1989). The HIV-1 protease accepts a broad range of amino acids in its subsites, although F*P, Y*P, L*A, M*M, F*L, F*Y, and L*F are the natural cleavage sites, and has a minimum length requirement of six residues (Meek *et al.* , 1990).

1.4.4 PEPTIDES AS DRUGS

Although many substrate-based and transition-state peptide inhibitors of the HIV-1 protease with K_i's in the nanomolar range have been reported (Dreyer *et al.* , 1989; Roberts *et al.* , 1990; Erickson *et al.* , 1990; Meek *et al.* , 1990; Sham *et al.* , 1991), inherent problems with peptide-drugs make the development of non-peptide therapeutic agents important. Peptides have a relatively low metabolic stability due to proteolytic susceptibility. Furthermore, often a single peptide has not just one activity, but affects several biological functions. Finally, peptides exhibit low oral bioavailability and poor penetration through the blood-brain-barrier.

CHAPTER 2

HALOPERIDOL AND ITS ANALOGUES AS INHIBITORS OF THE HIV-1 PROTEASE

2.1 THE DISCOVERY OF HALOPERIDOL AS AN INHIBITOR OF THE HIV-1 PROTEASE

The shape-matching algorithm DOCK 1.1 (briefly described in section 1.2.3), which scores and ranks putative ligands based on a function of the interatomic distances to the receptor (Desjarlais *et al.* , 1988), was run using the uncomplexed HIV-1 protease structure (Wlodower *et al.* , 1989). Both a search in which all the active site spheres were included and one where the DOCK spheres corresponding to the flaps were removed in order to select for molecules complementary to the peptide-binding site of the enzyme were carried out. The search was conducted on a subset of the Cambridge Structural Database containing about 10,000 molecules (Seibel, unpublished results). The program parameters used were: MATCH: dislim = 2.0 Å, nodlim = 8; SCORE: concut = 2.4 Å, dmin = 3.5 Å, discut = 5.0 Å (Desjarlais *et al.* , 1990)

The top 200 scoring molecules from each of the two searches were examined using the molecular graphics package MidasPlus (Huang, 1989). Three primary criteria were used to evaluate the candidates

as possible templates for the design of HIV-1 protease inhibitors. First, proximity (within 4 Å) of at least one atom of the template to the carboxyl oxygen atoms (OD2) of either Asp-25 or Asp-125 of the protease. This requirement was imposed so that the inhibitor would act competitively with the substrate. The potential to form hydrogen bonds to the occluded regions of the protein surface, in order to maximize protein-ligand interactions and selectivity to the target, was also considered important. Finally, since the scoring function evaluates the candidates on their shape complementarity to the receptor site, it was expected that modifications to the templates would be necessary to engineer the chemical complementarity. Therefore, a molecular scaffold requiring a modest synthetic effort flexible to atomic substitution, without spiro ring linkages or multiple chiral centers, was desired. Using these criteria, the field was narrowed down to eight candidates (Figure 2.1). Only one candidate originated from the search including the flap spheres, ranking 21st based on its DOCK score in that search. The templates from the other search were numbers 9, 27, 30, 47, 51, 105, and 155.

The primary candidate was bromperidol (Figure 2.2), candidate number 51. It was of particular interest because its best orientation from the DOCK program (Figures 2.3, 2.4, and 2.5) placed the hydroxyl group between the catalytic aspartates, corresponding closely to the position of the hydroxyl group in the co-crystal of a statine-based inhibitor and penicillopepsin (James and Sielecki, 1987). Other polar atoms of the protease within hydrogen-bonding distance (a 3 Å heavy atoms interatomic distance) were the N ω of

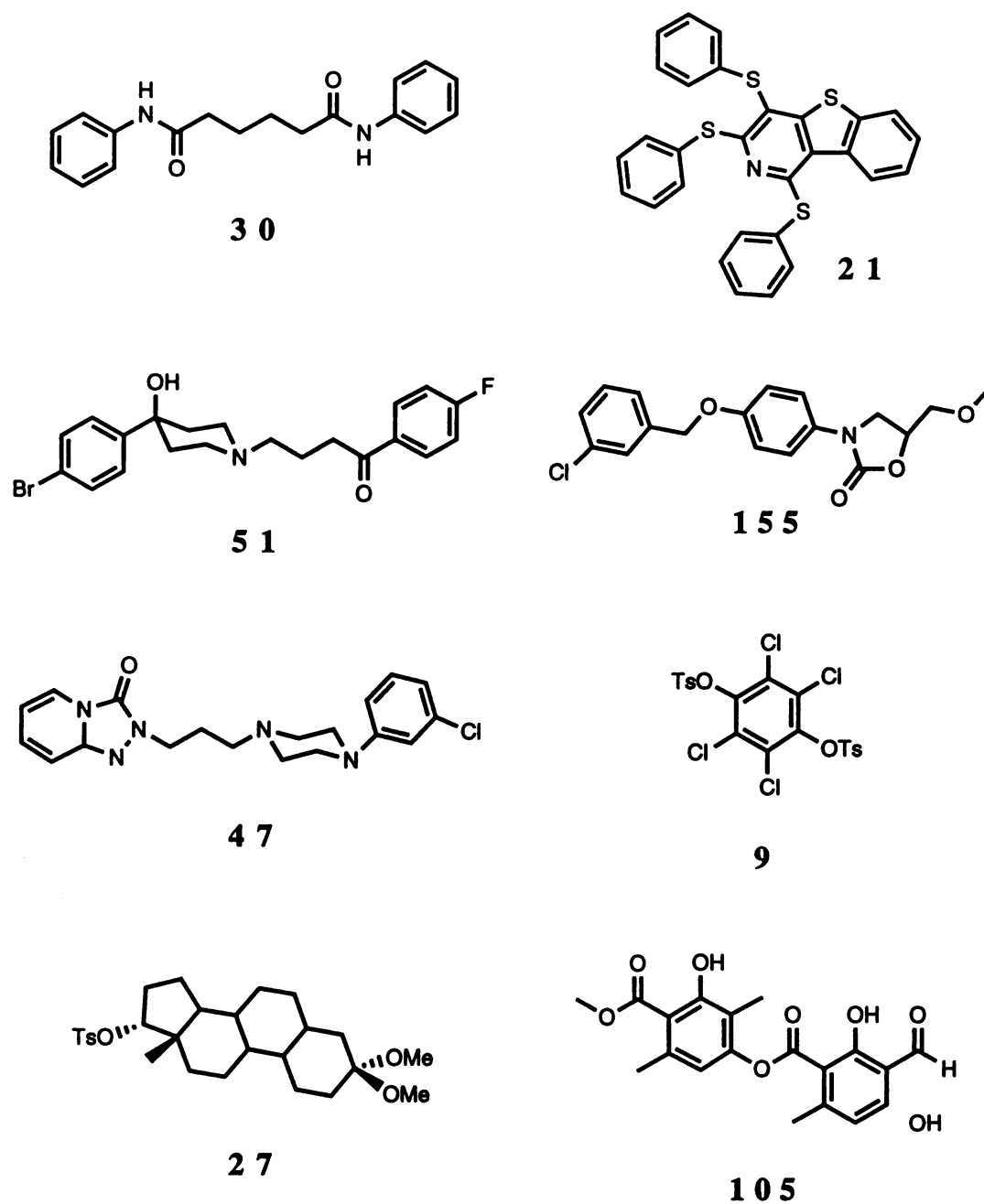


Figure 2.1: Template candidates obtained from the DOCK 1.1 search of a subset of the Cambridge Crystallographic Database. Only molecule number 21 was obtained from the search which included the flap spheres.

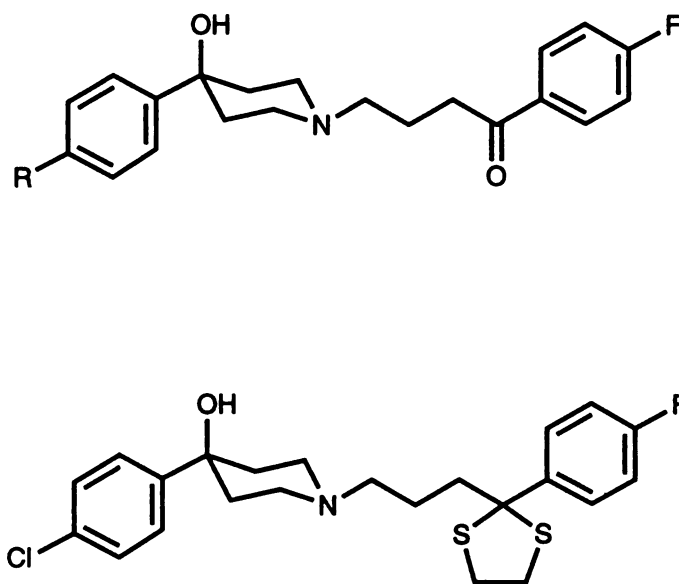


Figure 2.2: Structures of bromperidol, R = Br; and haloperidol, R = Cl (top); and UCSF8 (bottom).

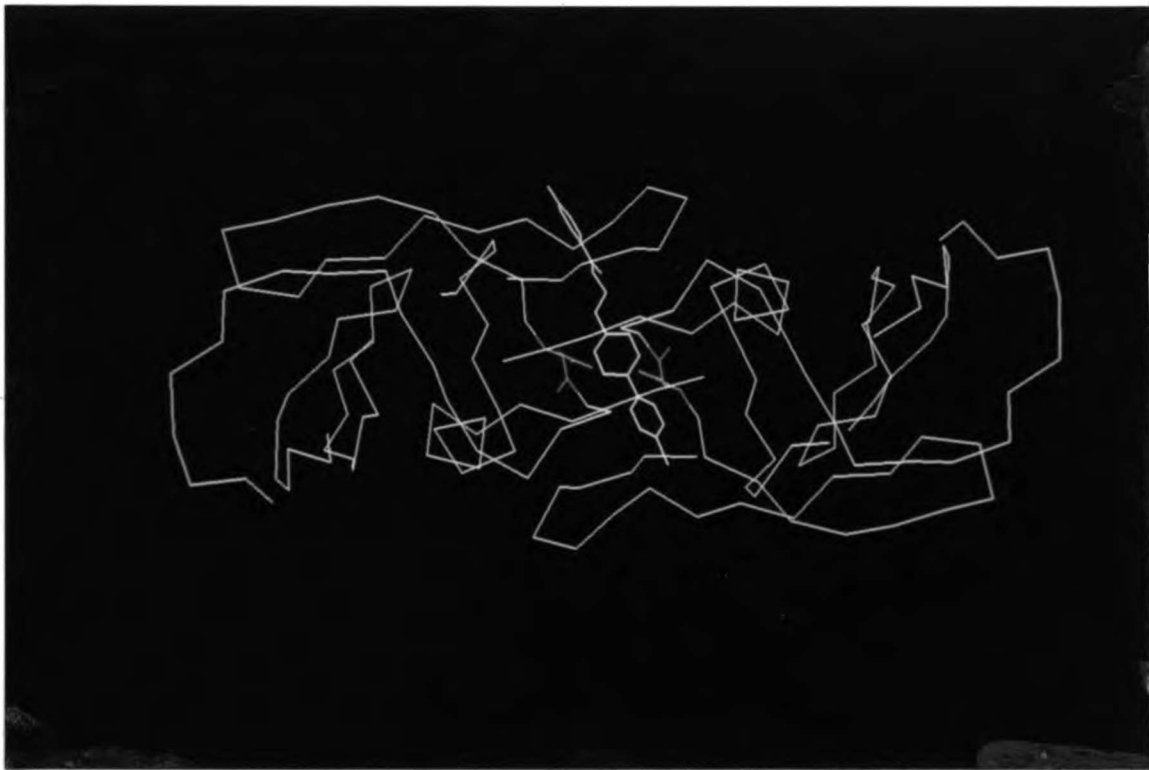


Figure 2.3: Top view of the highest scoring orientation obtained from DOCK 1.1 of bromperidol (yellow) within the HIV-1 protease active site (cyan). The flap residues have been removed, and only the alpha carbons of the protein are shown for clarity. The catalytic aspartate residues are shown in red.

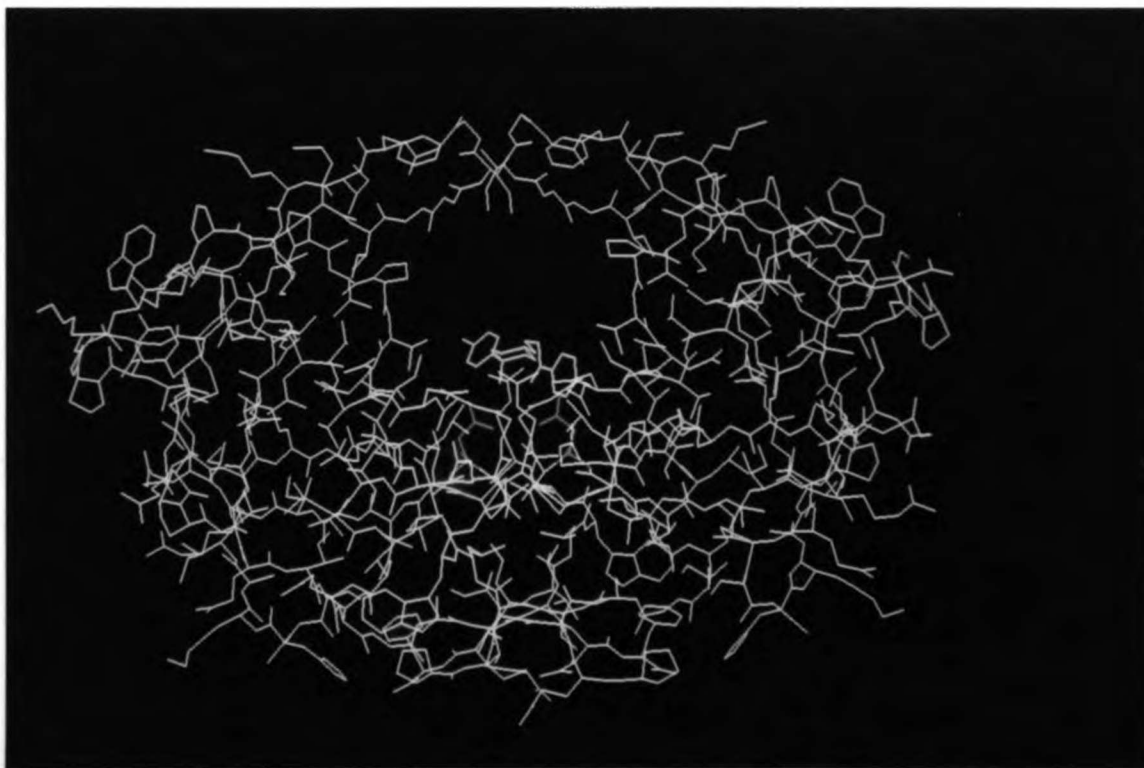


Figure 2.4: Side view of the highest scoring orientation obtained from DOCK 1.1 of bromperidol (yellow) within the HIV-1 protease active site (cyan). The catalytic aspartate residues are shown in red.

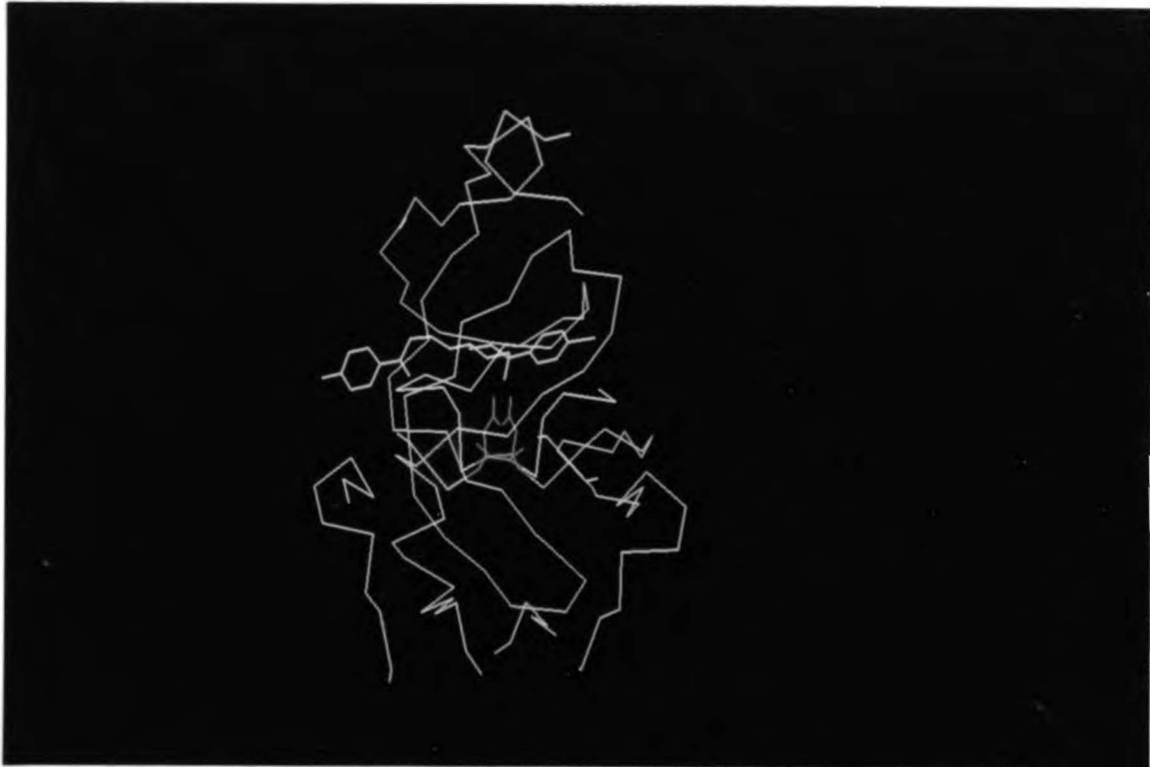


Figure 2.5: Side view of the highest scoring orientation obtained from DOCK 1.1 of bromperidol (yellow) within the HIV-1 protease active site (cyan). Only the alpha carbons of the protein are shown for clarity. The catalytic aspartate residues are in red. Note how the hydroxyl group of haloperidol can interact with both catalytic aspartate residues.

Arg-108 to the fluorophenyl meta- and para- positions, and the backbone carbonyl of Gly-27 to the ketone group of the ligand. Furthermore, the bromophenyl moiety filled the P1 pocket which is occupied by a phenylalanine sidechain in the natural substrate, and the fluorophenyl fit tightly within a notch created by residues R108, L110, L123, and V182. Other attractive features of this lead were the commercial availability of a close analogue, haloperidol (HAL), which only differs in the substitution of a chlorine atom for the bromine atom of bromperidol, and the fact that many of its pharmacological properties had been investigated because it is a known antipsychotic agent.

Haloperidol (1, UCSF1) (Figure 2.2) was tested for its ability to inhibit the hydrolysis of the decapeptide Ala-Thr-Leu-Asn-Phe*Pro-Ile-Ser-Pro-Trp by the HIV-1 protease. The kinetic parameters for the substrate were: $K_m = 2.5 \pm 0.44$ mM, $V_{max} = 23.9 \pm 2.3$ $\mu\text{mol}\cdot\text{min}^{-1}\cdot\text{mg}^{-1}$, and $k_{cat} = 514$ min^{-1} (DeCamp, Babé, and Craik in Desjarlais *et al.*, 1990). HAL inhibited the HIV-1 protease in a concentration-dependent manner with a K_i of 100 ± 20 μM , IC_{50} of 125 μM , and IC_{90} of 2.0 mM. Haloperidol is highly selective for the HIV protease exhibiting little inhibitory effect on pepsin, and no effect on renin or cathepsin D, but inhibiting the HIV-2 protease to a similar extent (Table 2.1). Cell viability assays using a colorimetric assay (Mossman, 1983) and COS-7 cells gave an LD_{50} of 500 μM for a four hour assay, and 150 μM for a 24 hour assay (Babé and Craik, unpublished results).

Protease	Percent Activity Remaining	IC ₅₀ (μM)
Human Renin	100	ND *
Bovine Cathepsin D	100	ND
Porcine Pepsin	72	1000
HIV-1 Protease	26	125
HIV-2 Protease	30	140

Table 2.1: Relative enzyme activity in the presence of 0.5 mM haloperidol and IC₅₀'s for various aspartic proteases. ND signifies not detectible (DeCamp and Craik, unpublished results; Desjarlais *et al.* , 1990).

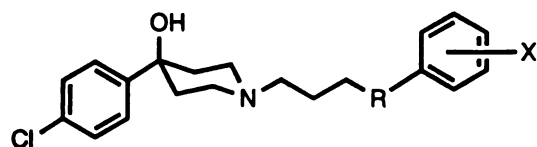
2.2 "RANDOM" MODIFICATIONS OF HALOPERIDOL

As stated in section 1.2.3, the binding orientations proposed by DOCK cannot be considered predictions, but they can be used as hypotheses to suggest initial modifications in lieu of an enzyme-inhibitor complex crystal structure. Thus, prior to unambiguous determination of the inhibitor's binding mode, modifications of the haldol skeleton were carried out to determine structure-activity relationships and to evaluate the DOCK binding orientation.

2.2.1 ADDITIONS TO THE HALOPERIDOL KETONE

Additions to the ketone moiety of haloperidol were accomplished using organometallic reagents. Reactions with phenyl lithium and benzyl magnesium bromide resulted in the phenyl diol (**2**, UCSF24) and the benzyl diol (**3**, UCSF25) derivatives of haldol, respectively. The addition of alkyl Grignard reagents was also attempted but the reaction was sluggish and none of the desired products was obtained.

Derivatives **2** and **3** inhibited the HIV-1 protease with IC_{50} 's of 62 μ M and 87 μ M, respectively (Table 2.2) (DeCamp and Craik, unpublished results). The decreases in the IC_{50} values observed for these derivatives, in conjunction with a slight increase in the IC_{50} of the haldol diol obtained by reduction of the ketone with lithium aluminum hydride (Desjarlais *et al.*, 1990), suggested that there is space available in the vicinity of the ketone, and that hydrophobic groups are adequate for filling this space. In addition, since the



Compound	R	X	IC ₅₀ (μM)
1		<u>p</u> - F	125
2		<u>p</u> - F	62
3		<u>p</u> - F	87
18		<u>o</u> - phenyl	40
19		<u>m</u> - phenyl	20
20		<u>p</u> - phenyl	32
21		<u>o</u> - phenyl	20
22		<u>m</u> - phenyl	10
23		<u>p</u> - phenyl	7
24		<u>m</u> - phenyl	8
25	N-oxide of 19		80

Table 2.2: Structures and IC₅₀'s of haloperidol-based inhibitors.

products of these reactions, and the analogous ones in section 2.2.3, generate racemic mixtures of the two enantiomers, it is possible that one enantiomer is a much more potent inhibitor than the other thus making the IC₅₀ of that isomer as much as 2-fold better than observed. The fact that the phenyl analogue was more inhibitory than the benzyl analogue suggests there are some steric or geometric constraints on the site.

2.2.2 BIPHENYL ANALOGUES OF HALOPERIDOL

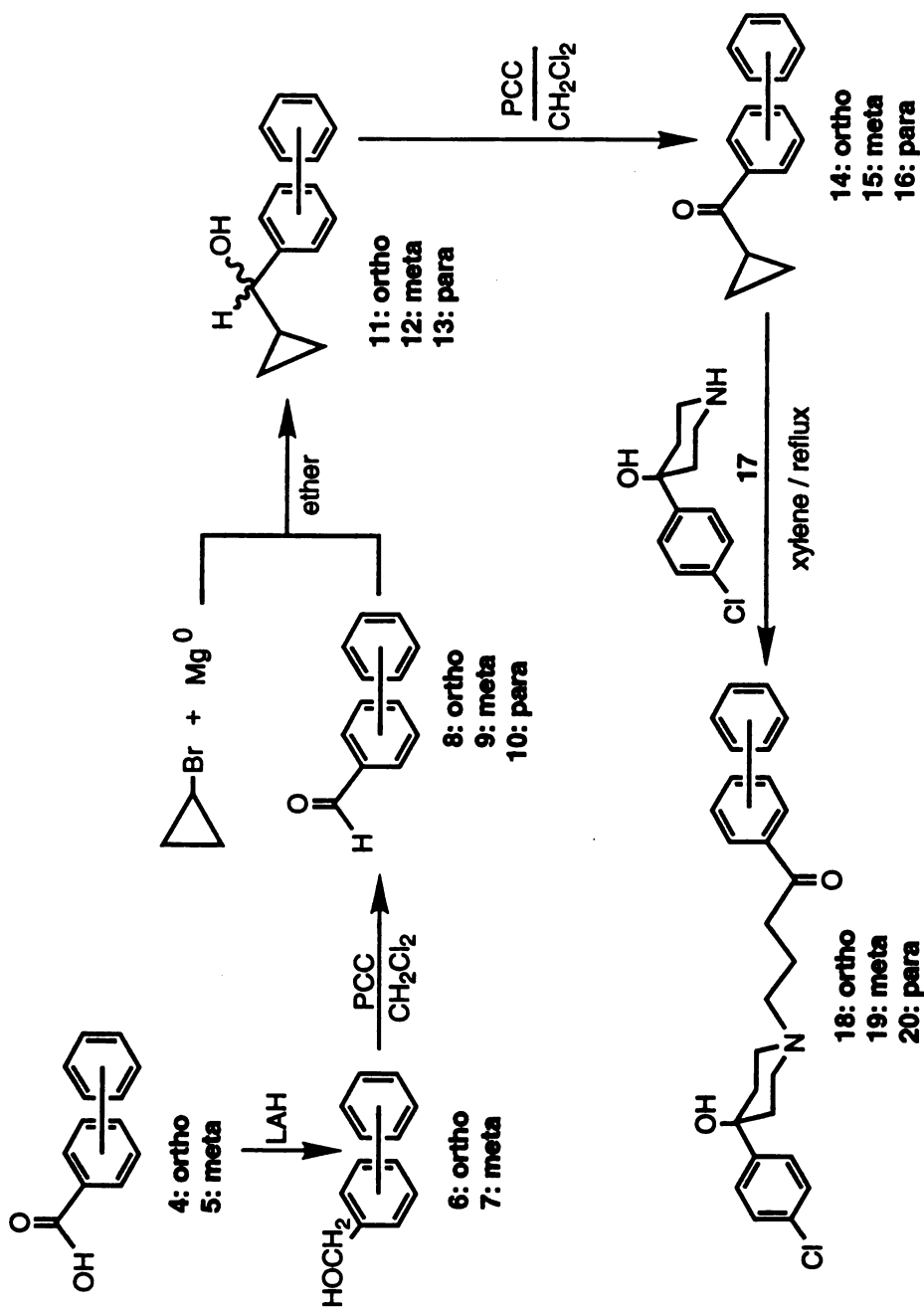
The reaction of phenyl lithium with haldol resulted in an additional product, which upon testing exhibited an IC₅₀ of 12 μM for the HIV-1 protease (DeCamp and Craik, unpublished results). Its NMR spectrum contained five extra protons in the aromatic region suggesting the addition of a second phenyl equivalent to the molecule. This was supported by a mass spectrum revealing a molecular weight 58 units above the expected one. It was postulated that the phenyl anion was adding to the fluorophenyl group of haloperidol resulting in the elimination of the fluorine atom thereby generating a biphenyl moiety.

This theory was confirmed by HRMS and ¹⁹F NMR. The accurate molecular weight of 511.22683 differed from a calculated mass of 511.22781 by only 1.9 ppm. In its ¹⁹F NMR, no fluorine signal was found, whereas the fluorine signal for haloperidol was found 28.36 ppm upfield from the external standard CF₃CH₂OH. The lack of occurrence of such a reaction between phenyl lithium and 2

suggested that the ketone is vital and that the mechanism was probably of the Michael type. In order to determine the effect of a phenyl group at each position of the fluorophenyl ring, haloperidol derivatives of all three biphenyl isomers were synthesized *de novo* (Scheme 2.1).

Biphenyl alcohols **6** and **7**, obtained from the LAH reduction of their corresponding acids, **4** and **5**, were oxidized to aldehydes **8** and **9**, respectively, with pyridinium chlorochromate (PCC). The commercial availability of para biphenyl aldehyde makes these two steps unnecessary for the para derivative. Addition of cyclopropyl magnesium bromide to the aldehydes followed by oxidation by PCC gave ketones **14**, **15**, and **16**. Finally, ring opening of the cyclopropyl moiety with 4-(4'-chlorophenyl)-4-piperidinol (**17**) generated the desired biphenyl analogues of haloperidol, **18** (UCSF51), **19** (UCSF52), and **20** (UCSF36).

Testing the three isomeric biphenyl derivatives for their inhibition of the HIV-1 protease revealed, in every instance, an improved activity over that of haloperidol itself (Table 2.2). The meta isomer (**19**) was the most potent with an IC_{50} of 20 μ M, followed by the para isomer (**20**), IC_{50} 32 μ M, and the ortho isomer (**18**), IC_{50} 40 μ M (DeCamp and Craik, unpublished results). Thus, the enzyme appears to be ample enough to accommodate a phenyl group off any position of the fluorophenyl ring, implying the ring does not lie within a "tight" pocket. Thus, at most only two (the ortho and meta positions



Scheme 2.1: Synthetic pathway for the de novo synthesis of the biphenyl analogues of haloperidol.

on the same side) of the ring's carbon atoms appear to be in contact with the enzyme in the radial direction.

2.2.3 DOUBLE MODIFICATIONS TO THE HALOPERIDOL STRUCTURE

The additivity of the modifications discussed in sections 2.2.2 and 2.2.3 was examined by the synthesis and testing of the products of phenyl addition to the ketone group of the haldol biphenyl analogues. In addition, the inhibitory potency of the thioketal and the N-oxide derivatives of the meta-biphenyl haloperidol, **19**, was also evaluated. The phenyl additions were carried out with phenyl lithium as in section 2.2.2, the thioketal derivative was synthesized using ethanedithiol and $\text{BF}_3 \cdot \text{OEt}_2$ in methanol, and the N-oxidation was accomplished with H_2O_2 .

The phenyl addition products of ortho-, meta-, and para-biphenyl haloperidol, **21** (UCSF56), **22** (UCSF57), and **23** (UCSF33), exhibited IC_{50} 's of 7, 10, and 20 μM , respectively (Table 2.2) (DeCamp and Craik, unpublished results). Thus, improvements in potency of about 4.5-fold in the case of the para-isomer and 2-fold for both the meta- and ortho- isomers were observed. These are similar enhancements to the one observed upon phenyl addition to haloperidol (also of about 2-fold), suggesting not only that the biphenyl analogues are binding in a fashion similar to that of haloperidol, but also that the biphenyl moiety, in particular that of

the ortho- isomer, is binding to a site distinct from the added phenyl group.

Conversion of the carbonyl group of meta-biphenyl haloperidol, **19**, to a thioketal, yielding **24** (UCSF59), improved the IC₅₀ to 8 μM (DeCamp and Craik, unpublished results), a factor of 2.5 (Table 2.2). This is somewhat less than the 8-fold improvement observed upon conversion of haloperidol to its thioketal derivative. This may suggest that, relative to the fluorophenyl group, the meta-biphenyl group is constrained in a less productive binding orientation for the thioketal moiety.

Finally, conversion of UCSF52 to its N-oxide, **25** (UCSF67), resulted in a 4-fold loss of activity (Table 2.2) (DeCamp and Craik, unpublished results). This compares unfavorably to the little change observed upon the N-oxidation of haloperidol. It is possible that the added length of the biphenyl derivative has forced a slight shift in the position of the piperidine nitrogen atom, and upon N-oxidation an unfavorable steric or electrostatic interaction with the enzyme has resulted.

2.3 X-RAY STRUCTURE OF THE COMPLEX OF HIV-1 PROTEASE AND THE THIOKETAL DERIVATIVE OF HALOPERIDOL (UCSF8)

The three-dimensional structure (to 2.2 Å resolution and an R factor of 17.7%) of a complex of the HIV-1 protease with the thioketal

derivative of haloperidol, UCSF8 - shown in Figure 2.2, (Rutenber *et al.*, 1992) is shown in Figure 2.6. The structure of the UCSF8-bound enzyme appears to be intermediate between that of the "open" uncomplexed form (Wlodawer *et al.*, 1989), Figure 1.4, and that of the "closed" form complexed with the reduced peptide inhibitor MVT-101 (Miller *et al.*, 1989), Figure 1.6. The structures of the three forms of the enzyme are compared in Figures 2.7 and 2.8. The enzyme flaps have the same polarity about the two-fold axis as in the peptidomimetic-bound structure and reversed to that on the unbound structure. However, they have closed down towards the catalytic aspartate residues only slightly relative to the "open" form, about 17° less than is observed in the "closed" structure (Rutenber *et al.*, 1992). An additional characteristic unique to the UCSF-bound structure is a coordinated chloride ion between the inhibitor and the almost symmetric amide nitrogens of I50 and I150 in the flap region of the enzyme. This may either reflect the need for a counter-ion for the piperidinium group of the inhibitor, or only be a result of the high salt concentration during crystallization.

UCSF8, unlike peptidomimetic inhibitors, binds near the flaps of the enzyme 5.3 Å at its closest point from the catalytic aspartate residues (Figure 2.9). Thus, the inhibitor appears to be acting as a "doorstop" preventing the flaps from fully closing. Two, two-fold related and partially overlapping binding modes, each at about 50% occupancy, are observed (Figure 2.10) (Rutenber *et al.*, 1992). Consequently, the electron density of the piperidine ring overlaps with that of the propyl chain making the positions of those atoms

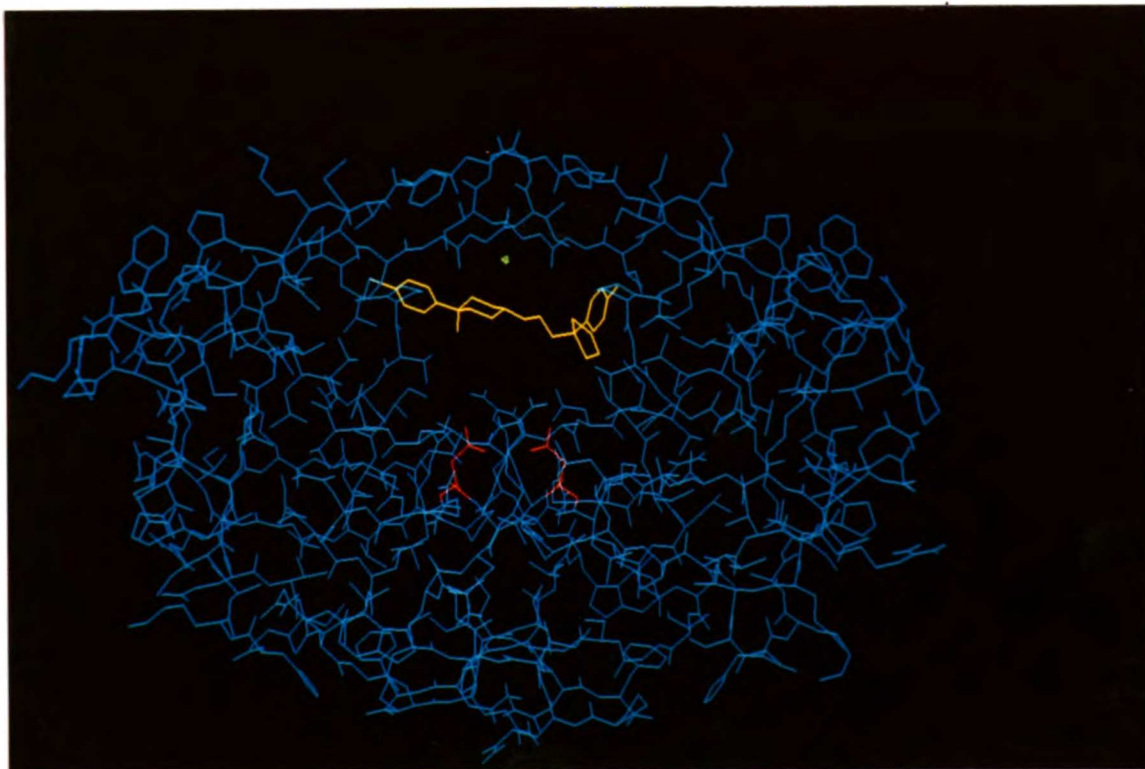


Figure 2.6: X-ray structure of the HIV-1 protease (blue) complexed with UCSF8 (yellow). The crystallographic chloride ion is shown in green, and the catalytic aspartate residues are shown in red. (Rutenber *et al.*, 1992)

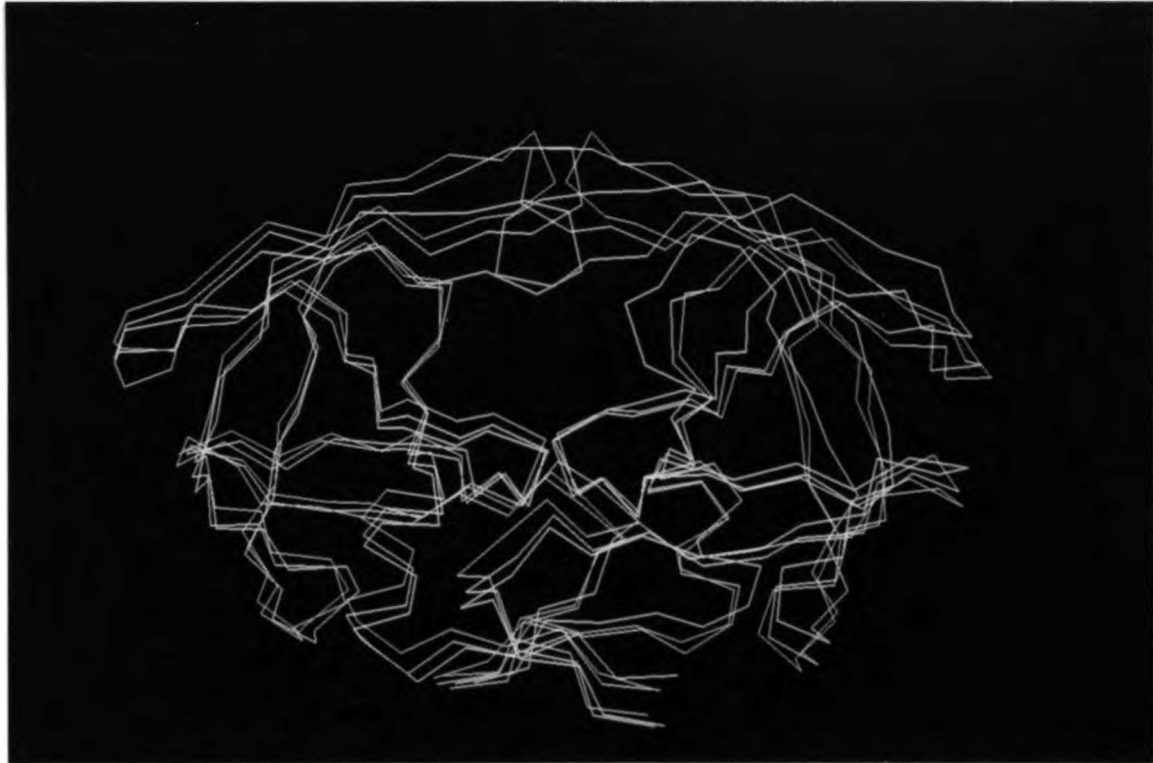


Figure 2.7: Side view comparison of the structures of the uncomplexed (cyan), peptide inhibitor bound (yellow), and UCSF8 bound (magenta) forms of the HIV-1 protease. Only the alpha carbon atoms are shown. The major differences among the structures occur in the flap residues. The flaps in the UCSF8 bound protease close down to a position intermediate between the uncomplexed and the peptide bound forms of the enzyme.

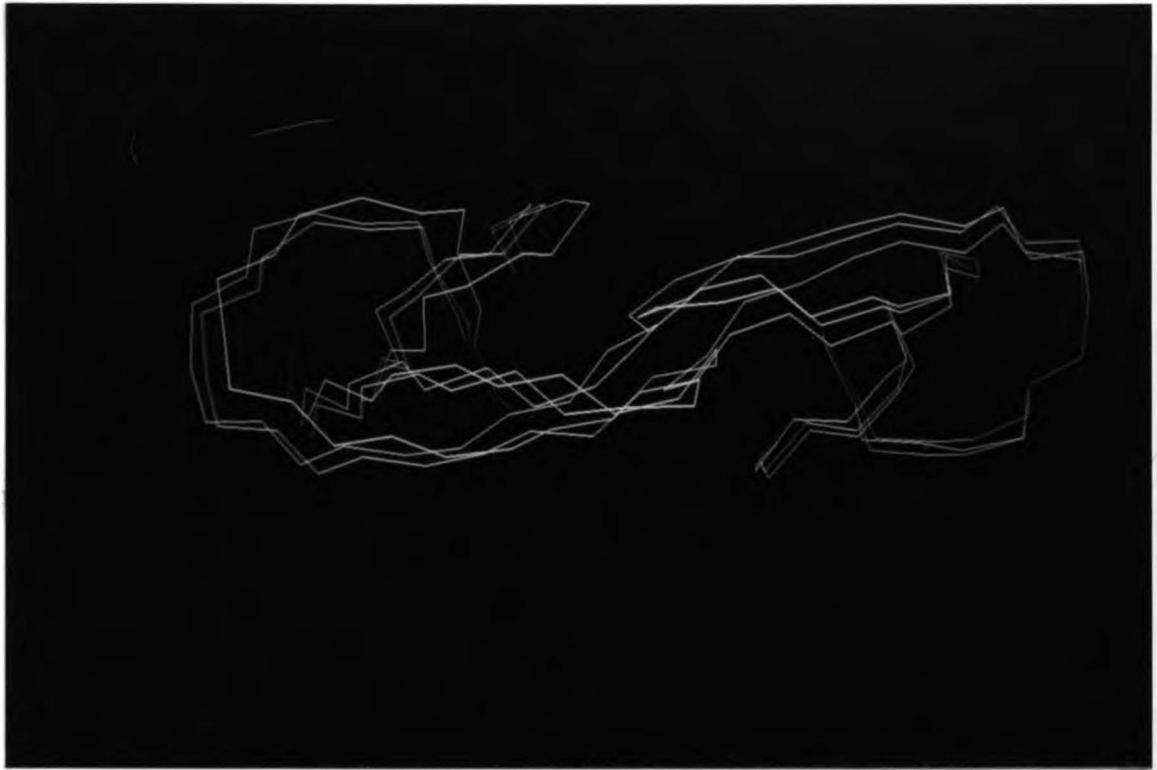


Figure 2.8: Top view comparison of the structures of the uncomplexed (cyan), the peptide inhibitor bound (yellow), and the UCSF8 bound (magenta) forms of the HIV-1 protease. Only the alpha carbon atoms, primarily of the flap residues, are shown. The flaps in the UCSF8 bound structure have the same polarity about the two-fold axis as in the peptide bound structure and reversed to that of the uncomplexed structure.

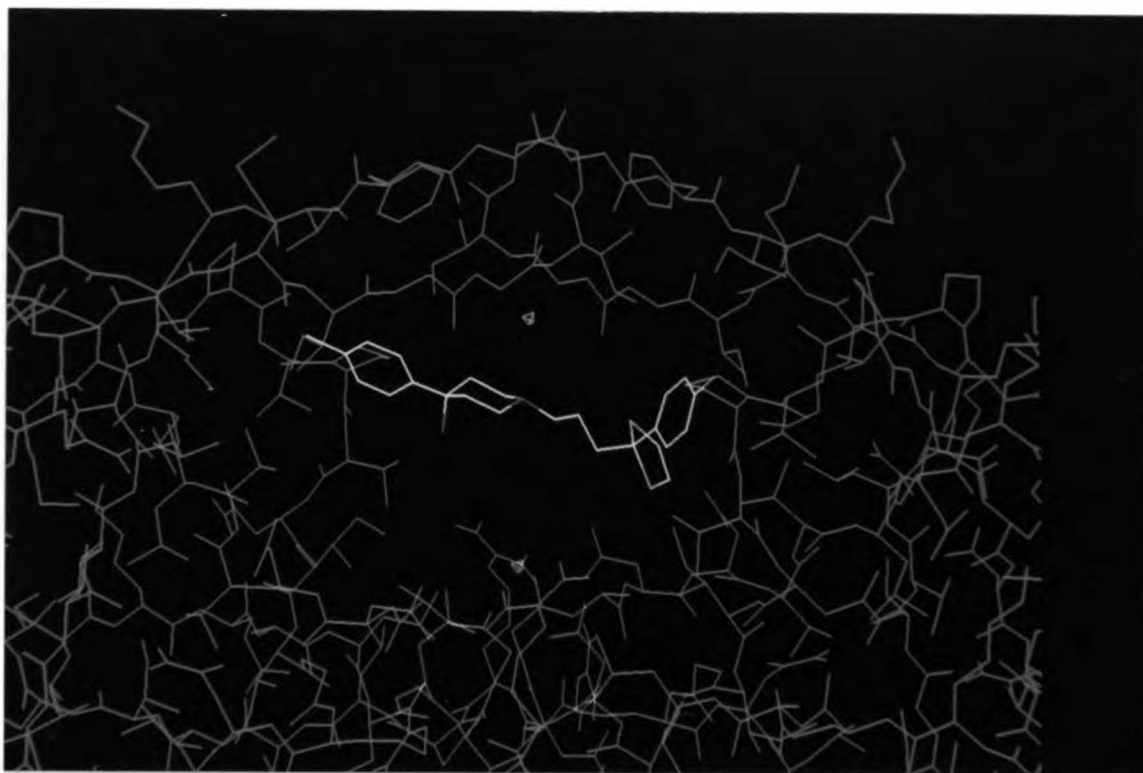


Figure 2.9: Close-up view of UCSF8 (colored by atom type) bound within the HIV-1 protease active site (cyan). The chloride ion is shown in green, and the catalytic aspartate residues are shown in red. The oxygen atom of the crystallographic water found between the aspartate residues is also shown.

uncertain. The observed electron density is most consistent with a chair conformation of the piperidinol moiety (Figure 2.9) with the nitrogen atom pointing towards the chloride ion and the hydroxyl group pointing towards the catalytic aspartates. Initially, a boat conformation for the piperidinol ring, where the hydroxyl either



D29 and D30. This represents the only overlap with the volume of the active site occupied by peptide-based inhibitors (Figure 2.10).

Figure 2.10: Both two-fold related binding modes observed crystallographically for UCSF8 within the HIV-1 protease active site (cyan). One UCSF8 molecule is shown in yellow, the other in magenta. The chloride ion is in green, and the catalytic aspartate residues and the ligated crystallographic water molecule are in red.

The observed orientation provides a model for the binding of other inhibitors. The major axis of the inhibitor is oriented $\sim 45^\circ$ and $\sim 100^\circ$ towards the flap region. It is suggested that halopiperidol derivatives may bind in the orientation proposed by D29, and upon formation of the thioether functionality, such an orientation would be

uncertain. The observed electron density is most consistent with a chair conformation of the piperidinol moiety (Figure 2.9) with the nitrogen atom pointing towards the chloride ion and the hydroxyl group pointing towards the catalytic aspartates. Initially, a boat conformation for the piperidinol ring, where the hydroxyl either interacts with the enzyme flaps or in conjunction with the nitrogen atom chelates the chloride ion, was assigned. Much of the design effort was based on the latter structure. An inflexibility towards its modification places strong importance on the hydroxyl group, possibly as a chelating atom (unpublished results); an observation more consistent with the boat structure. The positions of the aromatic rings and the thioketal moiety, however, are much better defined. The symmetry-related hydrophobic pockets surrounding the halogenated phenyl rings, one from each monomer, are defined by V32, I47, I54, V56, P79, T80, and P81. The thioketal ring interacts with the P2 binding pocket of the enzyme defined by the side chains of A28, V32, I47, I84 and the peptide plane of residues D29 and D30. This represents the only overlap with the volume of the active site occupied by peptide-based inhibitors (Figures 2.11 and 2.12) .

The observed binding mode for UCSF8 differs from the original orientation proposed for haloperidol by DOCK (Figures 2.13 and 2.14). The major axis of the inhibitor is rotated $\sim 79^\circ$ and translated by ~ 4.8 Å towards the flap region. It is conceivable that haloperidol itself may bind in the orientation proposed by DOCK, and upon formation of the thioketal functionality, such an orientation would be



Figure 2.11: Side view comparison of the binding modes of UCSF8 (yellow) and MVT-101 (magenta) (Miller *et al.*, 1989) within the active site of the HIV-1 protease (cyan). Only an alpha carbon tracing of the UCSF8-bound form of the enzyme is shown. The catalytic aspartates are in red. The only overlap between the two inhibitors occurs at the P2 binding site of the enzyme which is occupied by the thioketal moiety of UCSF8, and a norleucine sidechain of MVT-101.

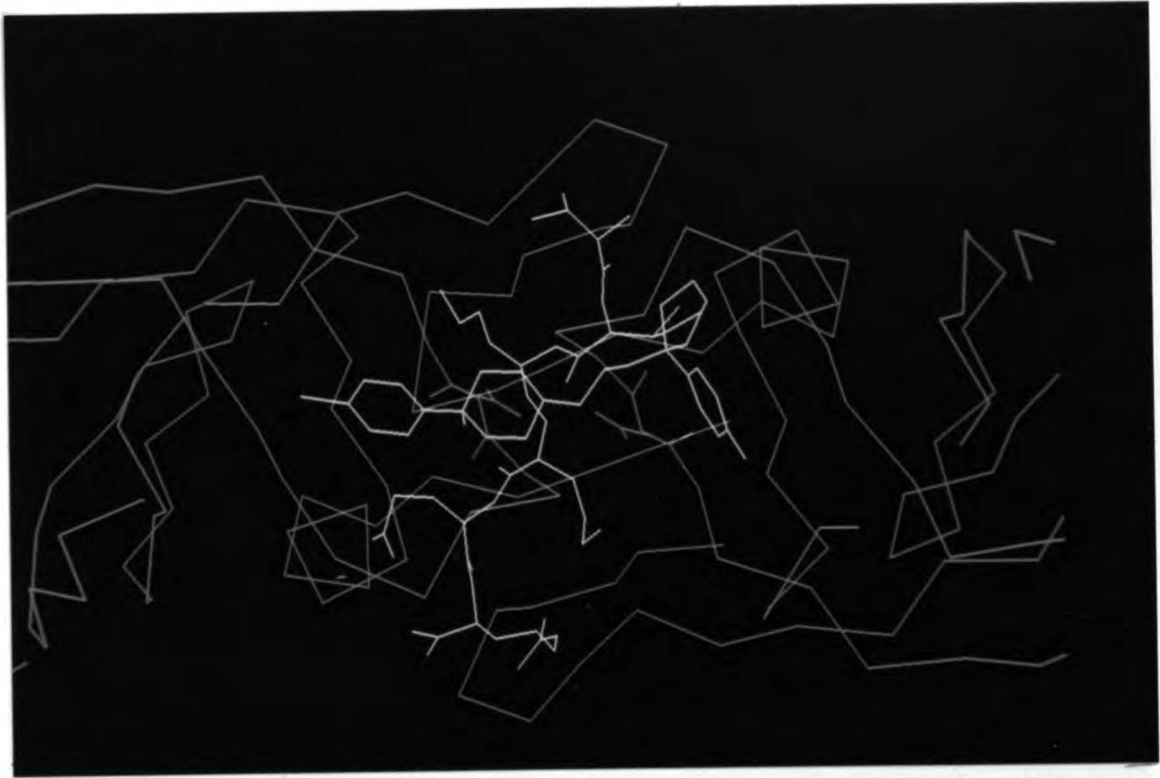


Figure 2.12: Top view comparison of the binding modes of UCSF8 (yellow) and MVT-101 (magenta) (Miller *et al.*, 1989) within the active site of the HIV-1 protease (cyan). The flap residues are removed, and only an alpha carbon tracing of the UCSF8-bound form of the enzyme is shown for clarity. The catalytic aspartates are in red. The directions of the major axes of the two inhibitors differ by about 70°, and UCSF8 is translated by 4.5 Å towards the flaps.

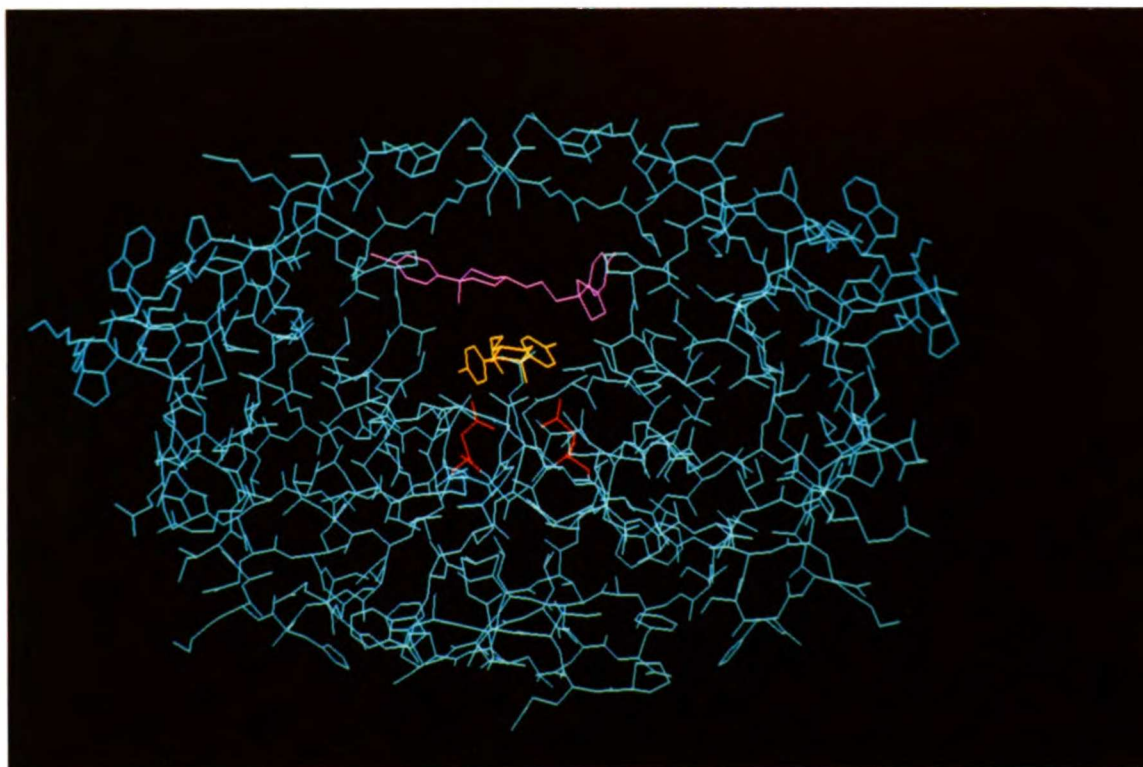


Figure 2.13: Side view comparison of the binding modes of UCSF8 proposed by DOCK (yellow) and observed in the x-ray structure (magenta) within the active site of the UCSF8 bound HIV-1 protease (cyan). The x-ray orientation is translated about 4.8 Å towards the flaps relative to the DOCK orientation.



Figure 2.14: Top view comparison of the binding modes of UCSF8 proposed by DOCK (yellow) and observed in the x-ray structure (magenta) within the active site of the HIV-1 protease (cyan). The flap residues have been removed, and only an alpha carbon tracing is shown for clarity. The directions of the major axes of the two orientations differ by about 79°.

disfavored relative to the one observed in the crystal structure. As a matter of fact, one would expect the thioetal derivative NOT to bind in the DOCK orientation. The carbonyl group of haloperidol points towards the enzyme surface and is within 3 Å of the backbone carbonyl of G27, making it impossible to accommodate the thioetal ring, even when bond rotations are allowed.

A second possibility is that haloperidol binds in a mode analogous to UCSF8 in the x-ray structure of its complex with the enzyme, and the discrepancy between the two structures is a result of the breakdown of some of the assumptions in the DOCK search: 1) scoring based exclusively on steric complementarity; 2) the treatment of the structures of the putative ligands and of the receptor as rigid and conformationally-fixed. Support for such a theory arises from the fact that docking of UCSF8 to the HIV-1 protease with a more recent version of the program (DOCK3.0) (Meng *et al.*, 1992) containing an electrostatic force-field scoring function essentially reproduces the observed UCSF8-HIV-1PR structure when the proper ligand conformation is used (Meng and Kuntz, unpublished results).

2.4 RATIONALIZATION OF THE INHIBITORY POTENCY OF HALOPERIDOL DERIVATIVES BASED ON THE STRUCTURE OF THE THIOKETAL DERIVATIVE (UCSF8)- HIV-1 PROTEASE COMPLEX

The increased inhibitory potency, relative to haloperidol, of the derivatives discussed in section 2.2 appears to be consistent with the

binding mode observed for the thioketal derivative (UCSF8) in the crystal structure.

Molecular models of the analogues were built using the program SYBYL (Tripos). Visualization was carried out on an Iris 4D/70 workstation (Silicon Graphics) with the molecular graphics package MidasPlus (Huang, 1989). The models were manually docked into the enzyme and their bonds rotated to adopt a conformation analogous to the thioketal derivative crystal structure. Keeping all other atoms fixed, different conformations of the modified groups were explored in an attempt to maximize surface contact and minimize overlap between the putative ligand and the enzyme.

2.4.1 PRODUCTS OF ADDITIONS TO THE HALOPERIDOL KETONE

The groups which were added to the haloperidol ketone could easily be accommodated by the enzyme in a conformation analogous to that of the thioketal derivative. Due to differences in the geometry of the main chain, the group added to the ketone cannot point in the identical direction as the thioketal group when the fluorophenyl groups are superimposed. The added phenyl or benzyl group must therefore be placed in the direction of one of the two sulfur atoms of the thioketal (Figures 2.15 and 2.16). It appears as though one of the structures, and consequently one of the enantiomers, is preferred based on the model. The R isomer can interact with the P2 site of the enzyme, whereas the S isomer overlaps significantly with residues

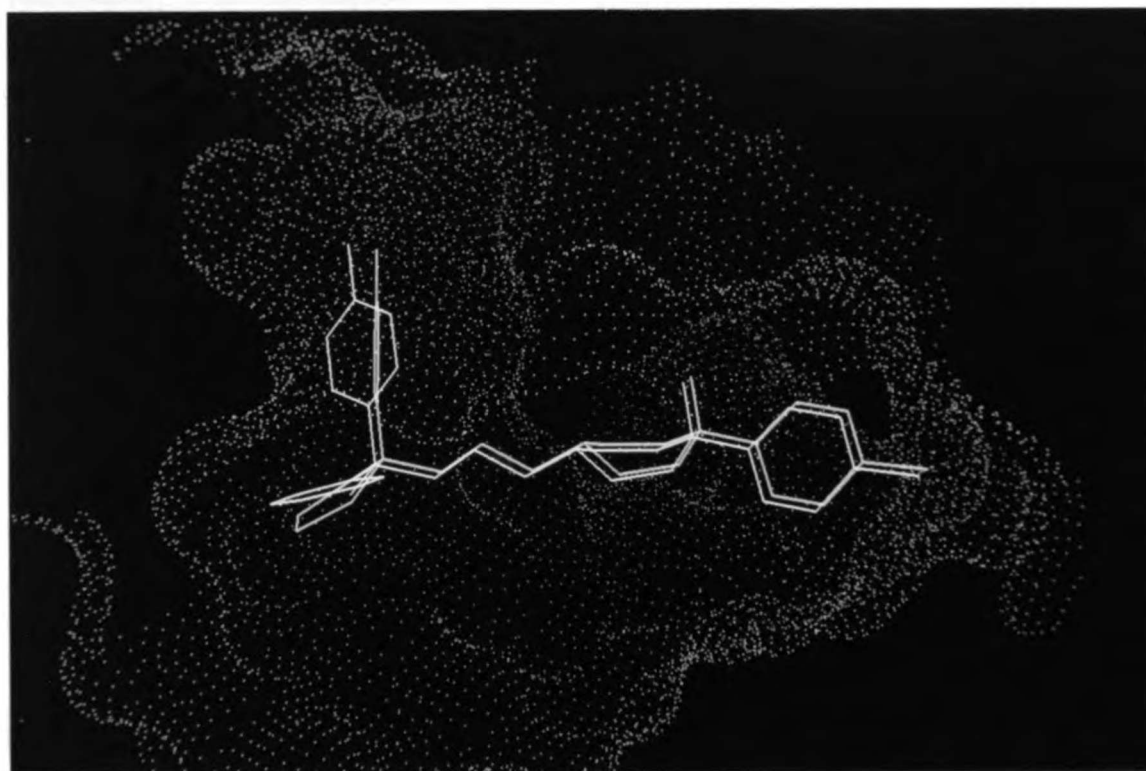


Figure 2.15: Result of the superposition of the R isomer of **2** (magenta) on the x-ray structure of UCSF8 (yellow) within the protease active site (cyan). A Van der Waals surface for **2** is included for evaluation of fit to the enzyme's solvent accessible surface.

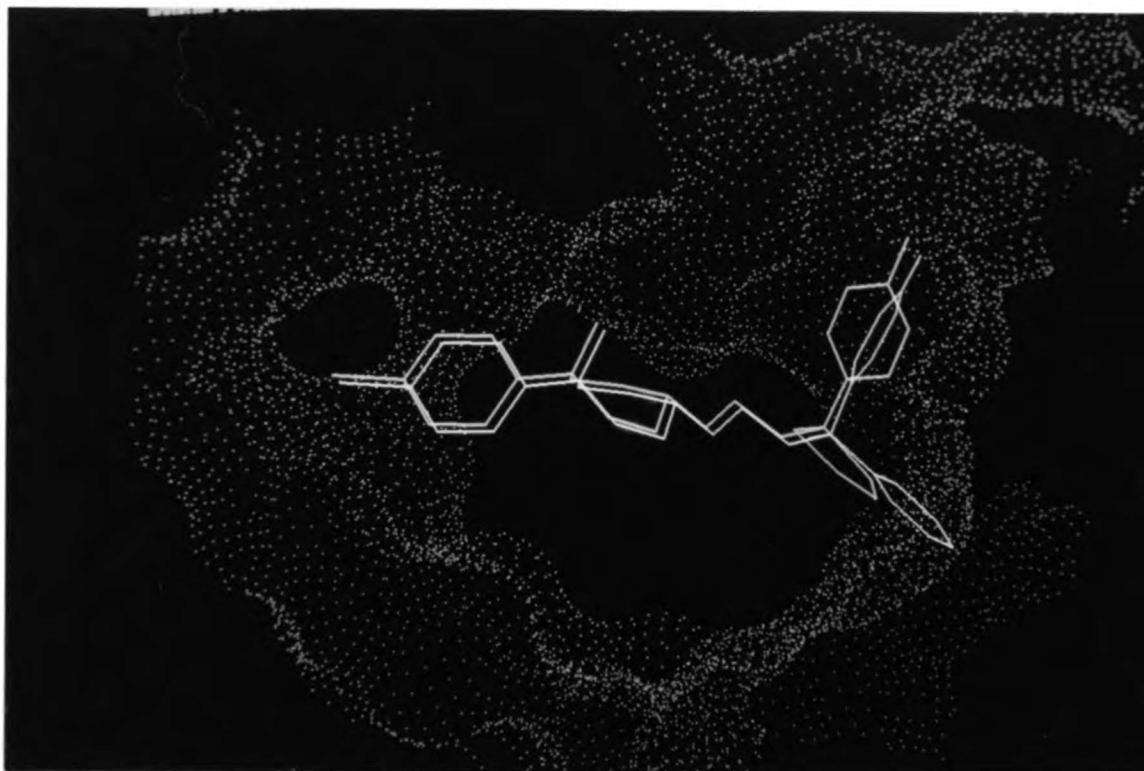


Figure 2.16: Result of the superposition of the S isomer of **2** (magenta) on the x-ray structure of UCSF8 (yellow) within the protease active site (cyan). Notice the overlap between the Van der Waals surface for **2** and the enzyme's solvent accessible surface.

A28, D30, V32, and I84 making it less attractive. Alternatively, the added phenyl or benzyl group can be placed in the direction of the fluorophenyl moiety of the crystal structure, and the fluorophenyl group in the P2 site of the enzyme (Figure 2.17). Consequently, in the latter model the S isomer is favored over the R isomer.

2.4.2 BIPHENYL ANALOGUES OF HALOPERIDOL

The biphenyl modifications also appear to be accommodated without major modifications in the structure of either ligand or enzyme. After rotation of the biphenyl groups, para- and meta-biphenyl moieties can be placed in a "cleft" created on one side by flap residues 32, 47, 54, and 56 and on the other by residues 79-81 (Figure 2.18). Unlike the para-biphenyl which has a favorable geometry when the proximal phenyl is superimposed on the fluorophenyl of UCSF8, the proximal phenyl of the meta isomer must be rotated about 25 degrees from the fluorophenyl axis (Figure 2.19). In this conformation, the meta isomer fills the cleft well without much overlap with the protein (Figures 2.20 and 2.21). On the other hand, the para isomer appears to be slightly too long, overlapping with the enzyme (Figure 2.22), with the shortest heavy atom-to-heavy atom distance being about 2.1 Å. Thus adjustments must be made by either the protein, the inhibitor, or both to accommodate this model. It is most likely that the necessary adjustments can be effected by the butyl chain of the inhibitor alone due to its flexibility and limited structural constraints. The binding cleft, however, does not extend far enough to also interact with the ortho biphenyl

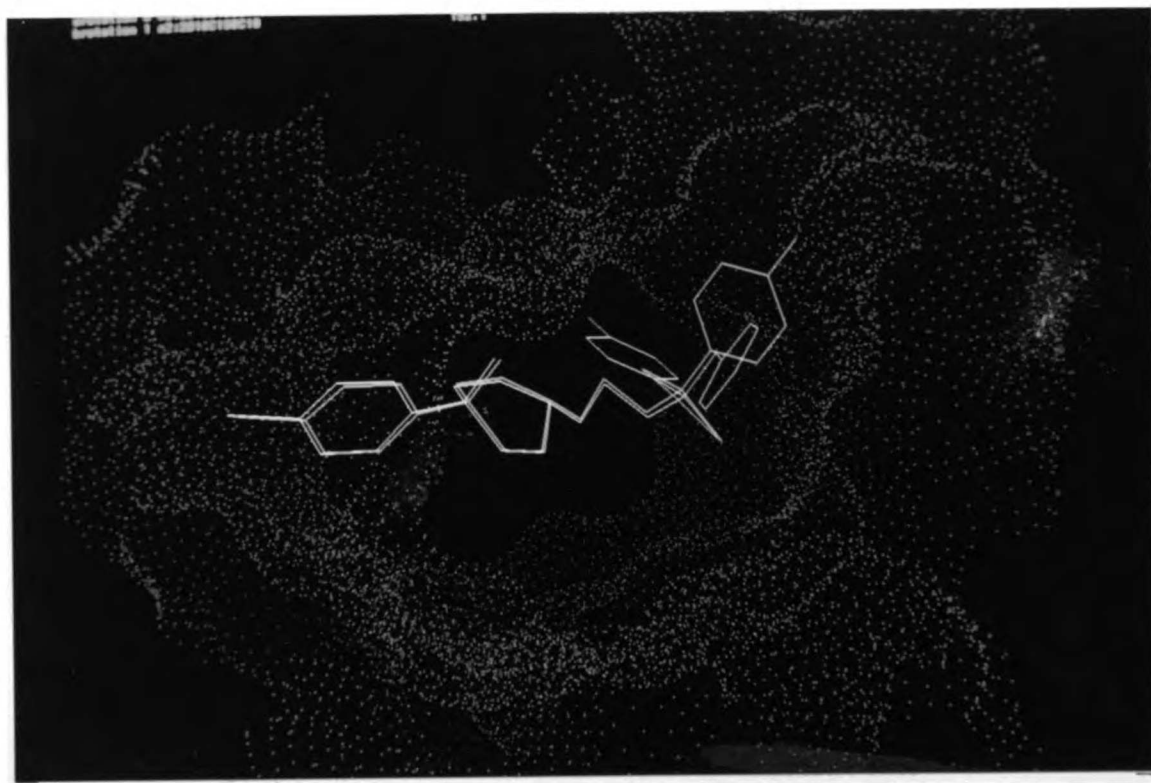


Figure 2.17: Alternative binding mode for the S isomer of **3** (magenta) obtained from its superposition on the x-ray structure of UCSF8 (yellow), followed by rotation of a single bond placing the benzyl group of **3** in the site occupied by the fluorenyl group of UCSF8.

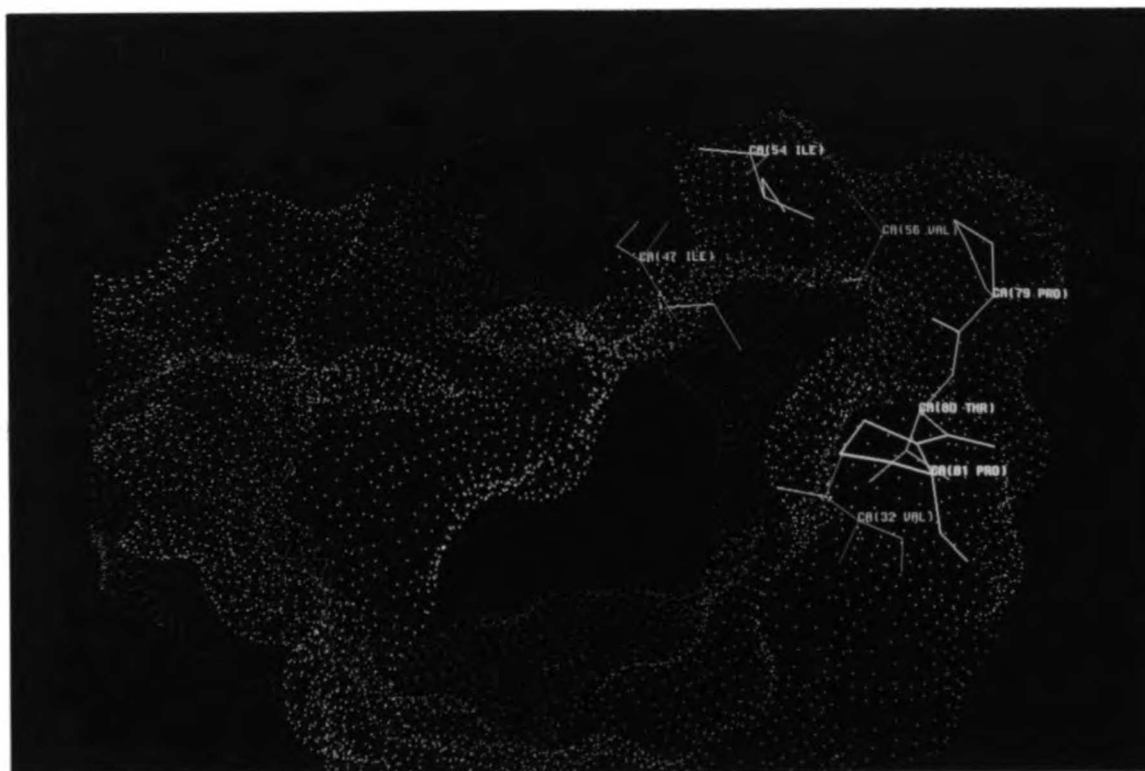


Figure 2.18: HIV-1 protease cleft created by residues 32, 47, 54, 56, and 79-81.

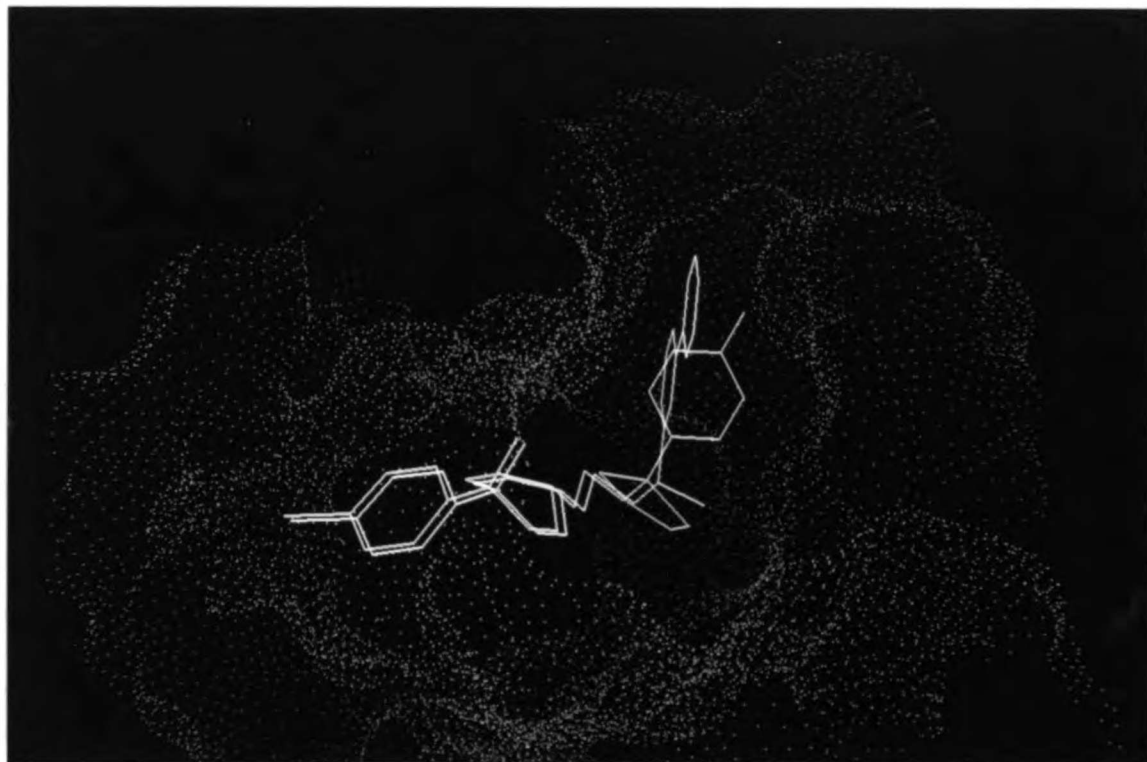


Figure 2.19: Comparison of the structures of UCSF8 (yellow) and the proposed binding orientation for the meta biphenyl analogue of haloperidol (**19**). About a 25° rotation of the biphenyl moiety of **19** from the fluorophenyl axis of UCSF8 is necessary to place it in the protease binding cleft without major overlap with the protein.

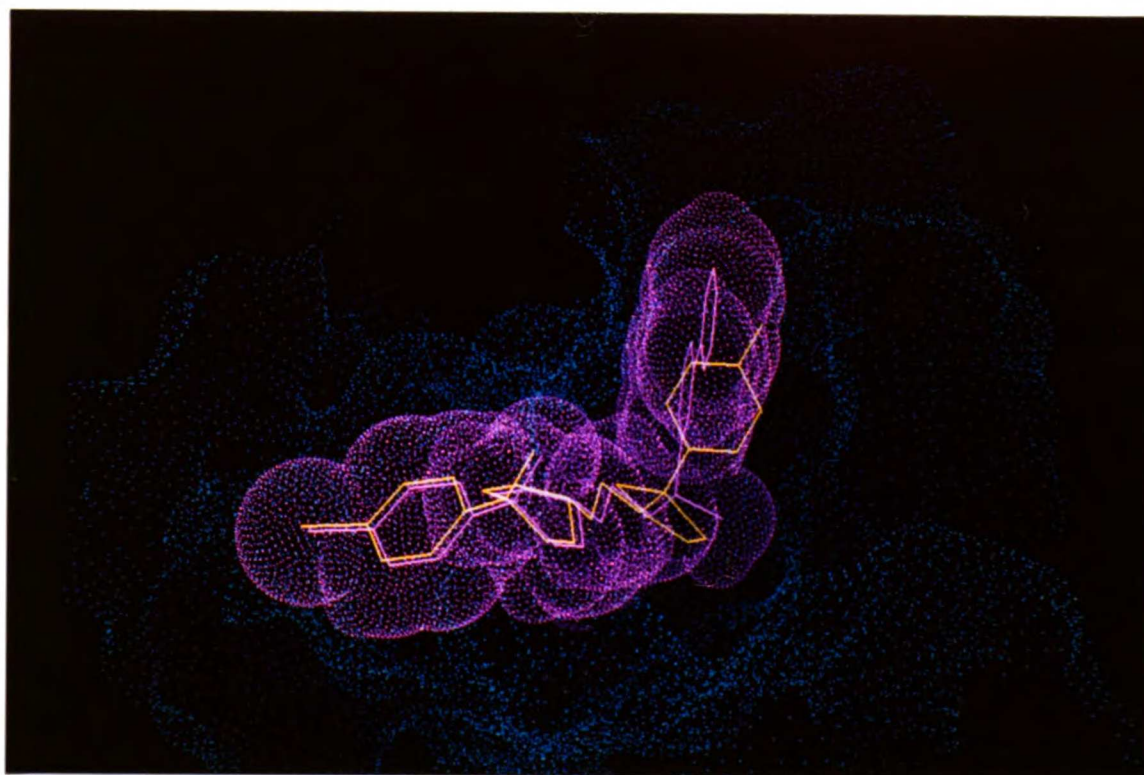


Figure 2.20: Proposed binding orientation for the meta biphenyl haloperidol derivative (magenta), **19**, to the HIV-1 protease (cyan). A Van der Waals surface for **19** is included for evaluation of fit to the enzyme's solvent accessible surface.

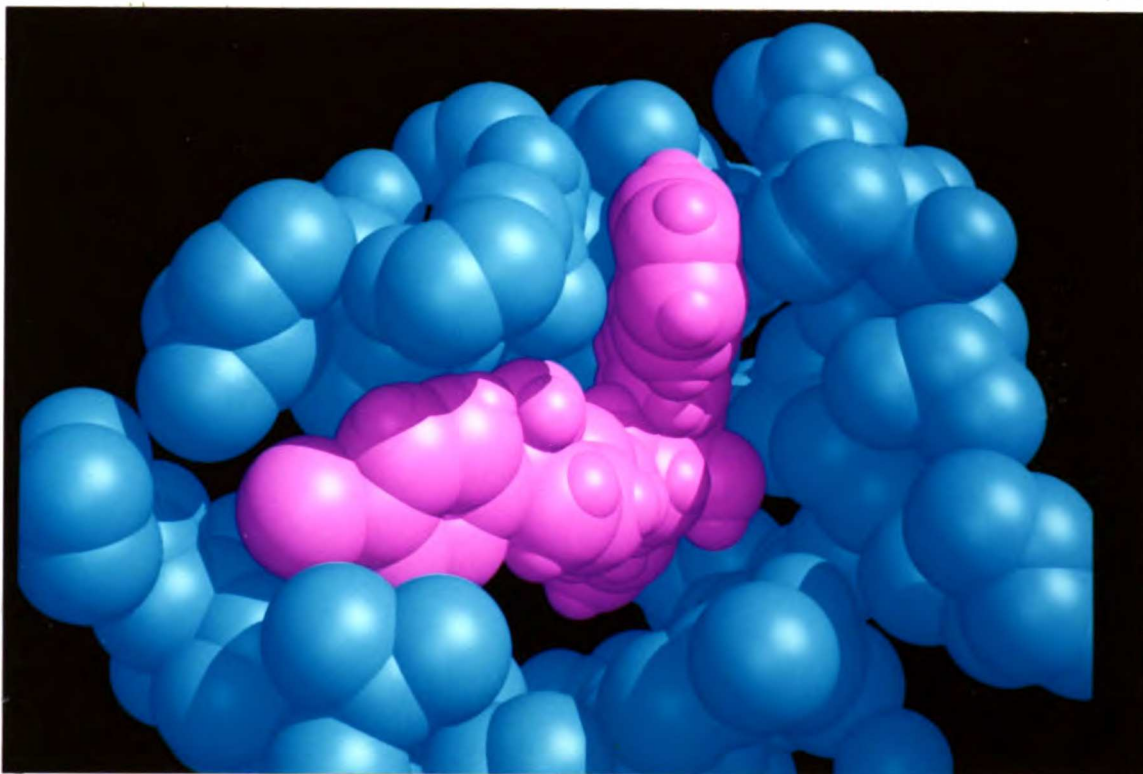


Figure 2.21: Space-filling representation of the proposed binding orientation for the meta biphenyl haloperidol derivative (magenta), **19**, to the HIV-1 protease (cyan).

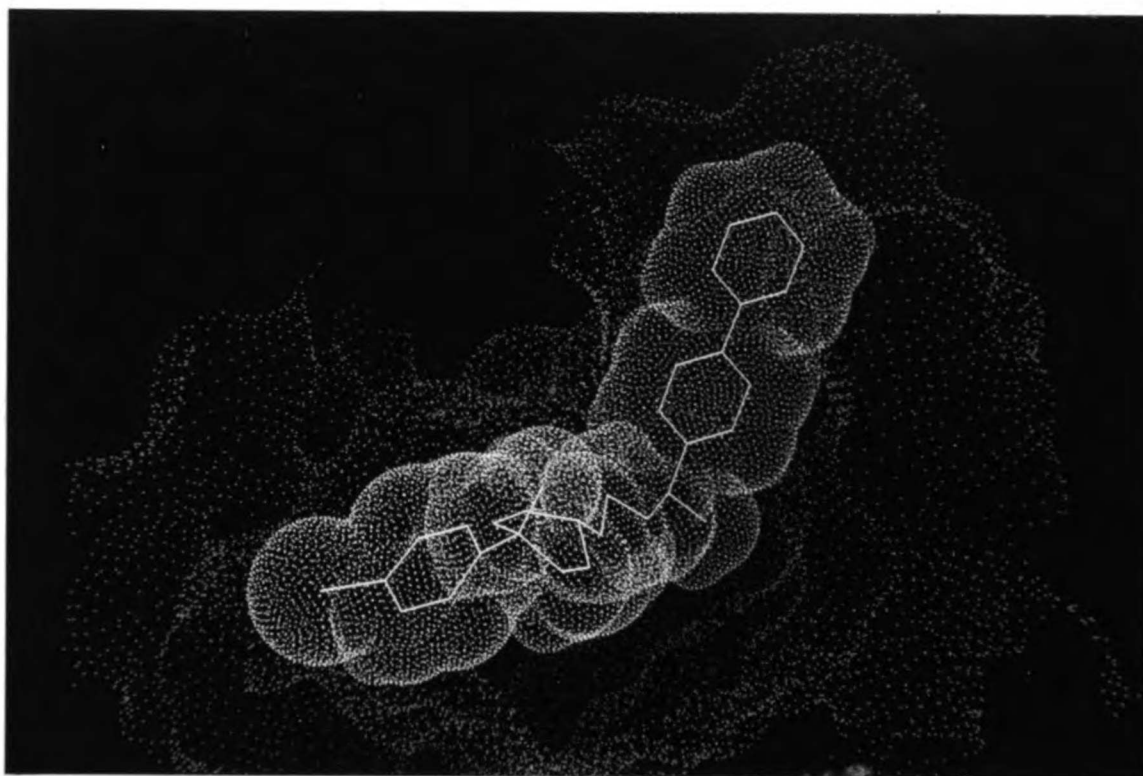


Figure 2.22: Proposed binding orientation for the para biphenyl haloperidol derivative (magenta), **20**, to the HIV-1 protease (cyan). Notice the slight overlap between the Van der Waals surface of the biphenyl moiety of **20** and the enzyme's solvent accessible surface.

isomer, and the group must be rotated, about a 30 degree deviation from the fluorophenyl axis, so as to not extrude into solvent (Figure 2.23). These results are consistent with the inhibition potency rankings of the haloperidol biphenyl analogues.

2.4.3 PRODUCTS WITH TWO MODIFICATIONS OF THE HALOPERIDOL STRUCTURE

For the derivatives where two modifications of the haloperidol structure have been created, the binding models are a combination of those for the single modification derivatives discussed above. The products of the phenyl addition to the biphenyl analogues of haloperidol are still capable of binding in the orientation described for their parent compounds in the preceding section. Unlike the analogues discussed in section 2.2.1, however, the second binding mode proposed seems less favorable, therefore a preference for the R isomer would be expected. The resulting models for the three biphenyl isomer derivatives are shown in Figures 2.24, 2.25, and 2.26. The modest 2.5-fold improvement in the inhibitory potency upon conversion of the meta biphenyl derivative to the thioketal, compared to the 8-fold improvement observed for the analogous derivatization of haloperidol, might be explained by the 25° rotation required to fit the biphenyl portion into the desired cleft, thereby reducing the favorable interaction of the thioketal ring with the P2 pocket.

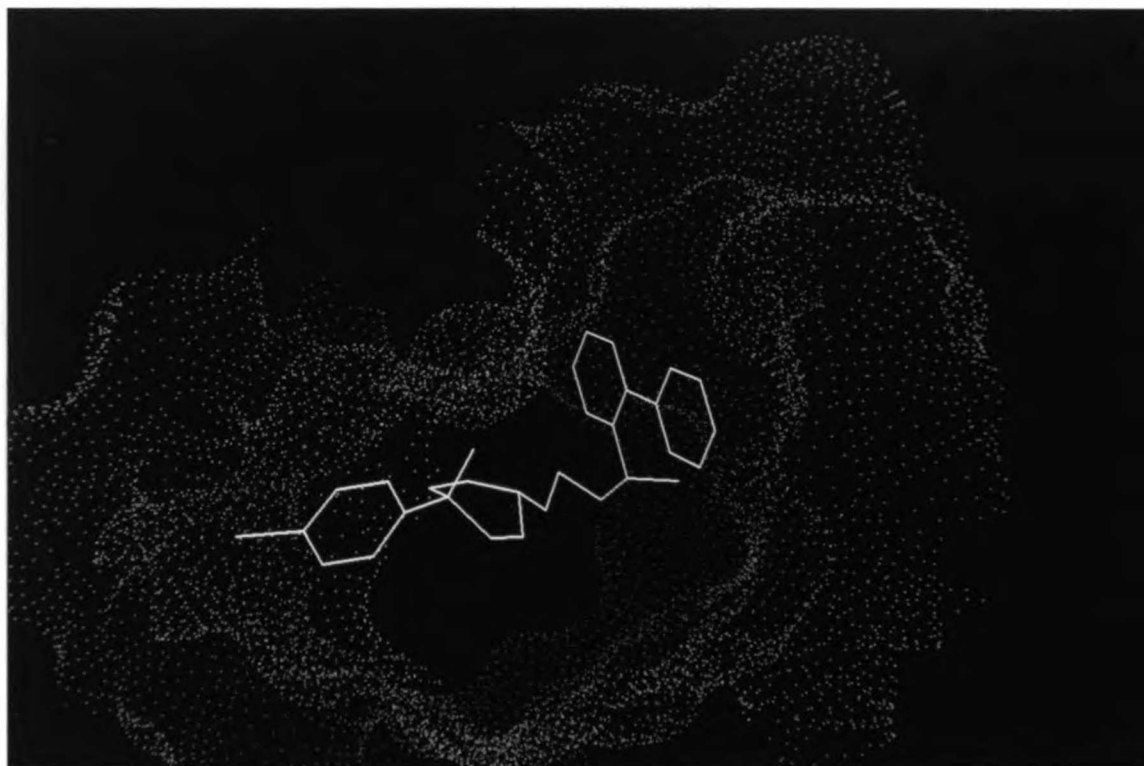


Figure 2.23: Proposed binding orientation for the ortho biphenyl haloperidol derivative (magenta), **18**, to the HIV-1 protease (cyan). The ortho phenyl moiety cannot be placed in the cleft analogous to the meta and para isomers and must be rotated until interaction with the enzyme's surface is achieved.

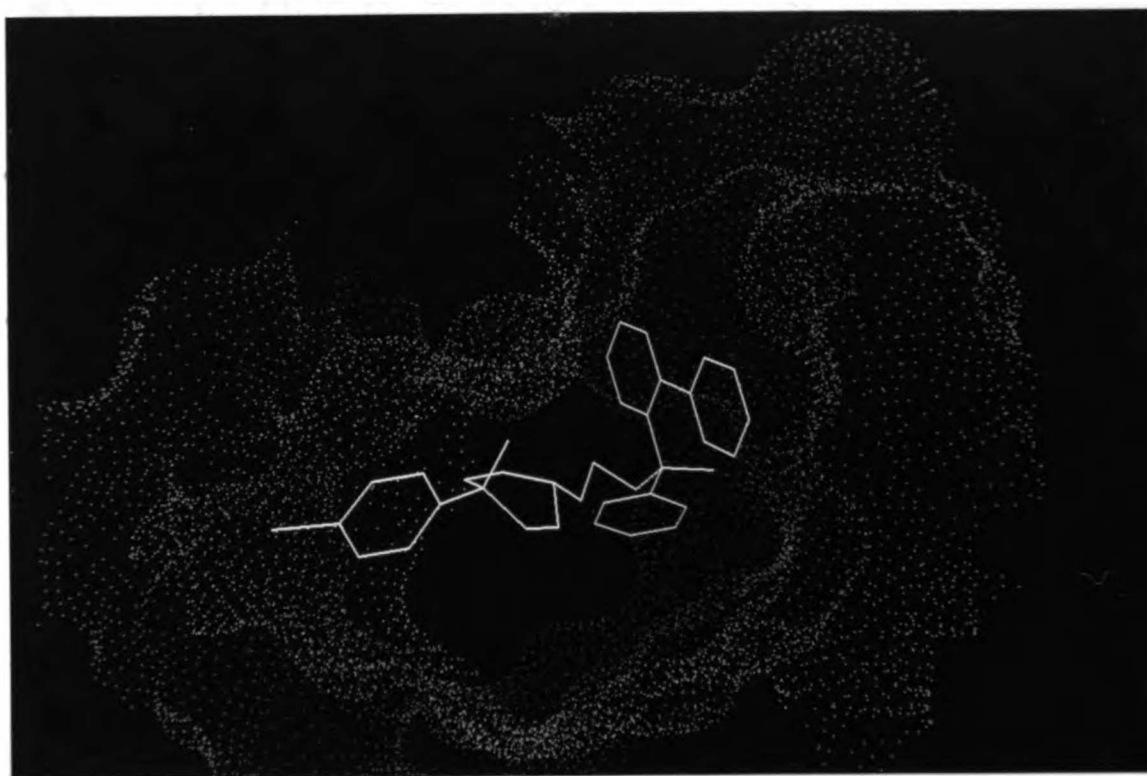


Figure 2.24: Proposed binding orientation for **21** (magenta), to the HIV-1 protease (cyan).

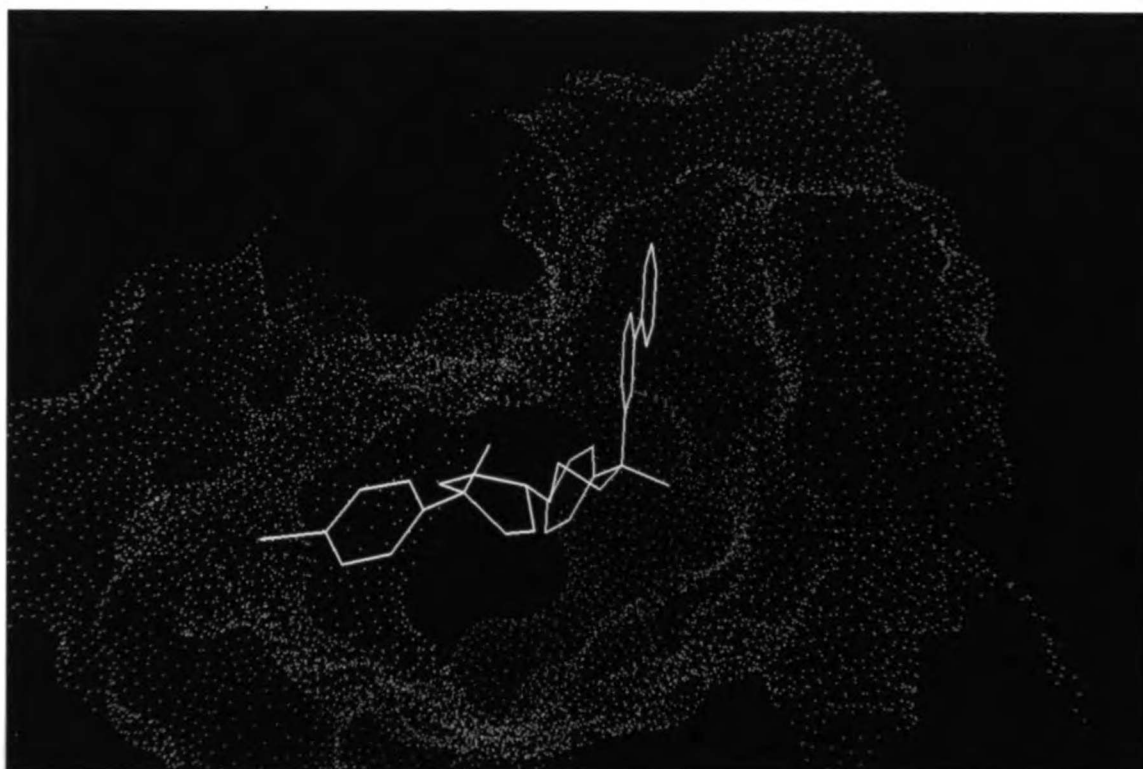


Figure 2.25: Proposed binding orientation for **22** (magenta), to the HIV-1 protease (cyan).

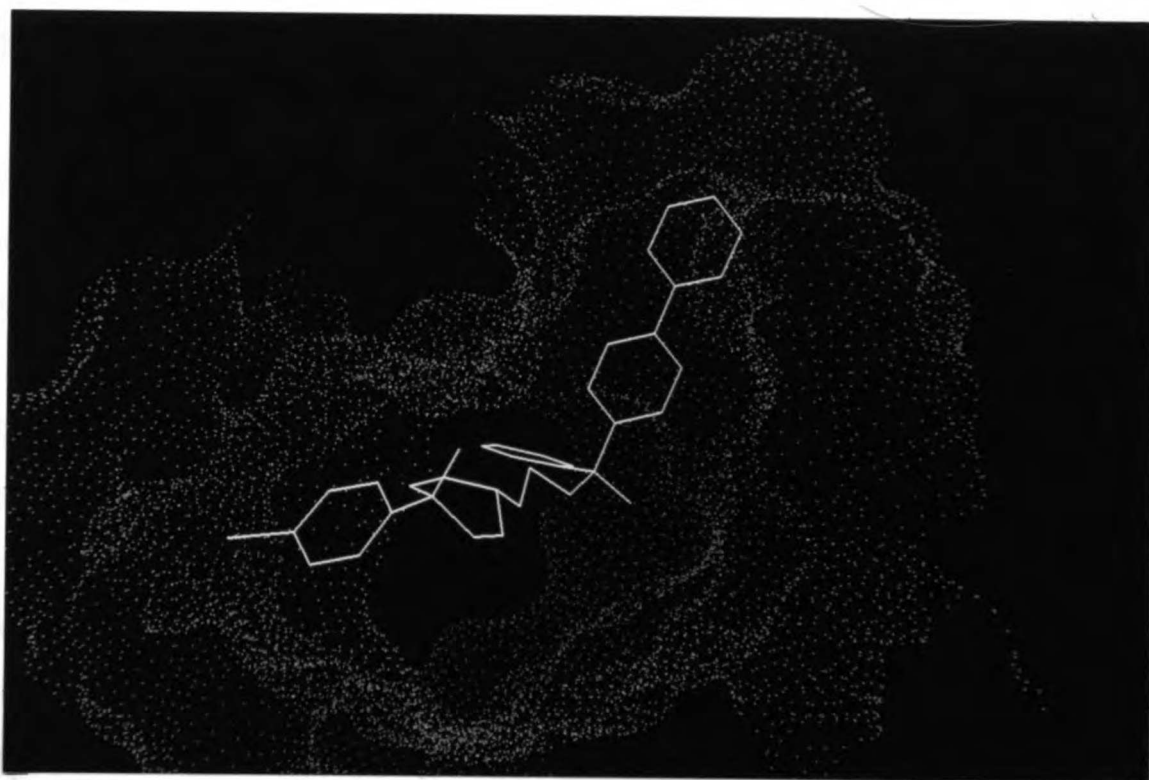


Figure 2.26: Proposed binding orientation for **23** (magenta), to the HIV-1 protease (cyan).

CHAPTER 3

THE SEARCH FOR ADDITIONAL INHIBITOR LEADS USING A PHARMACOPHORE-BASED APPROACH

3.1 INTRODUCTION

The development of haloperidol-based inhibitors of the HIV-1 protease with significant improvements in potency was experiencing several shortcomings. Testing of over one hundred derivatives had resulted in a maximum improvement of 18-fold over the parent compound, an IC_{50} of 7 μ M. In addition, only modest improvements, at best, had been obtained from modifications targeting specific interactions with the enzyme. Difficulties in the crystallization of additional inhibitor-protease complexes had limited the interpretation of observed results and the design of "rational" modifications. Furthermore, the weakness of the inhibition of haloperidol, combined with the shallowness and plasticity of the active site and flexibility of the inhibitor, which suggested multiple binding modes, made modeling efforts formidable. Finally, with the LD_{50} 's generally about equal to the IC_{50} 's, it had not been possible to observe any inhibitory effect in an *ex vivo* system. Furthermore, the high level of toxicity of these compounds provided little hope for their therapeutic value. Therefore, a quest for additional lead compounds using a pharmacophore-based search was initiated.

3.2 DEFINING THE PHARMACOPHORE

In order to take advantage of the knowledge accumulated from the haloperidol derivatives, the UCSF8 binding site from the structure of its complex with the protease was targeted. Based on the structure and on the inhibitory potency of many other derivatives features important for activity were established. The halogenated phenyl rings appear to interact closely with the enzyme, although the halogens themselves do not appear to be vital for activity.

Replacement of the ketone of haloperidol with large hydrophobic groups gave some of the largest single improvements in inhibition, evident in the interaction of the thioketal moiety of UCSF8 with the P2 site of the protease in the x-ray structure. Additional improvements were observed for the addition of phenyl residues off the butyl chain or fluorophenyl ring, with the latter yielding the biphenyl analogues discussed in chapter 2. The only other interaction apparent from the crystal structure was that of the chloride counterion with the enzyme flaps.

The features which seemed most desirable for a ligand at the haloperidol site were the potential to fill the hydrophobic "pockets" occupied by the two halogenated phenyl rings (defined by V32, I47, I54, V56, P79, T80, and P81; Rutenber *et al.*, 1992), the thioketal ring, and the symmetry related thioketal ring (defined by A28, V32, I47, and I84; Rutenber *et al.*, 1992). The additional characteristics outlined above were ignored to avoid limiting the search too

stringently. The query used for the search was generated from the distances between the centroids of the rings of UCSF8, in the bound conformation, both intramolecularly and intermolecularly with its symmetry related partner (Figure 3.1A). The interrelating distances can be approximated by a triangle with sides of 11.5 and 11.9 Å and a base of 4.0 when three of the four groups are considered and a rectangle with sides of similar distances when the fourth group is included.

The actual query used for the search is shown in Figure 3.1B. Centroids of phenyl rings were required to occupy the positions corresponding to the vertices of the triangle (only three vertices were defined by the query since compounds which contained a fourth group would already be included). This assumes that filling each of the hydrophobic pockets with a phenyl group results in a favorable interaction, a reasonable assumption given the fact that phenyl rings occupy two of these sites in the complex structure, and phenyl addition to the haloperidol ketone resulted in a two-fold increase in inhibitory potency. Centroid-to-centroid distance ranges of 9.5-14.0 Å and 3.0-8.0 Å were specified for the sides and the base of the triangle, respectively, so as to include conformationally flexible molecules capable of satisfying the desired constraints.

3.3 SEARCH RESULTS

The search was performed on the fine chemicals database (FCD) (Molecular Design), a collection of almost 60,000 commercially

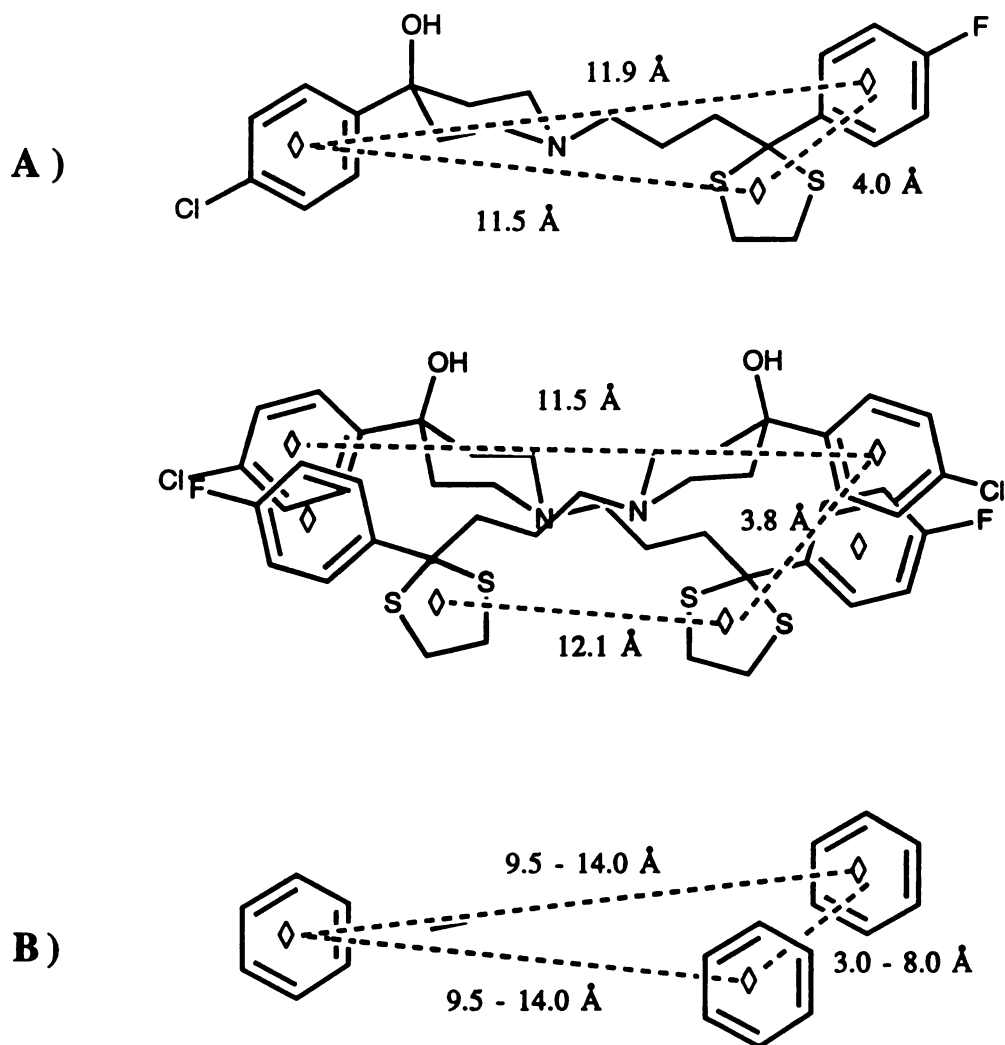


Figure 3.1: (A) Relative distances between the centroids of the chlorophenyl, fluorophenyl, and thioketal groups of UCSF8 in the HIV-1 protease bound conformation. Centroids are depicted as \diamond . Top: intramolecular distances; Bottom: intermolecular distances of the symmetry related inhibitor molecules observed crystallographically. (B) Query used for the pharmacophore search of the FCD using MACCS-3D.

available compounds, using the program MACCS-3D (Molecular Design). The query was satisfied by 171 molecules in the database. An initial visual screening immediately eliminated 40 compounds because of either their redundancy as multiple salts of the same compound or the presence of heavy metals. A query including a phenyl centroid at the fourth vertex selected 78 of the 131 remaining compounds.

3.4 EVALUATION OF COMPOUNDS

Although 131 compounds satisfied the query, due to the wide ranges allowed for the inter-centroid distances, not all of these were capable of interacting with the enzyme at the desired sites. The candidates were therefore docked into the protease, the UCSF8 complex structure with the inhibitor removed, using DOCK 3.0. Since the search was carried out using a pharmacophoric pattern for the haloperidol binding site, the UCSF8 atom coordinates were used in the matching procedure instead of sphere centers to insure placement of the putative ligands in the desired site. Both contact and force-field scoring were used for determining the orientation and rank of the molecules. The docked ligands were visually evaluated for their potential to fill the appropriate pockets using the molecular graphics package MidasPlus.

3.5 RESULTS OF INHIBITION ASSAYS

Some of the candidates whose inhibitory potency against the HIV-1 protease was evaluated are shown in Figure 3.2. The results of the assays are summarized in Table 3.1. Some inhibition at a 100 μM concentration was observed with 23 of the 27 compounds that were tested, with the following distribution: 1 : $\text{IC}_{50} < 10 \mu\text{M}$; 2 : $10 \mu\text{M} < \text{IC}_{50} < 50 \mu\text{M}$; 2 : $50 \mu\text{M} < \text{IC}_{50} < 100 \mu\text{M}$; 18 : $\text{IC}_{50} > 100 \mu\text{M}$. Of these, one compound, SF2 (pimozide), had been tested previously as a candidate from the original DOCK 1.0 search of the Cambridge Crystallographic Database (section 2.1). Its IC_{50} was 125 μM .

3.5.1 COMPOUNDS SIMILAR TO HALOPERIDOL

Several of the ligands, SF2, SF17, SF35, SF36, and SF49, were similar in structure to haloperidol. Included in this group were the most potent leads found: SF17 - cinnarizine, and its derivative, SF35 - flunarizine, exhibiting IC_{50} 's of 7 μM and 15 μM , respectively.

Flunarizine differs from cinnarizine only by the presence of fluorine atoms in the para position of the bis phenyl groups. Their low IC_{50} 's, relative to haloperidol, are probably due to their ability to fill three of the hydrophobic pockets combined with the additional rigidity of the double-bond in the backbone. Their placement within the protease active site by DOCK 3.0, using force-field scoring, is shown in Figure 3.3. The phenyl groups on the piperazine end fill the positions analogous to the fluorophenyl and thioketal rings of UCSF8, and the remaining phenyl group occupies the chlorophenyl binding pocket in

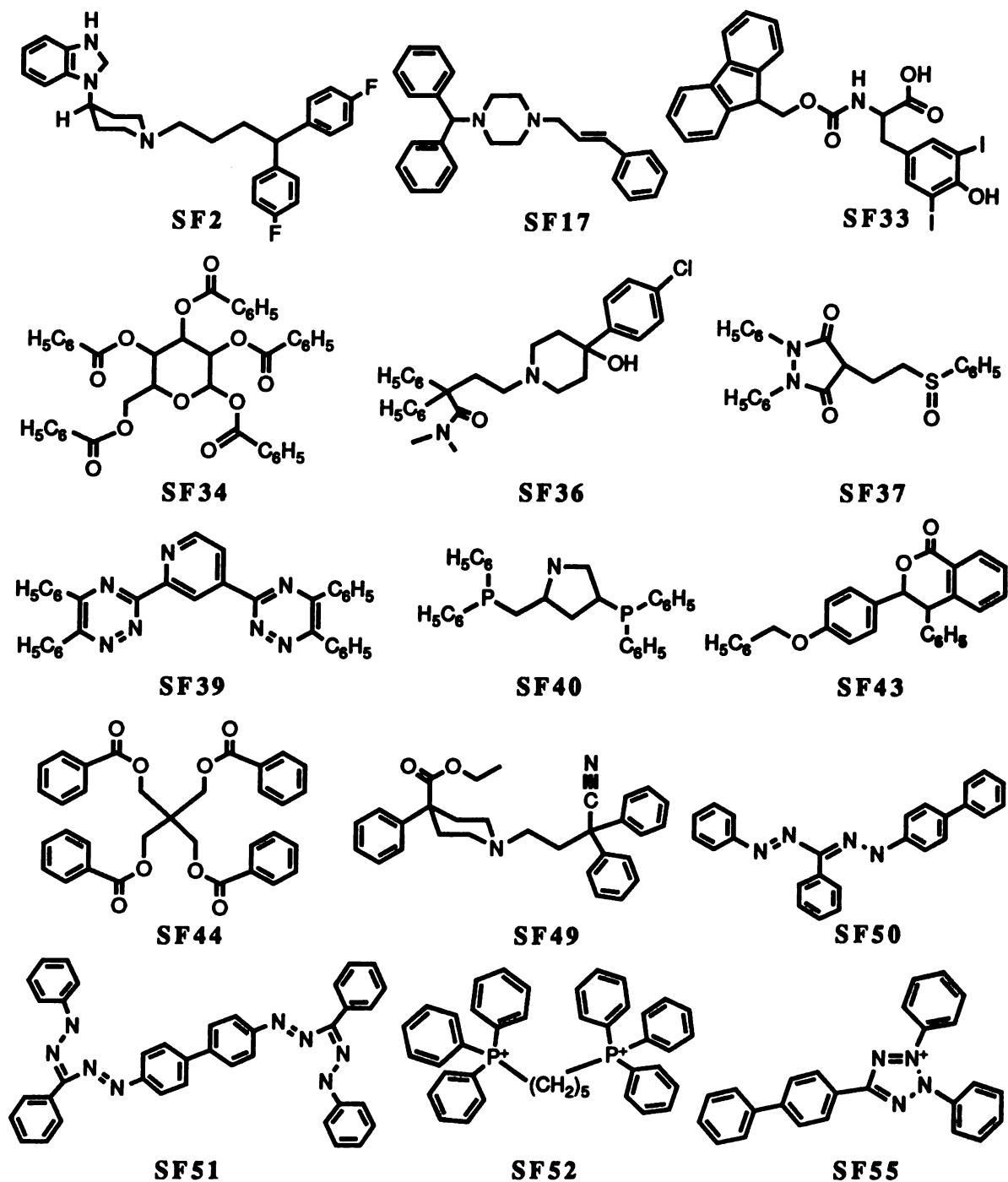


Figure 3.2: Structures of compounds originating from the pharmacophore-based search of the FCD using MACCS-3D which were tested for inhibition of the HIV-1 protease. The inhibition assay results are shown in Table 3.1.

Compound	Percent Inhibition at 100 μ M *	IC ₅₀ (μ M)
SF2	ND	125
SF17	ND	7
SF33	ND	40
SF34	15	ND
SF36	ND	190
SF37	None	ND
SF39	10	ND
SF40	54	100
SF43	12	ND
SF44	9	ND
SF49	20	ND
SF50	18	ND
SF51	29	ND
SF52	26	ND
SF55	32	ND

*nominal concentration
 ND = not determined

Table 3.1: Inhibitory potency for the HIV-1 protease of the compounds originating from the pharmacophore-based search of the FCD using MACCS-3D.

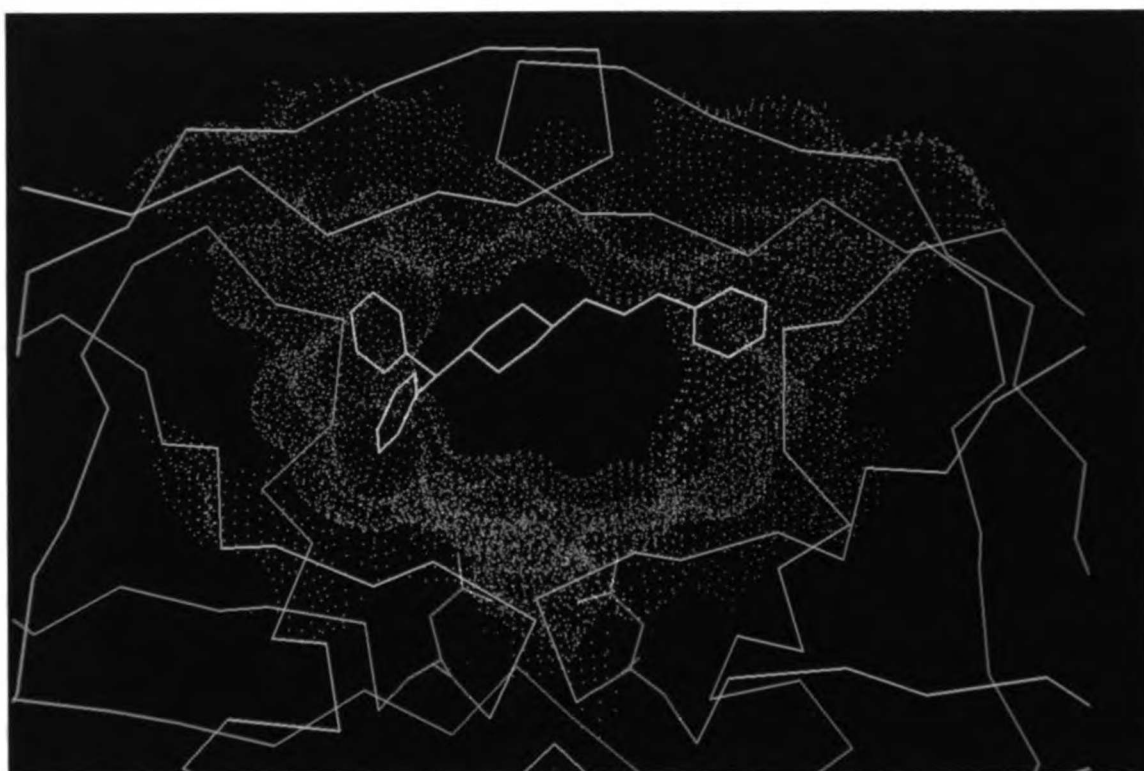


Figure 3.3: Orientation of cinnarizine, SF17, (yellow) within the HIV-1 protease active site (cyan) proposed by DOCK 3.0. The catalytic aspartate residues are shown in red.

the UCSF8-protease structure. An alternative orientation, in which the inhibitor is closer to the flaps (Figure 3.4), is obtained from DOCK 3.0 when contact scoring is used. In either case, an orientation similar to that of the inhibitor in the UCSF8 complex structure is proposed.

These compounds are interesting for various reasons. Their inhibitory potency ranks among the best of the haloperidol derivatives. With a molecular weight of 368 amu, cinnarizine is as potent as haloperidol derivatives larger than 500 amu, suggesting more efficient interactions with the protease. The presence of a second phenyl group on the heterocyclic end of the molecule supports the existence of the fourth hydrophobic pocket since the only modifications of haloperidol exploring additional pockets had occurred at the opposite end of the molecule. Finally, the second nitrogen atom of the piperazine moiety seems to adequately replace the hydroxyl group of haloperidol, a site very sensitive to modification and which, when modified previously, invariably resulted in significant loss of activity. A possible explanation is its ability to similarly interact with the crystallographically identified chloride counterion, which would support a boat conformation for the heterocycle. The shorter propyl chain of cinnarizine may result in a shift of the piperazine ring relative to the protein that allows both nitrogen atoms (one in the protonated state) to simultaneously interact with the chloride ion. The overall length of the molecule, however, is preserved by an additional carbon atom between the

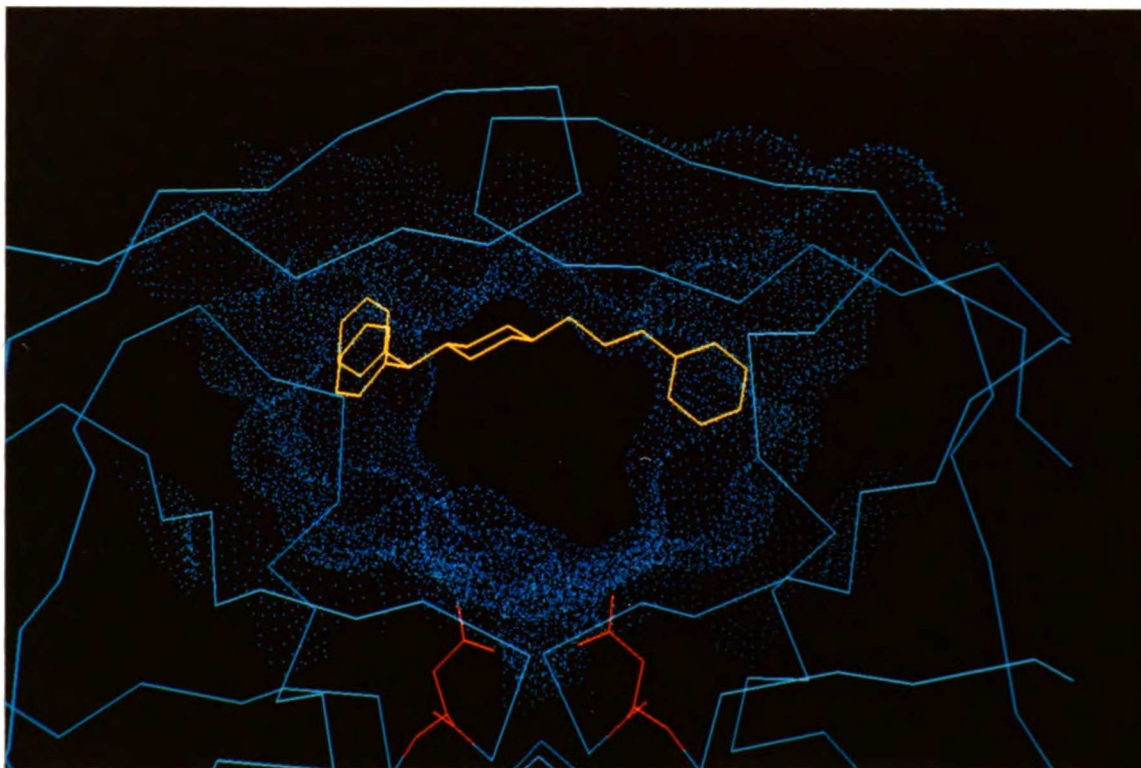


Figure 3.4: Alternative possible binding orientation, analogous to that of UCSF8, of cinnarizine, SF17, (yellow) within the HIV-1 protease active site (cyan). The catalytic aspartate residues are shown in red.

heterocycle and the aromatic groups at the opposite end of the molecule.

3.5.2 N-FMOC PROTECTED AMINO ACIDS

A family of 30 N-FMOC protected amino acids satisfied the query. These included aromatic amino acids protected exclusively at the amino terminus (Group I), but primarily consisted of other amino acids additionally protected at the carboxy terminus or sidechain by an activated phenyl ester (Group II). It is likely that the latter compounds are hydrolyzed under the acidic assay conditions. In their docked orientations, Figure 3.5, the FMOC group is placed either in the pockets occupied by the thioketal and the fluorophenyl in the crystal structure, or in the channel which is the proposed binding site of the biphenyl derivatives. Since the compounds are treated as rigid bodies by DOCK, the conformation probably dictates the site for the docking, but it is encouraging that both of these binding modes are sterically allowed.

A few representatives of this family were chosen for *in vitro* testing of inhibitory activity. Initially, only representatives of Group I were tested due to the potential hydrolysis of the Group II compounds. Of these, the most potent was SF33, which exhibited an IC₅₀ of 40 μM. In its DOCK orientation (Figure 3.6), the fluorene moiety occupies the UCSF8 thioketal and fluorophenyl pockets, and the diiodophenol group occupies the UCSF8 chlorophenyl pocket. Other candidates assayed from this group, however, were much less potent, with very

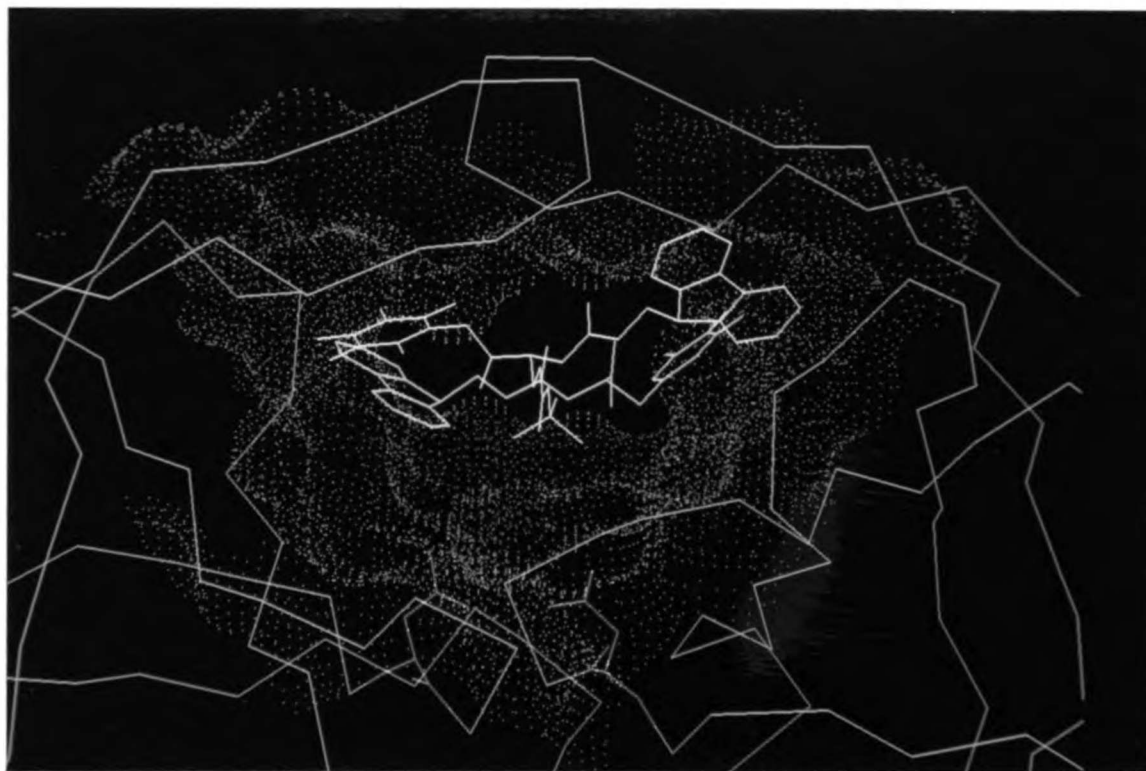


Figure 3.5: Possible orientations of the FMOC group proposed by DOCK 3.0 for $N\alpha$ -FMOC amino acid-based inhibitors of the HIV-1 protease. In most candidates of this type, the FMOC group is placed in the thioketal and fluorophenyl containing pockets of the UCSF8 complex structure (yellow), or in the cleft proposed to bind the biphenyl moiety in the biphenyl derivatives of haloperidol (magenta).

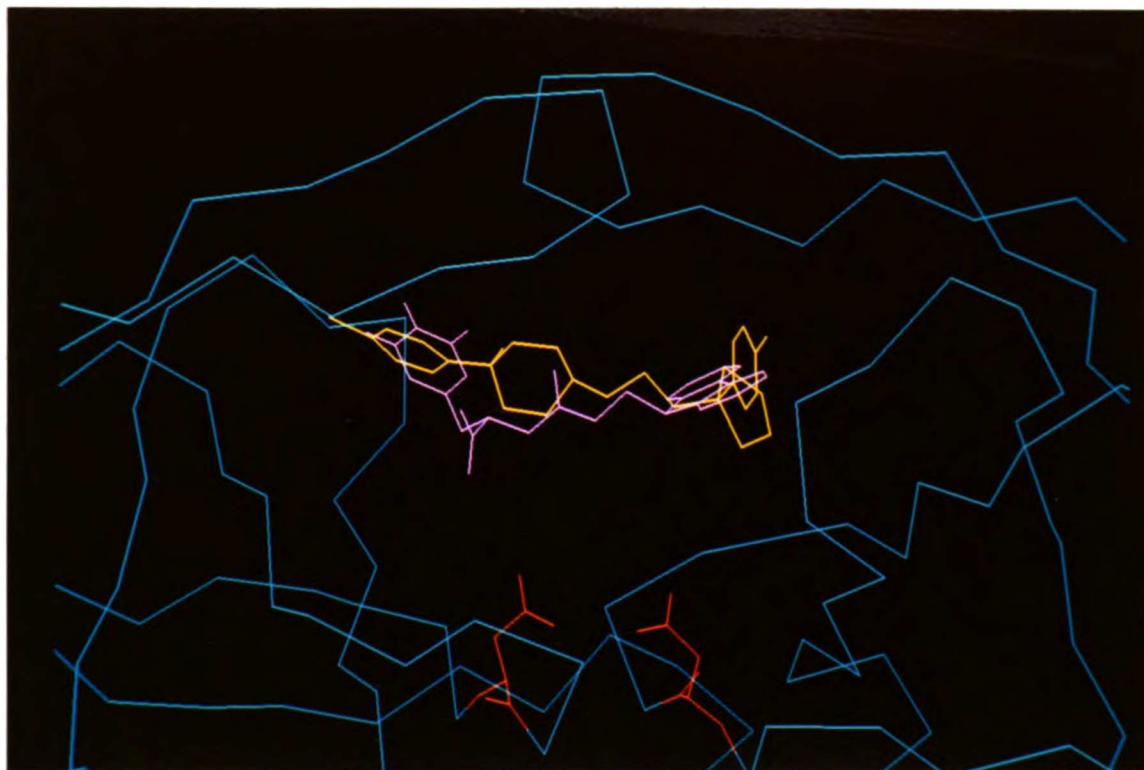


Figure 3.6: Comparison of binding orientations of SF33 (magenta) proposed by DOCK, and UCSF8 (yellow) within the HIV-1 protease. The Fmoc group is placed in the thioketal and fluorophenyl containing pockets and the diiodophenol occupies the chlorophenyl pocket of the UCSF8 complex structure.

little or no inhibition apparent at a concentration of 100 μM . Subsequently, some Group II candidates were tested. The para nitrophenyl esters of N-FMOC asparagine, SF67, and methionine, SF90, inhibited the protease with IC_{50} 's of 250 μM and 70 μM , respectively. In an attempt to occupy all four pockets simultaneously, the para nitrophenyl ester of N-FMOC phenylalanine was also assayed, but showed only nominal inhibition at 500 μM .

3.5.3 ADDITIONAL COMPOUNDS

The only other ligand with an IC_{50} below 100 μM was SF40, which exhibited 54% inhibition at that concentration. The inhibition is greatly reduced to only 8% for its t-butyl carbamate derivative, SF41. Based on their DOCK orientations, this loss in activity does not appear to be due to steric reasons and may reflect a preference for a positive charge, or the chloride counterion, in this region. This is supported by the relative DOCK scores of the two compounds. SF40 ranked 23rd, based on its force-field score, whereas SF41 was 63rd. Their order was reversed in the contact score with respective ranks of 64th and 70th. Based on this evidence and the apparent importance of the charged nitrogen atom in haloperidol derivatives, it may be necessary to include a positive charge in the pharmacophoric pattern for this binding site.

Of the compounds which exhibited no inhibition at 100 μM , SF37 was particularly surprising due to its strong resemblance to haloperidol. Although the molecule is shorter, haloperidol derivatives have not

shown a strong dependence on length. The orientation obtained from DOCK (Figure 3.7) reveals no obvious problems. One possible explanation for its incapacity to bind to the enzyme is the high negative potential at the sulfoxide oxygen atom. A factor of three improvement in inhibitory potency is observed when the haloperidol ketone oxygen atom, a much less electron-rich site, is replaced by a carbon atom. Thus, not only does a positive charge appear to be favored somewhere along this site, but a negative charge may not be tolerated.

3.6 CONCLUSIONS

Although most of the compounds selected in the pharmacophore-based search were weak inhibitors, one can draw several conclusions from the high success ratio (85%) observed. The four protease pockets occupied by the aromatic and thioketal rings of UCSF8 in the complex structure are viable targets for inhibitor design. Filling these sites with phenyl groups, although not sufficient, is a strong determinant of inhibitory activity. This is particularly striking when one considers the high variability in the structures and physical properties of the ligands. Finally, leads from this search have resulted in the discovery of more promising drug candidates. The low toxicity relative to haloperidol, as well as the ease of their modification and the abundance of commercially available derivatives, has made N-FMOC amino acids particularly attractive targets, a topic which is discussed further in chapter 5

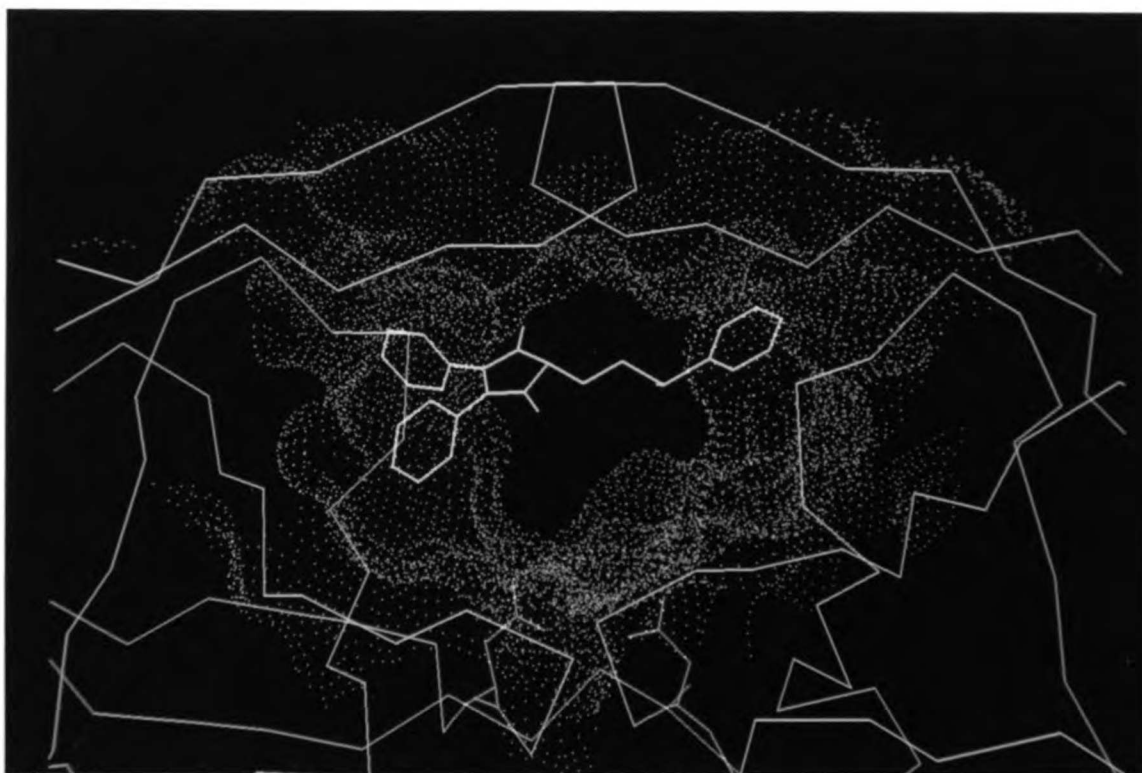


Figure 3.7: Orientation of SF37 (yellow) within the HIV-1 protease active site (cyan) proposed by DOCK 3.0.

CHAPTER 4

DERIVATIVES OF HALOPERIDOL AND CINNARIZINE ATTEMPTING TO FILL THE HYDROPHOBIC POCKETS DEFINED BY THE UCSF8-PROTEASE COMPLEX X-RAY STRUCTURE

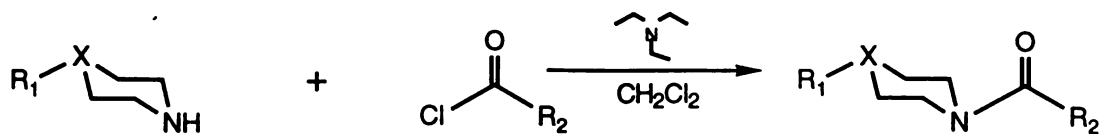
4.1 INTRODUCTION

As previously discussed in Chapters 2 and 3, four hydrophobic pockets are evident in the crystal structure of the complex between UCSF8 and the HIV-1 protease, the two occupied by the halogenated phenyl rings, and the two occupied by the symmetry-related thioketal groups. Haloperidol derivatives in which three of these pockets are occupied have several-fold lower IC_{50} 's than the parent compound, which can only fill two of them. Furthermore, cinnarizine, with an IC_{50} of 7 μ M, is a much more potent inhibitor of the protease than haloperidol, presumably because of: 1) energy gained from the interaction with three of the pockets via the hydrophobic effect, and 2) additional rigidity in the alkyl chain, which lowers the entropic cost of binding. Lower IC_{50} 's should be achievable by inhibitors capable of filling all four pockets simultaneously. With this goal in mind, haloperidol- and cinnarizine-like compounds having two phenyl groups at each end of the molecule were designed.

4.2 SYNTHESIS OF DERIVATIVES

The first set of derivatives targeted to fill the four pockets simultaneously were synthesized as shown in Scheme 4.1. The bisacylation of piperazine (26) and the mono-acylation of 4-(bis-(4'-fluorophenyl)methyl)piperazine (27) and 4-(diphenyl hydroxy methyl) piperidine (28) using diphenylacetyl chloride (29) gave compounds 31, 33, and 35, respectively. Acylation of the same heterocyclic amines with 3,3-diphenylpropionyl chloride (30) generated *in situ* resulted in amides 32, 34, and 36. The 4-(4'-chlorophenyl)-4-piperidinol (17) moiety of haloperidol was also acylated with 29 and 30, giving 37 and 38, for comparison purposes. These amide derivatives were not expected to be potent inhibitors of the protease, and were primarily synthesized as starting materials for more interesting compounds. The inactivity anticipated for 31, 32, and 35-38 is based on data obtained from other uncharged derivatives of haloperidol. Although compounds 33 and 34 are still capable of being ionized at pH 5.5, the protonation occurs at the 4 position of the heterocycle rather than at the 1 position, and may therefore be too distant to the chloride binding site to allow a productive interaction.

Compounds 39-42, Scheme 4.2, were generated by lithium aluminum hydride (LAH) reduction of the amide moiety of 31, 33, 35, and 37. Compared to cinnarizine (or haloperidol), derivatives 40 and 41 are both one methylene shorter. Compound 39 is the same length as cinnarizine and has the added feature of being



26: X=N R₁=H

29: R₂=CH(C₆H₅)₂

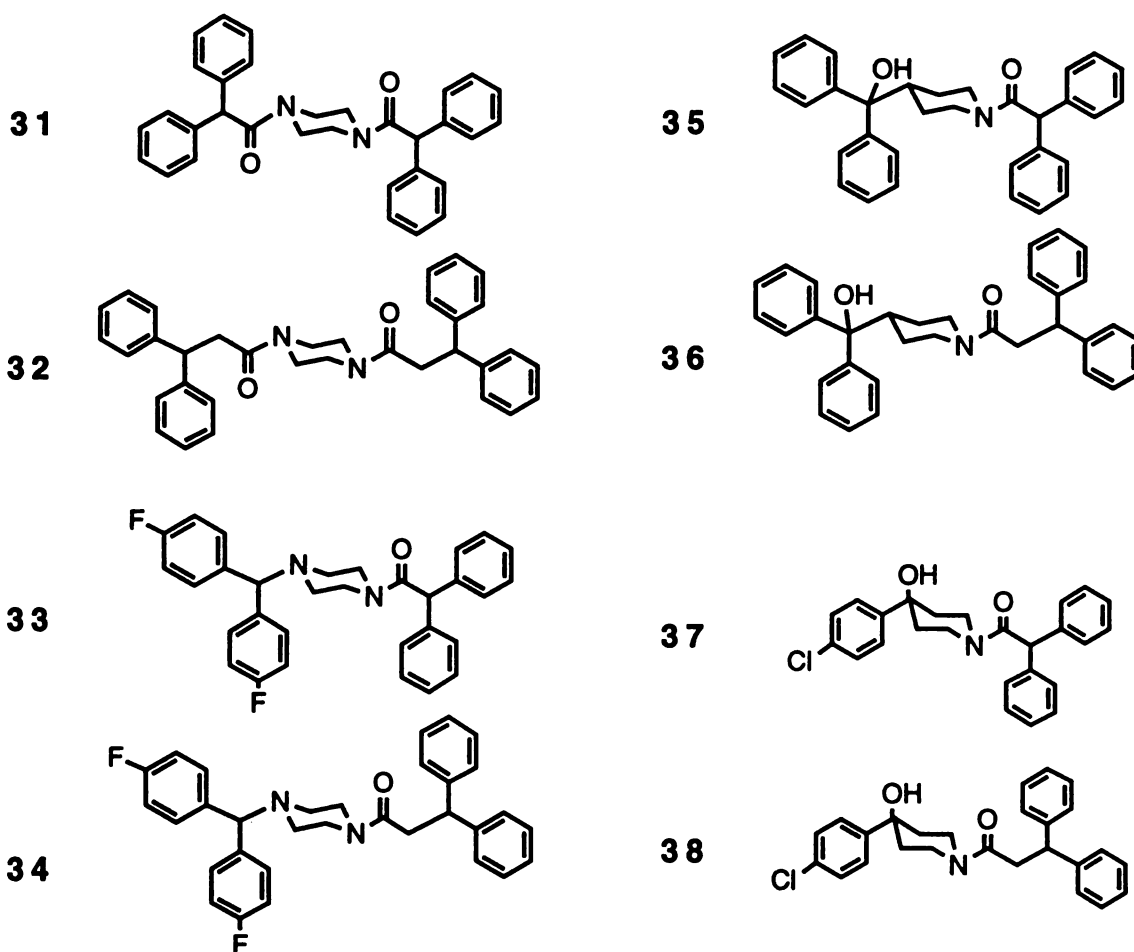
31-38

27: X=N R₁=CH(p-F-C₆H₅)₂

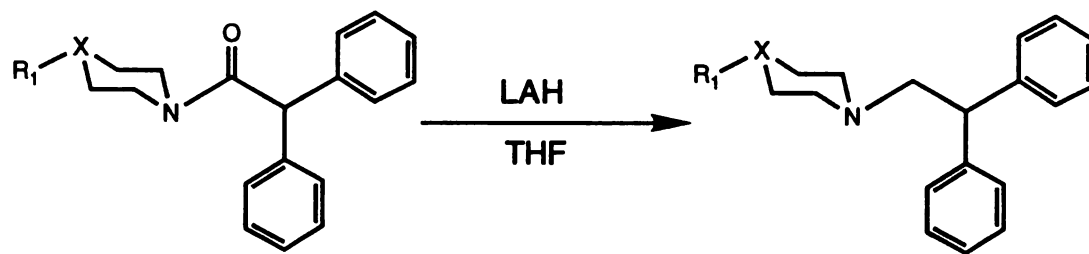
30: R₂=CH₂CH(C₆H₅)₂

28: X=CH R₁=C(OH)(C₆H₅)₂

17: X=C(OH) R₁=p-Cl-C₆H₄

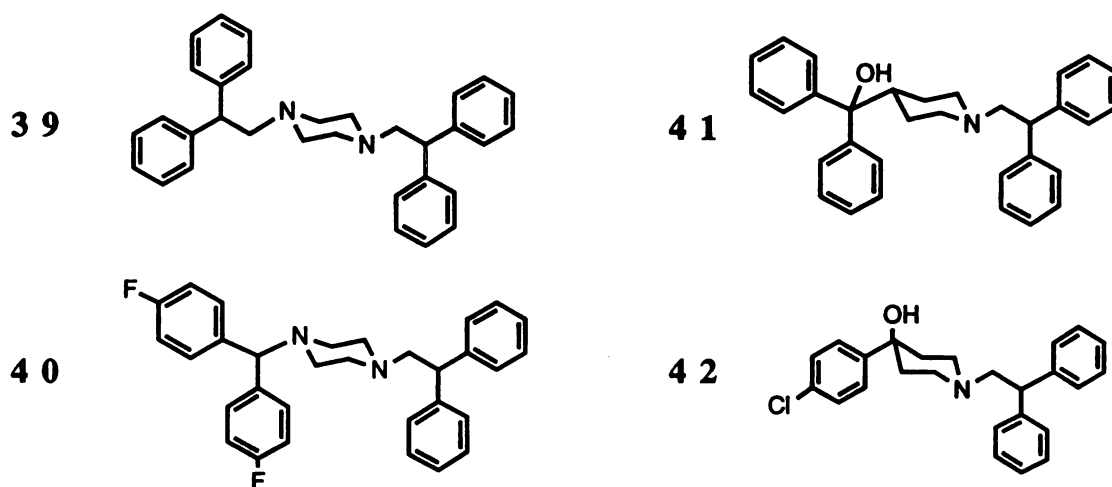


Scheme 4.1: Formation of cinnarizine and haloperidol amide derivatives by the acylation of various heterocyclic starting materials.



- 31:** X=N R₁=COCH(C₆H₅)₂
33: X=N R₁=CH(p-F-C₆H₄)₂
35: X=CH R₁=C(OH)(C₆H₅)₂
37: X=C(OH) R₁=p-Cl-C₆H₄

39-42



Scheme 4.2: Reduction of cinnarizine and haloperidol amide derivatives to generate the corresponding amines.

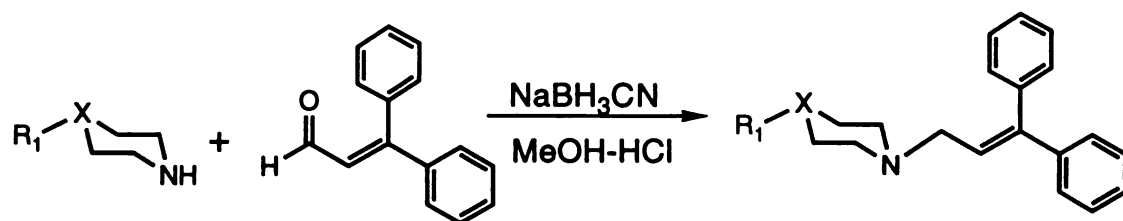
symmetrical, potentially allowing equivalent chelation of the chloride anion.

In situ reduction by NaBH₃CN of the imines generated from heterocyclic amines and 3-phenyl cinnamaldehyde produced derivatives **44-47**, Scheme 4.3. Compounds **44** and **45** are derivatives of cinnarizine and flunarizine with an additional terminal phenyl group on the propyl chain. Compound **46** is an analogue of haloperidol containing both an additional terminal phenyl group and the rigidity of an olefin in the alkyl chain. The double alkylation of piperazine yielded compound **47**.

The double bonds in compounds **44** and **46** were catalytically hydrogenated, Scheme 4.4. The fully saturated analogue of **44** is **48**. This compound, a structural isomer of **39**, is also related to **40**, being one methylene group longer and having hydrogen atoms in place of the fluorine atoms. Reduction of **46** gave compound **49**, which has one more methylene group than does **42**.

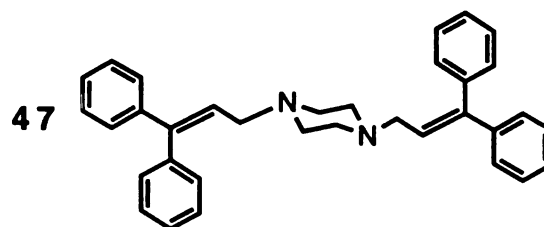
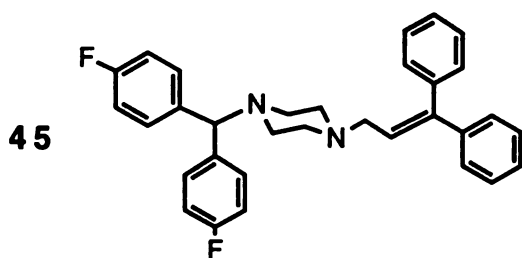
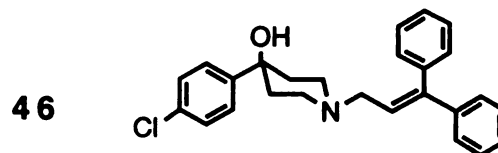
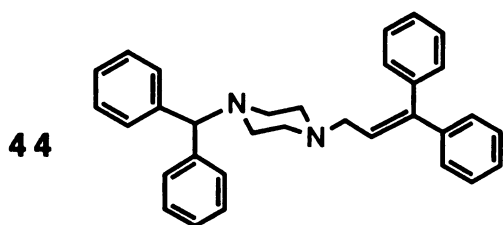
4.3 RESULTS OF HIV-1 PROTEASE INHIBITION ASSAYS

The results of the HIV-1 protease inhibition assays for **31-49** are summarized in Table 4.1 (Craig *et al.*, unpublished results). The amide derivatives, **31-38**, exhibited only minimal activity at 100 μ M. Dramatic improvements in inhibitory potency were observed upon conversion of **35**, **37**, and **38** to their corresponding amines **41**, **42**, and **49**, which have IC₅₀'s of 110 μ M, 100 μ M, and 125 μ M,

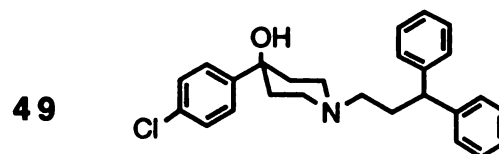
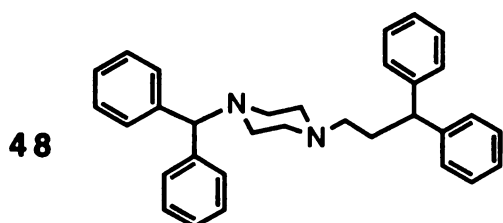
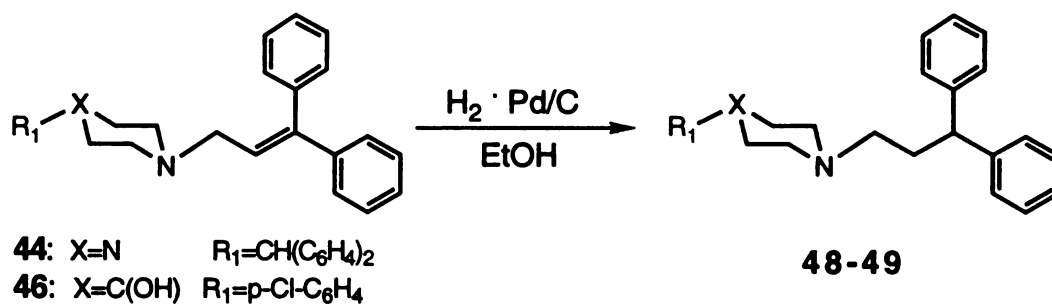


- 43:** X=N R₁=CH(C₆H₄)₂
27: X=N R₁=CH(p-F-C₆H₄)₂
17: X=C(OH) R₁=p-Cl-C₆H₄
26: X=N R₁=H

44-47



Scheme 4.3: Formation of cinnarizine and haloperidol olefin derivatives by alkylation of various heterocyclic starting materials.



Scheme 4.4: Reduction of cinnarizine and haloperidol olefin derivatives to generate the corresponding saturated compounds.

Compound	Percent Inhibition at 100 μ M *	IC ₅₀ (μ M)
31	8	nd
32	ND	nd
33	3	nd
34	7	nd
35	14	nd
36	nd	>500
37	nd	>250
38	nd	450
39	nd	>500
40	12	nd
41	nd	110
42	nd	100
44	nd	200
45	3	nd
46	nd	55
47	nd**	nd**
48	18	nd
49	nd	125

*nominal concentration

**insoluble

ND = none detected

nd = not determined

Table 4.1: HIV-1 protease inhibitory potencies for various derivatives of cinnarizine and haloperidol (Craig *et al.*, unpublished results).

respectively. Other compounds showed little improvement upon conversion of the amide moiety to an amine (compare **31** and **39**, **33** and **40**, and **34** and **48**). Introduction of an unsaturation into the alkyl chain of compounds **48** and **49**, yielding **44** and **46**, respectively, improved their inhibitory potency, resulting in IC₅₀'s of 200 μ M and 55 μ M, respectively. An assessment of the inhibitory potency of compound **47** was not possible due to solubility difficulties in the assay medium.

None of the compounds targeted to simultaneously occupy the four protease pockets exhibited the desired improvement in inhibitory potency. Although the expected general trend in potency amide < saturated amine < unsaturated amine was observed, all the derivatives were much weaker than was originally projected. In fact, the best inhibitors were those containing the haloperidol fragment which, at most, could only fill three pockets simultaneously, but even those, being one methylene shorter than the parent compound, were relatively weak inhibitors.

The symmetrical piperazine derivatives, **31**, **32**, and **39**, did not inhibit the protease significantly. Due to the inherent symmetry of the unliganded protease dimer, symmetrical ligands have always been of interest. In addition, in the UCSF8-protease structure, the chloride ion lies on the C₂ axis, coordinated to the amide nitrogen of Ile 50 from each monomer. Thus, it was hoped that these derivatives would bind in a symmetrical fashion with each nitrogen atom interacting with the chloride ion in an identical fashion. Their

inability to bind to the enzyme may reflect either an incapacity of the enzyme to accommodate the four phenyl groups simultaneously, or a preference by the chloride ion for a non-symmetrical coordination with compounds of this type. Under the assay conditions, it is likely that only one of the nitrogen atoms is protonated thereby introducing non-equivalence. Since the chloride ion may prefer greater proximity to one of the protonation states, probably the cation, non-symmetrical analogues may be favored by the enzyme.

About a 30-fold loss in inhibitory potency is observed for analogue **44** relative to cinnarizine. The two molecules differ only in the presence of a second phenyl group on the propyl chain of the former. Assuming a binding orientation similar to haloperidol in which a fourth pocket capable of accomodating the additional group appears to be present, this loss of activity may reflect the inability of the ligand to adopt a productive conformation, or an improper geometrical arrangement of the phenyl groups. Alternatively, it may not be possible to occupy all four pockets with phenyls simultaneously due to steric reasons, or the inhibitory binding mode of cinnarizine may differ from that of haloperidol, although the latter reason seems unlikely based on the strong similarities between the two inhibitors.

CHAPTER 5

N α -FMOC AMINO ACIDS AS INHIBITORS OF THE HIV-1 PROTEASE

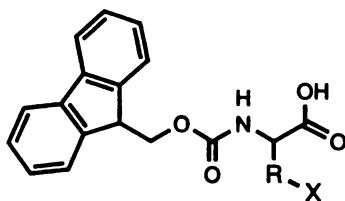
5.1 INTRODUCTION

N α -FMOC 3,5-diiodotyrosine, SF33, was found to inhibit the HIV-1 protease with an IC₅₀ of 40 μ M. The ligand was discovered by a pharmacophore-based search of the Fine Chemicals Database (FCD), as described in Chapter 3. The presence of three phenyl groups and their relative distances, as defined by the query, was satisfied by the two phenyls of the fluorenyl group and the phenyl of the tyrosine sidechain. Twenty-nine other N α -FMOC amino acid derivatives were also found in this search including singly protected aromatic amino acids, and other amino acids additionally protected by a phenyl-containing group at either the carboxy terminus or the sidechain. The relatively low toxicity observed for SF33 in a 24 hour cell culture assay, LD50 of >250 μ M (Babé and Craik, unpublished results), suggested that this family of compounds should be studied further.

5.2 EVALUATION OF POTENCY OF VARIOUS N α -FMOC AMINO ACIDS

A variety of N α -FMOC amino acids were tested for inhibition of the HIV-1 protease (Table 5.1). Additional compounds which were tested, whose results are not shown, include non-aromatic amino acids protected only on the amino terminus with the FMOC moiety, none of which exhibited any inhibition. In fact, the only compound of this type which inhibits the protease to any extent is the methionine derivative, SF60, with 24% inhibition at 100 μ M, and the inhibition improves to 34% at 50 μ M for its para nitrophenyl ester derivative, SF90. Similar results are observed with N α -FMOC glutamine, for which the unesterified compound is devoid of activity but the para-nitrophenyl ester inhibits with an IC₅₀ of 250 μ M. These results are consistent with the pharmacophore pattern proposed in which the presence of a third phenyl group contributes to binding.

None of the additional tyrosine derivatives assayed were more potent than SF33. N-FMOC tyrosine (SF87), differing from SF33 in the absence of iodine atoms at the positions ortho to the aryl hydroxyl group, showed no inhibition at 50 μ M. The iodine atoms of SF33 thus appear to be important for inhibitory activity. Their size and polarizability can provide a significant amount of binding energy, probably through the hydrophobic effect, in their interaction with the protein. The N-FMOC tyrosine derivative protected at the phenol with a t-butyl group, SF73, was also inactive. Protection of



	Amino Acid Side Chain (R)	Side Chain Protecting Group (X)	IC ₅₀ (μM)
SF33	3,5-Diiodo Tyr	—	40
SF48	His	Trt	30
SF60	Met	—	>100*
SF68	Cys	Trt	2.8
SF73	Tyr	t-Bu	>500
SF74	His	Bz	ND
SF75	Arg	Ts	2.0
SF81	His	Fmoc	ND
SF87	Tyr	—	ND
SF88	Tyr	Bz	>50**

* 24% inhibition observed at 100 μM

** 40% inhibition observed at 50 μM

ND = none detected

Abbreviations: Trt = trityl, t-Bu = t-butyl, Bz = benzyl, Ts = tosyl

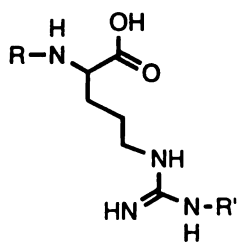
Table 5.1: Structures and inhibitory potencies (Craik *et al*, unpublished results) of Nα-Fmoc amino acids.

the phenol with a benzyl group (SF88), however, conveyed inhibitory activity (40% inhibition at 50 μM) to the molecule. The latter result is consistent with the binding orientation proposed by DOCK for SF33 (Section 3.5.2), in which the additional benzyl group occupies the cleft invoked for binding of the biphenyl derivatives of haloperidol (Section 2.4.2).

The $\text{N}\alpha$ -FMOC derivatives of histidine (SF48) and cysteine (SF68) with a trityl group added to the sidechain exhibited inhibition of the viral protease with respective IC_{50} 's of 30 μM and 2.8 μM . The inhibitory potency of the latter places it among the best of the haloperidol derivatives. Upon testing of other derivatives of these amino acids, it appears much of their potency is due to the large amount of hydrophobicity of the trityl group. Replacement of this group with a t-butyl in the case of the cysteine analogue (SF69), or with a benzyl or FMOC in the case of the histidine analogue (SF74 and SF81, respectively), abolishes all inhibitory activity at concentrations as high as 500 μM . Additional derivatives of these amino acids were therefore not pursued.

5.3 $\text{N}\alpha$ -FMOC ARGININE DERIVATIVES AS HIV-1 PROTEASE INHIBITORS

The most promising leads within the family of $\text{N}\alpha$ -FMOC amino acids have been derivatives of arginine (Table 5.2). The first of these compounds tested, SF47, inhibited the viral protease with an IC_{50} of 35 μM . The compound was chosen primarily because of the presence



	Stereochem.	R	R'	IC ₅₀ (μM)
SF47	L	FMOC		3.5
SF71	L	FMOC	H	>500
SF72	L	FMOC		5.2
SF75	L	FMOC		2.0
SF84	D	FMOC		ND
SF92	L	CBz		ND
SF93	L	t-BOC		ND

ND = none detected

Abbreviations: CBz = benzoyl carbonyl, t-BOC = t-butyl-O-carbonyl

Table 5.2: Structures and inhibitory potencies (Craik *et al.*, unpublished results) of arginine derivatives modified at the amino and guanidino groups.

of a third aryl group, which appeared to be important for inhibitory activity, on the amino acid sidechain. Trimming of the second ring of the sidechain aryl moiety, as in SF72, has a small effect (less than a factor of two) on the inhibitory potency. Further pruning of the aryl group to a tolyl (SF75), however, improves the IC₅₀ to 2 μM, a factor of 26 better than SF72. Removal of the aryl moiety from the sidechain altogether (SF71) results in total loss of inhibitory activity, consistent with previous observations. It is important to note that the latter compound differs from the other derivatives not only in the absence of the aryl moiety, but also in the positive charge present on the guanidino group at the relevant pH values. Although the loss of activity is primarily attributed to the removal of the aryl group, the possibility of a significant contribution from the change in the charge cannot be ruled out.

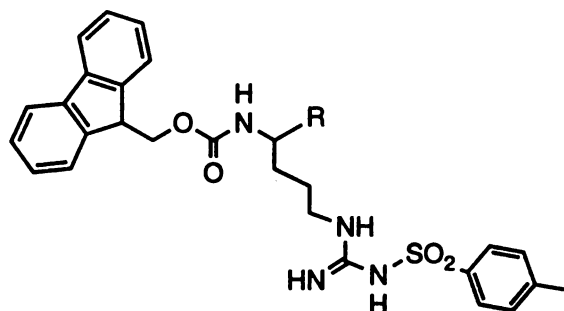
Unlike haloperidol derivatives, the affinity of this family of molecules for the protease exhibited a large sensitivity to relatively subtle changes in their structure. The 26-fold difference between the IC₅₀'s of SF72 and SF75 is essentially a result of the removal of four methyl groups. A more dramatic example of the sensitivity to small structural changes, however, is the difference in inhibitory potency between SF47 and its D isomer, SF84. The change in chirality about the asymmetric center is the most conservative modification possible since enantiomers exhibit identical physical properties and can only be differentiated by other chiral molecules. The L isomer, as stated above, inhibits the HIV-1 protease with an

IC₅₀ of 35 μM, whereas the D isomer is completely devoid of inhibitory activity in concentrations up to 50 μM.

The importance of the group attached to the alpha amino position was investigated. Although it was assumed that the FMOC moiety at this position was essential for inhibition, no evidence had been obtained to support this notion. Confirmation was established when the replacement of the FMOC of SF75 by either a CBz or a t-BOC, SF92 and SF93, respectively, completely abolished all inhibitory activity (Table 5.2).

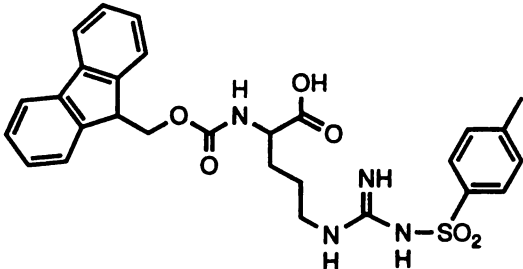
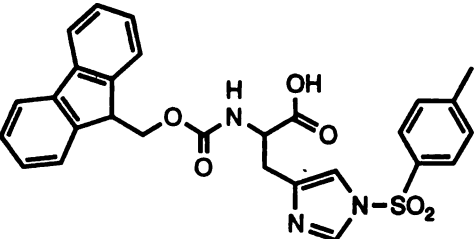
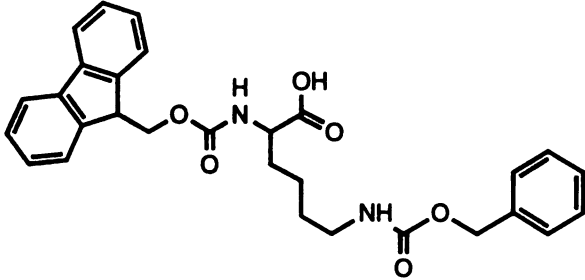
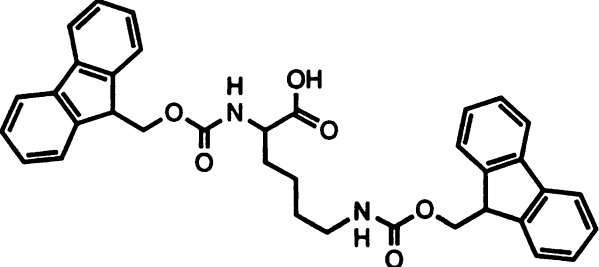
At the carboxy terminus, a free acid appears to be most complementary to the enzyme (Table 5.3). Losses in inhibition of 10-fold and 4-fold, respectively, are observed when the acid group is replaced by either an alcohol, or an amide. The latter is an isosteric modification engineered to investigate the sole effect of an uncharged moiety at this position. The enthalpic gain from having a negative charge is more significant when one considers the greater amount of energy required for its desolvation. Esterification of the alpha carboxy group with sequentially larger alcohols (DeVoss, 1992), also resulted in a concomitant loss of inhibitory activity. Thus, both steric and electronic factors are important at this position of the molecule.

The tolerance of the alkyl guanidino sidechain to structural modifications has also been briefly explored (Table 5.4). Gross modifications in length and geometry cannot be accommodated by



R	IC ₅₀ μM
COOH	2
CO ₂ Me	10
CO ₂ Et	>>25
CO ₂ CH ₂ CH ₂ OH	60
CO ₂ CH ₂ C ₆ H ₅	>100
CH ₂ OH	20
CONH ₂	8

Table 5.3: Structures and inhibitory potencies (Craig *et al.*, unpublished results) of N α -Fmoc N ω -tosylarginine derivatives modified at the carboxyl group (adapted from DeVoss, 1992).

		<u>IC₅₀ (μM)</u>
SF75		2
SF83		ND
SF85		>50
SF86		50

ND = none detected

Table 5.4: Structures and inhibitory potencies of N α -FMOC amino acid derivatives assayed to explore the tolerance of substitution in the alkyl guanidino sidechain of SF75.

the enzyme, as is apparent by the inactivity of SF83. Replacement of the arginyl sidechain and tosyl group of SF75 by a lysyl sidechain and a CBz group, respectively, (SF85) although detrimental, does not completely abolish activity with 30% inhibition observed at 50 μ M. The inhibition is improved to 50% at 50 μ M when an Fmoc group takes the place of the CBz (SF86). The chain of the latter two compounds is one methylene unit longer than SF75 and contains a urethane moiety in the position between the guanidino and sulfonamide groups. Thus, both the length and electronic, including hydrogen bonding, properties of the amino acid sidechain must be considered when designing more potent inhibitors.

5.4 ATTEMPTS AT ELUCIDATING THE BINDING ORIENTATION OF N α -FMOC N ω -TOSYLARGININE

Rational modifications of the ligand for improving the inhibitory potency require determination of its binding orientation and/or conformation. This information is generally obtained by x-ray crystallography or NMR. In lieu of such data, possible binding orientations can be generated by computational methods, and evaluated using the inhibitors' structure-activity relationships. The extent of conformational freedom of N α -FMOC N ω -tosylarginine (SF75), with a minimum of nine fully rotatable bonds, makes an extensive conformational search formidable. Therefore, a distance-geometry-based approach was chosen.

The program DGEOM (Blaney,1990) was used to generate multiple conformations of the ligand. Random conformers are created within the realm of the receptor atoms thereby reducing the total number of possible orientations. The active site of the UCSF8-bound form of the HIV-1 protease (without the inhibitor) was used in the calculations. Thirty different conformations, spanning the entire protease active site, were obtained. In addition, since the family of N α -FMOC amino acids was obtained through a pharmacophore-based search, a conformation which superimposed the FMOC aryl groups on the thioketal and fluorophenyl rings and the tosyl group on the symmetry-related thioketal ring of UCSF8 in its bound conformation was manually generated. The chain connecting the aromatic moieties was placed so as to follow the active site's solvent accessible surface. The DGEOM structures were evaluated for steric and electronic complementarity to the protease's active site using DOCK 3.0. The conformation derived from the UCSF8 binding orientation, a conformation derived from the MVT-101 (peptide-inhibitor) binding orientation, and a random extended conformation were also evaluated in an analogous fashion.

It was hoped that the structure derived from the UCSF8 conformation would rank the best, thereby supporting the rationality behind its discovery. Lamentably, such was not the case, although particularly close contacts, between the OD2 of Asp25 and a ligand carboxyl oxygen atom (2.4 Å), and between the C α of Ala28 and a guanidino nitrogen atom (3.5 Å), may have resulted in its elimination (Figure 5.1).

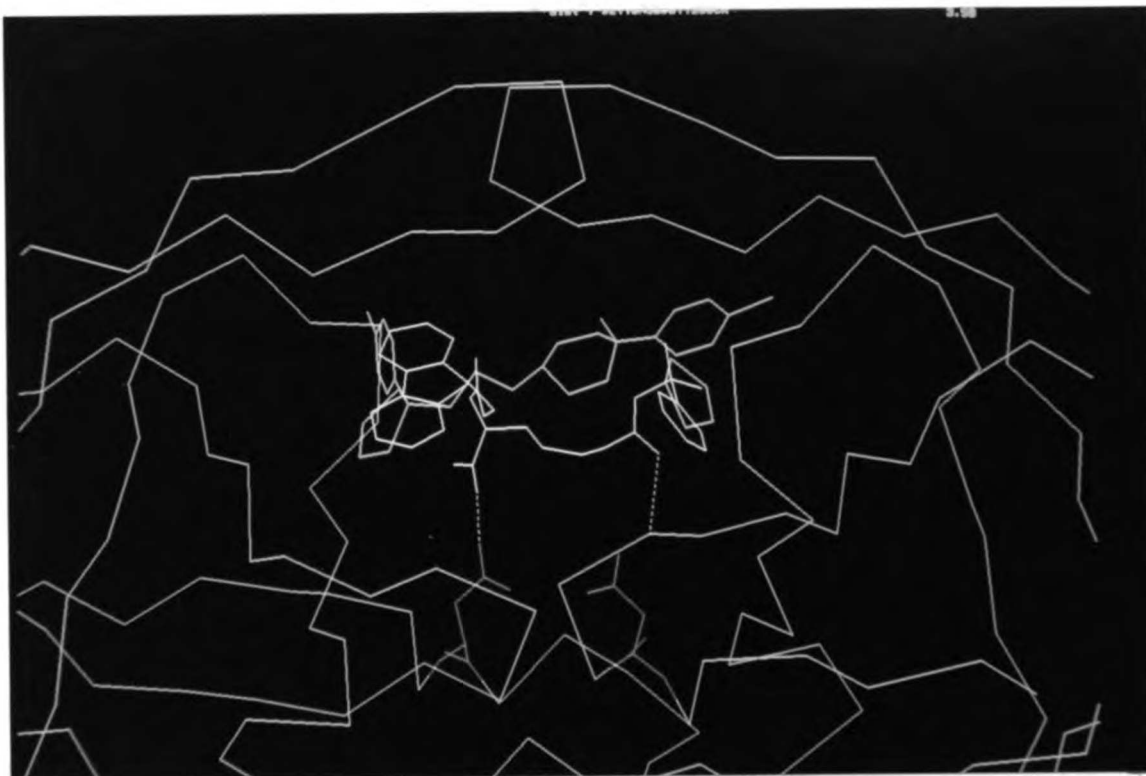


Figure 5.1: Superposition of manually generated conformation of $N\alpha$ -FMOC $N\omega$ -tosylarginine (magenta) on the x-ray structure of UCSF8 (yellow) in its bound conformation to the HIV-1 protease (cyan). Orange broken lines depict close contacts between the ligand and the protein. The catalytic aspartate residues are shown in red.

The highest scoring orientation, however, also concurs with a binding mode where the Fmoc and tosyl groups bind in pockets analogous to the UCSF8 rings (Figure 5.2). Although the fluorenyl moiety is not actually superimposed on the UCSF8 fluorophenyl and thioketal groups, its proximity to them is encouraging considering the conformation was randomly generated and held rigid during the docking procedure. The tosyl group exhibits an even larger overlap with the chlorophenyl ring of the bound inhibitor.

Several differences between the manually generated and the highest scoring orientations are observed (Figures 5.3 and 5.4). The major difference exists in the chain linking the aromatic groups. The chain of the computationally derived structure is in a more compact conformation, unable to follow the enzyme's surface. Furthermore, the tosyl group, which occupies the site analogous to the UCSF8 thioketal ring in the manually derived structure, is in the chlorophenyl pocket in the DGEOM conformation.

Although the structure is not proposed to be the actual binding orientation, particularly along the chain linking the aromatic residues, it contains features which are attractive based on observed experimental results. The importance of the fluorenyl and tosyl groups is evident, serving as anchors for the rest of the molecule. Furthermore, proximity of the acid functionality to the sidechain of Asp125 (Figure 5.5) is consistent with the observed effect of pH on inhibition. The inhibitory potency of SF75 decreases at higher pHs with a profile (pKa) identical to that of enzymatic activity, whereas



Figure 5.2: Superposition of the highest scoring DOCK orientation of a computationally generated conformation of $N\alpha$ -FMOC $N\omega$ -tosylarginine (magenta) on the x-ray structure of UCSF8 (yellow) in its bound conformation to the HIV-1 protease (cyan). The catalytic aspartate residues are shown in red.



Figure 5.3: Side view comparison of the orientations of N α -FMOC N ω -tosylarginine obtained manually (yellow) and by computational methods (magenta) within the HIV-1 protease (cyan). The catalytic aspartate residues are shown in red.



Figure 5.4: Top view comparison of the orientations of $N\alpha$ -FMOC $N\omega$ -tosylarginine obtained manually (yellow) and by computational methods (magenta) within the HIV-1 protease (cyan). The catalytic aspartate residues are shown in red.



Figure 5.5: Close-up view of the acid functionality the highest scoring orientation of N α -FMOC N ω -tosylarginine. Distances to protein residues within 5 Å of the acid group of the ligand are denoted by orange broken lines. Only the sidechains of those residues are shown. The enzyme backbone atoms are in white, all other atoms are colored by atom type.

the amide derivative exhibits no pH dependence (Salto and Craik, unpublished results). The pH dependence of enzymatic activity is attributed to deprotonation of the second catalytic aspartate residue, providing strong evidence for its proximity to the acid group of SF75 (i.e., once both catalytic aspartates are unprotonated, a repulsion between the negatively charged residue and inhibitor is created). An additional residue near the ligand's acid moiety is Arg108. Disruption of the putative salt bridge to this residue may explain the lowered activity of derivatives in which the acid is replaced by an uncharged group, particularly when their desolvation energy is expected to be less than that of the charged parent compound.

Finally, the presence of a valine residue in position 182, which is an isoleucine in the HIV-2 protease (Figure 5.6), near the acid functionality of the ligand may rationalize observed differences in the effect of esterification on inhibition of the two enzymes. The activity of the methyl ester of SF75 is 10-fold less than the parent compound for the HIV-1 enzyme whereas little effect is observed for the HIV-2 enzyme. On the other hand, upon formation of the ethyl ester a 10-fold loss in activity is seen for the HIV-2 protease (Salto and Craik, unpublished results). It is counterintuitive that the HIV-1 enzyme, whose residue 82 has one less methyl group, could only accommodate the smaller ligand, and the HIV-2 enzyme, with one extra methyl group on residue 82, could accommodate the one methyl larger ligand. It is a possibility that the larger sidechain forces motions in other residues thus "opening" a small pocket; it is equally possible, however, that this discrepancy speaks against the

proposed placement of the acid moiety and an alternative hypothesis is necessary.

```

                20
P Q F S L W K R P V V T A Y I E G Q P V
                V
E V L L D T G A D D S I V A G I E L G N                40
                I
N Y S P K I V G G I G G F I N T K E Y K                60
                L
N V E I E V L N K K V R A T I M T G D T                80
                V
P I N I F G R N I L T A L G M S L N L                99

```

Figure 5.6: Primary structure of the HIV-2 protease. Active site residues are underlined. Active site residues differing from those of the HIV-1 protease are in bold with the corresponding HIV-1 residue above them.

CHAPTER 6

CONCLUSIONS AND FUTURE DIRECTIONS

Using the shape-fitting algorithm DOCK, haloperidol, a known antipsychotic, was identified as a competitive inhibitor of the HIV-1 protease with a K_i of 100 μM . Systematic modification of the haloperidol skeleton by traditional medicinal chemistry methods has yielded improvements in inhibitory potency as high as 18-fold. The modifications which have resulted in the largest decreases in IC_{50} 's have mostly been those which have either increased the rigidity in the ligand, or additions of large lipophilic moieties in areas where the enzyme is ample enough to accommodate such changes.

Modifications targeted for hydrogen bonding to specific groups of the protein have been less successful in increasing inhibition. These results are in agreement with the notion that although hydrogen bonding contributes to specificity it is not an important driving force for intermolecular association, and the primary source of binding energy is derived from the hydrophobic effect (Santi and Kenyon, 1980).

Various important implications arise from the binding orientation observed for the thioketal derivative of haloperidol (UCSF8) in the x-ray structure of its complex with the HIV-1 protease solved by

Rutenber *et al.* (unpublished results). A previously unknown conformation of the protease, intermediate between the unliganded form (Wlodawer *et al.*, 1989) and the peptide-bound form (Miller *et al.*, 1989), is apparent, a consequence of the inhibitor binding near the enzyme flaps away from the catalytic machinery. Thus, new binding pockets of the protein were identified and, through structure-function analysis of multiple derivatives, characterized.

Does the difference between the binding modes proposed for haloperidol by DOCK and observed crystallographically for UCSF8 question the validity, and rationality, of the method for the discovery of lead compounds? First, as was pointed out in Section 2.3, an orientation for UCSF8 analogous to that proposed for haloperidol is unfavored due to steric clashes between the protein and the thioketal group of the inhibitor, raising the possibility that the DOCK orientation may be one of several binding modes represented. In fact, the relative weakness of inhibition and lack of sensitivity to subtle modifications of haloperidol makes it likely that multiple binding orientations exist. Secondly, DOCK, particularly version 1.0, was not meant to predict binding in an absolute fashion, only to find structures which are sterically competent requiring subsequent chemical modification to optimize protein-ligand interactions. That is, as long as the structures of the target and the putative ligand are in an accessible (i.e., relatively low energy) conformation, the orientation proposed by DOCK, already devoid of steric clashes, should also be accessible if the chemical complementarity is engineered correctly. As the scoring functions are improved

(accounting for chemical complementarity, entropic loss of binding, desolvation energy, ligand flexibility, etc.) the energy gap between the "starting" molecule and the target molecule narrows. As one engineers the modifications based on the proposed binding mode, such an orientation may become increasingly stabilized, and eventually achieved regardless of the actual binding mode of the original ligand.

The importance of crystallographic support in the inhibitor improvement cycle cannot be overstated. Without it, the synthetic and computational efforts are formidable, particularly in the case of a weakly-binding lead where multiple binding modes are probable. Concomitant changes in inhibitory potency are often not observed from subtle, and sometimes not so subtle, changes in the ligand's structure, and even when significant improvements are observed, these could occur from changes in the binding orientation. The initial protein-ligand complex crystallographic structure is invaluable for determining an accessible binding mode and designing modifications in the ligand. The presence of the desired effects engineered in subsequent generations of compounds, however, must also be corroborated by crystallography.

The structure of the complex of UCSF8 with the HIV-1 protease and structure-activity relationships of haloperidol derivatives led to the proposal of a pharmacophore pattern for the novel binding site identified in the enzyme. A high (85%) success ratio for the discovery of HIV-1 protease inhibitors resulted from a database

search based on this pattern. Inhibitors obtained by this method have resulted in potent second generation lead compounds.

N α -FMOC amino acids, and in particular, N α -FMOC N ω -tosylarginine derivatives, appear to be promising drug leads. N α -FMOC N ω -tosylarginine itself, with an IC₅₀ of 2.0 μ M for the HIV-1 protease (Craik *et al.*, unpublished results) and an IC₅₀ of 700 nM for the HIV-2 protease (Salto and Craik, unpublished results), is a potent non-peptide inhibitor for the HIV proteases. In addition, preliminary cell viability assays suggest that these compounds, with LD50's of greater than 250 μ M (Babé and Craik, unpublished results), are much less toxic than haloperidol derivatives.

Unlike for haloperidol derivatives, the inhibitory potencies of derivatives of N α -FMOC N ω -tosylarginine exhibit a high sensitivity to subtle modifications in their structure. Inversion of the chirality of one derivative, SF47, whose IC₅₀ is 35 μ M, to the D isomer abolishes all inhibitory activity in concentrations up to 50 μ M. Likewise, a difference of four methyl groups in the N ω protecting groups of SF72 and SF75 results in a 26-fold difference in inhibitory activity. Conversion of the FMOC moiety to either a CBz or t-BOC, or removal of the tosyl group, renders the compound inactive. Finally, stepwise enlargement of an ester functionality at the carboxy terminus of the ligand is paralleled by a concomitant decrease in inhibitory potency. These results suggest the existence of tight, specific interactions between the inhibitor and the protein.

Although these compounds were not selected by the pharmacophore-based search, it is likely that, in their binding orientation, they occupy the analogous pockets which were targeted. In an extended conformation, as they exist in the database, the distance between the aromatic groups is too large to fit the query. The flexibility of the molecule, however, allows it to adopt a more compact conformation whereby the aryl groups are at the specified distances while the rest of the chain conforms to the surface of the protein active site.

The above case illustrates a major limitation of discovering lead compounds by searching a database. By fixing the ligand molecules to a single conformation, potential ligands to the target molecule can be eliminated. On the other hand, examination of multiple conformers of the ligands becomes computationally prohibitive and does not guarantee that the relevant conformer will be evaluated. The number of molecules examined does not appear to be the limiting factor in the discovery of a lead compound; in the present study, several inhibitors were identified. Furthermore, rigid compounds, not requiring a conformational search, are preferred as inhibitors due to a smaller loss of entropic energy upon binding.

Unambiguous determination of the binding orientation of N α -FMOC N ω -tosylarginine derivatives is essential for the rational design of more potent inhibitors. Using a distance geometry and rigid-body docking approach, a binding orientation in agreement with experimental evidence has been generated. Furthermore, the resulting orientation is consistent to that proposed for N α -FMOC

amino acids based on the pharmacophore pattern derived from the binding mode of UCSF8. Such a binding mode supports the rationality behind the discovery of these compounds as HIV-1 protease inhibitors. Recently, advances have been made in the determination of the binding conformation of N α -FMOC N ω -tosylarginine by NMR (Benjamin and Kuntz, unpublished results) and in the growth of protein-inhibitor crystals (Salto and Craik, unpublished results), suggesting a three-dimensional structure for the complex may soon be obtained.

6.1 PERSPECTIVE

To date, two approaches for the design of haloperidol derivatives have been taken: 1) the systematic modification of the different functionalities of the lead compound to determine their effect on inhibitory activity (a traditional medicinal chemistry approach); 2) "targeted" modifications where potential interactions with the enzyme are engineered in the ligand based on the binding mode observed in the inhibitor-protein complex crystal structure. A third, more automated, computational method for designing modifications in the ligand may also be possible.

By performing the DOCK calculations on the enzyme-inhibitor complex, the shape of the remaining active site volume can be defined, and a database search for complementary compounds carried out. Compounds can be selected for joint (cooperative?)

testing with the original ligand, or for attachment to the ligand at favorable sites.

The x-ray structure of the UCSF8-HIV-1 protease complex was used as a test case for the methodology described above. A cross-section of the DOCK spheres occupying the remaining active site volume is shown in Figure 6.1. Four different scoring options within the DOCK program were used in ranking the putative ligands obtained from the FCD: 1) force-field, 2) contact, 3) normalized force-field, 4) normalized contact. The non-normalized scoring, being a summation of the protein-ligand interactions over all the ligand atoms, tends to favor larger molecules, whereas normalized scoring tends to favor smaller molecules which complement the enzyme well. The top 250 molecules of each scoring method were evaluated visually.

Differences among the various scoring methods in the distribution of the ligand molecules are obvious (Figures 6.2-6.5). As expected, smaller molecules were selected when the scoring was normalized (compare Figures 6.4 and 6.5 with Figures 6.2 and 6.3, respectively). An unexpected preference for the fluorophenyl side (the right-hand side in the figures) of the active site by the ligands ranked using a force-field scoring function was observed (none of the compounds transversed the active site). No distinct preference was obvious in the ligands from the contact (non-normalized) scoring list, with a large portion of those transversing the active site. Finally, a strong preference for the thioketal side (the left-hand side in the figures) was detected when normalized contact scoring was utilized.

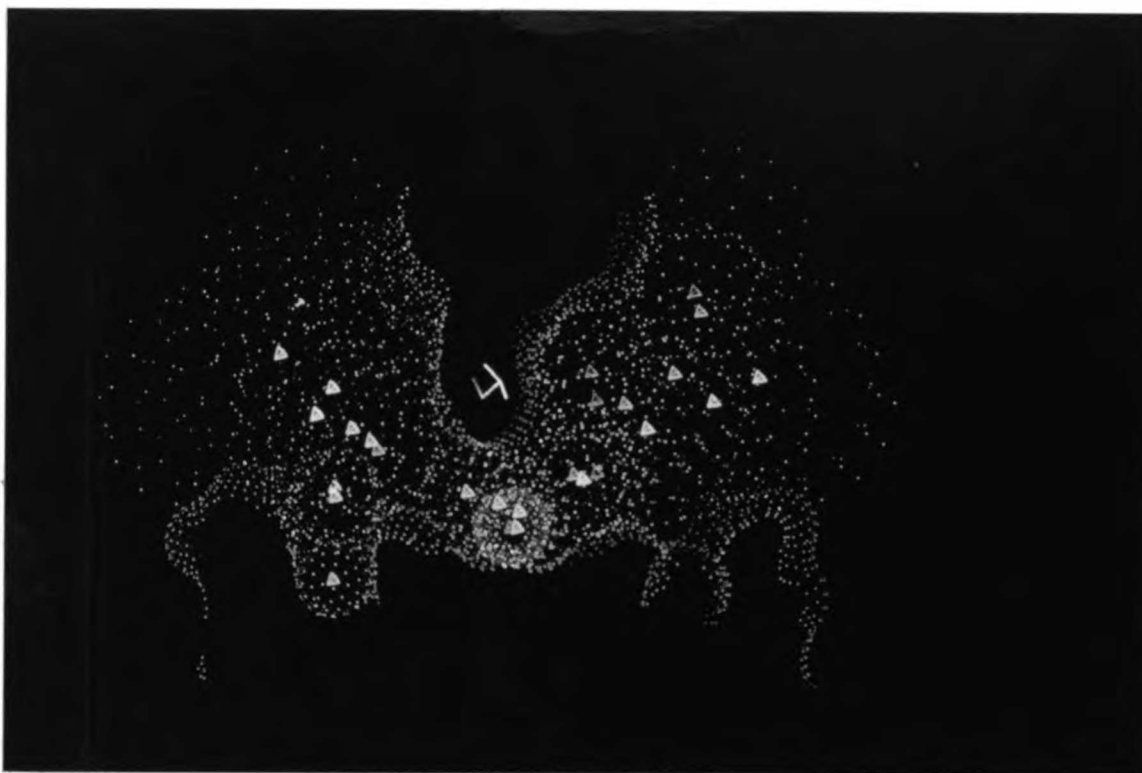


Figure 6.1: A thin cross-section of the spheres generated by DOCK within the remaining volume in the UCSF8-bound active site of the HIV-1 protease. The solvent accessible surface for the inhibitor-enzyme complex is shown in cyan. UCSF8 is in magenta, the spheres and their centers (triangles) are shown in yellow. The crystallographically determined water molecule bound to the catalytic aspartate residues of the enzyme with a Van der Waals surface is in red. The flaps of the enzyme are above the UCSF8 molecule, all of which perpendicularly intersect the page.

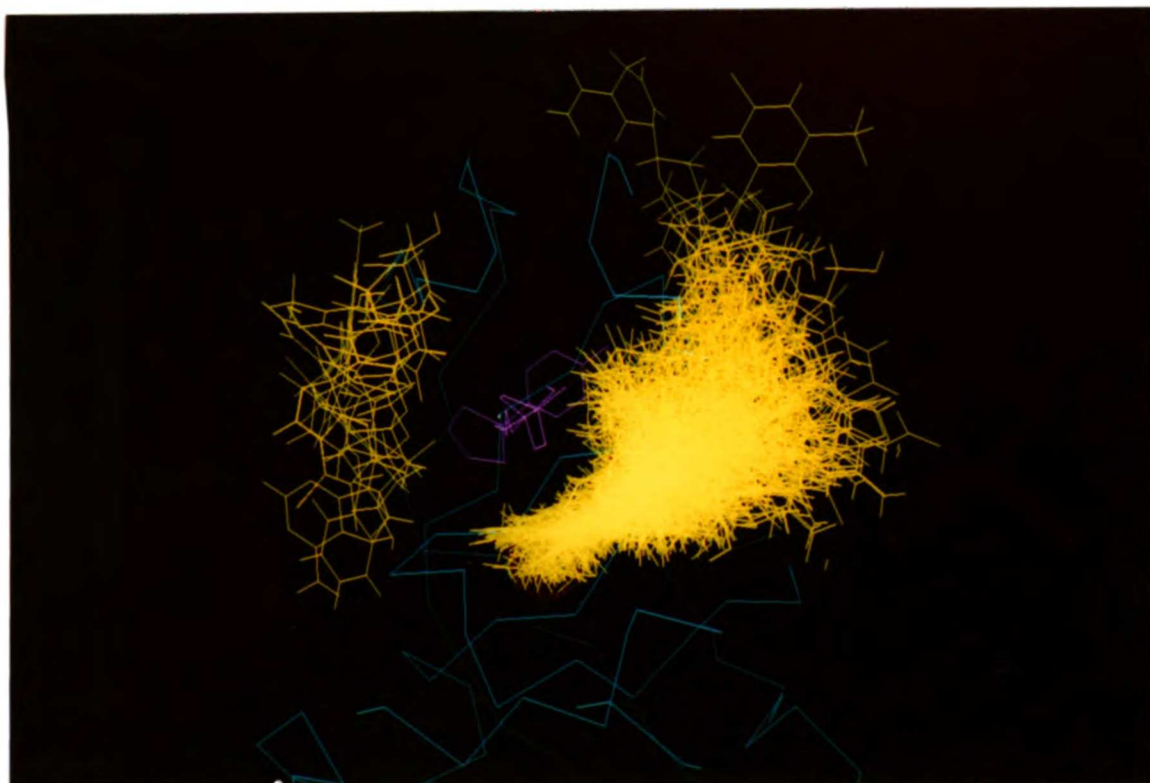


Figure 6.2: Results of the DOCK search of the FCD for ligands complementary to the remaining volume in the UCSF8-bound active site of the HIV-1 protease using the force-field scoring option. The putative ligands are shown in yellow, UCSF8 in magenta, and the enzyme in cyan. Peptide-based inhibitors bind from left to right in this orientation.

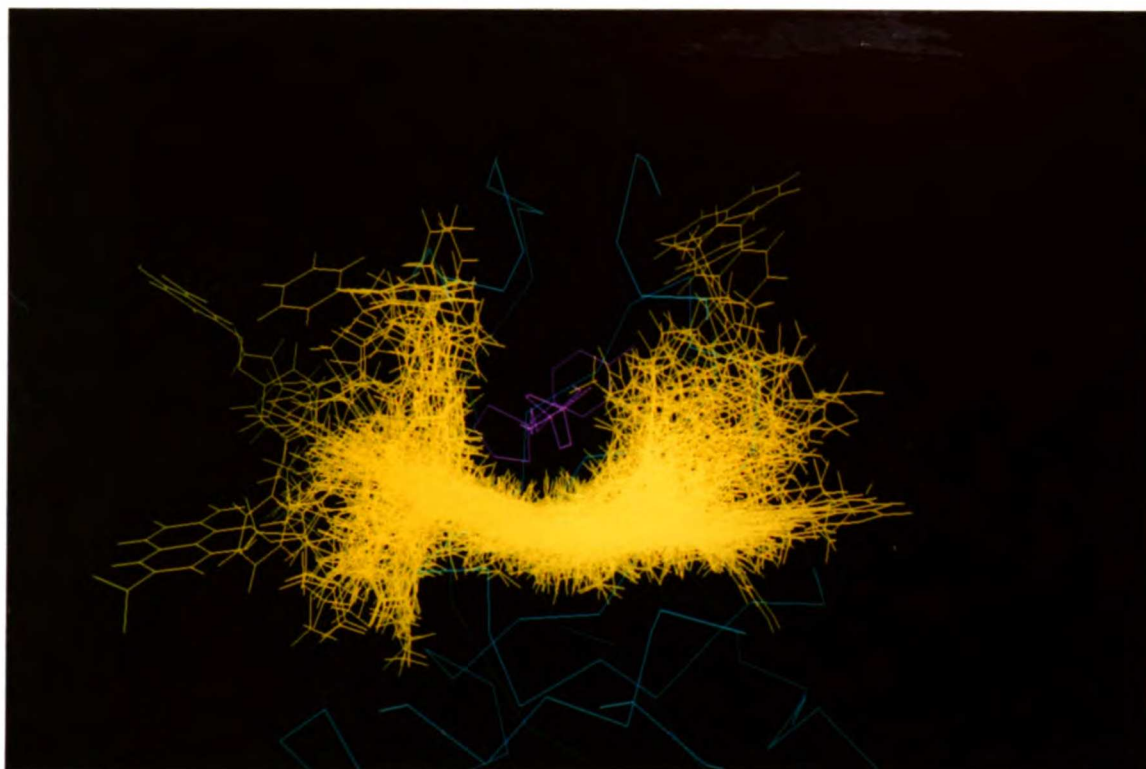


Figure 6.3: Results of the DOCK search of the FCD for ligands complementary to the remaining volume in the UCSF8-bound active site of the HIV-1 protease using the contact only scoring option. The putative ligands are shown in yellow, UCSF8 in magenta, and the enzyme in cyan. Peptide-based inhibitors bind from left to right in this orientation.

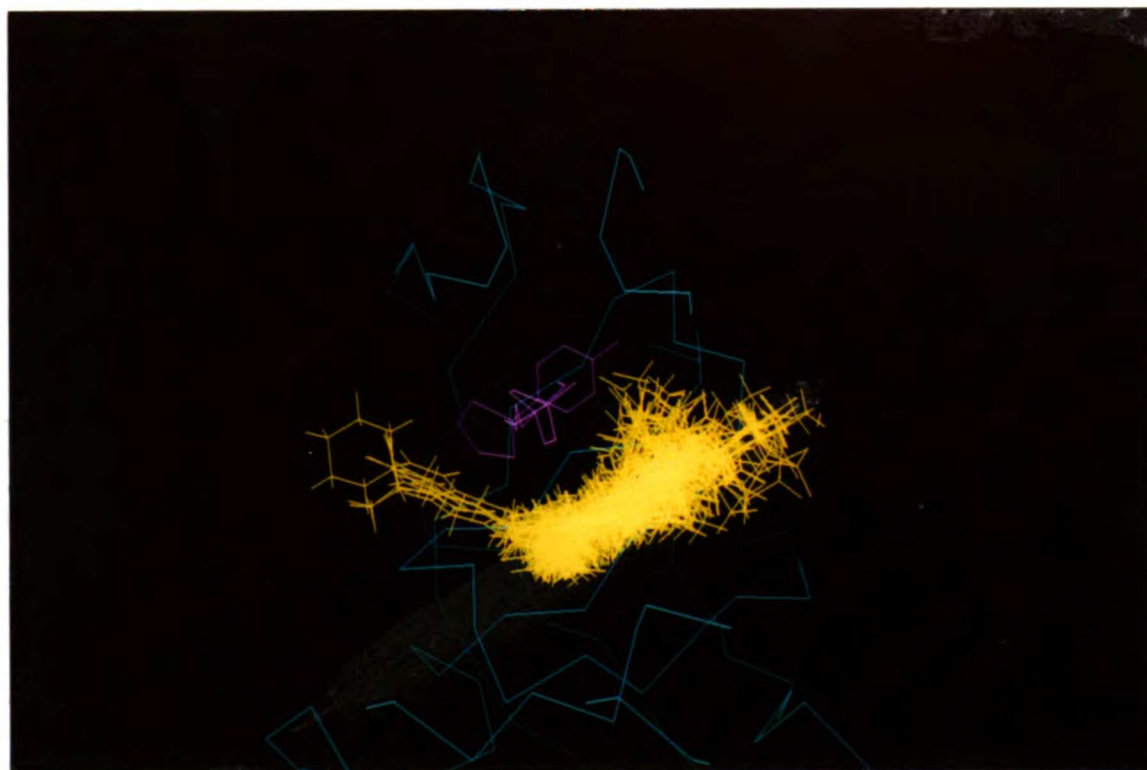


Figure 6.4: Result of the DOCK search of the FCD for ligands complementary to the remaining volume in the UCSF8-bound active site of the HIV-1 protease using the normalized force-field scoring option. The putative ligands are shown in yellow, UCSF8 in magenta, and the enzyme in cyan. Peptide-based inhibitors bind from left to right in this orientation.

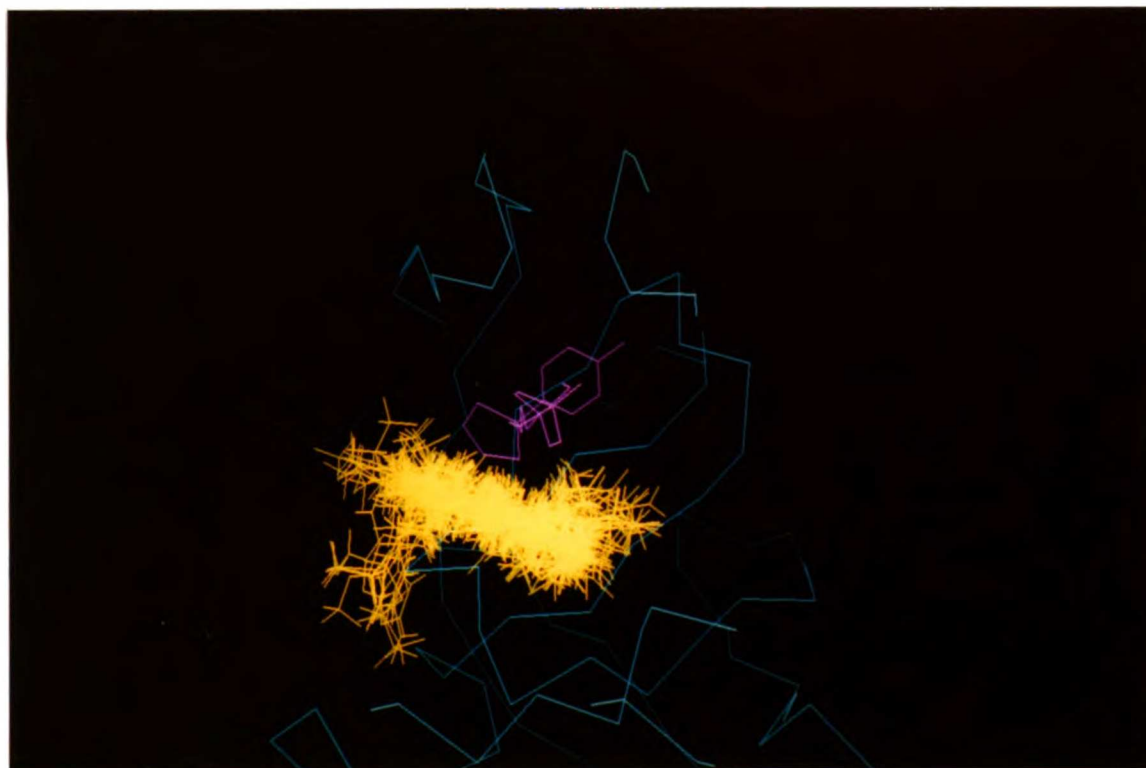


Figure 6.5: Result of the DOCK search of the FCD for ligands complementary to the remaining volume in the UCSF8-bound active site of the HIV-1 protease using the normalized contact scoring option. The putative ligands are shown in yellow, UCSF8 in magenta, and the enzyme in cyan. Peptide-based inhibitors bind from left to right in this orientation.

The observed preferences reflect inherent properties of the remaining volume in the active site. Interaction with the catalytic aspartate residues appears to be a strong determinant for selection when force-field scoring is employed, a task more easily achieved from the fluorophenyl side of the active site. The preference for molecules transversing the site for the ligands scored by contact alone (non-normalized) arises from the interaction with the enzyme surface on their underside and with the bound inhibitor (UCSF8) on the top.

Top candidates from the list of compounds ranked using non-normalized force-field scoring can be assayed for cooperative inhibition in conjunction with UCSF8. The highest scoring molecule was methyl-4-azidobenzoimidate (Figure 6.6). The DOCK orientation places the terminal azido nitrogen atom within hydrogen bonding distance of the catalytic aspartate residues. Most of the steric component of its score is derived from interactions between the aryl moiety of the ligand with the piperidine ring of the bound inhibitor.

Molecules obtained from the lists ranked by normalized scoring, generally being smaller in size, can be considered fragments for attachment to the known inhibitor. Relative to the fragments scored exclusively by the contact method, those scored using the force-field method would presumably require fewer atomic substitutions when engineering chemical complementarity to the protein. A potential attachment site to UCSF8 which has recently been explored (Furth and Caldera, unpublished results) exists at the methylene groups of

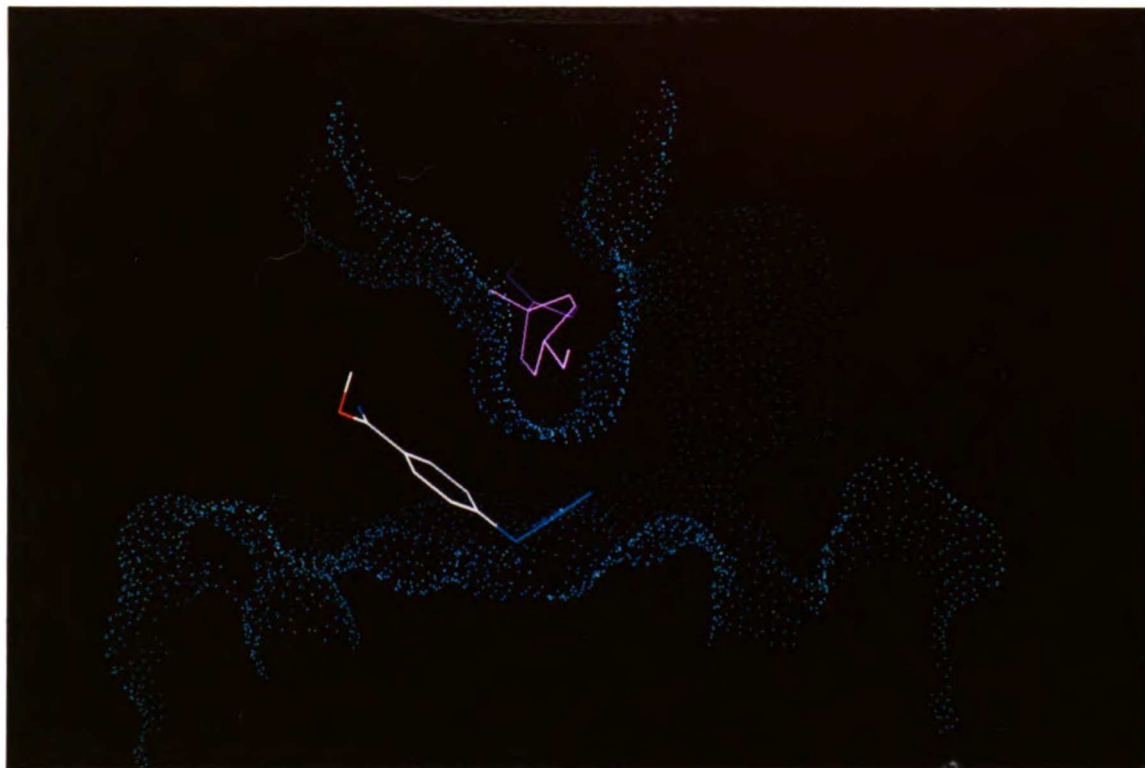
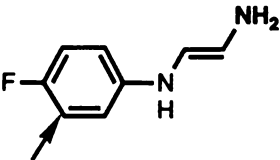

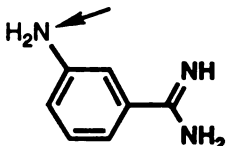
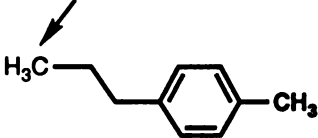
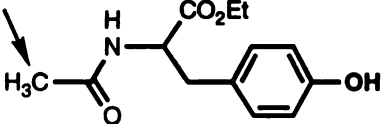
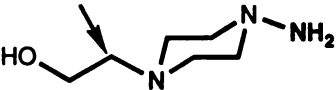


Figure 6.6: DOCK orientation of the top scoring molecule (methyl-4-azidobenzoimidate) obtained from the search for ligands complementary to the remaining volume in the UCSF8-bound active site of the HIV-1 protease. The candidate was selected from those ranked using the force-field scoring option. The putative ligand colored by atom (carbon, white; nitrogen, blue; and oxygen, red) , UCSF8 in magenta, and the solvent accessible surface of the enzyme in cyan.

the thioketal moiety. The DOCK candidates were screened for compounds containing an atom within 5.0 Å, heavy atom-to-heavy atom distance, to one these atoms. Various candidates which fulfilled the criteria are shown in Table 6.1. An analogous procedure can be followed for any synthetically flexible position of the inhibitor.

Methodology for the structure-based discovery of novel HIV-1 protease inhibitors has been described. Lead compounds are initially modified by traditional means, although it may be possible to automate the design of later generation compounds. These techniques can be applied to any target for which the three dimensional structure is known, and therefore comprise a powerful tool for the discovery of drugs.

Compound Ranking*		Distance** to UCSF8 Thioketal Methylene	Distance** to HOH-301†
77FF		4.2 Å	3.0 Å
129FF		4.8 Å	3.1 Å
212FF		4.8 Å	3.0 Å
6CON		3.3 Å	3.1 Å
10CON		2.8 Å	3.2 Å
15CON		3.2 Å	3.2 Å

* FF and CON suffixes indicate the compound was obtained from the normalized force-field and contact scoring lists, respectively.

** Distances are to the closest ligand atom

† HOH-301: water molecule bound to the catalytic aspartate residues

Table 6.1: DOCK candidates with the potential of being attached to a thioketal methylene group of UCSF8.

CHAPTER 7

EXPERIMENTAL

7.1 EQUIPMENT

NMR spectra were obtained on a General Electric QE-300 instrument in CDCl₃. Chemical shifts are reported in parts per million downfield from the internal standard (TMS). Mass spectra were obtained on a VG-70-SE. Infrared spectra were recorded on a Nicolet 5DX FTIR and are reported as cm⁻¹. The programs MidasPlus (Ferrin *et al.*, 1988), SYBYL (Tripos), DGEOM (Blaney, 1990; obtainable through Quantum Chemical Program Exchange), and all versions of DOCK (Desjarlais *et al.*, 1988; Meng *et al.*, 1992) were carried out on an Iris 4D/70 workstation. MACCS-3D (Christie, 1990; Molecular Design) was run on a Vax station 3100 (Digital). The Cambridge Structural Database was obtained from the Cambridge Crystallographic Data Centre. The Fine Chemicals Database (FCD) was obtained as part of the MACCS-3D package (Molecular Design).

7.2 CHEMICALS

Haloperidol (UCSF1), cinnarizine (SF17), flunarizine (SF35), N-FMOC-3,5-diiodo-L-tyrosine (SF33), loperamide (SF36), (±)sulfinpyrazone (SF37), 1,2,3,5-tetra-O-benzoyl xylofuranose (SF38), and

diphenoxylate (SF49) were purchased from Sigma (St. Louis, MO). Pentaerythritol tetrabenzoate (SF44) was purchased from Chemalog (South Plainfield, NJ). 2,5-diphenyl-3-(p-diphenyl)-tetrazolium formazan (SF50) and 2,3-diphenyl-5-(p-diphenyl)-tetrazolium chloride (SF55) were purchased from TCI (Portland, OR). Neotetrazolium chloride diformazan (SF51) was purchased from K&K (Costa Mesa, CA). Pentamethylene bis[triphenyl phosphonium bromide] was purchased from Alfa (Danvers, MA). Protected amino acids were purchased from Bachem (Torrance, CA). Piperidine and piperazine derivatives were purchased from Janssen (distributed through Spectrum, New Brunswick, NJ). All other chemicals and solvents were purchased from Aldrich Chemical Co. (Milwaukee, WI).

7.3 SYNTHETIC METHODS

7.3.1 PURIFICATION OF HALOPERIDOL (UCSF1)

Commercial haldol (Sigma) was recrystallized from diethyl ether/chloroform, 4:1 (vol/vol). The recrystallized material, colorless needles, was shown to be pure by its melting point (mp 148.2-149 °C; lit. 148.0-149.4 °C) (Janssen *et al.*, 1959), NMR, and elemental analysis. An R_f of 0.28 was determined from TLC in 10% MeOH in ethyl acetate.

7.3.2 ADDITIONS TO KETONES BY ORGANOMETALLIC REAGENTS

Procedure 1: To the ketone dissolved in THF, 3-5 equivalents of the organometallic reagent were added by syringe under an argon atmosphere while the solution was stirring over an ice-water bath. The reaction was then allowed to reach room temperature and stirring was continued for two hours. When TLC showed complete disappearance of the starting material, the reaction was stopped by pouring it into a beaker of ice-water. The product was extracted into ether, dried over sodium sulfate, filtered, and rotoevaporated to dryness.

4-[4-(4-Chlorophenyl)-4-hydroxy-1-piperidinyll]-1-(4-fluorophenyl)-1-phenyl-1-butanol (2, UCSF24): Compound 2 was obtained from the reaction of haloperidol with phenyllithium in 90% yield (white powder, melting point 69-71 °C). A single spot with an R_f of 0.68 is observed by TLC (10% methanol in ethyl acetate). The ^1H NMR, IR, and MS are consistent with the assigned structure. The IR spectrum shows loss of the carbonyl stretch present for haldol at 1679 cm^{-1} . Loss of carbonyl is also indicated by the lack of peaks downfield of 8.0 in the ^1H NMR. ^1H NMR δ 6.95 (t, $J = 8.7\text{ Hz}$, 2 H, aromatic α to fluorine), 7.15-7.61 (m, 11 H, other aromatic), 1.5-2.8 ppm (m, broad, 16H, alkyl). MS-CI (NH_3) (m/e) 454 ($\text{M}^+ + 1$). MS-EI (m/e) 376 ($\text{M}^+ - \text{C}_6\text{H}_5$), 224 ($\text{M}^+ - \text{CH}_2\text{CH}_2\text{C}(\text{OH})(\text{C}_6\text{H}_5)(\text{C}_6\text{H}_4\text{F})$). HREI (m/e): Calcd for $\text{C}_{27}\text{H}_{27}\text{NOFCl}$ ($-\text{H}_2\text{O}$): 435.1765. Found: 435.1742.

4-[4-(4-Chlorophenyl)-4-hydroxy-1-piperidinyl]-1-(4-fluorophenyl)-1-benzyl-1-butanol (3. UCSF25): The crude product of the reaction of haldol with benzylmagnesium bromide was purified by column chromatography. The purified product (yellow solid, mp 88-90 °C) was obtained in 73% yield. A single spot with an R_f of 0.65 is observed by TLC in 10% methanol in ethyl acetate. All the spectral data obtained support the desired structure. Both the IR spectrum and the ^1H NMR confirm the loss of the carbonyl group. ^1H NMR δ 6.95 (t, $J = 8.7$ Hz, 2H, aromatic α to fluorine), 6.88-7.47 (m, 11H, other aromatic), 3.06 (s, 2H, benzyl), 1.5-3.3 ppm (m, broad, 16H, alkyl). MS-CI (NH_3) (m/e) 467 ($\text{M}^+ + 1$). MS-EI (m/e) 449 ($\text{M}^+ - \text{HOH}$), 376 ($\text{M}^+ - \text{CH}_2\text{C}_6\text{H}_5$), 358 ($\text{M}^+ - \text{CH}_2\text{C}_6\text{H}_5, -\text{HOH}$), 224 ($\text{M}^+ - \text{CH}_2\text{CH}_2\text{C}(\text{OH})(\text{CH}_2\text{C}_6\text{H}_5) (\text{C}_6\text{H}_4\text{F})$). HREI (m/e): Calcd for $\text{C}_{28}\text{H}_{29}\text{NOFCI} (-\text{H}_2\text{O})$: 449.1922. Found: 449.1915.

4-[4-(4-Chlorophenyl)-4-hydroxy-1-piperidinyl]-1-(2-biphenyl)-1-phenyl-1-butanol (21. UCSF56): The ortho isomer of phenyl diol biphenyl haloperidol was obtained from the reaction of phenyl lithium with 18. Recrystallization from hexane gave a white powder (mp 75-76 °C). The reaction proceeded with a 56% yield. In ethyl acetate, a TLC R_f of 0.49 was obtained. The NMR spectrum was consistent with the structure of the desired compound. Although the resolution is slightly better than for the other phenyl addition compounds, the alkyl proton signals are still quite broad. ^1H NMR δ 7.24-7.97 (m, 18H, aromatic), 2.97 (t, $J = 7.1$ Hz, 2H, butyl α to N), 2.62 (m, 2H, piperidine (eq) α to N), 2.35 (t, $J = 7.1$ Hz, 2H, butyl γ to

N), 2.13-2.26 (m, 2H, piperidine (ax) α to N), 1.92 (m, 2H, butyl β to N), 1.82 (m, 2H, piperidine (ax) β to N), 1.60 ppm (m, 2H, piperidine (eq) β to N). MS-CI (NH₃) (*m/e*) 512 (M⁺ + 1), 494 (- HOH), 476 (- 2HOH), 224 (- CH₂CH₂C(OH)(CH₂C₆H₅) (C₁₂H₉)). HREI (*m/e*): Calcd for C₃₃H₃₄NO₂Cl: 511.2278. Found: 511.2238.

4-[4-(4-Chlorophenyl)-4-hydroxy-1-piperidinyl]-1-(3-biphenyl)-1-phenyl-1-butanol (22, UCSF57): The meta isomer of phenyl diol biphenyl haldol was obtained from the reaction of phenyl lithium with 19. Recrystallization from hexane gave a white powder (mp 70-72 °C). The product was obtained in 61 % yield. In ethyl acetate, a TLC R_f of 0.52 was obtained. The NMR spectrum was consistent with the structure of the desired compound. ¹H NMR δ 7.84 (s, 1H, aromatic α to main chain and phenyl), 7.15-7.56 (m, 17H, other aromatic), 1.26-2.66 ppm (m, 16H, alkyl). MS-CI (NH₃) (*m/e*) 512 (M⁺ + 1), 494 (- HOH), 476 (- 2HOH), 224 (- CH₂CH₂C(OH)(CH₂C₆H₅) (C₁₂H₉)). HREI (*m/e*): Calcd for C₃₃H₃₄NO₂Cl: 511.2278. Found: 511.2276.

4-[4-(4-Chlorophenyl)-4-hydroxy-1-piperidinyl]-1-(4-biphenyl)-1-phenyl-1-butanol (23, UCSF33): Phenyl diol p-biphenyl haldol was obtained from the reaction of 20 with phenyl lithium. A single spot is evident by TLC, R_f of 0.67 (10% methanol in ethyl acetate). The product was purified by flash chromatography using a gradient from 100% CH₂Cl₂ to 100% ethyl acetate as eluent. No suitable recrystallization solvent system was found; however, the desired

compound is somewhat soluble in hot hexane whereas the impurities seem to remain behind. The resulting white powder (mp 100-101 °C) was obtained in 50% yield. The spectral data collected on the product confirms its desired structure. ¹H NMR δ 7.17-7.56 (m, 18H, aromatic), 1.25-2.62 ppm (m, 16H, alkyl). MS-CI (NH₃) (*m/e*) 512 (M⁺ + 1), 494 (- HOH). HREI (*m/e*): Calcd for C₃₃H₃₄NO₂Cl: 511.2278. Found: 511.2268.

Procedure 2: To a 100 ml 3-neck round-bottom flask equipped with a stirrer and a condenser, magnesium turnings (1 eq.) were added to 50 ml of dry ether before 0.7 equivalents of cyclopropyl bromide were added slowly by syringe through a septum. The reaction began refluxing spontaneously and was allowed to proceed under argon until the refluxing stopped. At this point, the reaction vessel was cooled with an ice-water bath and the biphenylcarboxaldehydes (0.5 eq.) were added in a minimal amount of ether. The reaction was then removed from the ice-water bath and allowed to proceed at room temperature for several hours. A more polar product and disappearance of starting material were evident by TLC. The reaction was quenched by pouring it into a beaker of ice-water. The ether layer was separated and collected, and the aqueous layer was extracted with two volumes of ether. The combined ether washings were dried with sodium sulfate, filtered, and rotoevaporated to dryness.

Ortho-biphenyl cyclopropyl methanol (11): The crude product of the reaction of **8** with cyclopropyl magnesium bromide was separated by

flash chromatography using a gradient from 50:50 pentane:CH₂Cl₂ to 100% ethyl acetate. Initially, a clear, viscous liquid was obtained which slowly crystallized (mp 84-85.5 °C) with an overall yield of 80%. The R_f by TLC in CH₂Cl₂ is 0.26. IR (KBr disk) 3369 (b) OH. ¹H NMR δ 7.22-7.77 (m, 9H, aromatic), 4.16 (dd, *J* = 2.7 Hz, *J* = 8.0 Hz, 1H, -CHOH-), 1.81 (d, *J* = 3.0 Hz, 1H, -OH), 1.22 (m, 1H, cyclopropyl methyne), 0.26-0.57 ppm (m, 4H, cyclopropyl methylenes). MS-EI (*m/e*) 224 (M⁺), 206 (-HOH), 196 (-CH₂CH₂), 178 (-CH₂CH₂ & HOH), 165 (-C₃H₅ & HOH), and 152 (biphenyl). HREI (*m/e*): Calcd for C₁₆H₁₆O: 224.1201. Found: 224.1196.

Meta-biphenyl cyclopropyl methanol (12): The crude product of the reaction of **9** with cyclopropyl magnesium bromide was separated by flash chromatography using a gradient from 50:50 pentane:CH₂Cl₂ to 100% ethyl acetate. Compound **12**, a clear liquid, was obtained with an overall yield of 85%. The R_f by TLC in CH₂Cl₂ is 0.26. IR (neat) 3369 (b) OH. ¹H NMR δ 7.26-7.66 (m, 9H, aromatic), 4.09 (dd, *J* = 2.9 Hz, *J* = 8.3 Hz, 1H, -CHOH-), 1.99 (d, *J* = 2.9 Hz, 1H, -OH), 1.27 (m, 1H, cyclopropyl methyne), 0.40-0.69 ppm (m, 4H, cyclopropyl methylenes). MS-EI (*m/e*) 224 (M⁺), 196 (-CH₂CH₂), 181, 167, and 152 (biphenyl). HREI (*m/e*): Calcd for C₁₆H₁₆O: 224.1201. Found: 224.1196.

Para-biphenyl cyclopropyl methanol (13): The para isomer of biphenyl cyclopropyl methanol (**13**), obtained from the reaction of **10** with cyclopropyl magnesium bromide (65% crude yield), was

used in the subsequent reaction without further purification or characterization.

7.3.3 LAH REDUCTIONS OF BIPHENYL ACIDS

General Procedure: The carboxylic acid was dissolved in ether in a round-bottom flask. Excess LAH was added slowly while the solution was stirring over an ice-water bath. The mixture was removed from the ice bath and stirring was continued for one hour at room temperature. Upon disappearance of the starting material by TLC, the reaction was quenched by addition of ethyl acetate followed by a small amount of water. The reaction mixture was filtered, and the filtrate was dried over sodium sulfate, filtered, and rotoevaporated to dryness.

Ortho-biphenyl methanol (6): The product of the LAH reduction of **4** was a liquid at room temperature and proceeded in near quantitative yield. An R_f of 0.74 was found in ethyl acetate and about 0.27 in dichloromethane. The loss of the carbonyl group and presence of the alcohol was evident from the IR spectrum. IR (neat) 3444 (b) OH. ^1H NMR δ 7.24-7.54 (m, 9H, aromatic), 4.56 ppm (s, 2H, methylene). MS-EI (m/e) 184 (M^+), 167 ($M^+ - \text{OH}$). The product was used in the next step without further purification.

Meta-biphenyl methanol (7): Compound **7** was obtained from the reduction of **5** by LAH. The product, which was a liquid at room

temperature, was obtained in nearly quantitative yield. The R_f of 7 was about 0.74 in ethyl acetate, and about 0.27 in CH_2Cl_2 . The product was characterized by MS, IR, and NMR. The loss of the carbonyl group and presence of the alcohol was evident from the IR spectrum. IR (neat) 3447 (b) OH. ^1H NMR δ 7.20-7.69 (m, 9H, aromatic), 4.56 ppm (s, 2H, methylene). MS-EI (m/e) 184 (M^+), 165 ($\text{M}^+ - \text{HOH}$). The product was used in the next step without further purification.

7.3.4 PYRIDINIUM CHLOROCHROMATE (PCC) OXIDATIONS

General Procedure: PCC oxidations were carried out using the method of Corey and Suggs (1975). 2-3 equivalents of pyridinium chlorochromate were suspended in CH_2Cl_2 and the alcohol was rapidly added at room temperature. The solution turned brown before a black solid, the reduced reagent, slowly precipitated out. The mixture was allowed to stir at room temperature for 3 hours, at which time a small amount was removed, worked up as described below, and analyzed by TLC. If starting material was still present, more PCC was added and the reaction was continued. When the reaction seemed complete, the mixture was diluted with several volumes of ether and was filtered through a sintered glass funnel filled with Florisil (the solution became clear). The black solid was washed several times with ether and the solvent was filtered as above. The filtrates were combined and rotoevaporated to dryness.

Ortho-phenylbenzaldehyde (8): Ortho biphenyl alcohol (6) was oxidized to aldehyde 8 with PCC. Purification by flash chromatography using a gradient from 100% pentane to 100% CH₂Cl₂ as eluent resulted in a clear liquid. An R_f of 0.71 was found in CH₂Cl₂. The reaction proceeded with a yield of 79%. IR (neat) 1694 (s) carbonyl. ¹H NMR δ 9.99 (s, 1H, aldehydic proton), 7.36-8.05 ppm (m, 9H, aromatic). MS-EI (*m/e*) 182 (M⁺), 152 (M⁺ - CHO).

Meta-phenylbenzaldehyde (9): Compound 7 was oxidized to meta-phenylbenzaldehyde (9) using PCC. A clear liquid was obtained after purification by flash chromatography using a gradient from 100% pentane to 100% CH₂Cl₂. 9 has an R_f of 0.71 in CH₂Cl₂. The reaction proceeded in 85% yield. IR (neat) 1694 (s) carbonyl. ¹H NMR δ 10.09 (s, 1H, aldehydic proton), 8.11 (s, 1H, aromatic α to aldehyde and phenyl), 7.40-7.88 ppm (m, 8H, aromatic). MS-EI (*m/e*) 182 (M⁺), 152 (M⁺ - CHO).

Ortho-biphenyl cyclopropyl ketone (14): Ortho-biphenyl cyclopropyl ketone, 14, was obtained from the oxidation of 11 by PCC. Purification by flash chromatography (pentane to CH₂Cl₂ gradient) yielded a viscous liquid which crystallized (mp 81-82.5 °C) during refrigerated storage. The overall yield of the reaction was 60%. IR (KBr disk) 1673 (s) carbonyl. ¹H NMR δ 7.30-7.68 (m, 9H, aromatic), 1.70 (m, 1H, cyclopropyl methyne), 1.05 (m, 2H) and 0.62 ppm (m, 2H) cyclopropyl methylenes. MS-EI (*m/e*) 222 (M⁺), 194 (M⁺ - C₂H₄), 181 (M⁺ - C₃H₅), 165 (M⁺ - OC₃H₅), 152 (biphenyl). HREI (*m/e*): Calcd for C₁₆H₁₄O: 222.1045. Found: 222.1038.

Meta-biphenyl cyclopropyl ketone (15): Meta-biphenyl cyclopropyl ketone, **15**, was obtained from the oxidation of **12** by PCC. Purification by flash chromatography (pentane to CH₂Cl₂ gradient), yielded a viscous liquid. A 71% yield for the reaction was obtained. IR (KBr disk) 1673 (s) carbonyl. ¹H NMR δ 7.35-8.24 (m, 9H, aromatic), 2.74 (m, 1H, cyclopropyl methyne), 1.28 (m, 2H) and 1.09 ppm (m, 2H) cyclopropyl methylenes. MS-EI (*m/e*) 222 (M⁺), 181 (M⁺ - C₃H₅), 165 (M⁺ - OC₃H₅), 152 (biphenyl). HREI (*m/e*): Calcd for C₁₆H₁₄O: 222.1045. Found: 222.1047.

Para-biphenyl cyclopropyl ketone (16): The alcohol functionality of **13** was oxidized to a ketone using PCC. A TLC of the reaction products revealed a major product spot with an R_f of 0.71 in CH₂Cl₂. The product was purified by flash chromatography using a slow gradient from 100% pentane to 100% CH₂Cl₂ as the eluent. The resulting white solid had a melting point of 106-108 °C. A 70% yield for the reaction was obtained. IR (KBr disk) 1666 (s) carbonyl. ¹H NMR δ 7.40-8.19 (m, 9H, aromatic), 2.72 (m, 1H, cyclopropyl methyne), 1.27 (m, 2H) and 1.06 ppm (m, 2H) cyclopropyl methylenes. MS-EI (*m/e*) 222 (M⁺), 181 (M⁺ - C₃H₅), 152 (biphenyl). HREI (*m/e*): Calcd for C₁₆H₁₄O: 222.1045,. Found: 222.1032.

7.3.5 ALPHA KETO CYCLOPROPYL RING OPENINGS

General Procedure: To the biphenyl cyclopropyl ketone in approximately 50 ml of xylene in a 100 ml pear-shaped flask, a slight excess of 4-(4 chlorophenyl)-4-hydroxypiperidine (**17**) was added by pipet as a suspension in xylene (**17** is not soluble in xylene at room temperature, but dissolves completely at reflux temperature). The flask was equipped with a condenser and heated in an oil bath with stirring until the solution began to reflux. Refluxing was continued for 3-5 days. The reaction was allowed to cool to room temperature at which point a large amount of solid precipitated out. The xylene was removed using a rotary evaporator.

4-[4-(4-Chlorophenyl)-4-hydroxy-1-piperidinyl]-1-(2-biphenyl)-1-butanone (**18**, UCSF51): The crude product of the reaction of **14** and **17** was purified by flash chromatography using a slow gradient from 100% CH₂Cl₂ to 10% methanol in ethyl acetate as eluent. The product off the column was an orange liquid. Recrystallization from hexane afforded white crystals (mp 96-97 °C) in 10% yield. Spectral data supports the assigned structure. IR (KBr disk) 1694 (s) carbonyl. ¹H NMR δ 7.31-7.55 (m, 13H, aromatic), 2.62 (td, *J* = 2.4 Hz, *J* = 11.6 Hz, 2H, piperidine (eq) α to N), 2.31 (t, *J* = 7.2 Hz, 2H, butyl α to N), 2.28 (dt, *J* = 2.4 Hz, *J* = 11.6 Hz, 2H, piperidine (ax) α to N), 2.17 (t, *J* = 7.4 Hz, 2H, butyl α to carbonyl), 1.99 (dt, *J* = 4.3 Hz, *J* = 13.0 Hz, 2H, piperidine (ax) β to N), 1.66 ppm (m, 4H, butyl β to N and piperidine

(eq) β to N). MS-CI (NH_3) (m/e) 434 ($M + 1$), 416 ($- \text{HOH}$), 237, 224. HREI (m/e): Calcd for $\text{C}_{27}\text{H}_{28}\text{NO}_2\text{Cl}$: (433.1809). Found: (433.1822).

4-[4-(4-Chlorophenyl)-4-hydroxy-1-piperidinyl]-1-(3-biphenyl)-1-butanone (19, UCSF52): The products of the reaction of **15** and **17** were purified by flash chromatography using a slow gradient from 100% CH_2Cl_2 to 10% methanol in ethyl acetate as eluent. The desired compound was recrystallized from hexane, resulting in white crystals with a melting point of 99-100 °C (20% yield). Spectral data supports the assigned structure. IR (KBr disk) 1687 (s) carbonyl. ^1H NMR δ 8.23 (s, 1H, aromatic α to carbonyl and phenyl), 7.22-7.98 (m, 12H, other aromatic), 3.05 (t, $J = 6.9$ Hz, 2H, butyl α to carbonyl), 2.78 (td, $J = 2.9$ Hz, $J = 11.3$ Hz, 2H, piperidine (eq) α to N), 2.50 (t, $J = 7.0$ Hz, 2H, butyl α to N), 2.40 (dt, $J = 2.2$ Hz, $J = 11.3$ Hz, 2H, piperidine (ax) α to N), 2.04 (m, 2H, butyl β to N), 1.93 (dt, $J = 3.9$ Hz, $J = 12.6$ Hz, 2H, piperidine (ax) β to N), 1.63 ppm (d, $J = 12.0$ Hz, 2H, piperidine (eq) β to N). MS-EI (m/e) 433.(M^+), 415 ($M^+ - \text{HOH}$), 237, 224. HREI (m/e): Calcd for $\text{C}_{27}\text{H}_{28}\text{NO}_2\text{Cl}$: (433.1809). Found: (433.1828).

4-[4-(4-Chlorophenyl)-4-hydroxy-1-piperidinyl]-1-(4-biphenyl)-1-butanone (20, UCSF36): The crude product mixture of the alkylation of **17** by **16** was separated by flash chromatography using a slow gradient from 100% CH_2Cl_2 to 10% methanol in ethyl acetate as eluent. The desired product was the most polar of the components, with and R_f of 0.41 in 10% methanol in ethyl acetate. The yellowish solid was recrystallized from CH_2Cl_2 yielding colorless needles (mp 166-167 °C (d)) of **20** in 12% yield. Spectral analysis supported the

assigned structure. IR (KBr disk) 1680 (s) carbonyl, 3093 (b) OH. ^1H NMR δ 7.27-8.08 (m, 13H, aromatic), 3.04 (t, $J = 6.7$ Hz, 2H, butyl α to carbonyl), 2.80 (td, $J = 2.7$ Hz, $J = 11.2$ Hz, 2H, piperidine (eq) α to N), 2.70 (t, $J = 6.9$ Hz, 2H, butyl α to N), 2.42 (dt, $J = 2.3$ Hz, $J = 11.2$ Hz, 2H, piperidine (ax) α to N), 2.03 (m, 2H, butyl β to N), 1.99 (dt, $J = 3.9$ Hz, $J = 12.5$ Hz, 2H, piperidine (ax) β to N), 1.67 ppm (d, $J = 12.2$ Hz, 2H, piperidine (eq) β to N). MS-CI (NH_3) (m/e) 434 ($\text{M}+1$), 416 (-HOH). HREI (m/e): Calcd for $\text{C}_{27}\text{H}_{26}\text{NOCl}$ (-HOH): 415.1702. Found: 415.1671.

7.3.6 THIOKETALIZATION

4-[4-(4-Chlorophenyl)-4-hydroxy-1-piperidinyl]-1-(3-biphenyl)-1-(2,5-dithiane) butane (24, UCSF59): To 150 mg (0.346 mmol) of **20** and 100 μl of ethanedithiol (1.2 mmol) in dry methanol, 500 μl of $\text{BF}_3 \cdot \text{OEt}_2$ was added dropwise. The solution was allowed to stir for 2 days. Quenching was accomplished by transferring the reaction mixture into saturated NaHCO_3 followed by extraction into ether. The ether layer was washed with saturated NaCl . The aqueous layers were combined and re-extracted with ether. The combined ether extracts were dried over Na_2SO_4 , filtered, and rotoevaporated to dryness. The product was separated by flash chromatography using a slow gradient from 100% CH_2Cl_2 to 100% ethyl acetate as eluent. A sticky yellowish solid was obtained after the purification. The ^1H NMR spectrum supports the assigned structure. ^1H NMR δ 7.94 (s, 1H, aromatic α to carbonyl and phenyl), 7.28-7.69 (m, 12H, other aromatic), 3.29 (m, 2H) and 3.40 (m, 2H) thioketal methylenes, 2.70

(d, $J = 10.7$ Hz, 2H, piperidine (eq) α to N), 2.28-2.46 (m, 6H, butyl α to carbonyl, piperidine (ax) α to N, and butyl β to N), 2.05 (dt, $J = 3.0$ Hz, $J = 12.2$ Hz, 2H, piperidine (ax) β to N), 1.50-1.67 ppm (m, 4H, butyl α to thioketal and piperidine (eq) β to N). MS-CI (NH_3) (m/e) 510 ($M+1$), 492 (-HOH), 450 (- $\text{CH}_2\text{CH}_2\text{S}$). HREI (m/e): Calcd for $\text{C}_{29}\text{H}_{30}\text{NS}_2\text{Cl}$ (-HOH): 491.1508. Found: 491.1489.

7.3.7 N-OXIDATION

4-[4-(4-Chlorophenyl)-4-hydroxy-1-oxo-1-piperidinyl]-1-(3-biphenyl)-1-butanone (25, UCSF67): The N-oxide of meta-biphenyl haloperidol was prepared by the reaction of **19** with hydrogen peroxide. To 70 mg (160 μM) of crude **19** in about 5 ml of CH_2Cl_2 , 800 μl of 30% H_2O_2 (about a 50-fold excess) was added slowly via a syringe while the solution was stirring over an ice-water bath. The ice bath was removed and the solution was allowed to stir at room temperature. After 20 hours, TLC revealed that all the starting material was gone. The desired product, a white precipitate, coated the reaction vessel. The product did not move from the origin by TLC. Recrystallization from acetone gave a white powder (mp 177-179 $^\circ\text{C}$ (d)) in 82% yield. Spectral data supported the desired structure. IR (KBr disk) 1684 (s) carbonyl, 1560 (s) N-O. ^1H NMR δ 8.15 (s, 1H, aromatic α to carbonyl and phenyl), 7.28-7.92 (m, 12H, other aromatic), 3.65 (t, $J = 11.3$ Hz, 2H, butyl α to N), 3.20-3.50 (m, 6H, piperidine (eq) α to N, butyl α to N, and piperidine (ax) α to N), 2.64 (dt, $J = 3.4$ Hz, $J = 13.1$ Hz, 2H, piperidine (ax) β to N), 2.25 (m, 2H, butyl β to N), 1.62 ppm (d, $J = 13.7$ Hz, 2H, piperidine (eq) β to N).

MS-CI (NH₃) (*m/e*) 450 (M+1) 434 (- O). HREI (*m/e*): Calcd for C₂₇H₂₄NOCl (-2HOH): 413.1546. Found: 413.1525.

7.3.8 ACYLATION OF HETEROCYCLIC AMINES

The general procedure for the preparation of **31-38** is: To 1.0 mmol of the heterocyclic amine in CH₂Cl₂ containing 1 equivalent of triethyl amine, 1 equivalent of the acid chloride, also in CH₂Cl₂, is added (2 equivalents of triethyl amine and acid chloride are added when reacting with both nitrogen atoms of piperazine). The reaction was allowed to stir at room temperature for one hour. The products were partitioned between brine and CH₂Cl₂. The organic layer was dried with Na₂SO₄, filtered through a silica gel plug with ethyl acetate, and rotoevaporated to dryness. The products were purified by flash chromatography using an ethyl acetate-hexane gradient as eluent.

3,3-Diphenyl propionoyl chloride (30): A 0.5 M solution of **30** in CH₂Cl₂ was prepared. To 2.263 g (10 mmol) of 3,3-diphenyl propionic acid in 20 ml of solvent stirring in an ice-water bath, 0.87 ml (10 mmol) of oxalyl chloride was added. A few drops of DMF were added to catalyze the reaction, which resulted in gas evolution. The reaction was complete after 15 min of stirring. The resulting solution was used in subsequent reactions without further purification.

1,4-Bis-(2,2-diphenylethyl)piperazine diamide (31, UCSF135): The reaction of diphenyl acetyl chloride (**29**) and piperazine proceeded

with an 84% yield. The product was a white powder (mp >270 °C) ¹H NMR δ 7.19-7.33 (m, 20H, aromatic), 5.16 (s, 1H) and 5.06 (s, 1H) benzyl (2 isomers), 3.67 (s, 2H), 3.42 (s, 2H), 3.40 (s, 2H), and 3.11 ppm (s, 2H) piperidino. MS-CI (NH₃) (*m/e*) 475 (M+1), 308 (-C(C₆H₅)₂), 281 (-COCH(C₆H₅)₂), 168. HREI (*m/e*): Calcd for C₃₂H₃₀N₂O₂: 474.2307. Found: 474.2299.

1.4-Bis-(3.3-diphenylpropyl)piperazine diamide (32, UCSF136): A white solid (mp 186-187 °C) was obtained from the reaction of **30** and piperazine (32% yield). The TLC had a single spot with an R_f of 0.24 in 40% ethyl acetate. ¹H NMR δ 7.16-7.41 (m, 20H, aromatic), 4.61 (t, *J* = 7.5 Hz, 2H, benzyl), 3.02 (d, *J* = 7.5 Hz, 4H, -CO-CH₂-), 3.37 (s, 2H), 3.15 (s, 2H), 3.16 (s, 2H), and 2.87 ppm (s, 2H) piperidino. MS-CI (NH₃) (*m/e*) 503 (M+1), 295 (-COCH₂CH(C₆H₅)₂), 180, 167. HREI (*m/e*): Calcd for C₃₄H₃₄N₂O₂: 502.2620. Found: 502.2607.

1-(2.2-Diphenyl-1-oxoethyl)-4-(bis-(4'-fluorophenyl)methyl)piperazine (33, UCSF137): A viscous clear liquid was obtained from acylation of **27** with **29** (90% yield). The TLC had a single spot with an R_f of 0.55 in 40% ethyl acetate. ¹H NMR δ 7.25-7.34 (m, 10H, phenyl), 7.20 (t, *J*=7.5 Hz, 4H) and 6.95 (t, *J* = 8.6 Hz, 4H) fluorophenyl β and α to the fluorine respectively, 5.15 (s, 0.5H) and 5.05 (s, 0.5H) -CH(C₆H₅)₂ (2 isomers), 4.15 (s, 1H, -CH(*p*-F-C₆H₄)₂), 3.69 (t, *J* = 5.0 Hz, 2H) and 3.43 (t, *J* = 4.7 Hz, 2H) -(CH₂)₂N-CO-, 2.33 (t, *J* = 4.8 Hz, 2H) and 2.12 ppm (t, *J* = 4.7 Hz, 2H) -(CH₂)₂N-CH(*p*-F-C₆H₄)₂. MS-CI (NH₃) (*m/e*) 483 (M+1), 280 (- (C₆H₄F)₂CH), 203 ((C₆H₄F)₂CH), 183,

167. HREI (*m/e*): Calcd for C₃₁H₂₈N₂O₂F₂: 482.2170. Found: 482.2182.

1-(3,3-Diphenyl-1-oxopropyl)-4-(bis-(4'-fluorophenyl)methyl)piperazine (34, UCSF138): A sticky solid was obtained from the acylation of **27** with **30** (56% yield). The TLC had a single spot with an R_f of 0.40 in 40% ethyl acetate. ¹H NMR δ 7.14-7.46 (m, 14H, phenyl and fluorophenyl β to the fluorine), 6.96 (t, *J* = 8.5 Hz, 4H, fluorophenyl α to the fluorine), 4.62 (t, *J* = 7.4 Hz, 1H, -CH₂-CH(C₆H₅)₂), 4.11 (s, 1H, -CH(*p*-F-C₆H₄)₂), 3.52 (t, *J* = 5.4 Hz, 4H) and 3.31 (t, *J* = 4.5 Hz, 4H) -(CH₂)₂N-CO-, 3.01 (d, *J* = 7.5 Hz, 2H, -CO-CH₂-), 2.19 (t, *J* = 4.6 Hz, 2H) and 2.03 ppm (s, 2H) -(CH₂)₂N-CH(*p*-F-C₆H₄)₂. MS-CI (NH₃) (*m/e*) 497 (M+1), 293 (- (C₆H₄F)₂CH), 245, 203 ((C₆H₄F)₂CH), 167. HREI (*m/e*): Calcd for C₃₂H₃₀N₂OF₂: 496.2326. Found: 496.2321.

4-(Diphenylhydroxymethyl)-1-(2,2-diphenyl-1-oxoethyl)piperidine (35, UCSF139): A white powder (mp 83-85 °C) was obtained from the reaction of diphenyl acetyl chloride (**29**) and 4-(diphenyl hydroxymethyl) piperidine, **28**, after purification by flash chromatography. The product had an R_f of 0.45 on silica TLC in 40% EtOAc-hexane and was recovered in 87% yield. ¹H NMR δ 7.15-7.44 (m, 20H, aromatic), 5.17 (s, 1H, benzyl), 4.77 (d, *J* = 13.2 Hz, 1H, -CH(eq)H-N *cis* to carbonyl), 3.95 (d, *J* = 13.5 Hz, 1H, -CH(eq)H-N *trans* to carbonyl), 2.92 (dt, *J* = 2.4 Hz, *J* = 13.3 Hz, 1H, -CH(ax)H-N *cis* to carbonyl), 2.60 (m, 1H, -CH(ax)H-N *trans* to carbonyl), 2.56 (m, 1H, 4-piperidino proton), 1.57 (m, 2H, -CH(eq)H-CH₂-N-), 1.33 (m, 1H, -

CH(ax)H-CH₂-N- *cis* to carbonyl), 1.00 ppm (m, 1H, -CH(ax)H-CH₂-N-*trans* to carbonyl). MS-CI (NH₃) (*m/e*) 462 (M+1), 444 (-HOH). HREI (*m/e*): Calcd for C₃₂H₂₉NO (-HOH): 443.2249. Found: 443.2240.

4-(Diphenylhydroxymethyl)-1-(3,3-diphenyl-1-oxopropyl)

piperidine (36, UCSF163): A white solid (mp 83-84 °C) was obtained in 30% yield from the reaction of 28 and 3,3-diphenyl propionoyl chloride (30). An R_f of 0.34 was determined in 40% EtOAc-hexane. ¹H NMR δ 7.15-7.47 (m, 20H, aromatic), 4.62 (t, *J* = 7.5 Hz, 1H, benzyl), 3.80 (d, *J* = 13.3 Hz, 1H, -CH(eq)H-N *cis* to carbonyl), 2.93-3.10 (q_{AB}, 2H, -CO-CH₂-), 3.06 (m, 1H, -CH(eq)H-N *trans* to carbonyl), 2.83 (dt, *J* = 2.3 Hz, *J* = 13.2 Hz, 1H, -CH(ax)H-N *cis* to carbonyl), 2.53 (m, 1H, 4-piperidino proton), 2.43 (dt, *J* = 2.4 Hz, *J* = 13.0 Hz, 1H, -CH(ax)H-N *trans* to carbonyl), 1.50 (d, *J* = 13.3 Hz, 1H, -CH(eq)H-CH₂-N- *cis* to carbonyl), 1.34 (d, *J* = 13.2 Hz, 1H, -CH(eq)H-CH₂-N- *trans* to carbonyl), 1.14 (m, 1H, -CH(ax)H-CH₂-N- *cis* to carbonyl), 0.86 ppm (m, 1H, -CH(ax)H-CH₂-N-*trans* to carbonyl). MS-EI (*m/e*) 475 (M⁺), 457 (-HOH), 290, 167. HREI (*m/e*): Calcd for C₃₃H₃₃NO₂: 475.2511. Found: 475.2494.

1-(2,2-Diphenyl-1-oxoethyl)-4-(4'-chlorophenyl)-4-piperidinol (37, UCSF164): Compound 37 was obtained in quantitative yield from the reaction of 17 and 29. The product had an R_f of 0.22 on silica TLC in 40% EtOAc-hexane. The white solid had a melting point of 173-175 °C. ¹H NMR δ 7.20-7.44 (m, 14H, aromatic), 5.27 (s, 1H, benzyl), 4.67 (td, *J* = 2.2 Hz, *J* = 13.3 Hz, 1H, -CH(eq)H-N *cis* to carbonyl), 3.84 (td, *J* = 2.1 Hz, *J* = 13.5 Hz, 1H, -CH(eq)H-N *trans* to carbonyl), 3.46 (dt, *J* =

2.8 Hz, $J = 13.0$ Hz, 1H, -CH(ax)H-N *cis* to carbonyl), 3.12 (dt, $J = 2.9$ Hz, $J = 12.9$ Hz, 1H, -CH(ax)H-N *trans* to carbonyl), 1.94 (dt, $J = 4.6$ Hz, $J = 13.4$ Hz, 1H, -CH(ax)H-CH₂-N- *cis* to carbonyl), 1.68 (dd, $J = 2.5$ Hz, $J = 13.9$ Hz, 1H, -CH(eq)H-CH₂-N- *cis* to carbonyl), 1.50 (dd, $J = 2.6$ Hz, $J = 13.9$ Hz, 1H, -CH(eq)H-CH₂-N-*trans* to carbonyl), 1.37 ppm (dt, $J = 4.5$ Hz, $J = 13.1$ Hz, 1H, -CH(ax)H-CH₂-N-*trans* to carbonyl). MS-EI (m/e) 405 (M⁺), 387 (-HOH), 238, 189, 167. HREI (m/e): Calcd for C₂₅H₂₄NO₂Cl: 405.1495. Found: 405.1482.

1-(3,3-Diphenyl-1-oxopropyl)-4-(4'-chlorophenyl)-4-piperidinol (38, UCSF165): Compound **38** (a sticky white solid) was obtained from the reaction of **17** with 3,3-diphenyl propionoyl chloride (**30**) in a 15% yield. The product had an R_f of 0.17 on silica TLC in 60% EtOAc-hexane. ¹H NMR δ 7.13-7.31 (m, 14H, aromatic), 4.66 (t, $J = 7.5$ Hz, 1H, benzyl), 4.51 (d, $J = 12.7$ Hz, 1H, -CH(eq)H-N *cis* to carbonyl), 3.68 (d, $J = 13.2$ Hz, 1H, -CH(eq)H-N *trans* to carbonyl), 3.38 (dt, $J = 2.4$ Hz, $J = 13.2$ Hz, 1H, -CH(ax)H-N *cis* to carbonyl), 2.95-3.21 (q_{AB}, 2H, -CO-CH₂-), 2.95 (m, 1H, -CH(ax)H-N *trans* to carbonyl), 1.71 (m, 1H, -CH(ax)H-CH₂-N- *cis* to carbonyl), 1.60 (m, 1H, -CH(eq)H-CH₂-N- *cis* to carbonyl), 1.54 (m, 1H, -CH(eq)H-CH₂-N-*trans* to carbonyl), 1.28 ppm (m, 1H, -CH(ax)H-CH₂-N-*trans* to carbonyl). MS-EI (m/e) 419 (M⁺), 401 (-HOH), 234, 189. HREI (m/e): Calcd for C₂₆H₂₆NO₂Cl: 419.1652. Found: 419.1663.

7.3.9 LAH REDUCTION OF AMIDES

The general procedure for the reduction is: To 150 mg of the amide in THF, 5 equivalents of LAH are added. The reaction is heated to reflux temperature and the reaction is allowed to proceed until the starting amide disappears by TLC. After allowing the reaction to cool, the excess LAH is quenched by the stepwise addition of 1.0 μ l H₂O, 1.0 μ l 15% NaOH, and 3.0 μ l H₂O per mg of LAH. The resulting suspension is filtered and the filtrate rotoevaporated to dryness. The products are partitioned between brine and CH₂Cl₂. The organic layer is dried with Na₂SO₄ and filtered through a silica gel plug with ethyl acetate, and the solvent is removed *in vacuo*. The products are purified by flash chromatography using an ethyl acetate-hexane gradient.

1,4-Bis-(2,2-diphenylethyl)piperazine (39, UCSF167): The reduction of 31 by LAH proceeded in 50% yield. The white solid (mp 116-118 °C) had an R_f = 0.36 in 20% EtOAc-hexane. ¹H NMR δ 7.12-7.39 (m, 20H, aromatic), 4.16 (t, *J* = 7.4 Hz, 2H, benzyl), 2.92 (d, *J* = 7.5 Hz, 4H, acyclic methylene), 2.39 ppm (s, broad, 8H, piperazine). MS-CI (NH₃) (*m/e*) 447 (M+1), 280 (-CH(C₆H₅)₂). HREI (*m/e*): Calcd for C₁₉H₂₃N₂ (-CH(C₆H₅)₂): 279.1861. Found: 279.1850.

1-(2,2-Diphenylethyl)-4-(bis-(4'-fluorophenyl)methyl)piperazine (40, UCSF182): The reduction of 33 by LAH yielded 40 in 58% yield. The product, a sticky, yellowish solid, had an R_f of 0.26 in 20% EtOAc-hexane. ¹H NMR δ 7.15-7.32 (m, 14H, aromatic), 6.93 (t, *J* =

7.7 Hz, 4H, aromatic α to the fluorine), 4.22 (t, broad, $J = 7.2$ Hz, 1H, -CH(C₆H₅)₂), 4.13 (s, 1H, -CH(p-F-C₆H₄)₂), 3.00 (d, $J = 7.0$ Hz, 2H, acyclic methylene), 2.48 (s, broad, 4H) and 2.30 ppm (s, broad, 4H) piperazine methylenes. MS-CI (NH₃) (m/e) 469 (M+1), 302 (-CH(C₆H₅)₂). HREI (m/e): Calcd for C₁₈H₁₉N₂F₂ (-CH(C₆H₅)₂): 301.1516. Found: 301.1501.

4-(Diphenylhydroxymethyl)-1-(2,2-diphenylethyl)piperidine (41, UCSF185): A sticky, clear solid was obtained from the reduction of **35** by LAH in a 35% yield. A single spot with an R_f of 0.45 in 40% ethyl acetate-hexane was observed by TLC. ¹H NMR δ 7.12-7.49 (m, 20H, aromatic), 4.17 (t, $J = 7.5$ Hz, 1H, benzyl), 2.96 (d, $J = 7.3$ Hz, 2H, exocyclic methylene), 2.91 (d, $J = 11.5$ Hz, 2H, -CH(eq)H-N), 2.37 (m, 1H, 4-piperidino proton), 2.00 (m, 2H, -CH(ax)H-N), 1.37 ppm (m, 4H, -CH(eq)H-CH₂-N- and -CH(ax)H-CH₂-N-). MS-CI (NH₃) (m/e) 448 (M+1), 281 (-CH(C₆H₅)₂), 263 (-CH(C₆H₅)₂ & HOH). HREI (m/e): Calcd for C₁₉H₂₂NO (-CH(C₆H₅)₂): 280.1701. Found: 280.1672.

1-(2,2-Diphenylethyl)-4-(4'-chlorophenyl)-4-piperidinol (42, UCSF186): Compound **42** was obtained from the reduction of **37** in 75% yield. The product, a sticky, yellowish solid, had an R_f of 0.18 on silica TLC in 20% EtOAc-hexane. ¹H NMR δ 7.15-7.54 (m, 14H, aromatic), 4.24 (m, 1H, benzyl), 3.05 (dd, $J = 2.9$ Hz, $J = 7.4$ Hz, 2H, exocyclic methylene), 2.79 (d, $J = 11.3$ Hz, 2H, -CH(eq)H-N), 2.51 (t, $J = 11.7$ Hz, 2H, -CH(ax)H-N), 2.04 (m, 2H, -CH(eq)H-CH₂-N-), 1.64 ppm (t, $J = 12.1$ Hz, 2H, -CH(ax)H-CH₂-N-). MS-CI (NH₃) (m/e) 392 (M+1),

374 (-HOH), 225 (-CH(C₆H₅)₂), 207 (-CH(C₆H₅)₂ & HOH). HREI (*m/e*):
Calcd for C₂₅H₂₄NCl (-HOH): 373.1597. Found: 373.1584.

7.3.10 REDUCTIVE AMINATION OF 3-PHENYLCINNAMAL- DEHYDE WITH HETEROCYCLIC AMINES

The general procedure for the reductive amination is: To the amine in methanol, HCl (gas)-saturated methanol was added dropwise until the solution reached a pH of about 7. 3-Phenyl-cinnamaldehyde (0.5 equiv.) were added and the solution was stirred over molecular sieves for 1 hour prior to the addition of 1.0 equivalents of NaBH₃CN. The reaction was worked up after stirring for 2 days. Concentrated HCl was added until the pH reached less than 2. The methanol was removed *in vacuo* and the residue was dissolved in water and extracted with ether. Brine and KOH (to pH greater than 10) were added to the aqueous layer and a second ether extraction was performed. The combined organic layers were dried over sodium sulfate, filtered through a silica gel plug with ethyl acetate, and rotoevaporated to dryness. The crude products were purified by flash chromatography with an ethyl acetate-hexane gradient.

1-(3,3-Diphenyl-2-propenyl)-4-(diphenylmethyl)piperazine (44, UCSF166): The crude product mixture of the reductive alkylation of 43 with 3-phenylcinnamaldehyde was separated by column chromatography. Compound 44 (yellowish crystals, mp 116-118 °C) was obtained in 50% yield. A single spot with an R_f of 0.31 in 20% EtOAc-hexane was observed by TLC. ¹H NMR δ 7.12-7.45 (m, 20H,

aromatic), 6.21 (t, $J = 6.8$ Hz, 1H, vinyl), 4.21 (s, 1H, benzyl), 3.07 (d, $J = 6.8$ Hz, 2H, allylic), 2.45 ppm (s, broad, 8H, piperazine). MS-EI (m/e) 444 (M^+), 277 (-CH(C₆H₅)₂), 251 (-CH₂CHC(C₆H₅)₂). HREI (m/e): Calcd for C₃₂H₃₂N₂: 444.2565. Found: 444.2547.

1-(3,3-Diphenyl-2-propenyl)-4-(bis-(4'-fluorophenyl)methyl) piperazine (45, UCSF183): Compound 27 was alkylated with 3-phenylcinnamaldehyde under reducing conditions. A white solid (mp 130-132 °C) was obtained in 75% yield after purification by column chromatography. A single spot with an R_f of 0.16 in 20% EtOAc-hexane was observed by TLC. ¹H NMR δ 7.15-7.40 (m, 18H, aromatic), 6.93 (t, $J = 8.5$ Hz, 4H, aromatic α to the fluorine), 6.22 (t, 6.7 Hz, 1H, vinyl), 4.24 (s, 1H, benzyl), 3.08 (d, 6.7 Hz, 2H, allylic), 2.43 ppm (s, broad, 8H, piperazine). MS-EI (m/e) 480 (M^+), 287 (-CH₂CHC(C₆H₅)₂), 277 (-CH(C₆H₄F)₂). HREI (m/e): Calcd for C₃₂H₃₀N₂F₂: 480.2377. Found: 480.2376.

1-(3,3-Diphenyl-2-propenyl)-4-(4'-chlorophenyl)-4-piperidinol (46, UCSF184): Compound 46 was obtained from the reductive alkylation of 17 with 3-phenylcinnamaldehyde in 80% yield. The product (white solid, mp 112-113 °C) had an R_f of 0.17 on silica TLC in 60% EtOAc-hexane. ¹H NMR δ 7.15-7.54 (m, 14H, aromatic), 6.24 (t, $J = 6.8$ Hz, 1H, vinyl), 3.17 (d, $J = 6.8$ Hz, 2H, allylic), 2.80 (d, $J = 11.2$ Hz, 2H, -CH(eq)H-N), 2.41 (t, $J = 11.4$ Hz, 2H, -CH(ax)H-N), 2.05 (t, $J = 12.4$ Hz, 2H, -CH(ax)H-CH₂-N-), 1.62 ppm (d, $J = 12.2$ Hz, 2H, -CH(eq)H-CH₂-N-). MS-EI (m/e) 403 (M^+), 385 (-HOH). HREI (m/e): Calcd for C₂₆H₂₆NOCl: 403.1702. Found: 403.1700.

1.4-Bis(3,3-diphenyl-2-propenyl)piperazine (47, UCSF189): The major product of the bis alkylation of piperazine with 3-phenylcinnamaldehyde was purified by column chromatography (30% yield). The product (white solid, mp 178-179 °C) had an R_f of 0.27 in 60% EtOAc-hexane. $^1\text{H NMR}$ δ 7.13-7.42 (m, 20H, aromatic), 6.20 (t, $J = 6.7$ Hz, 2H, vinyl), 3.07 (d, $J = 6.7$ Hz, 4H, allylic), 2.49 ppm (s, broad, 8H, piperazine). MS-EI (m/e) 470 (M^+), 277 ($-\text{CH}_2\text{CHC}(\text{C}_6\text{H}_5)_2$). HREI (m/e): Calcd for $\text{C}_{34}\text{H}_{34}\text{N}_2$: 470.2722. Found: 470.2707.

7.3.11 CATALYTIC HYDROGENATION

The olefinic group in compounds **44** and **46** was reduced to the alkane by catalytic hydrogenation. To 100 mg of the olefin in ethanol, a spatula tip of palladium/charcoal catalyst was added. A stopcock was added to the flask and fitted with a balloon filled with H_2 . The flask was evacuated followed by purging with hydrogen for several cycles before finally leaving it under the hydrogen atmosphere. The reaction was stirred at room temperature for three hours after which a TLC showed mostly starting material present. Addition of more catalyst, repeating the gas cycling, and stirring overnight allowed the reaction to proceed to completion. The reaction mixture was filtered through celite and the solvent removed *in vacuo*. The residue was dissolved in CH_2Cl_2 , dried with Na_2SO_4 , filtered through a silica gel plug with ethyl acetate, and rotoevaporated to dryness. The products were purified by flash chromatography using an ethyl acetate-hexane gradient as eluent.

1-(3,3-Diphenylpropyl)-4-(diphenylmethyl)piperazine (48,

UCSF187): The reduction of **44** by catalytic hydrogenation proceeded in 65% yield. The desired product (white powder, mp 123-125 °C) had an $R_f = 0.36$ in 20% EtOAc-hexane $^1\text{H NMR } \delta$ 7.12-7.42 (m, 20H, aromatic), 4.21 (s, 1H, -NCH(C₆H₅)₂), 3.95 (t, $J = 7.5$ Hz, 1H, -CH₂CH(C₆H₅)₂), 2.42 (s, broad, 8H, piperazine), 2.26 (m, 2H, -CH₂CH₂CH(C₆H₅)₂), 1.27 ppm (m, 2H, -CH₂CH(C₆H₅)₂). MS-EI (m/e) 446 (M⁺), 279 (-CH(C₆H₅)₂). HREI (m/e): Calcd for C₃₂H₃₄N₂: 446.2722. Found: 446.2702.

1-(3,3-Diphenylpropyl)-4-(4'-chlorophenyl)-4-piperidinol (49,

UCSF188): Compound **49** was obtained from the reduction of **46** in 40% yield. The product (white powder, mp 85-86.5 °C) had an R_f of 0.23 on silica TLC in 60% EtOAc-hexane. $^1\text{H NMR } \delta$ 7.16-7.52 (m, 14H, aromatic), 3.99 (t, $J = 7.4$ Hz, 1H, benzyl), 2.78 (d, $J = 11.1$ Hz, 2H, -CH(eq)H-N), 2.38 (m, 4H, -CH(ax)H-N and (C₆H₅)₂CHCH₂CH₂N-), 2.11 (m, 2H, -CH(ax)H-CH₂-N-), 1.71 (m, 2H, (C₆H₅)₂CHCH₂CH₂N-), 1.26 ppm (m, 2H, -CH(eq)H-CH₂-N). MS-EI (m/e) 405 (M⁺), 387 (-HOH), 224. HREI (m/e): Calcd for C₂₆H₂₈NOCl: 405.1859. Found: 405.1840.

7.4 CALCULATIONS

7.4.1 DOCK

The parameters for DOCK 1.1 used in the search of a subset the Cambridge Structural Database (Chapter 2), which have been reported previously (Desjarlais *et al.*, 1990), were: MATCH: dislim = 2.0 Å, nodlim = 8; SCORE: concut = 2.4 Å, dmin = 3.5 Å, discut = 5.0 Å. The structure of the uncomplexed HIV-1 protease reported by Wlodawer *et al.* was used in the calculations. The top 200 molecules were saved and evaluated for complementarity to the enzyme active site visually using MidasPlus as described in Chapter 2.

DOCK 3.0 parameters for orienting the putative ligands, obtained from the MACCS-3D search of the FCD, to the thioketal atom centers (Chapter 3) were: dislim = 1.7, nodlim = 4, ratiom = 0.0, lowno4, lbinsz = 0.2, lovlap = 0.0, sbinsz = 1.0, sovlap = 0.0.

DOCK 3.0 parameters for orienting the 33 N α -Fmoc N ω -tosylarginine conformations obtained from distance geometry into the HIV-1 protease, the UCSF8-bound enzyme conformation without the inhibitor, (Chapter 5) were: dislim = 1.5, nodlim = 5, ratiom = 0.0, lowno4, lbinsz = 0.2, lovlap = 0.0, sbinsz = 1.0, sovlap = 0.0. The partial charges for the ligands were generated by the Gasteiger and Marsili method within the SYBYL software.

Identical parameters to those immediately above were also used in the search of the FCD for compounds complementary to the UCSF8-bound protease (Chapter 6). The partial charges for UCSF8 were generated by the Gasteiger and Marsili method within the SYBYL software. The top 250 molecules in each of the searches, scored using 1) force-field; 2) normalized force-field; 3) contact; and 4) normalized contact, were evaluated visually using MidasPlus.

7.4.2 MACCS-3D

The query for the MACCS-3D search of the FCD (Chapter 3) was three phenyl groups forming a triangle with centroid-to-centroid distances of 9.5-14.0 Å, 9.5-14.0 Å, and 3.0-8.0 Å. The compounds obtained from the search were evaluated by docking them into the enzyme using DOCK 3.0.

7.4.3 DGEOM

Multiple conformations of N α -Fmoc N ω -tosylarginine within the UCSF8-HIV-1 protease structure (Rutenber et al., 1992), with the inhibitor removed, were generated by distance geometry using the program DGEOM (Chapter 5). Additional constraints placed on the calculation were: 1) the enzyme was kept rigid; 2) enzyme-substrate closest contacts were set as their van der Waals radii; 3) an atom in each the Fmoc group and the tosyl group were required to remain within the active site boundaries defined by the Cz atom of Arg 8 and Arg 108, and the C α atom of Ile 50 and Ile 150. 4) the

atoms of the carbamate group and the guanidino-sulfonamide group were constrained to a planar conformation.

REFERENCES

- Blaney, J. and Crippen, G. (1990) DGEOM, Quantum Chemistry Program Exchange, Indiana University, Bloomington.
- Christie, B., Henry, D., Güner, O. and Moock, T. (1990) In Online Information 90, *14th International Online Proceedings; Learned Information* 137-161.
- Corey, E. J. and Suggs, J. W. (1975) Pyridinium Chlorochromate: An efficient Reagent for Oxidation of Primary and Secondary Alcohols to Carbonyl Compounds, *Tet. Lett.* **31**, 2647-2650.
- Dalgleish, A., Beverley, P. C. L., Clapham, M. R., Crawford, D. H., Greaves, M. F. and Weiss, R. A. (1984) The CD4 (T4) Antigen is an Essential Component of the Receptor for the AIDS Retrovirus, *Nature* **312**, 763-767.
- Darke, P. L., Leu, C.-T., Heimbach, J. C., Sigal, I. S., Springer, J. P., Navia, M. A., Fitzgerald, P. M. D. and McKeever, B. M. (1990) Human Immunodeficiency Virus (Type 1) Protease: Enzymology and Three-Dimensional Structure of a New AIDS Drug Target., in *Human Immunodeficiency Virus (Type 1) Protease: Enzymology and Three-Dimensional Structure of a New AIDS Drug Target.* (Laver, W. G. and Air, G. M., eds) Vol. pp. 321-334, Academic Press, San Diego.
- DeCamp, D., Babé, L., Salto, R., Lucich, J., Koo, M.-S., Kahl, S. and Craik, C. (1992) Inhibition of HIV-1 Protease by Boronated Porphyrins, *J. Med. Chem.* **35**, (in press).
- Desjarlais, R. L., Seibel, G. L., Kuntz, I. D., Furth, P. S., Alvarez, J. C., Ortiz de Montellano, P. R., DeCamp, D. L., Babé, L. M. and Craik, C. S. (1990) Structure-Based Design of Nonpeptide Inhibitors Specific for the Human Immunodeficiency Virus 1 Protease, *Proc. Natl. Acad. Sci.* **87**, 6644-6648.
- Desjarlais, R. L., Sheridan, R. P., Seibel, G. L., Dixon, J. S. and Kuntz, I. D. (1988) Using Shape Complementarity as an Initial Screen in Designing Ligands for a Receptor Binding Site of Known Three-Dimensional Structure, *J. Med. Chem.* **31**, 722-729.

- DeVoss, J. (1992) July Research Report, Ortiz de Montellano Laboratory, UCSF.
- Dreyer, G. B., Metcalf, B. W., Tomaszek Jr., T. A., Carr, T. J., Chandler III, A. C., Hyland, L., Fakhoury, S. A., Magaard, V. W., Moore, M. L., Strickler, J. E., Debouck, C. and Meek, T. D. (1989) Inhibition of Human Immunodeficiency Virus 1 Protease *In Vitro*: Rational Design of Substrate Analogue Inhibitors, *Proc. Natl. Acad. Sci. USA* **86**, 9752-9756.
- Ehrlich, P. (1909) Veber den Jetzigen Stand der Chemotherapie, *Ber. Dtsch. Chem. Ges.* **42**, 17.
- Erickson, J., Neidhart, D. J., VanDrie, J., Kempf, D. J., Wang, X. C., Norbeck, D. W., Plattner, J. J., Rittenhouse, J. W., Turon, M., Wideburg, N., Kohlbrenner, W. E., Simmer, R., Helfrich, R., Paul, D. A. and Knigge, M. (1990) Design, Activity, and 2.8 Å Crystal Structure of a C₂ Symmetric Inhibitor Complexed to HIV-1 Protease, *Science* **249**, 527-533.
- Eyring, H. (1935) The Activated Complex and the Absolute Rate of Chemical Reactions, *Chem. Rev.* **17**, 65-77.
- Ferrin, T. E., Huang, C. C., Jarvis, L. E. and Langridge, R. (1988) The MIDAS Display System, *J. Mol. Graphics* **6**, 13-37.
- Fischer, E. (1894) Einfluss der Configuration auf die Wirkung der Enzyme, *Ber. Deutsch. Chem. Ges.* **27**, 2984-2993.
- Fischi, M. A., Richman, D. D., Grieco, M. H., Gottlieb, M. S., Volberding, P. A., Laskin, O. L., Leedom, J. M., Groopman, J. E., Mildvan, D., Schooley, R. T., Jackson, G. G., Durack, D. T. and King, D. (1987) The Efficacy of Azidothymidine (AZT) in the Treatment of Patients with AIDS and AIDS-Related Complex: A Double-Blind, Placebo-Controlled Trial, *N. Engl. J. Med.* **317**, 185-191.
- Gallo, R. C. and Montagnier, L. (1988) AIDS in 1988, *Scient. Am.* **259**, 41-48.
- Gottlinger, H., Sodroski, J. and Haseltine, W. (1989) Role of Capsid Precursor Processing and Myristoylation on Morphogenesis and Infectivity of Human Immunodeficiency Virus Type 1, *Proc. Natl. Acad. Sci. USA* **86**, 5781-5785.

- Haldane, J. B. S. (1930), *Enzymes*, M.I.T. Press, Cambridge.
- Haseltine, W. A. and Wong-Staal, F. (1988) The Molecular Biology of the AIDS Virus, *Scient. Am.* **259**, 52-62.
- Janssen, P., van de Westeringh, C., Jageneau, A., Demoen, P., Hermans, B., van Daele, G., Schellekens, K., van der Eycken, C. and Niemegeers, C. (1959) *Med. Pharm. Chem.* **1**, 281-297.
- Kohl, N. E., Emini, E. A., Schleif, W. A., Davis, L. J., Heimbach, J. C., Dixon, R. A. F., Scolnick, E. M. and Sigal, I. S. (1988) Active Human Immunodeficiency Virus Protease is Required for Viral Infectivity, *Proc. Natl. Acad. Sci. USA* **85**, 4686-4690.
- Kuntz, I. D., Blaney, J. M., Oatley, S. J., Langridge, R. and Ferrin, T. E. (1982) A Geometric Approach to Macromolecule-Ligand Interactions, *J. Mol. Biol.* **161**, 269-288.
- Langley, J. N. (1878) On the Physiology fo the Salivary Secretion, *Journ. of Physiol.* **1**, 339-369.
- Larder, B. A., Darby, G. and Richman, D. D. (1989) HIV with Reduced Sensitivity to Zidovudine (AZT) Isolated During Prolonged Therapy, *Science* **243**, 1731-1734.
- McDougal, J. S., Kennedy, M. S., Sligh, J. M., Cort, S. P., Mawle, A. and Nicholson, J. K. A. (1986) Binding of HTLV-III/LAV to T4+ T Cells by a Complex of the 110K Viral Protein and the T4 Molecule, *Science* **231**, 382-385.
- Meek, T. D., Dayton, B. D., Metcalf, B. W., Dreyer, G. B., Strickler, J. E., Gorniak, J. G., Rosenberg, M., Moore, M. L., Magaard, V. W. and Debouck, C. (1989) Human Immunodeficiency Virus 1 Protease Expressed in Escherichia Coli Behaves as a Dimeric Aspartic Protease, *Proc. Natl. Acad. Sci. USA* **86**, 1841-1845.
- Meek, T. D., Lambert, D. M., Metcalf, B. W., Petteway Jr., S. R. and Dreyer, G. B. (1990) HIV-1 Protease as a Target for Potential Anti-AIDS Drugs, in *HIV-1 Protease as a Target for Potential Anti-AIDS Drugs* (De Clercq, E. and Callebaut, C., eds) Vol. pp. 225-256, Elsevier, Amsterdam.

- Meng, E. C., Shoichet, B. K. and Kuntz, I. D. (1992) Automated Docking with Grid-Based Energy Evaluation, *J. Comp. Chem* **13**, 505-524.
- Miller, M., Schneider, J., Sathyanarayana, B. K., Toth, M. V., Marshall, G. R., Clawson, L., Selk, L., Kent, S. B. H. and Wlodawer, A. (1989) Structure of a Complex of Synthetic HIV-1 Protease with a Substrate-Based Inhibitor at 2.3 Å Resolution, *Science* **246**, 1149-1152.
- Mosmann, T. (1983) Rapid Colorimetric Assay for Cellular Growth and Survival: Application to Proliferation and Cytotoxicity Assays., *J. Immunol. Meth.* **65**, 55-63.
- Navia, M. A., Fitzgerald, P. M. D., McKeever, B. M., Leu, C.-T., Heimbach, J. C., Herber, W. K., Sigal, I. S., Darke, P. L. and Springer, J. P. (1989) Three-Dimensional Structure of Aspartyl Protease from Human Immunodeficiency Virus HIV-1, *Nature* **337**, 615-620.
- Page, K. A., Landau, N. R. and Littman, D. R. (1990) Construction and use of a human immunodeficiency virus vector for analysis of virus infectivity, *J. Virol.* **64**, 5270-5276.
- Pearl, L. H. and Taylor, W. R. (1987) A Structural Model for the Retroviral Proteases, *Nature* **329**, 351-354.
- Pichuantes, S., Babé, L. M., Barr, P. J. and Craik, C. S. (1989) Recombinant HIV1 Protease Secreted by *Saccharomyces Cerevisiae* Correctly Processes Myristylated GAG Polyprotein, *Proteins* **6**, 324-337.
- Propst, C. L. and Perun, T. J. (1989) Introduction to Computer-Aided Drug Design, in *Introduction to Computer-Aided Drug Design* (Perun, T. J. and Propst, C. L., eds) Vol. pp. 1-16, Marcel Dekker, Inc., New York.
- Richards, A. D., Roberts, R., Dunn, B. M., Graves, M. C. and Kay, J. (1989) Effective blocking of HIV-1 proteinase activity by characteristic inhibitors of aspartic proteinases., *FEBS Lett.* **247**, 113-117.
- Richardson, J. S. (1985) Schematic Drawings of Protein Structures, *Methods Enzymol.* **115**, 359-380.

- Richman, D. D., Fischl, M. A., Grieco, M. H., Gottlieb, M. S., Volberding, P. A., Laskin, O. L., Leedom, J. M., Groopman, J. E., Mildvan, D., Hirsch, M. S., Jackson, G. G., Durack, D. T. and Nusinoff-Lehrman, S. (1987) The Toxicity of Azidothymidine (AZT) in the Treatment of Patients with AIDS and AIDS-Related Complex, *N. Engl. J. Med.* **317**, 192.
- Roberts, N. A., Martin, J. A., Kinchington, D., Broadhurst, A. V., Craig, J. C., Duncan, I. B., Galpin, S. A., Handa, B. K., Kay, J., Krohn, A., Lambert, R. W., Merrett, J. H., Mills, J. S., Parkes, K. E. B., Redshaw, S., Ritchie, A. J., Taylor, D. L., Thomas, G. J. and Machin, P. J. (1990) Rational Design of Peptide-Based HIV Proteinase Inhibitors, *Science* **248**, 358-361.
- Roberts, R. M. (1989), *Serendipity: Accidental Discoveries in Science*, Wiley, New York.
- Rutenber, E., Fauman, E., Fong, S., Furth, P., Ortiz de Montellano, P., Meng, E., Kuntz, I., DeCamp, D., Salto, R., Craik, C. and Stroud, R. (1992) Structure of HIV-1 Protease Complexed with a Non-Peptide Inhibitor: Initiating a Cycle of Structure-Based Drug Design,
- Seelmeier, S., Schmidt, H., Turk, V. and von der Helm, K. (1988) Human Immunodeficiency Virus has an Aspartic-Type Protease that can be Inhibited by Pepstatin A, *Proc. Natl. Acad. Sci. USA* **85**, 6612-6616.
- Sheridan, R. P. and Venkataraghavan, R. (1987) New Methods in Computer-Aided Drug Design, *Acc. Chem. Res.* **20**, 322-329.
- Smith, D. H., Byrn, R. A., Marsters, S. A., Gregory, T., Groopman, J. E. and Capon, D. J. (1987) Blocking of HIV-1 Infectivity by a Soluble, Secreted Form of the CD4 Antigen, *Science* **238**, 1704-1707.
- Tang, J., James, M. N. G., Hsu, I. N., Jenkins, J. A. and Blundell, T. L. (1978) Structural Evidence for Gene Duplication in the Evolution of the Acid Proteases, *Nature* **271**, 618-621.
- Toh, H., Ono, M., Saigo, K. and Miyata, T. (1985) Retroviral Protease-Like Sequence in the Yeast Transposon Ty1, *Nature (London)* **315**, 691-692.

Tripes Associates (1990) St. Louis, Missouri, SYBYL Molecular Modeling Software, Version 5.3.

Wlodawer, A., Miller, M., Jaskolski, M., Sathyanarayana, B. K., Baldwin, E., Weber, I. T., Selk, L. M., Clawson, L., Schneider, J. and Kent, S. B. H. (1989) Conserved Folding in Retroviral Proteases: Crystal Structure of a Synthetic HIV-1 Protease, *Science* **245**, 616-621.

II. THIANTHRENE 5-OXIDE AS A PROBE OF THE ELECTRONIC PROPERTIES OF HEMOPROTEIN OXIDIZING SPECIES

CHAPTER 1

INTRODUCTION

1.1 HEMOPROTEINS

Hemoproteins are capable of carrying out a multitude of catalytic functions by virtue of their heme prosthetic group. Included in this repertoire are peroxidation, peroxygenation, monooxygenation, and dioxygenation. All of these catalytic functions are thought to involve a two electron oxidation of the heme to a ferryl $[\text{FeO}]^{3+}$ species and a radical centered either on the porphyrin or the protein (Ortiz de Montellano, 1987). Thus, differences in catalytic properties among hemoproteins are largely due to the environment created by the protein.

Monooxygenation reactions catalyzed by cytochrome P450 involve the direct transfer of the ferryl oxygen to the substrate (Ortiz de Montellano, 1986, 1987). An analogous mechanism has been implicated in chloroperoxidase-catalyzed monooxygenations (Ortiz de Montellano et al., 1987; Kobayashi et al., 1986). The dominance of this ferryl oxygen transfer mechanism is largely attributed to the fact that a cysteine thiolate is present as the fifth ligand to the heme iron atom (Dawson & Sono, 1987). Hemoproteins which contain a histidine imidazole as the heme ligand, however, do not transfer the ferryl oxygen atom to substrates as readily, and additional

intermediates have been invoked in oxygenations catalyzed by these hemoproteins (Ortiz de Montellano & Catalano, 1985; Catalano & Ortiz de Montellano, 1987; Dordick et al., 1986).

1.2 THIANTHRENE 5-OXIDE AS A PROBE OF THE ELECTRONIC CHARACTER OF CHEMICAL OXIDANTS

Thianthrene 5-oxide, T-5-O (1), has been used previously as a mechanistic probe to investigate the electronic character of *chemical* oxygen-transfer agents (Adam et al., 1984, 1987, 1991; Ballisteri et al., 1991). Whereas T-5-O is converted to the 5,10-dioxide (2) by electrophilic agents, nucleophilic oxidants result in its conversion to the 5,5-dioxide (3) (Figure 1.1). This is due to the presence of both electron-rich (sulfide) and electron deficient (sulfoxide) oxidation sites. Furthermore, preferential conversion of the 5,5- and 5,10-dioxides to the 5,5,10-trioxide (4) by electrophilic and nucleophilic oxidants, respectively, is also observed. An exception to this general trend is the oxidation of T-5-O to the 5,5-dioxide by electrophilic radicals with a high ($E_{OX} > \sim 1.76$ V) oxidation potential. These electrophilic radicals initially abstract an electron from the T-5-O generating the radical cation, which in a second step collapses with the reduced oxidant to give the nominally nucleophilic product (Adam et al., 1991; Ballisteri et al., 1991).

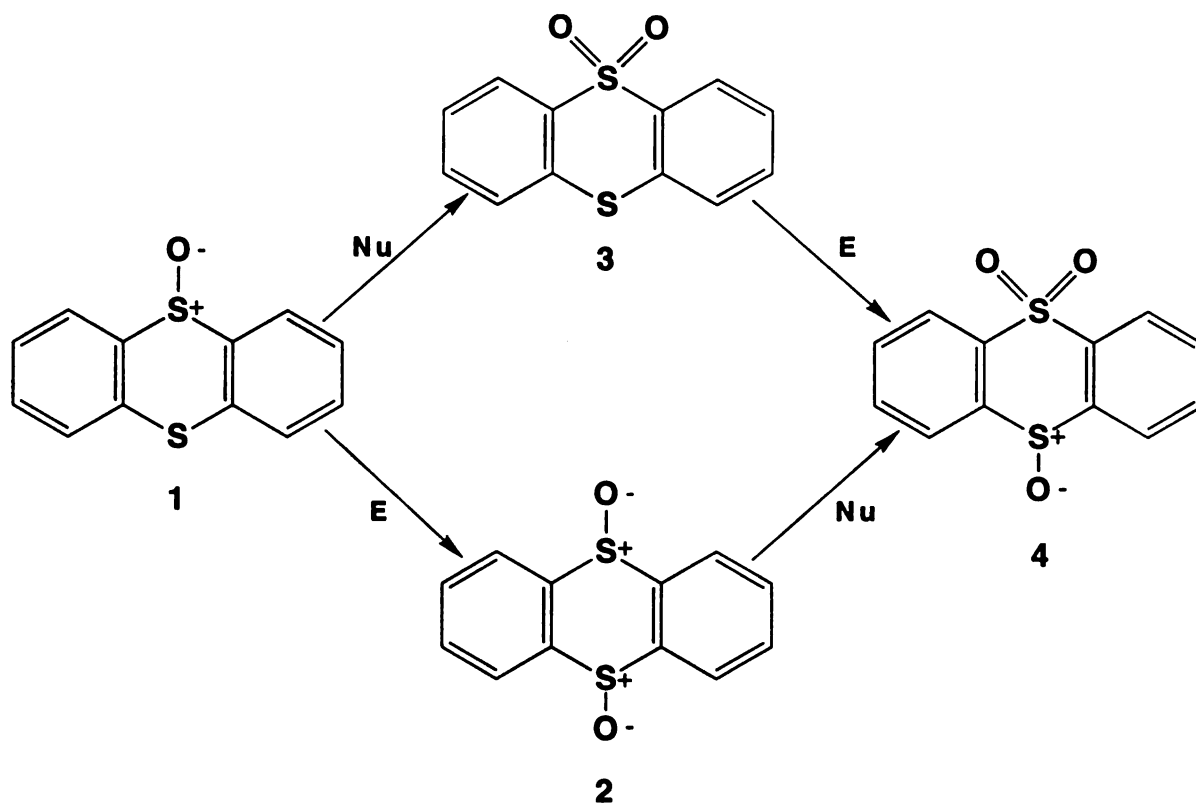


Figure 1.1: Oxidation of thianthrene-5-oxide (1) to the 5,10-dioxide (2), 5,5-dioxide (3), and subsequently to the 5,5,10-trioxide (4) by electrophilic (E) or nucleophilic (Nu) oxygen-transfer agents.

1.2.3 T-5-O AS A PROBE OF THE ELECTRONIC CHARACTER OF OXYGENATIONS IN BIOLOGICAL SYSTEMS

T-5-O is particularly attractive as a biological probe due to the intramolecular competition between the nucleophilic and electrophilic oxidation sites. Thus, problems associated with differential substrate binding and rate determining steps other than actual substrate oxidation are circumvented. Furthermore, oxidation

at the sulfide site can give rise to *cis* and *trans* diastereomers of the 5,10-dioxide (Figure 1.2) potentially yielding information as to the stereochemical restrictions imposed on the substrate by the enzyme. The present studies were undertaken to (a) demonstrate the utility of thianthrene 5-oxide as a mechanistic probe in biological systems, and (b) clarify the electronic character of several poorly understood hemoprotein oxidizing agents, thus providing insight into the mechanisms of transformations catalyzed by them.

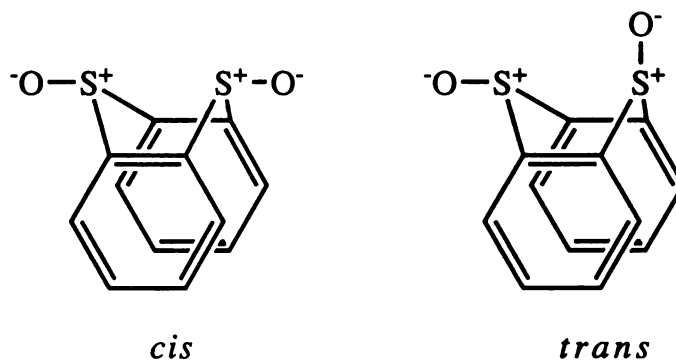


Figure 1.2: *Cis* and *trans* isomers of thianthrene 5,10-dioxide.

CHAPTER 2

DIRECT OXIDATION OF THIANTHRENE 5-OXIDE BY THE FERRYL SPECIES OF CYTOCHROME P450

2.1 INTRODUCTION

Cytochrome P450's catalyze the insertion of an oxygen atom into a substrate. The overriding feature of the cytochrome P450 catalytic cycle (Figure 2.1) is the activation of oxygen by heterolysis of the O-O bond generating the reactive oxidant $[\text{FeO}]^{3+}$. It is this ferryl oxygen atom which is then directly transferred to the substrate (Ortiz de Montellano, 1986).

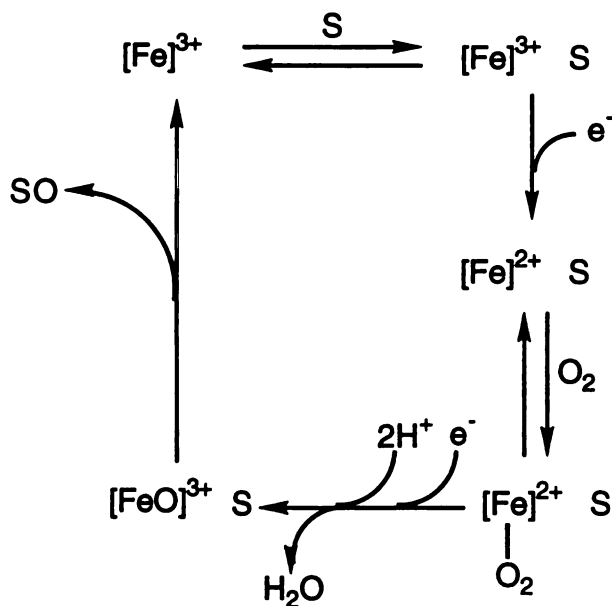


Figure 2.1: The catalytic cycle of cytochrome P450. The prosthetic heme group is represented by the brackets around the iron; substrate is denoted as S. Reproduced from Ortiz de Montellano (1986).

2.2 OXIDATION OF THIANTHRENE 5-OXIDE BY CYTOCHROME P450

T-5-O was incubated with hepatic microsomes from phenobarbital-pretreated rats in the presence of NADPH and the products extracted and analyzed by HPLC. The major metabolites of the reaction were the 5,10-dioxide and 5,5,10-trioxide of thianthrene. No product formation was observed in control experiments containing all the incubation components except NADPH. A quantitative study of the time course of the reaction (Figure 2.2) shows that the substrate is rapidly converted to the 5,10-dioxide with about 10% conversion 30 seconds into the reaction. Product formation is paralleled by the disappearance of T-5-O. It is not until a significant amount of the 5,10-dioxide has accumulated that appearance of the 5,5,10-trioxide commences. At no point in these incubations is more than a trace of the 5,5-dioxide detected. An initial rate of approximately 32 nmol/nmol P450/min is observed for 5,10-dioxide formation.

Preincubation of the microsomes with 1-aminobenzotriazole (1-ABT) confirmed the involvement of cytochrome P450 in the transformations. 1-ABT is a mechanism-based inactivator of cytochrome P450 (Ortiz de Montellano & Mathews, 1981) which has previously been shown to have no effect on microsomal flavin monooxygenase, another enzyme capable carrying out sulfoxidations (Cashman, 1987). An 80% reduction in the product formation was observed for microsomes preincubated for 17 min with 5 mM 1-ABT.

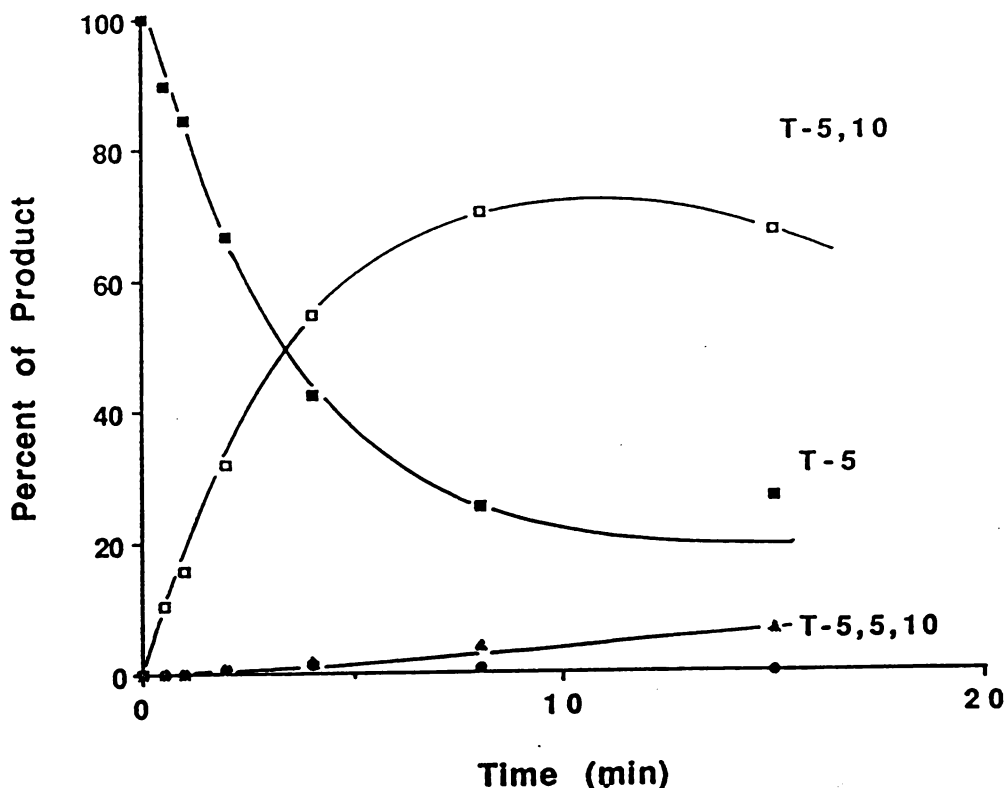


Figure 2.2: Time course for the oxidation of T-5-O (■) to T-5,10-dioxide (□) and T-5,5,10-trioxide (▲) by microsomal cytochrome P450. T-5,5-dioxide (●) is not detectably formed.

Thianthrene 5,5-dioxide as well as both isomers of T-5,10-dioxide are further oxidized to the trioxide by the microsomal cytochrome P450 system (Figure 2.3). Of the three, the 5,5-dioxide is most rapidly oxidized followed by the *cis*-5,10-dioxide and the *trans*-5,10-dioxide; approximate initial rates of 8, 4, and 2 nmol (nmol of enzyme)⁻¹ min⁻¹, respectively, were determined.

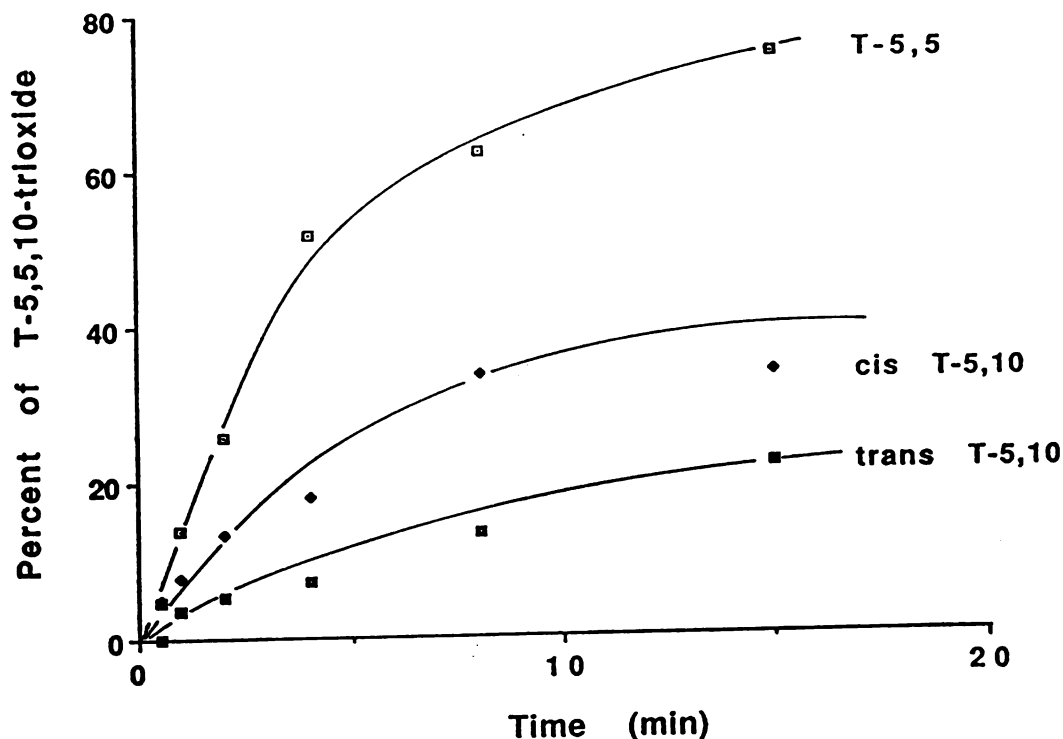


Figure 2.3: Time courses for T-5,5,10-trioxide formation from the microsomal cytochrome P450-catalyzed oxidation of T-5,5-dioxide (□), *cis*-T-5,10-dioxide (◆), and *trans*-T-5,10-dioxide (■).

2.3 STEREOCHEMICAL COURSE FOR THE OXIDATION OF T-5-O BY CYTOCHROME P450 2B1

Analysis of the stereoisomer composition of the T-5,10-dioxide produced from the oxidation of T-5-O revealed little stereoselectivity in the cytochrome P450-catalyzed reaction. A *cis/trans* isomer ratio of approximately 1.3 ($57.1 \pm 0.9\%$ *cis*) was observed. This result is not surprising given the fact that cytochrome P450 2B1, an isozyme whose primary function is that of detoxification, is the major cytochrome P450 component in phenobarbital-induced microsomes.

The nature of the enzyme's function necessitates the ability to accommodate a broad spectrum of substrates (Guengerich, 1987). Thus, the enzyme is endowed with a large, malleable active site permitting substantial rotational freedom for smaller substrates such as T-5-O.

2.4 DISCUSSION OF THE RESULTS OF THE CYTOCHROME P450-CATALYZED OXIDATION OF T-5-O

Thianthrene 5,10-dioxide, the product expected for an electrophilic oxidant is the product of the oxidation of T-5-O by phenobarbital-induced hepatic microsomes. Furthermore, synthetic T-5,5-dioxide is converted to the 5,5,10-trioxide much more rapidly than either T-5,10-dioxide isomer. All the observed results are in agreement with current opinion implicating an electron deficient ferryl oxygen as the active oxidant in cytochrome P450 (Ortiz de Montellano, 1986). In addition, they are consistent with observed linear relationships between V_{max} and substrate oxidation potentials in the cytochrome P450-catalyzed oxidation of substituted thioanisoles ($\rho = -0.16$ *versus* σ^+) (Watanabe et al., 1981) and substituted sulfoxides ($\rho = -0.2$ *versus* σ^+) (Watanabe et al., 1982)

CHAPTER 3

CHLOROPEROXIDASE: ANOTHER FERRYL OXYGEN TRANSFER REACTION

3.1 INTRODUCTION

Chloroperoxidase, a heme protein isolated from the mold *Caldariomyces fumago*, has been found to be capable of catalyzing cytochrome P450-like reactions such as N-dealkylation (Hollenberg, 1992), epoxidation (Ortiz de Montellano et al., 1987), and sulfoxidation (Kobayashi et al., 1986). In these cases, mechanisms analogous to those of cytochrome P450 whereby the substrate directly interacts with the ferryl oxygen atom have been implicated. Evidence for such mechanisms includes the incorporation of a hydrogen peroxide-derived oxygen atom into the sulfoxides formed from thioanisole and p-methylthioanisole (Kobayashi et al., 1986) and the epoxide produced from styrene (Ortiz de Montellano et al., 1987). Moreover, the N-demethylation of N,N-dimethylaniline catalyzed by chloroperoxidase exhibits a small ($k_H/k_D = 2.5$) intramolecular isotope effect implying a deprotonation step similar to cytochrome P450, making it unique among peroxidases (Hollenberg, 1992). The divergence in catalytic breadth from that of classical peroxidases, which carry out one electron oxidations of substrates, has been partially attributed to the presence of a thiolate, as in

cytochrome P450, rather than an imidazole as the fifth ligand to the heme iron.

3.2 CHLOROPEROXIDASE-CATALYZED OXIDATION OF T-5-O

T-5-O is oxidized by chloroperoxidase to the 5,10-dioxide with no T-5,5-dioxide or T-5,5,10-trioxide produced (Figure 3.1). The appearance of product is paralleled by disappearance of the parent compound. Control incubations containing hydrogen peroxide but no enzyme exhibited no product formation. An initial rate of approximately $1.5 \text{ nmol (nmol of enzyme)}^{-1} \text{ min}^{-1}$ was calculated from the time course of the reaction.

Incubations in which the T-5-O was replaced by each of the thianthrene dioxides were also carried out. The T-5,10-dioxide isomers were both only very slowly converted to the 5,5,10-trioxide by chloroperoxidase. Only a trace of product was detected in the incubation of the trans isomer, and the cis isomer was oxidized at a rate of less than $0.03 \text{ nmol (nmol of enzyme)}^{-1} \text{ min}^{-1}$. In contrast, the 5,5-dioxide is readily oxidized to the 5,5,10-trioxide (Figure 3.2). An initial rate of approximately $0.06 \text{ nmol (nmol of enzyme)}^{-1} \text{ min}^{-1}$ was calculated. This, however, represents a lower limit for the turnover number since only a concentration of $13.5 \mu\text{M}$, a value probably too low to saturate the enzyme, was achieved for the substrate due to solubility problems.

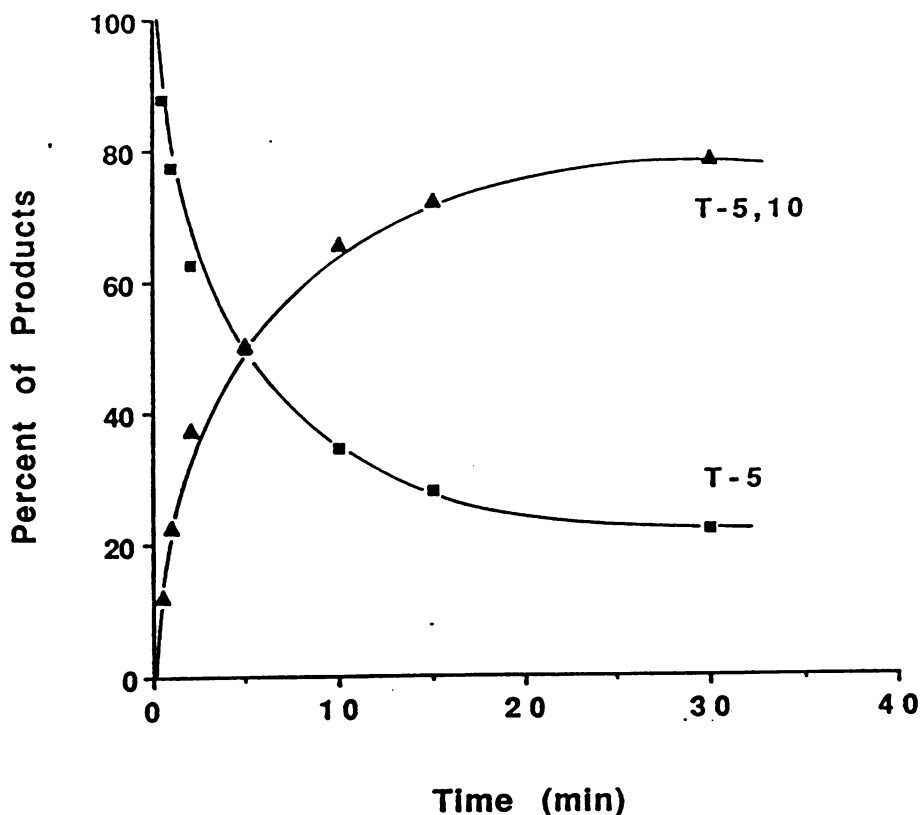


Figure 3.1: Time course for the oxidation of T-5-O (squares) to T-5,10-dioxide (triangles) by chloroperoxidase. Neither T-5,5-dioxide nor T-5,5,10-trioxide are detectably formed.

3.3 STEREOCHEMICAL COURSE FOR THE OXIDATION OF T-5-O BY CHLOROPEROXIDASE

Unlike cytochrome P450, chloroperoxidase exhibits a slight stereoselectivity in its oxidation of T-5-O to the 5,10-dioxide. The *cis* isomer accounted for 71.3 ± 1.3 % of the total 5,10-dioxide produced. Thus, although the primary metabolite observed for both cytochrome P450 and chloroperoxidase is the same, differences in the isomeric

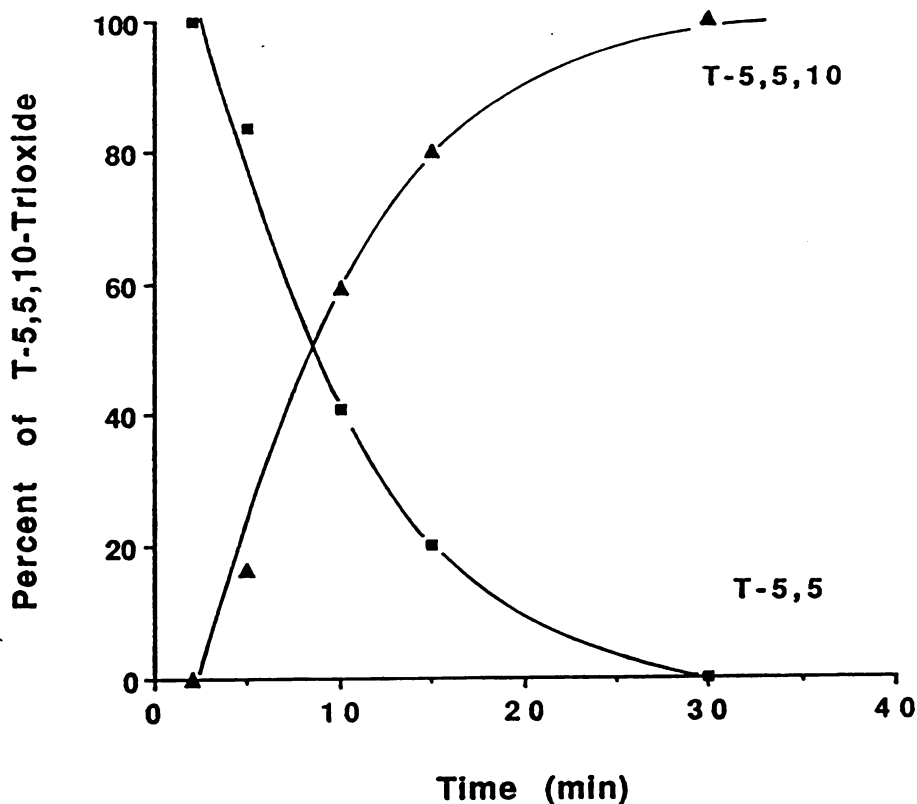


Figure 3.2: Time course for the chloroperoxidase-catalyzed conversion of T-5,5-dioxide to T-5,5,10-trioxide.

ratio of the product may reflect differences in active-site structures. It is likely the chloroperoxidase active-site is smaller, and consequently more restrictive towards rotational freedom of the substrate, limiting access to the sulfide lone pair of electrons *trans* to the sulfoxide oxygen.

Alternatively, orientation of the substrate in the active-site may occur via a polar interaction (i.e., electrostatic or hydrogen-bonding) between the sulfoxide of the substrate and an enzymatic residue. This is consistent with data suggesting a higher polarity for the

chloroperoxidase active-site relative to that of cytochrome P450 (Ortiz de Montellano et al., 1987; Dawson & Sono, 1987; Sono et al., 1986). Equilibrium binding studies of various ligands to the ferrous form of chloroperoxidase at pH's ranging from 2 to 7 have identified a single ionizable protein residue with a K_a of 5.5 as having an effect on binding (Sono et al., 1986). It was postulated that this ionizable group is a histidine, perhaps the residue involved in the cleavage of the peroxide O-O bond by analogy to the mechanism of cytochrome c peroxidase proposed on the basis of its crystal structure (Poulos & Kraut, 1980). Furthermore, the oxidation of styrene by chloroperoxidase generates a substantially higher ratio of phenylacetaldehyde to styrene oxide than cytochrome P450 (Ortiz de Montellano et al., 1987). The proposed origin of the former product was from a 1,2-rearrangement process accelerated by a more polar environment (Ortiz de Montellano et al., 1987).

3.4 DISCUSSION OF THE RESULTS OF THE CHLOROPEROXIDASE-CATALYZED OXIDATION OF T-5-O

The major metabolite isolated from the incubation of T-5-O with chloroperoxidase, as for cytochrome P450, is T-5,10-dioxide. This indicates that its oxidizing species is electrophilic in nature, a result expected for direct oxidation of the substrate by the ferryl species. The present results concur with those of chloroperoxidase-catalyzed oxidations of sulfides (Kobayashi et al., 1986) and styrene (Ortiz de Montellano et al., 1987) in the presence of $[^{18}\text{O}]\text{H}_2\text{O}_2$, in which the label was incorporated into the products. They also agree with an

observed correlation ($\rho = -1.40$, correlation coefficient $r = 0.824$) between the log of the sulfoxidation rate of *para*-substituted thioanisoles and the σ substituent constant (Kobayashi et al., 1987). In contrast, there is a reported lack of correlation between the oxidation rates of benzyl methylsulfide, thioanisole, and thiobenzamide and their electrochemical oxidation potentials, $E_{1/2} = 1.71$, $E_{1/2} = 1.44$, and $E_{1/2} = 1.30$ vs. SCE, respectively (Doerge, 1986).

Differences between chloroperoxidase- and cytochrome P450-catalyzed oxidations of the thianthrene oxides could be a reflection of the relative potencies of their respective catalytic species. Thus, the relative ease with which cytochrome P450 converts both T-5,10-dioxides to the 5,5,10-trioxide would make it a more powerful oxidant than chloroperoxidase. The postulated differences in the reactivities of the two ferryl species must be explained by differences in their active-site environments such as the aforementioned proposed higher polarity for the chloroperoxidase active-site (Ortiz de Montellano et al., 1987; Sono et al., 1986; Dawson & Sono, 1987).

Alternatively, the nominally weaker oxidative potency of chloroperoxidase may be due to its sensitivity to self-inactivation by H_2O_2 in the absence of a good substrate. Kobayashi et al. (1986) have reported the inactivation of chloroperoxidase during the catalytic turnover of substituted thioanisoles. As T-5-O is replaced by the less readily oxidized 5,10-dioxides, the rate of inactivation may increase.

CHAPTER 4

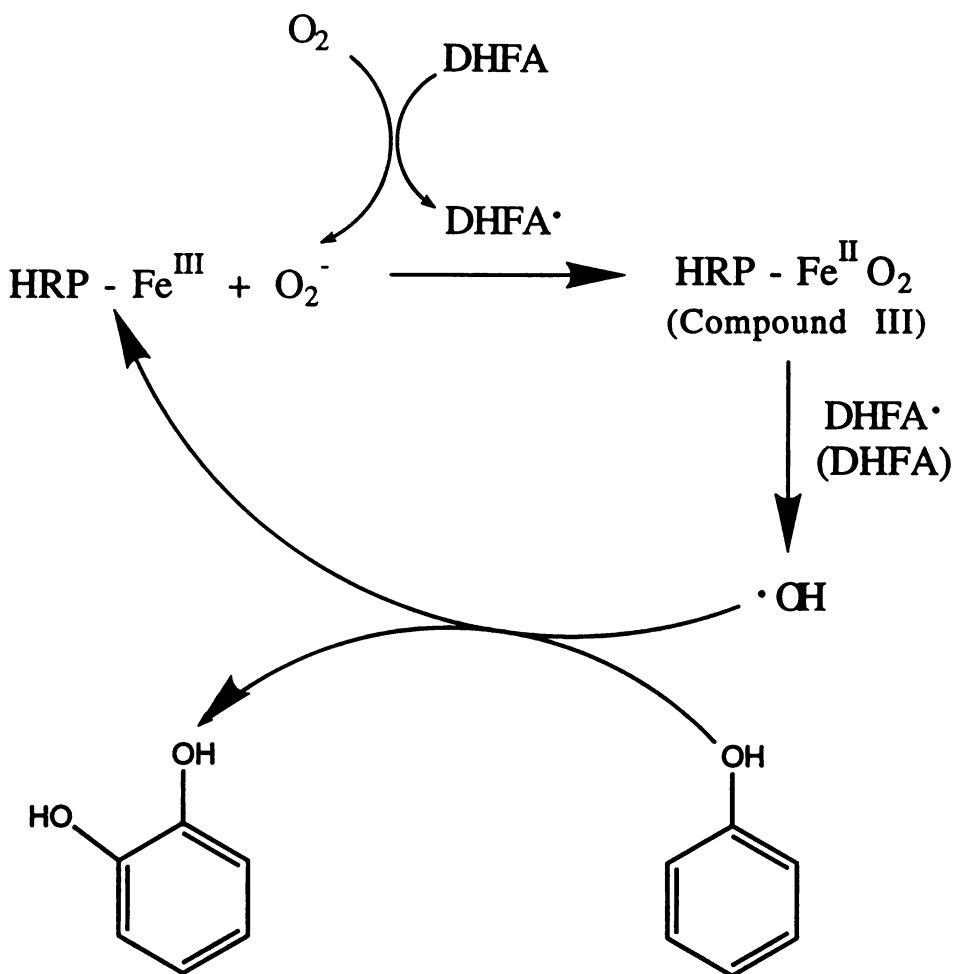
THE HORSERADISH PEROXIDASE/DIHYDROXYFUMARATE/O₂ OXIDIZING SYSTEM

4.1 INTRODUCTION

Under aerobic conditions in the presence of dihydroxyfumaric acid (DHFA), horseradish peroxidase (HRP) catalyzes the hydroxylation of aromatic compounds (Mason et al., 1957; Buhler & Mason, 1961; Yamazaki & Piette, 1963; Halliwell & Ahluwalia, 1976). DHFA cannot be replaced by ascorbate, NADH, cysteine, sulfite or H₂O₂ (Halliwell & Ahluwalia, 1976). Conflicting reports as to the effect of catalase on the reaction, however, have left it unclear as to whether low concentrations of H₂O₂, endogenously produced from the dismutation of superoxide, facilitate catalysis (Halliwell & Ahluwalia, 1976; Yamazaki & Piette, 1963; Dordick et al., 1986). The reaction is not highly coupled, with about 12 moles of DHFA being consumed per mole of hydroxylated product (Dordick et al., 1986). The oxygen atom incorporated into the hydroxylated aromatic product has been reported to originate from molecular oxygen (Mason, 1958). In contrast to cytochrome P450, the HRP-catalyzed aromatic hydroxylation proceeds without migration of the aromatic hydrogen to a vicinal position (the NIH shift) (Daly & Jerina, 1970).

Indirect evidence has led to the proposal by several groups that the active oxidant in the HRP/DHFA/O₂ system is a radical species (Buhler & Mason, 1961; Yamazaki & Piette, 1963; Daly & Jerina, 1970; Halliwell & Ahluwalia, 1976; Dordick et al., 1986). Included in this evidence are: 1) product distributions, notably the formation of all three isomers of nitrophenol from nitrobenzene, as well as the relative yields obtained from various substitutions on the aryl ring (Buhler & Mason, 1961), and 2) inhibition of the reaction by superoxide dismutase and by radical scavengers including mannitol, ethanol, formate, and DMSO (Halliwell & Ahluwalia, 1976; Dordick et al., 1986).

Although earlier investigators did not define the identity of the radical species ultimately responsible for the transformation, both Halliwell & Ahluwalia (1976) and Dordick et al. (1986), albeit through different mechanisms, both invoked the hydroxyl radical. The former group concluded that superoxide generated during the oxidation of DHFA by HRP reacts with endogenously generated H₂O₂ to produce the hydroxyl radical. In contrast, Dordick et al. (1986) proposed the mechanism shown in Scheme 4.1 for the generation of hydroxyl radicals. HRP compound III is formed by reaction of the ferric hemoprotein with the superoxide radical anion. Spectroscopically they determined that DHFA is required not only for the formation of compound III but also for hydroxylation by compound III to occur. Thus, it is compound III that, after receiving an electron from DHFA, formally breaks down to a hydroxyl radical, a hydroxyl anion, and ferric HRP.



Scheme 4.1: Proposed mechanism for the DHFA/O₂-dependent aromatic hydroxylation catalyzed by HRP (Dordick et al., 1986).

Some inconsistencies exist, however, between hydroxyl radical involvement and the observed data. The regioselectivity of the peroxidase-catalyzed hydroxylation of benzoic acid and nitrobenzene disagrees with that observed for reactions with free hydroxyl radicals generated by the Fenton reaction, by x-radiation of water, or by ultraviolet radiation of H₂O₂ (Buhler & Mason, 1961).

Furthermore, there are discrepancies between the concentrations of alcohol required to inhibit the DHFA-supported reactions and the concentrations required to inhibit the hydroxylation of *p*-nitrosodimethylaniline and other reactions mediated by radiolytically generated hydroxyl radicals (Bors et al., 1979).

4.2 THE AEROBIC OXIDATION OF T-5-O BY HORSERADISH PEROXIDASE AND DIHYDROXYFUMARATE

Under aerobic conditions, T-5-O is converted exclusively to T-5,5-dioxide by horseradish peroxidase in the presence of DHFA and O₂. As has been reported for aromatic hydroxylations by this system, exogenously added H₂O₂ cannot replace the DHFA. A time course for the reaction, Figure 4.1, reveals the tapering off of T-5,5-dioxide production after a few minutes due to depletion of the DHFA. Thus, upon re-addition of fresh DHFA, product formation recommences (Figure 4.1). Approximately 5-7 nmol of DHFA are consumed per nmole of T-5-O oxidized. An initial rate of approximately 5.7 nmol (nmol of enzyme)⁻¹ min⁻¹ was estimated for the reaction. Although formation of T-5,5-dioxide can be detected in control incubations lacking the enzyme, it is at a rate much lower than that for the horseradish peroxidase-catalyzed reaction.

Identification of the source of the oxygen atom incorporated into the T-5,5-dioxide was attempted by comparison of the product isolated from an incubation run under an ¹⁸O₂ atmosphere with that from the standard ¹⁶O₂ incubation. Mass spectrometric analysis of the two

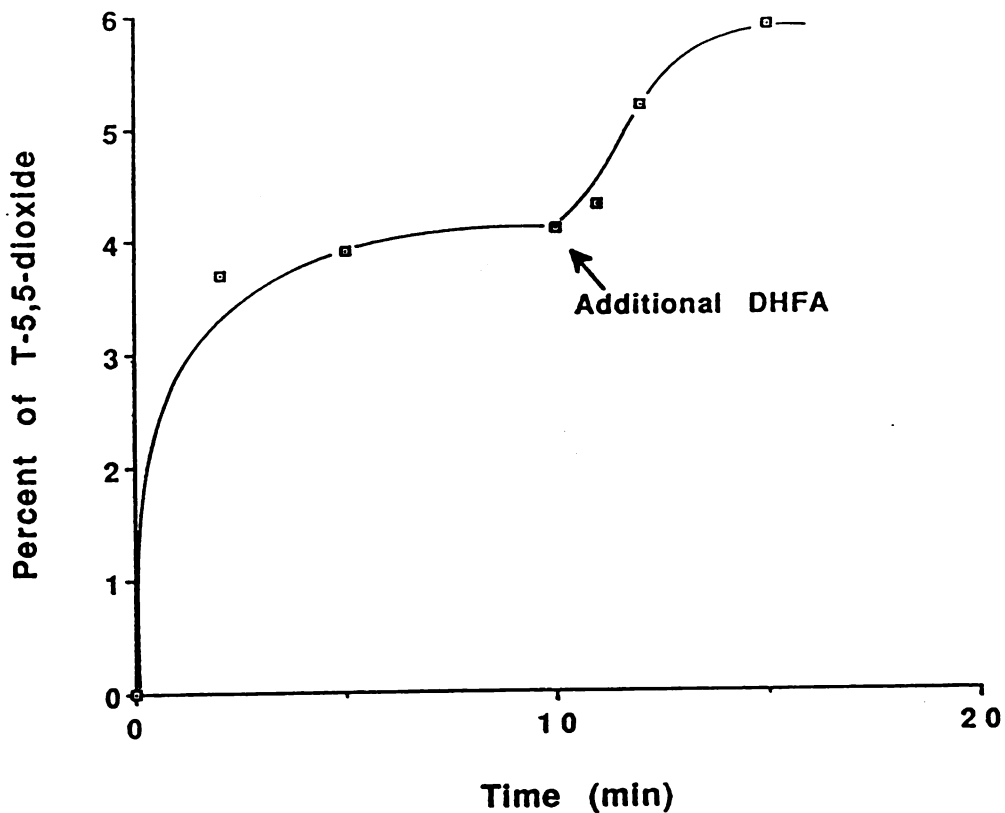


Figure 4.1: Time course of the conversion of T-5-O to the 5,5-dioxide by horseradish peroxidase in the presence of DHFA and O_2 . The arrow indicates the time point at which a second supply of DHFA (in one half the amount of the first) was added to the incubation.

products revealed a nearly complete shift of the T-5,5-dioxide molecular ion from m/z 248 to 250 in the incubation with the labeled oxygen. Thus, it is clear that the oxygen atom incorporated into the product originates from molecular oxygen.

Methanol, in mM concentrations, inhibits the oxidation of T-5-O by the HRP/DHFA/O₂ system in a dose dependent fashion (Figure 4.2). The IC₅₀ for methanol is estimated to be near 100 mM. Although the mechanism for the inhibition by methanol has not been unambiguously determined, it is presumably quenching radical species essential in the oxidative mechanism.

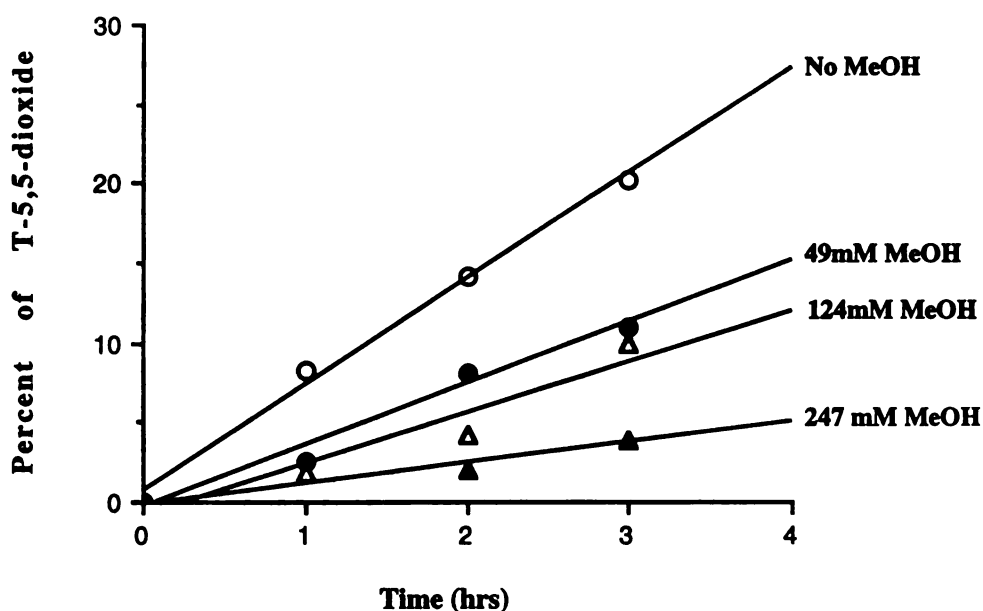


Figure 4.2: Dose-dependent inhibition of HRP/DHFA/O₂-mediated oxidation of T-5-O. Methanol concentrations: None (open circles), 49 mM (filled circles), 124 mM (open triangles), 247 mM (filled triangles).

The involvement of hydrogen peroxide and superoxide in the oxidation was also investigated. Superoxide dismutase completely inhibited product formation, an effect which could not be reversed by the addition of exogenous peroxide. Thus, superoxide is essential

in HRP/DHFA-mediated oxidation, and its role is not limited to generation of hydrogen peroxide by dismutation. In contrast to the report of Dordick et al. (1986) addition of exogenous hydrogen peroxide or catalase had an effect on the reaction. Slight inhibition was observed for incubations containing catalase and slight acceleration for reactions to which exogenous H_2O_2 was added (Figure 4.3). Little effect, however, was observed on the total amount of product generated as observed by Dordick et al. (1986).

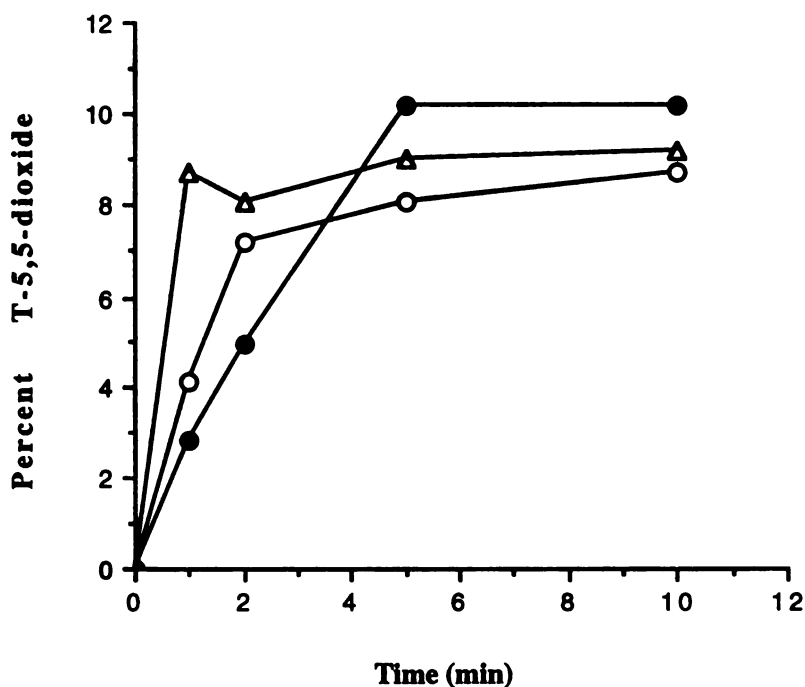


Figure 4.3: Effect of catalase and exogenous H_2O_2 on the HRP/DHFA/ O_2 -mediated oxidation of T-5-O. Standard incubation (open circles), + catalase (0.1 mg) (filled circles), + H_2O_2 (100 μ M) (open triangles).

Dordick et al. (1986) showed that compound III is stable and does not hydroxylate aromatic compounds unless DHFA is present. Analogous results were obtained for the reactivity of compound III itself with T-5-O. Compound III was formed by the reaction of horseradish peroxidase with superoxide generated from the autooxidation of DHFA followed by passage of the reaction mixture through Sephadex G25 to remove excess DHFA and other small redox-active substances. Compound III was reasonably stable in the absence of DHFA, with very little decay observed after 6 min. In the presence of DHFA, however, a half-life of approximately 3 min was determined. In the absence of DHFA, addition of T-5-O to compound III did not promote the decay of the iron-oxygen complex and did not give rise to oxygenated products. Thus, the requirement for DHFA in the HRP-catalyzed oxidation of T-5-O cannot be dismissed by compound III.

4.3 OXIDATION OF THE THIANTHRENE DIOXIDES BY THE HRP/DHFA/O₂ SYSTEM

The three thianthrene dioxide isomers were incubated with the HRP/DHFA/O₂ system. No 5,5,10-trioxide was detected in the 5,5-dioxide incubations, but both isomers of the 5,10-dioxide were converted to the trioxide. The time course for oxidation of the *cis*-5,10-dioxide (Figure 4.4) shows that, as in the case of the oxidation of T-5-O, the reaction is limited by the exhaustion of DHFA. An initial rate of approximately 7.6 nmol (nmol of enzyme)⁻¹ min⁻¹ was determined for product formation. Although the *trans*-5,10-dioxide

isomer is also oxidized to the trioxide, the rate is too slow to accurately estimate it.

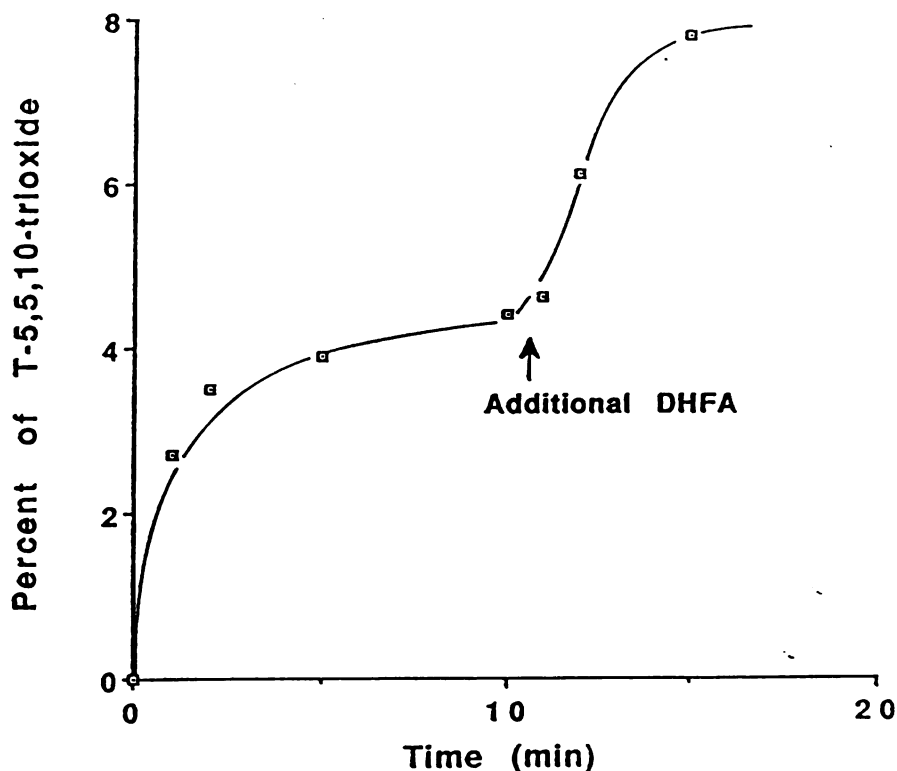


Figure 4.4: Time course of the conversion of *cis*-T-5-O to the 5,5,10-trioxide by horseradish peroxidase in the presence of DHFA and O₂. The arrow indicates the time point at which a second supply of DHFA was added to the incubation.

4.4 INVOLVEMENT OF HYDROXYL RADICAL IN THE AEROBIC OXIDATION OF T-5-O BY HORSERADISH PEROXIDASE AND DIHYDROXYFUMARATE

Hydroxyl radical has been proposed to be the active oxidant in the DHFA/HRP system based primarily on ambiguous inhibitory data. Although, due to its inherent reactivity, the hydroxyl radical is relatively non-selective as an oxidant, based on its electronic

properties it would be expected to behave as an electrophile rather than a nucleophile. To determine the products of the reaction of hydroxyl radical with T-5-O, the substrate was incubated with various "hydroxyl radical" generating systems.

Ferrous iron reacts with H_2O_2 in the Fenton reaction to produce different active oxidants depending on its chelation state. It has been proposed that with EDTA-complexed iron, approximately 90% of the oxidant formed appears to be the hydroxyl radical, whereas in the unchelated reaction it is not a significant product (Winterbourn, 1987). Chelation of the iron by diethylenetriamine-N,N,N',N'',N''-pentaacetate (DTPA) or ethylenediamine-N,N'-diacetate (EDDA) have been reported to produce oxidizing species other than hydroxyl radical (Rahhal & Richter, 1988; Rush & Koppenol, 1988). Incubation of T-5-O with nonchelated iron and H_2O_2 leads to the formation of both the 5,5-dioxide and 5,10-dioxide, with the 5,10-dioxide being formed in about a 5-fold excess. Chelation of the iron by EDTA, EDDA, or DTPA all resulted in the production of almost exclusively T-5,5-dioxide. Quantitative analysis revealed that no more 5,5-dioxide was being generated than in the unchelated reaction. Thus, the reaction leading to the 5,10-dioxide was being suppressed. The lack of differences between the "hydroxyl radical generating" EDTA reaction and the "non-hydroxyl radical generating" EDDA and DTPA reactions made it necessary to explore an alternative, less ambiguous system.

Incubation of T-5-O with hydroxyl radicals generated by the γ -radiolysis of nitrous oxide-saturated water by ^{60}Co produces the 5,5-dioxide as the only detectable product. The amount of product formed, however, can only account for a small fraction of the parent compound lost, suggesting that it is only a minor product of the reaction and that non-detected products, such as various states of aromatic hydroxylation, represent the majority of products. Furthermore, when the radiolysis was carried out in the acetate buffer used in the HRP/dihydroxyfumarate reactions, no thianthrene-5-oxide product or loss of the parent compound was detected. Apparently, hydroxyl radical is scavenged too rapidly by the 50 mM acetate for the T-5-O to be oxidized.

4.5 IMPLICATIONS OF T-5-O OXIDATION DATA ON THE MECHANISM OF HRP/DHFA-MEDIATED REACTIONS

Oxidation of T-5-O exclusively to the 5,5-dioxide (Figure 4.2), as well as the ability to convert the 5,10- but not the 5,5-dioxide to the 5,5,10-trioxide (Figure 4.4), suggests a nucleophilic oxidant in the HRP/DHFA/O₂ system. Thus, direct oxygenation by a P450- or chloroperoxidase-like electrophilic ferryl oxygen species is eliminated. Furthermore, the lack of product formation in the incubation of T-5-O with hydroxyl radical generated by γ -radiolysis in a buffer system analogous to that used for the HRP/DHFA incubation suggests it is unlikely that the oxidizing species in the DHFA/HRP system is the free hydroxyl radical.

An alternative for the oxidizing species in the DHFA/HRP system is a peroxy anion or peroxy radical, both of which would be expected to be nucleophilic in nature. One such possibility is an iron-dioxygen [$\text{Fe}^{\text{II}}\text{O}-\text{O}^-$] complex resulting from a one electron reduction of compound III. This would be consistent with the finding that DHFA is required for the oxidation of T-5-O even if compound III is preformed. The recent finding that an iron-peroxide complex (non-heme) catalyzes the hydrolysis of peptide bonds (Rana & Meares, 1991) lends support to this possibility.

A second alternative is the formation of a DHFA-peroxyl radical or anion by the recombination of a DHFA radical and either molecular oxygen or superoxide (Figure 4.5). The primary function of horseradish peroxidase in this co-oxidation process is to accelerate the generation of DHFA radicals by the classical peroxidase one electron abstraction using endogenously produced H_2O_2 . The initial steps of the mechanism are comparable to those proposed by MacDonald & Dunford (1989) for the HRP-catalyzed oxidation of malonaldehyde, a molecule similar to DHFA. The finding that low yields of T-5,5-dioxide are detected in control incubations with DHFA but no enzyme, as well as the probable involvement of H_2O_2 , are most consistent with this mechanism.

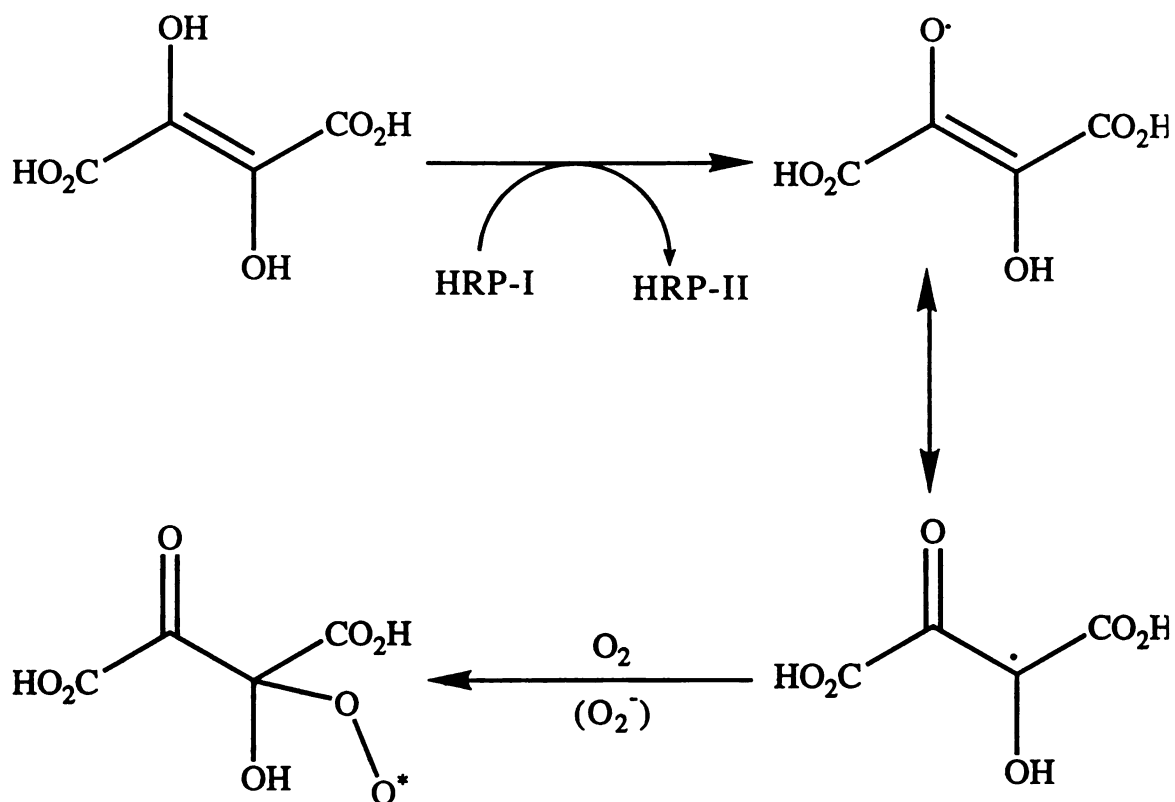


Figure 4.5: Mechanism for the formation of a hypothetical DHFA-peroxyl species ultimately responsible for the conversion of T-5-O to T-5,5-dioxide in the HRP/DHFA system. * The oxidizing species could be either the peroxy radical or the peroxy anion.

CHAPTER 5

HEMOGLOBIN-MEDIATED OXIDATION OF THIANTHRENE 5-OXIDE

5.1 INTRODUCTION

Hemoglobin and myoglobin catalyze the H_2O_2 -dependent epoxidation of olefins. Hemoglobin is oxidized by hydrogen peroxide to an iron-oxo species analogous to that of cytochrome P450 and a protein radical. Stereochemical analyses of the products of styrene, trans-stilbene, cis-stilbene, and 7,8-dihydroxy-7,8-dihydrobenzo[a]pyrene, in addition to determination of the origin of the incorporated oxygen atom, have resulted in the proposal of three mechanisms for the transformation (Ortiz de Montellano & Catalano, 1985, Catalano & Ortiz de Montellano, 1987). A fraction of the reaction proceeds with retention of the olefin stereochemistry and incorporation of an oxygen from the peroxide into the product, suggesting a cytochrome P450-like ferryl oxygen transfer to the olefin. A cooxidation mechanism in which the substrate is oxidized by a peroxy radical formed from the addition of oxygen to the protein radical was proposed for the fraction of the epoxidation that proceeds with loss of stereochemistry and incorporation of oxygen from O_2 rather than H_2O_2 (Figure 5.1) (Ortiz de Montellano & Catalano, 1985, Catalano & Ortiz de Montellano, 1987). A third mechanism, perhaps involving oxidation of the polycyclic aromatic hydrocarbon to a radical cation, is required to explain the incorporation of oxygen from water

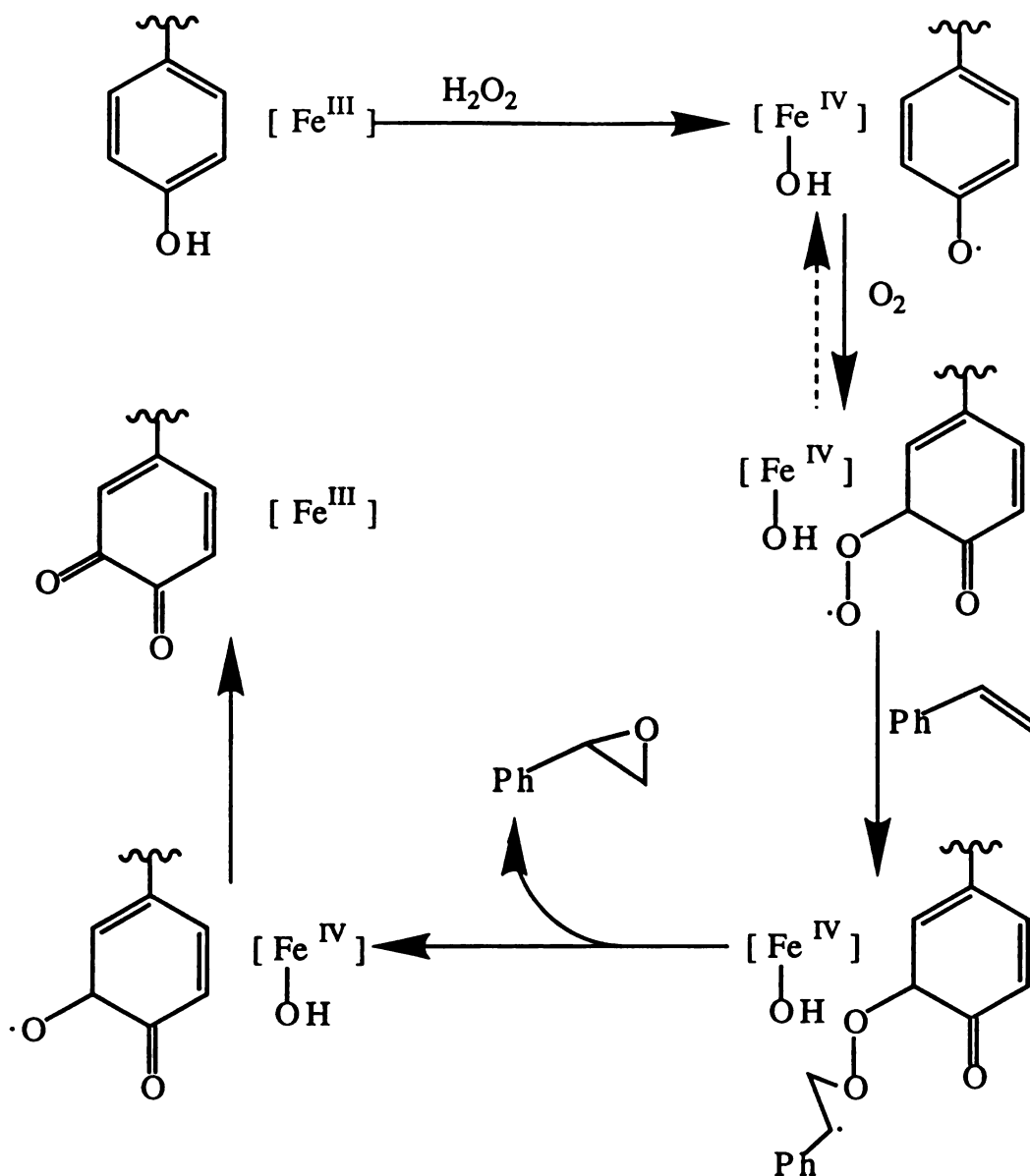


Figure 5.1: Mechanism proposed by Ortiz de Montellano & Catalano (1985) for the incorporation of molecular oxygen into styrene oxide in the H₂O₂-dependent oxidation of styrene by hemoglobin.

into the tetrol produced by epoxidation of 7,8-dihydro-7,8-dihydroxybenzo[a]pyrene by hemoglobin (Catalano & Ortiz de Montellano, 1987).

5.2 OXIDATION OF T-5-O BY THE HEMOGLOBIN/H₂O₂ SYSTEM

Incubation of T-5-O with human hemoglobin and H₂O₂ results in its conversion to the 5,5-dioxide, 5,10-dioxide, and 5,5,10-trioxide (Figure 5.2). No products were detected in control incubations lacking either hemoglobin or H₂O₂. Initial rates of 50 nmol (mg of hemoglobin)⁻¹ (min)⁻¹ and 160 nmol (mg hemoglobin)⁻¹ (min)⁻¹ for T-5,5-dioxide and T-5,10-dioxide formation, respectively, were determined. The ratio of the 5,10-dioxide to 5,5-dioxide produced was 5:1. Incubation of T-5,5-dioxide or either *cis*- or *trans*-T-5,10-dioxide with hemoglobin and H₂O₂ establishes that all three dioxides are converted to the trioxide, although oxidation of the *trans*-T-5,10-dioxide is somewhat sluggish in comparison to the other two.

Neither molecular oxygen nor superoxide appear to be involved in the oxidation of T-5-O. Neither running the incubation under anaerobic conditions nor in the presence of superoxide dismutase had much effect on product distribution or yields. Furthermore, mass spectrometric analysis of the products isolated from an incubation run under an ¹⁸O₂ atmosphere confirmed the results observed in the anaerobic incubation. None of the products showed

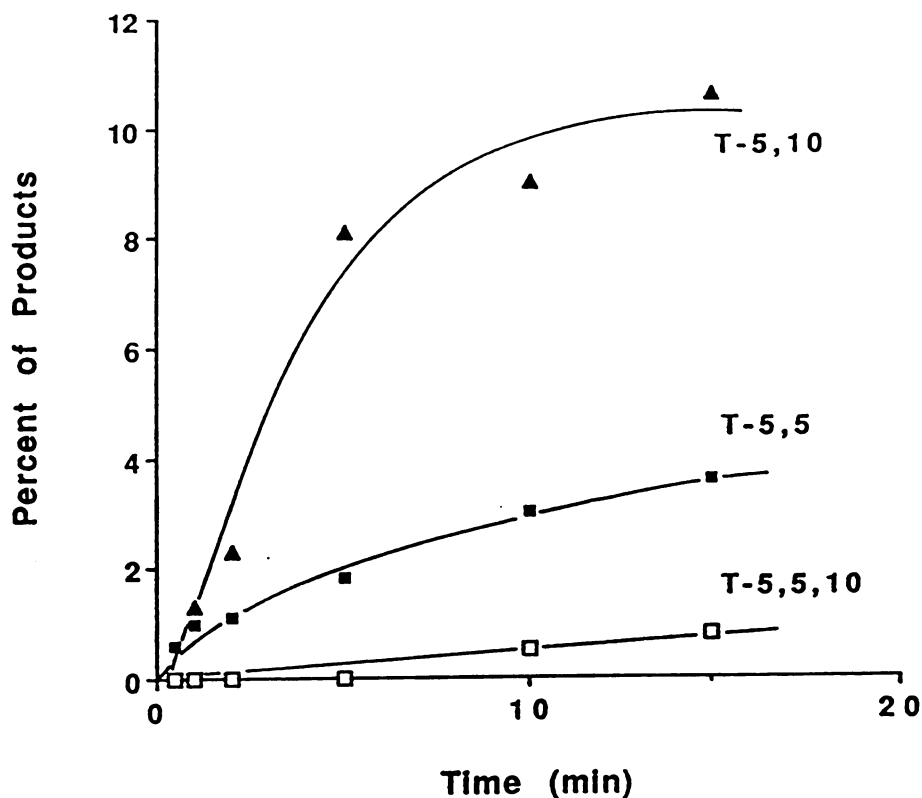


Figure 5.2: Time course for the conversion of T-5-O by human hemoglobin and H₂O₂ to T-5,5-dioxide (filled squares), T-5,10-dioxide (filled triangles), and T-5,5,10-dioxide (open squares).

significant (> 5% above natural abundance background) incorporation of labeled oxygen.

In contrast, incubations with [¹⁸O]H₂O₂ implicate hydrogen peroxide as the source of the oxygen atom incorporated into both products. Incorporation of the label into 92% and 85% (after correction for the specific ¹⁸O-content of the peroxide) of the T-5,5-dioxide was found in two different incubations. Likewise, the ¹⁸O-content of the 5,10-

dioxide product was found to be 90% and 94% in two different experiments. Thus, it appears as though most, if not all, of the incorporated oxygen atoms originate from H_2O_2 .

5.3 STEREOSELECTIVITY OF THE CONVERSION OF T-5-O TO T-5,10-DIOXIDE BY HEMOGLOBIN/ H_2O_2

Analysis of the stereochemical identity of the T-5,10-dioxide produced from the oxidation of T-5-O by the hemoglobin/ H_2O_2 system reveals a high degree of stereoselectivity for the reaction. The ratio of *cis:trans* 5,10-dioxide is almost 1:10 (9.3 ± 2.0 *cis*). Thus, the geometry of the substrate appears to be highly constrained within the enzyme's active site. This is in agreement with the crystal structures of sperm whale myoglobin (Takano, 1977a,b) and human hemoglobin (Fermi & Perutz, 1977), in which the heme is located near the surface of a congested crevice capped by a histidine residue. Ligands can be somewhat accommodated by displacement of the histidine, as is observed in the crystal structures of the myoglobin phenyl-iron complex (Ringe et al., 1984), the ethylisocyanide complex of myoglobin (Johnson et al., 1989), and the complex of methemoglobin with imidazole (Bell et al. 1981). Nonetheless, there is only sufficient room to bind T-5-O in a very highly constrained geometry. Interestingly, chlorpromazine, a substrate resembling T-5-O, has been shown to bind to hemoglobin, perturbing its heme crevice (Bhattacharyya et al., 1989, 1990). Furthermore, chlorpromazine is oxidized by hemoglobin/ H_2O_2 , and binds

covalently to the protein as a result of its catalytic turnover (Kelder et al., 1991; Magee & Marletta, 1989).

5.4 IMPLICATIONS OF THE RESULTS OF T-5-O OXIDATION BY HEMOGLOBIN/H₂O₂ ON THE MECHANISM

Human methemoglobin catalyzes the H₂O₂-dependent oxidation of T-5-O to both the 5,5- and 5,10-dioxide metabolites (Figure 5.2), making it unique among the systems examined. Thus, the enzyme produces an electrophilic and either a nucleophilic or high oxidation potential radical oxidant.

Production of the 5,10-dioxide, the product of an electrophilic oxidant, is consistent with direct oxidation of the substrate by a cytochrome P450-like ferryl species. The fact that the incorporated oxygen atom incorporated into this product originates either primarily or exclusively from H₂O₂ supports such a mechanism. A ferryl species, which is known to be formed in the reaction of methemoglobin with H₂O₂, has been previously implicated in the epoxidation of styrene and stilbene (Ortiz de Montellano & Catalano, 1985; Catalano & Ortiz de Montellano, 1987).

A mechanism rationalizing the oxidation of T-5-O to the 5,5-dioxide, however, is less readily devised. A co-oxidation mechanism analogous to that proposed for the methemoglobin-catalyzed conversion of styrene to styrene oxide (Ortiz de Montellano & Catalano, 1985; Catalano & Ortiz de Montellano, 1987) is eliminated

by the lack of incorporation of label from $[^{18}\text{O}]\text{-O}_2$, and incorporation of a peroxide-derived oxygen atom, into the product. The lack of effect of superoxide dismutase both on extent of product formation and product distribution also rules out a mechanism involving a superoxide radical anion produced by autooxidation of the hemoglobin ferrous dioxygen complex. One possibility for the oxidant is an activated ferrous dioxygen complex such as $\text{Fe}^{\text{II}}\text{-O-O}^-$, derived from the transfer of an electron to oxyhemoglobin.

CHAPTER 6

SUMMARY AND CONCLUSIONS

Thianthrene 5-oxide (T-5-O), a compound previously used to probe the electronic character of chemical oxidants, was used to help characterize the active oxidant in various hemoprotein oxygenating systems. Cytochrome P450 and chloroperoxidase, which are thought to transfer an electrophilic ferryl oxygen to the substrate, convert T-5-O exclusively to the 5,10-dioxide, as expected. The active site environment of cytochrome P450, however, appears to endow its oxidant with more oxidative power than that of chloroperoxidase based on its ability to more efficiently oxidize the T-5,10-dioxides to the 5,5,10-trioxide.

Horseradish peroxidase catalyzes the DHFA-dependent aerobic oxidation of T-5-O to the T-5,5-dioxide, the product of a nucleophilic oxidant. [¹⁸O] Experiments indicate the oxygen atom incorporated into the product is derived from molecular oxygen. It has been suggested, based primarily on product distribution and inhibition by radical scavengers, that the hydroxyl radical is responsible for the transformation. However, γ -radiolytically-generated hydroxyl radicals fail to oxidize T-5-O under conditions analogous to those used for the HRP/DHFA incubations. Thus, a co-oxidative mechanism for the transformation has been proposed.

Hemoglobin is unique among the enzymes examined in that it converts T-5-O efficiently to both the 5,5- and 5,10- dioxides. Thus, it appears as though multiple oxidative mechanisms are taking place. Neither superoxide nor molecular oxygen appear to be involved in the transformation because incubations with ^{18}O -labeled hydrogen peroxide have identified it as the primary source of the transferred oxygen atom in both products. The electrophilic oxidant product (T-5,10-dioxide) is consistent with oxidation by a cytochrome P450-like ferryl species, whereas a mechanism invoking an activated ferrous dioxygen complex ($\text{Fe}^{\text{II}}\text{-O-O}^-$) is proposed for the formation of the 5,5-dioxide.

An additional feature of T-5-O as a mechanistic probe in biological systems is its ability to investigate the stereoselectivity of the reaction of electrophilic oxidants due to the existence of *cis*- and *trans*- T-5,10-dioxides. Stereochemical analysis of the 5,10-dioxide reveals that, although all three products are thought to be generated by analogous mechanisms, there are significant differences in the T-5,10-dioxide isomer distributions that are produced. Thus, cytochrome P450, chloroperoxidase, and hemoglobin exhibit *cis:trans* ratios of about 1.3:1, 2.5:1, and 1:10, respectively (Table 6.1). These differences in the isomer ratio are thought to reflect the geometrical constraints imposed on the substrate by the protein.

The utility of T-5-O as a tool for characterizing the electronic properties of biological oxidants has been demonstrated. Although it is not a mechanistic panacea, it can provide valuable insight into the

Table 6.1. Isomeric composition of the T-5,10-dioxide product

<u>Enzyme system</u>	<u>% cis</u>	<u>% trans</u>	<u>cis/trans</u>
Cytochrome P450	57.1 ± 0.9	42.9 ± 0.9	1.3
Chloroperoxidase	71.3 ± 1.3	28.7 ± 1.3	2.5
Hemoglobin	9.3 ± 2.0	90.7 ± 2.0	0.1

electronic properties of the oxidant and eliminate otherwise viable alternatives. Furthermore, by the fact that cis and trans isomers can be generated by electrophilic oxidants, T-5-O can also serve to probe geometrical constraints imposed on the substrate by the enzyme. T-5-O has, in the present study, aided in the development of mechanisms for several hemoprotein oxidative systems and should prove similarly useful in the characterization of other heme and non-heme oxidants.

CHAPTER 7

EXPERIMENTAL

7.1 EQUIPMENT

NMR spectra were obtained on a General Electric QE-300 instrument in CDCl_3 . Chemical shifts are reported in parts per million downfield from the internal standard (TMS). Infrared spectra were recorded on a Nicolet 5DX FTIR and are reported in cm^{-1} . Absorption spectra were recorded on a Hewlett-Packard 8450A diode array spectrophotometer. High pressure liquid chromatography was performed on a system consisting of two Beckman 110A pumps, an Altex gradient controller, and a Hewlett-Packard 1040A diode array detector interfaced with a Hewlett-Packard Work Station. Electron impact mass spectra were obtained on a Kratos MS-25 instrument at 70 eV ionizing current.

7.2 MATERIALS

Horseradish peroxidase (Type VI), chloroperoxidase from *Caldariomyces fumago*, human hemoglobin (Type IV), NADP, superoxide dismutase, glucose-6-phosphate, glucose-6-phosphate dehydrogenase, 30% H_2O_2 , and DHFA were purchased from Sigma (St. Louis, MO). Thianthrene was purchased from Aldrich Chemical Co. $^{18}\text{O}_2$ (97.6 atom% ^{18}O) was purchased from MSD Isotopes. $[^{18}\text{O}]\text{H}_2\text{O}_2$

was prepared from $^{18}\text{O}_2$ by the method of Sawaki and Foote (1979) as described below or was purchased from ICON (Summit, New Jersey). The concentration of the $[\text{}^{18}\text{O}]\text{H}_2\text{O}_2$, determined by iodimetric titration (Pesez and Bartos, 1974), was 62 and 800 mM, respectively, for the synthetic and commercial samples. The ^{18}O -content of the peroxide was determined by gas chromatography-mass spectrometry of the menadione epoxide generated by reaction of the peroxide with menadione under basic conditions (Ortiz de Montellano and Catalano, 1985). The ^{18}O -content was 52.8% and 97.9%, respectively, for the synthetic and commercial samples. 1-Aminobenzotriazole was synthesized by Dr. Ralph Stearns according to the procedure of Campbell and Rees (1969). All buffers were Chelex-treated to remove trace metal ions.

7.3 SYNTHETIC PROCEDURES

Thianthrene 5-oxide: T-5-O was synthesized by refluxing a solution of thianthrene and nitric acid in glacial acetic acid (Gilman and Swayampati, 1955a). The product was shown to be pure by high pressure liquid chromatography. The compound had infrared, NMR, and mass spectra consistent with the assigned structure and a melting point in good agreement with the literature value. Melting point: 142-143 °C (reported 143-143.5 °C) (Gilman and Swayampati, 1955a). Absorption maxima for the compound were observed at 201 and 245 nm.

Thianthrene 5,10-dioxides: The 5,10-dioxides of thianthrene were synthesized by bubbling chlorine at a rapid rate through a suspension of thianthrene in boiling 90% acetic acid (Gilman and Swayampati, 1955b). The *cis*-T-5,10-dioxide crystallized from the reaction mixture when the heating was discontinued. The *trans*-T-5,10-dioxide, which remained in the reaction solvent after cooling, was purified by column chromatography with 10% methanol in toluene. The 5,10-dioxides were shown to be pure by high pressure liquid chromatography. The compounds had infrared, NMR, and mass spectra consistent with the assigned structures and melting points in good agreement with literature values. Melting points: *cis*-T-5,10-dioxide, 281-282 °C (reported 284 °C) (Hosoya, 1966); *trans*-T-5,10-dioxide, 250-251 °C (reported 249 °C) (Hosoya, 1966). Both compounds had a maximum in their absorption spectra at 213 nm.

Thianthrene 5,5-dioxide: T-5,5-dioxide was prepared by refluxing T-5,5,10-trioxide with zinc dust in 90% acetic acid (Gilman and Swayampati, 1955b). The product was recrystallized from acetic acid, and was shown to be pure by high pressure liquid chromatography. The compound had infrared, NMR, and mass spectra consistent with the assigned structure and a melting point in good agreement with literature values. Melting point: 164-165 °C (reported 168-169 °C) (Gilman and Swayampati, 1955b). Absorption maxima for the compound were observed at 225, 263, 281, and 311 nm.

Thianthrene 5,5,10-trioxide: T-5,5,10-trioxide was synthesized by continuing the oxidation of thianthrene with chlorine gas in acetic acid beyond the T-5,10-dioxide stage (Gilman and Swayampati, 1955b). The product was recrystallized from 90% acetic acid. The 5,5,10-trioxide was shown to be pure by high pressure liquid chromatography. The compound had infrared, NMR, and mass spectra consistent with the assigned structure and a melting point in good agreement with literature values. Melting point: 220-221.5 °C (reported 221.5-222.5 °C) (Gilman and Swayampati, 1955b). Absorption maxima for the compound were observed at 217, 243, 275 nm

$[^{18}\text{O}]\text{H}_2\text{O}_2$: ^{18}O -labeled hydrogen peroxide was prepared by the base-catalyzed oxidation of benzhydrol by $^{18}\text{O}_2$ (Sawaki and Foote, 1979; Grassi *et al.*, 1983). The resulting $[^{18}\text{O}]\text{-KOOH}$ was washed with ether and dissolved in 30 ml of 1N HCl containing 1 mM EDTA. The concentration of the $[^{18}\text{O}]\text{H}_2\text{O}_2$ was determined to be 62 mM by iodimetric titration (Pesez and Bartos, 1974). The ^{18}O -content of the peroxide was determined to be 52.8% by gas chromatography-mass spectrometry of the menadione epoxide generated by reaction of the peroxide with menadione under basic conditions (Ortiz de Montellano and Catalano, 1985).

7.4 INCUBATION PROCEDURES

Microsomal cytochrome P450 incubations: Liver microsomes were prepared from Sprague-Dawley male rats pretreated with sodium

phenobarbital (80 mg Kg⁻¹ day⁻¹ for 4 days) as previously reported (Ortiz de Montellano et al., 1981). Incubations contained 1 μM microsomal cytochrome P450, 200 μM T-5-O, 1 mM NADPH, 3 mM glucose-6-phosphate, 2 mM MgCl₂, 14 units of glucose-6-phosphate dehydrogenase, 150 mM KCl, and 1.5 mM DTPA in 7 ml of chelexed 100 mM phosphate buffer (pH 7.4). Incubations were carried out at 37 °C. Aliquots of 1 ml each were withdrawn at appropriate time periods and were combined with 17.5 μl of 10 mM phenyl sulfone, the internal standard. The reaction was quenched by extraction into 7 ml of methylene chloride. The extracts were concentrated to dryness on a rotary evaporator and the residue taken up in the mobile phase used for HPLC analysis. Control incubations which differed only in the absence of the NADPH regenerating system were also carried out. The T-5-O was replaced in some incubations by T-5,5-dioxide (50 μM) or either *cis*- (100 μM) or *trans*-T-5,10-dioxide (130 μM). In some experiments, the complete liver microsomal mixture was incubated with 500 μM or 5 mM of 1-aminobenzotriazole for 17 min prior to the addition of the T-5-O. The mixture was incubated for an additional 10 min after the addition of the substrate.

Chloroperoxidase incubations: A solution of chloroperoxidase (6.66 μM), H₂O₂ (233 μM), and 50 μM T-5-O in 100 mM acetate buffer (pH 5.0) was incubated at 25 °C. Phenyl sulfone was added as an internal standard to aliquots withdrawn from the incubation at various time points prior to their extraction with methylene chloride. The extracts were concentrated on a rotary evaporator and analyzed by high

pressure liquid chromatography. Analogous incubations were carried out replacing the T-5-O with *trans*-T-5,10-dioxide (50 μ M), *cis*-T-5,10-dioxide (50 μ M), or T-5,5-dioxide (13.5 μ M) as the substrate.

Horseradish peroxidase/DHFA incubations: Horseradish peroxidase (200 nM), 50 μ M T-5-O, and 3 mg of DHFA in 20 ml of chelex-treated 50 mM sodium acetate buffer (pH 5.0) were incubated at 25 °C with oxygen continuously bubbled through the incubation mixture. Additional DHFA (1.5 mg) was added in some experiments after 10 min. Aliquots (1 ml) removed at the desired time points were combined with 5 μ l of a 10 mM phenyl sulfone solution and were then immediately extracted with methylene chloride. The extracts were concentrated to dryness on a rotary evaporator and the product residues were analyzed by high pressure liquid chromatography. In some incubations, the T-5-O was replaced by the 5,5-dioxide (50 μ M), *cis*-5,10-dioxide (50 μ M), or *trans*-5,10-dioxide (50 μ M). Some incubations contained superoxide dismutase (2 mg, 7100 units), catalase (0.1 mg), or H₂O₂ (100 μ M). Methanol (49, 124, 247 mM) was added to a set of smaller (5 ml) incubations and 1 ml aliquots were periodically removed and analyzed for metabolite formation. Control incubations were carried out in the absence of horseradish peroxidase.

In some experiments, compound III was preformed by aerobic incubation of horseradish peroxidase with DHFA. The reaction was then passed through a Sephadex G-25 column to remove excess DHFA

and other small molecules. The compound III solution thus obtained was diluted with an equal amount of buffer. The half-life of compound III was determined spectrophotometrically in the absence and presence of 50 μ M T-5-O.

Incubation of Horseradish Peroxidase/DHFA with T-5-O and $^{18}\text{O}_2$: Approximately 25 ml of a 1 μ M solution of horseradish peroxidase in 50 mM sodium acetate buffer (pH 5.0) was placed in a three neck round bottom flask equipped with a pressure equalizing funnel containing 45 mg of DHFA in 10 ml of the same buffer. An ampule containing 250 ml of $^{18}\text{O}_2$ and a vacuum manifold were attached to the other two necks. The system was repeatedly evacuated and purged with nitrogen and was finally left under a slightly negative pressure of nitrogen. The vigorously stirred mixture was then cooled in an ice bath, the oxygen ampule was opened, and one third of the DHFA was added to initiate the reaction. The remaining DHFA was added in two further equal portions after the first and second hours of the incubation. After three hours, the mixture was extracted with methylene chloride, the extracts were concentrated to dryness on a rotary evaporator, and the product residues were analyzed by high pressure liquid chromatography. The T-5,5-dioxide product was collected and was analyzed by mass spectrometry.

Hemoglobin incubations: To a solution of human hemoglobin (40 μ M heme) and T-5-O (50 μ M) in 5 ml of 200 mM phosphate buffer (pH 7.4) was added enough H_2O_2 to bring its final concentration to 600 μ M. The mixture was incubated at 25 $^\circ\text{C}$. Aliquots were removed at

various time points and were combined with 5 μ l of 10 mM phenyl sulfone prior to extraction into methylene chloride. The methylene chloride extracts were concentrated and analyzed by high pressure liquid chromatography. Control incubations differed only in the absence of the hemoglobin. Analogous incubations in which the T-5-O was replaced by equal concentrations of *trans*- or *cis*-T-5,10-dioxide or T-5,5-dioxide were also carried out. Superoxide dismutase (2 mg, 7200 units) was added to some incubations.

The origin of the incorporated oxygen atom was determined by analogous incubations either under an $^{18}\text{O}_2$ atmosphere, or by replacing the hydrogen peroxide with $^{18}\text{O}]\text{H}_2\text{O}_2$. For the $^{18}\text{O}_2$ incubations, hemoglobin (80 mg) was added to 20 ml of chelex-treated 200 mM phosphate buffer (pH 7.4) containing 50 μ M T-5-O. After several evacuation/argon purge cycles, $^{18}\text{O}_2$ was admitted to the flask by breaking the gas ampule seal. The reaction was commenced by the addition of 150 μ l of 0.1 M H_2O_2 . After 20 min, the reaction was worked up and the products separated and collected by HPLC. The 5,5-dioxide, 5,10-dioxide, and 5,5,10-trioxide products were then analyzed by mass spectrometry. $^{18}\text{O}]\text{H}_2\text{O}_2$ incubations contained 40 mg of hemoglobin and 100 μ M T-5-O in a total of 10 ml of buffer. These reactions were initiated, without the argon purge step, by adding either 350 μ l of 62 mM $^{18}\text{O}]\text{H}_2\text{O}_2$ or 70 μ l of 100 mM $^{18}\text{O}]\text{H}_2\text{O}_2$.

Fenton Oxidations: To a mixture of ferrous sulfate (1 mM) and thianthrene-5-oxide (100 μ M) in 100 mM acetate buffer (pH 5.0) was

added H₂O₂ (100 μM). Aliquots (1 ml) were periodically removed and combined with phenyl sulfone prior to extraction with CH₂Cl₂. The methylene chloride extracts were concentrated and analyzed by HPLC. Control incubations were run in the absence of ferrous sulfate. In some incubations, ferrous sulfate was replaced by ferric chloride. To other incubations, a 1.5-fold molar excess of EDTA, DTPA, or EDDA relative to the ferrous sulfate concentration was added.

γ-Radiolysis experiments: Two sets of four 10 ml samples were prepared. The samples of the first set contained 50 μM thianthrene-5-oxide in double glass-distilled water and those of the second set the same amount of compound in 50 mM Chelex-treated acetate buffer (pH 5.0). Each sample was sealed in a glass ampule under nitrous oxide gas after vigorously bubbling with the gas. The samples were irradiated with a Motorola ⁶⁰Co source calibrated at a dose rate of 70 rad/30 sec at 64 cm. The samples were irradiated with doses of 5,000 (8.9 min), 10,000 (17.8 min), or 20,000 (35.8 min) rads. The ampules were then opened, phenyl sulfone added as the internal standard, and the products extracted and analyzed by HPLC.

7.5 PRODUCT IDENTIFICATION

The identity of the products was routinely confirmed by comparison of their HPLC retention times and absorption spectra with those of authentic samples. The mass spectra of the metabolites were also compared with those of the standards in early experiments. The HPLC analysis was carried out isocratically (hexane : tetrahydrofuran

: methanol 95 : 5 : 0.5) on a Partisil silica gel column at a solvent flow rate of 3.0 ml/min with the variable wavelength detector set at 215 nm. A standard curve was prepared using phenyl sulfone, which is well separated from the thianthrene oxides in this system, as an internal standard. Known amounts of the sulfone and of each of the thianthrene oxides were added to phosphate buffer, the mixture was extracted into methylene chloride, and the solvent was removed on a rotary evaporator. The residues were taken up in the mobile phase used for HPLC analysis. The standard curves were based on five points each and had correlation coefficients greater than 0.970. A typical chromatogram of the thianthrene oxide standards and the phenyl sulfone is shown in Figure 7.1.

The *cis*- and *trans*-T-5,10-dioxide isomers are not resolved in the above HPLC system but are resolved by elution from the same column with 2.9% methanol in methylene chloride at a flow rate of 0.35 ml/min with the variable wavelength detector set at 225 nm. This gives retention times of approximately 10, 12, 14, and 16 min for the 5,5-dioxide, 5,5,10-trioxide, 5-oxide, and *cis*-5,10-dioxide, respectively. The *trans*-5,10-dioxide has a much longer retention time in this system and is therefore eluted by increasing the flow rate to 2 ml/min after the elution of the *cis* isomer. The concentrations of the two isomers were calculated based on a standard curve prepared with known amounts of the two isomers.

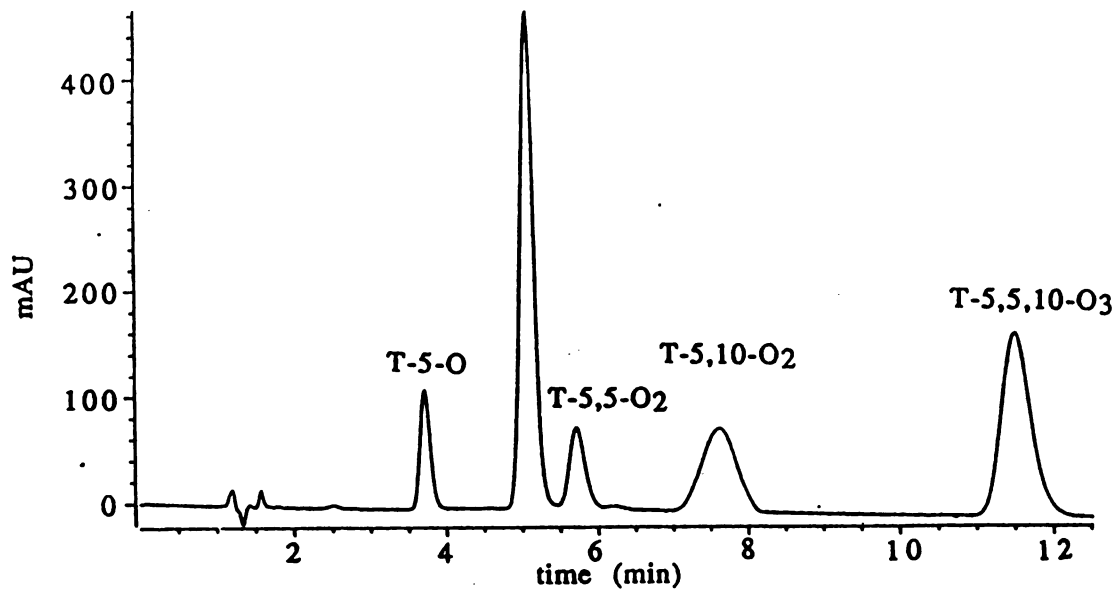


Figure 7.1. High pressure liquid chromatogram of the thianthrene oxides standards and phenyl sulfone (internal standard). The peaks at 3.7, 5.0, 5.7, 7.6, and 11.5 minutes correspond to T-5-O, phenyl sulfone, T-5,5-O₂, T-5,10-O₂, and T-5,5,10-O₃, respectively.

REFERENCES

- Adam, W., Chan, Y. Y., Cremer, D., Gauss, J., Scheutzow, D. and Schindler, M. (1987) Spectral and Chemical Properties of Dimethyldioxirane as Determined by Experiment and ab Initio Calculations, *J. Org. Chem.* **52**, 2800-2803.
- Adam, W., Haas, W. and Lohray, B. B. (1991) Thianthrene 5-Oxide as a Mechanistic Probe for Assessing the Electronic Character of Oxygen-Transfer Agents, *J. Am. Chem. Soc.* **113**, 6202-6208.
- Adam, W., Haas, W. and Sieker, G. (1984) Thianthrene 5-Oxide as a Mechanistic Probe in Oxygen-Transfer Reactions: The Case of Carbonyl Oxides vs. Dioxiranes, *J. Am. Chem. Soc.* **106**, 5020-5022.
- Ballisteri, F. P., Tomaselli, G. A., Toscano, R. M., Conte, V. and Di Furia, F. (1991) Application of the Thianthrene 5-Oxide Mechanistic Probe to Peroxometal Complexes, *J. Am. Chem. Soc.* **113**, 6209-6212.
- Bell, J. A., Korszun, Z. R. and Moffat, K. (1981) Structure of Imidazole Methemoglobin, *J. Mol. Biol.* **147**, 325-335.
- Bhattacharyya, M., Chaudhuri, U. and Poddar, R. K. (1989) Cooperative Binding of Chlorpromazine with Hemoglobin, *Biochem. International* **19**, 1363-1372.
- Bhattacharyya, M., Chaudhuri, U. and Poddar, R. K. (1990) Evidence for Cooperative Binding of Chlorpromazine with Hemoglobin: Equilibrium Dialysis, Fluorescence Quenching, and Oxygen Release Studies, *Biochem. Biophys. Res. Commun.* **167**, 1146-1153.
- Bors, W., Michel, C. and Saran, M. (1979) On the Nature of Biochemically Generated Hydroxyl Radicals. Studies Using the Bleaching of p-Nitosodimethylaniline as a Direct Assay Method, *Eur. J. Biochem.* **95**, 621-627.
- Buhler, D. R. and Mason, H. S. (1961) Hydroxylation Catalyzed by Peroxidase, *Arch. Biochem. Biophys.* **92**, 424-437.

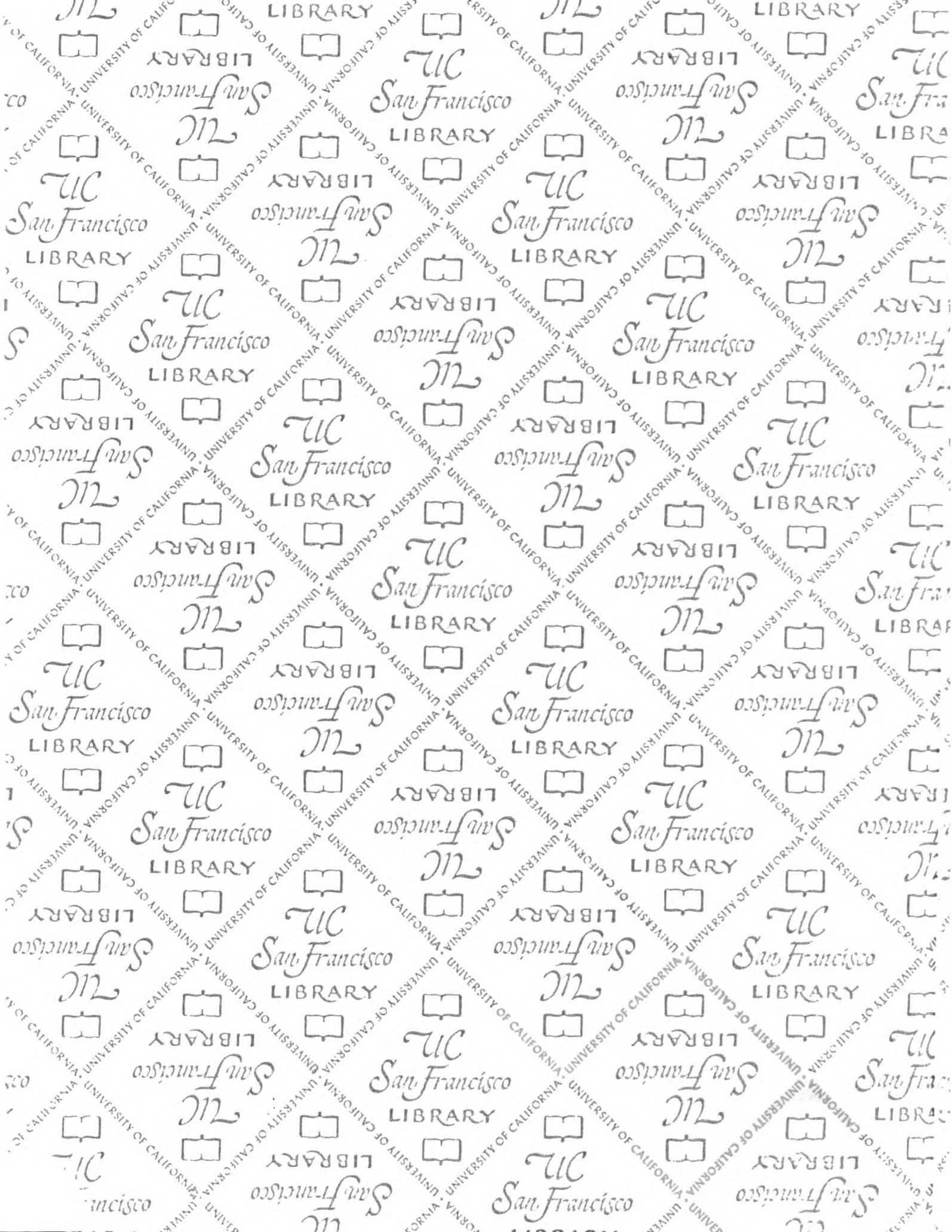
- Campbell, C. D. and Rees, C. W. (1969) Reactive Intermediates. I. Synthesis and Oxidation of 1- and 2-Aminobenzotriazole, *J. Chem. Soc. C* 742-747.
- Cashman, J. R. (1987) A Convenient Radiometric Assay for Flavin-Containing Monooxygenase Activity, *Anal. Biochem* **160**, 294-300.
- Catalano, C. E. and Ortiz de Montellano, P. R. (1987) Oxene Transfer, Electron Abstraction, and Cooxidation in the Epoxidation of Stilbene and 7,8-Dihydroxy-7,8-dihydrobenzo[a]pyrene by Hemoglobin, *Biochemistry* **26**, 8373-8380.
- Daly, J. W. and Jerina, D. M. (1970) Aerobic Aromatic Hydroxylation Catalyzed by Horseradish Peroxidase: Absence of NIH Shift, *Biochim. Biophys. Acta* **208**, 340-342.
- Dawson, J. H. (1988) Probing Structure-Function Relations in Heme-Containing Oxygenases and Peroxidases, *Science* **240**, 433-439.
- Dawson, J. H. and Sono, M. (1987) Cytochrome P-450 and Chloroperoxidase: Thiolate-ligated Heme Enzymes. Spectroscopic Determination of their Active-site Structures and Mechanistic Implications of Thiolate Ligation, *Chem. Rev.* **87**, 1255-1276.
- Doerge, D. R. (1986) Oxygenation of Organosulfur Compounds by Peroxidases: Evidence of an Electron Transfer Mechanism for Lactoperoxidase, *Arch. Biochem. Biophys.* **244**, 678-685.
- Dordick, J. S., Klibanov, A. M. and Marletta, M. A. (1986) Horseradish Peroxidase Catalyzed Hydroxylations: Mechanistic Studies, *Biochemistry* **25**, 2946-2951.
- Fermi, G. and Perutz, M. F. (1977) Structure of Human Fluoromethaemoglobin with Inositol Hexaphosphate, *J. Mol. Biol.* **114**, 421-431.
- Gilman, H. and Swayampati, D. (1955a) Conversion of Thianthrene-5-oxide to Dibenzothiophene by *n*-Butyllithium, *J. Am. Chem. Soc.* **77**, 3387-3389.
- Gilman, H. and Swayampati, D. (1955b) Studies in the Thianthrene System: Bromination and Reductive Bromination, *J. Am. Chem. Soc.* **77**, 5944-5948.

- Grassi, Oldani and Bauder (1983) Synthesis of Concentrated ^{18}O -Labeled Hydrogen Peroxide and of ^2H -, ^{13}C - and ^{18}O -Labeled Peroxyformic Acid, *Helv. Chim Acta* **66**, 400-404.
- Guengerich, F. P. (1987) *Mammalian Cytochromes P-450* (Guengerich, F. P., ed) Vol. 1, pp. 2-54, CRC Press, Boca Raton, Florida.
- Halliwell, B. and Ahluwalia, S. (1976) Hydroxylation of *p*-Coumaric Acid by Horseradish Peroxidase, *Biochem. J.* **153**, 513-518.
- Hollenberg, P. F. (1992) Mechanisms of Cytochrome P450 and Peroxidase-Catalyzed Xenobiotic Metabolism, *FASEB J.* **6**, 686-694.
- Hosoya, S. (1966) The Crystal and Molecular Structure of β -Thianthrene Dioxide, $\text{C}_6\text{H}_4\text{-(SO)}_2\text{-C}_6\text{H}_4$, *Acta Cryst.* **21**, 21-26.
- Johnson, K. A., Olson, J. S. and Phillips, G. N. (1989) Structure of Myoglobin-Ethyl Isocyanide: Histidine as a Swinging Door for Ligand Entry, *J. Mol. Biol.* **207**, 459-463.
- Kelder, P. P., Fischer, M. J. E., de Mol, N. J. and Janssen, L. H. M. (1991) Oxidation of Chlorpromazine by Methemoglobin in the Presence of Hydrogen Peroxide. Formation of Chlorpromazine Radical Cation and its Covalent Binding to Methemoglobin, *Arch. Biochem. Biophys.* **284**, 313-319.
- Kobayashi, S., Nakano, M., Goto, T., Kimura, T. and Schaap, A. P. (1986) An Evidence of the Peroxidase-Dependent Oxygen Transfer from Hydrogen Peroxide to Sulfides, *Biochem. Biophys. Res. Commun.* **135**, 166-171.
- Kobayashi, S., Nakano, M., Kimura, T. and Schaap, A. P. (1987) On the Mechanism of the Peroxidase-Catalyzed Oxygen-Transfer Reaction, *Biochemistry* **26**, 5019-5022.
- MacDonald, I. D. and Dunford, H. B. (1989) Mechanism of Horseradish Peroxidase-Catalyzed Oxidation of Malonaldehyde, *Arch. Biochem. Biophys.* **272**, 185-193.
- Mason, H. S., Onopryenko, I. and Buhler, D. (1957) Hydroxylation: The Activation of Oxygen by Peroxidase, *Biochim. Biophys. Acta* **24**, 225-226.

- Ortiz de Montellano, P. R. (1986) Oxygen Activation and Transfer, in *Cytochrome P-450: Structure, Mechanism, and Biochemistry* (Ortiz de Montellano, P. R., ed) pp. 217-272, Plenum Press, New York.
- Ortiz de Montellano, P. R. (1987) Control of the Catalytic Activity of Prosthetic Heme by the Structure of Hemoproteins, *Accts. Chem. Res.* **20**, 289-294.
- Ortiz de Montellano, P. R. and Catalano, C. E. (1985) Epoxidation of Styrene by Hemoglobin and Myoglobin: Transfer of Oxidizing Equivalents to the Protein Surface, *J. Biol. Chem.* **260**, 9265-9271.
- Ortiz de Montellano, P. R., Choe, Y. S., DePillis, G. and Catalano, C. E. (1987) Structure-Mechanism Relationships in Hemoproteins: Woxygenations Catalyzed by Chloroperoxidase and Horseradish Peroxidase, *J. Biol. Chem.* **262**, 11641-11646.
- Ortiz de Montellano, P. R. and Mathews, J. M. (1981) Autocatalytic Alkylation of the Cytochrome P-450 Prosthetic Haem Group by 1-Aminobenzotriazole, *Biochem. J.* **195**, 761-764.
- Ortiz de Montellano, P. R., Mico, B. A., Mathews, J. M., Kunze, K. L., Miwa, G. T. and Lu, A. Y. H. (1981) Selective Inactivation of Cytochrome P-450 Isozymes by Suicide Substrates, *Arch. Biochem. Biophys.* **210**, 717-728.
- Pesez, M. and Bartos, J. (1974) Colorimetric and Fluorimetric Determination of Organic Compounds (Schwartz, M., ed) pp. 329-331, Marcel Dekker, Inc., New York.
- Rahhal, S. and Richter, H. W. (1988) Reduction of Hydrogen Peroxide by the Ferrous Iron Chelate of Diethylenetriamine-N,N,N',N'',N'''-pentaacetate, *J. Am. Chem. Soc.* **110**, 3126-3133.
- Rana, T. M. and Meares, C. F. (1991) Transfer of Oxygen from a Artificial Protease to Peptide Carbon During Proteolysis, *Proc. Natl. Acad. Sci. U.S.A.* **88**, 10578-10582.
- Ringe, D., Petsko, G. A., Kerr, D. E. and Ortiz de Montellano, P. R. (1984) Reaction of Myoglobin with Phenylhydrazine: a Molecular Doorstop, *Biochemistry* **23**, 2-4.

- Rush, J. D. and Koppenol, W. H. (1988) Reactions of Fe^{II}nta and Fe^{II}edda with Hydrogen Peroxide, *J. Am. Chem. Soc.* **110**, 4957-4963.
- Sawaki, Y. and Foote, C. (1979) Acyclic Mechanism in the Cleavage of Benzils with Alkaline Hydrogen Peroxide, *J. Am. Chem. Soc.* **101**, 6292-6296.
- Sono, M., Dawson, J. H., Hall, K. and Hager, L. P. (1986) Ligand and Halide Binding Properties of Chloroperoxidase: Peroxidase-Type Active Site Heme Environment with Cytochrome P-450 Type Endogenous Axial Ligand and Spectroscopic Properties, *Biochemistry* **25**, 347-356.
- Takano, T. (1977a) Structure of Myoglobin Refined at 2.0 Å Resolution. I. Crystallographic Refinement of Metmyoglobin from Sperm Whale, *J. Mol. Biol.* **110**, 537-568.
- Takano, T. (1977b) Structure of Myoglobin Refined at 2.0 Å Resolution. II. Structure of Deoxymyoglobin from Sperm Whale, *J. Mol. Biol.* **110**, 569-584.
- Watanabe, Y., Iyanagi, T. and Oae, S. (1981) Kinetic Study on Enzymatic S-Oxygenation Promoted by a Reconstituted System with Purified Cytochrome P-450, *Tet. Letters* **21**, 3685-3688.
- Watanabe, Y., Iyanagi, T. and Oae, S. (1982) 1 Electron Transfer Mechanism in the Enzymatic Oxygenation of Sulfoxide to Sulfone Promoted by a Reconstituted System with Purified Cytochrome P-450, *Tet. Letters* **23**, 533-536.
- Winterbourn, C. C. (1987) The Ability of Scavengers to Distinguish OH· Production in the Iron-Catalyzed Haber-Weiss Reaction: Comparison of Four Assays for OH·, *J. Free Radicals Biol. Med.* **3**, 33-39.
- Yamazaki, I. and Piette, L. H. (1963) The Mechanism of Aerobic Oxidase Reaction Catalyzed by Peroxidase, *Biochim. Biophys. Acta* **77**, 47-64.

197950



FOR REFERENCE

NOT TO BE TAKEN FROM THE ROOM

CAT. NO. 23 012

609973



3 1378 00609 9736

